

Surface Organometallic Chemistry: Molecular Approaches to Surface Catalysis

NATO ASI Series

Advanced Science Institutes Series

A Series presenting the results of activities sponsored by the NATO Science Committee, which aims at the dissemination of advanced scientific and technological knowledge, with a view to strengthening links between scientific communities.

The Series is published by an international board of publishers in conjunction with the NATO Scientific Affairs Division

A Life Sciences	Plenum Publishing Corporation
B Physics	London and New York
C Mathematical and Physical Sciences	Kluwer Academic Publishers Dordrecht, Boston and London
D Behavioural and Social Sciences	
E Applied Sciences	
F Computer and Systems Sciences	Springer-Verlag
G Ecological Sciences	Berlin, Heidelberg, New York, London,
H Cell Biology	Paris and Tokyo



Surface Organometallic Chemistry: Molecular Approaches to Surface Catalysis

edited by

Jean-Marie Basset

Institut de Recherches sur la Catalyse, CNRS,
Villeurbanne, France

Bruce C. Gates

Center for Catalytic Science and Technology,
Department of Chemical Engineering,
University of Delaware, Newark, Delaware, U.S.A.

**Jean-Pierre Candy, Agnès Choplin, Michel Leconte,
Françoise Quignard and Catherine Santini**

Institut de Recherches sur la Catalyse, CNRS,
Villeurbanne, France



Kluwer Academic Publishers

Dordrecht / Boston / London

Published in cooperation with NATO Scientific Affairs Division

Proceedings of the NATO Advanced Research Workshop on
Surface Organometallic Chemistry:
Molecular Approaches to Surface Catalysis
Le Rouet (Ardèche), France
May 26 -30, 1986

Library of Congress Cataloging in Publication Data

NATO Advanced Research Workshop on Surface Organometallic Chemistry:
Molecular Approaches to Surface Catalysis (1986 : Ardèche, France)
Surface organometallic chemistry : molecular approaches to surface
catalysis : proceedings of the NATO advanced research workshop held
in Le Rouet, (Ardèche), France, May 26-30, 1986 / edited by Jean
-Marie Basset ... [et al.].
p. cm. -- (NATO ASI series. Series C, Mathematical and
physical sciences : vol. 231)
"Proceedings of the NATO Advanced Research Workshop on Surface
Organometallic Chemistry: Molecular Approaches to Surface
Catalysis"--T.p. verso.
"Published in cooperation with NATO Scientific Affairs Division."
Includes index.
ISBN-13: 978-94-010-7834-4
1. Organometallic chemistry--Congresses. 2. Catalysis--
-Congresses. 3. Surface chemistry--Congresses. I. Basset, Jean
-Marie. II. North Atlantic Treaty Organization. Scientific Affairs
Division. III. Title. IV. Series: NATO ASI series. Series C,
Mathematical and physical sciences : no. 231.
QD410.N33 1986
547'.05045453--dc19

88-4394
CIP

ISBN-13: 978-94-010-7834-4 e-ISBN-13: 978-94-009-2971-5
DOI: 10.1007/978-94-009-2971-5

Published by Kluwer Academic Publishers,
P.O. Box 17, 3300 AA Dordrecht, The Netherlands.

Kluwer Academic Publishers incorporates the publishing programmes of
D. Reidel, Martinus Nijhoff, Dr W. Junk, and MTP Press.

Sold and distributed in the U.S.A. and Canada
by Kluwer Academic Publishers,
101 Philip Drive, Norwell, MA 02061, U.S.A.

In all other countries, sold and distributed
by Kluwer Academic Publishers Group,
P.O. Box 322, 3300 AH Dordrecht, The Netherlands.

All Rights Reserved
© 1988 by Kluwer Academic Publishers
Softcover reprint of the hardcover 1st edition 1988

No part of the material protected by this copyright notice may be reproduced or utilized
in any form or by any means, electronic or mechanical, including photocopying, recording
or by any information storage and retrieval system, without written permission from the
copyright owner.

**ALL ASI SERIES BOOKS PUBLISHED AS A RESULT OF ACTIVITIES OF THE
SPECIAL PROGRAMME ON SELECTIVE ACTIVATION OF MOLECULES**

This book contains the proceedings of a NATO Advanced Research Workshop held within the programme of activities of the NATO Special Programme on Selective Activation of Molecules running from 1983 to 1988 as part of the activities of the NATO Science Committee.

Other books previously published as a result of the activities of the Special Programme are

BOSNICH, B. (Ed.) – *Asymmetric Catalysis* (E103), 1986

PELIZZETTI, E. and SERPONE, N. (Eds.) – *Homogeneous and Heterogeneous Photocatalysis* (C174) 1986

SCHNEIDER, M. P. (Ed.) – *Enzymes as Catalysts in Organic Synthesis* (C178) 1986

SETTON, R. (Ed.) – *Chemical Reactions in Organic and Inorganic Constrained Systems* (C165) 1986

VIEHE, H. G., JANOUSEK, Z., and MERÉNYI, R. (Eds.) – *Substituent Effects in Radical Chemistry* (C189) 1987

BALZANI, V. (Ed.) – *Supramolecular Photochemistry* (C214) 1987

FONTANILLE, M. and GUYOT, A. (Eds.) – *Recent Advances in Mechanistic and Synthetic Aspects of Polymerization* (C215) 1987

LAINÉ, R. M. (Ed.) – *Transformation of Organometallics into Common and Exotic Materials: Design and Activation* (E141) 1988

TABLE OF CONTENTS

Foreword	ix
List of Participants	xiii
List of Contributors	xvii
REPORT OF THE NATO WORKSHOP: "SURFACE ORGANOMETALLIC CHEMISTRY: MOLECULAR APPROACHES TO SURFACE CATALYSIS"	1
THE SURFACES OF OXIDES AT A MOLECULAR LEVEL Helmut Knözinger	35
REACTION OF ORGANOMETALLICS WITH SURFACES OF METAL OXIDES John Evans	47
CATALYTIC REACTIONS CARRIED OUT WITH METALS DERIVED FROM CLUSTERS Robin Whyman	75
SOLUBLE AND SUPPORTED METAL CATALYSTS FOR HYDROCARBON OXIDATION IN LIQUID AND VAPOR PHASE James E. Lyons	97
REACTIONS OF ORGANOMETALLIC COMPOUNDS WITH SURFACES OF SUPPORTED AND UNSUPPORTED METALS Yuri A. Ryndin and Yuri I. Yermakov	127
LOW-NUCLEARITY METAL CLUSTERS: STRUCTURE AND REACTIVITY Pierre Gallezot	143

LARGE MOLECULAR METAL CARBONYL CLUSTERS: MODELS OF METAL PARTICLES Giuliano Longoni, Alessandro Ceriotti, Mario Marchionna, and Giampietro Piro	157
MOLECULAR MODELS OF EARLY TRANSITION METAL OXIDES: POLYOXOANIONS AS ORGANIC FUNCTIONAL GROUPS Victor W. Day, Walter G. Klemperer, Curtis Schwartz, and Ren-Chain Wang	173
HOMOGENEOUS MODELS FOR MECHANISMS OF SURFACE REACTIONS: PROPENE AMMOXIDATION Dominic M. T. Chan, William A. Nugent, William C. Fultz, D. Christopher Roe, and Thomas H. Tulip	187
ORGANOMETALLIC OXIDES: FUTURE MODELS IN CATALYSIS? THE EXAMPLE OF TRIOXO(η^5 -PENTAMETHYLCYCLOPENTADIENYL)RHENIUM(VII) Wolfgang A. Herrmann	197
ZEOLITE SYNTHESIS: AN OVERVIEW Richard M. Barrer	221
NEW DIRECTIONS IN MOLECULAR SIEVE SCIENCE AND TECHNOLOGY Jule A. Rabo	245
RECENT ADVANCES IN PILLARED CLAYS AND GROUP IV METAL PHOSPHATES Abraham Clearfield	271
REACTION OF ORGANOMETALLICS WITH THE SURFACES OF ZEOLITES Eric G. Derouane	299
Index	311

FOREWORD

Surface organometallic chemistry is a new field bringing together researchers from organometallic, inorganic, and surface chemistry and catalysis. Topics ranging from reaction mechanisms to catalyst preparation are considered from a molecular basis, according to which the "active site" on a catalyst surface has a supra-molecular character. This, the first book on the subject, is the outcome of a NATO Workshop held in Le Rouet, France, in May, 1986. It is our hope that the following chapters and the concluding summary of recommendations for research may help to provide a definition of surface organometallic chemistry.

Besides catalysis, the central theme of the Workshop, four main topics are considered:

- 1) Reactions of organometallics with surfaces of metal oxides, metals, and zeolites;
- 2) Molecular models of surfaces, metal oxides, and metals;
- 3) Molecular approaches to the mechanisms of surface reactions;
- 4) Synthesis and modification of zeolites and related microporous solids.

Most surface organometallic chemistry has been carried out on amorphous high-surface-area metal oxides such as silica, alumina, magnesia, and titania. The first chapter, contributed by KNÖZINGER, gives a short summary of the structure and reactivity of metal oxide surfaces. Most of our understanding of these surfaces is based on acid-base and redox chemistry; this chemistry has developed from X-ray and spectroscopic data, and much has been inferred from the structures and reactivities of adsorbed organic probe molecules. There are major opportunities for extending this understanding by use of well-defined (single crystal) oxide surfaces and organometallic probe molecules.

EVANS provides a summary of the reactions of organometallics with oxide surfaces that lead to well-defined surface species including mononuclear and polynuclear complexes and monometallic and bimetallic particles. These surface reactions are described by the same principles encountered in molecular chemistry; the reaction classes include nucleophilic attack at the ligands, electrophilic attack at the metal-carbon bond, oxidative addition, Lewis base adduct formation, redox reactions, etc. The synthesis of well-defined reactive sites on surfaces by these organometallic routes will facilitate the study of elementary steps in surface chemistry.

The surface-bound organometallics, which may have either a "molecular like" or a "metal like" character, have been probed with a number of catalytic test reactions, including Fischer-Tropsch synthesis, as described by WHYMAN. New catalysts have been made, and there has been encouraging progress in tailoring specific organometallic surface structures for catalytic applications. LYONS provides an account of the varieties of industrially important catalytic oxidation reactions, offering suggestions for the application of surface organometallic chemistry in tailoring of new catalysts.

Organometallics (especially of main group elements) have been allowed to react with metal particles already on supports, leading to intermetallic phases and resulting in a new class of catalyst, which is already being used in a commercial process. RYNDIN, representing the group of the late Professor YERMAKOV, describes how these catalysts can be made and opens the way to a more systematic investigation.

Monometallic and bimetallic particles derived from molecular metal clusters can now be characterized by a wide range of powerful physical techniques, described by GALLEZOT. In the future, we can expect to be able to distinguish surface ligands and bulk compositions in bimetallic particles as well as dynamics of ligands and metal frameworks. Better understanding of structure and dynamics of metal particles will be based in part on comparisons with high-nuclearity molecular metal clusters, which are excellent models having well-known structures. LONGONI describes this class of molecules, which are truly at the borderline between the metallic state and the molecular state.

Compelling molecular models also include complexes of early transition metals in higher oxidation states. These complexes mimic oxide surface structure at a molecular level, including extended oxide structures. These models, described by KLEMPERER, can also be used to mimic some elementary steps in heterogeneous oxidation reactions.

Another facet of surface organometallic chemistry involves modelling of the mechanisms of surface reactions on the basis of the reactivity of molecular models. For example, the reactivity of metal-imine complexes of molybdenum is considered by CHAN, who proposes elementary steps constituting the catalytic cycle of the surface-catalyzed alkene ammoxidation reaction, which is of great industrial importance. HERRMANN provides some very fine examples of molecular models of the rhenium oxide catalysts used commercially in the alkene metathesis reaction.

The opportunities for tailoring the properties of catalysts and adsorbents extend beyond amorphous metal oxides, and some of the most compelling opportunities are offered by metal oxides with regular structures. Zeolite molecular sieves (crystalline aluminosilicates) are the most important industrial examples, and BARRER provides a review of the synthesis chemistry, which may just be entering the realm of molecular design. RABO's chapter is concerned with a new and structurally analogous class of materials, the ALPO's, SAPO's, and the like, which have dramatically extended the class of molecular sieves. CLEARFIELD's review completes this section, providing an introduction to aluminosilicate clays, which consist of layer structures with large intracrystalline spaces and molecular sieving properties. The intracrystalline spaces of all these molecular sieves offer whole new chemistries of their own and exciting opportunities for design of new supported structures, including organometallics. This subject is in its infancy, as described in the brief summary by DEROUANE.

Neither the Workshop nor this book would have been possible without the generous help and support of a number of people and organizations. The advice and financial support of the NATO Division of Scientific Affairs (Dr. Craig SINCLAIR) was essential. Travel and lodging grants and other funds were also generously provided by the CNRS (France), the NSF (USA), the British Petroleum Company (UK), the Charbonnages de France Chimie (France), Imperial Chemical Industries (UK), Rhône-Poulenc (France), and the Société Nationale Elf-Aquitaine (France). We also appreciate the efforts of those who were able to reduce the cost of the Workshop by obtaining financial assistance from their universities, companies, and governments. D. Reidel Publishing Company has provided the help and advice necessary for publication of this volume. We especially thank Mrs. N. M. POLS-v.d. HEIJDEN and Mrs. T. AMMERDORFFER-v.d. HOEK of the Reidel Staff.

Most important, we appreciate the time and effort contributed by the participants of the Workshop who have written portions of the report included in this volume. We thank the authors of the chapters for their efforts to provide clear descriptions of the state of the art in their fields.

Finally, we will be forever grateful to Mrs. Lydie BADOLLO, who typed the report during and after the meeting, and to Mrs. Françoise REYMOND, who had the difficult task of retyping the total volume in a new format. Without her, this book could never have been brought to fruition.

J. M. BASSET
B. C. GATES
J. P. CANDY
A. CHOPLIN
M. LECONTE
F. QUIGNARD
C. SANTINI

October, 1987

LIST OF PARTICIPANTS

Dr. D. BALLIVET-TKATCHENKO
CNRS - Laboratoire de Chimie de
Coordination
205 route de Narbonne
31400 TOULOUSE
FRANCE

Prof. R. M. BARRER
Department of Chemistry
Imperial College
South Kensington
LONDON SW7 2AY
ENGLAND

Dr. D. BARTHOMEUF
Laboratoire de Réactivité de
Surface et Structure
Université Pierre et Marie Curie
4 place Jussieu
75252 PARIS CEDEX 05
FRANCE

Dr. J. M. BASSET
CNRS - Institut de Recherches sur
la Catalyse
2 avenue Albert Einstein
69626 VILLEURBANNE CEDEX
FRANCE

Dr. D. M. T. CHAN
E.I. Du Pont de Nemours and Co.
Experimental Station
Imaging Systems Department
Building 352
WILMINGTON, DELAWARE 19898
U.S.A.

Prof. A. CLEARFIELD
Department of Chemistry
Texas A&M University
COLLEGE STATION, TEXAS 77843
U.S.A.

Dr. R. A. DALLA BETTA
Catalytica Associates
430 Ferguson Drive
Building 3
MOUNTAIN VIEW, CA 94043
U.S.A.

Prof. E. DEROUANE
Facultés Universitaires Notre
Dame de la Paix
Laboratoire de Catalyse
61 rue de Bruxelles
B-5000 NAMUR
BELGIUM

Prof. J. EVANS
Department of Chemistry
The University
SOUTHAMPTON SO9 5NH
ENGLAND

Dr. P. GALLEZOT
CNRS - Institut de Recherches sur
la Catalyse
2 avenue Albert Einstein
69626 VILLEURBANNE CEDEX
FRANCE

Prof. B. C. GATES
Center for Catalytic Science and
Technology
Department of Chemical
Engineering
University of Delaware
NEWARK, DELAWARE 19716
U.S.A.

Prof. W. A. GODDARD III
Chemistry Department
Mail Code 127-72
California Institute of
Technology
PASADENA, CA 91125
U.S.A.

Prof. R. H. GRUBBS
Division of Chemistry and
Chemical Engineering
California Institute of
Technology
PASADENA, CA 91125
U.S.A.

Prof. W. A. HERRMANN
Anorganisch-Chemisches Institut
Lichtenbergstrasse 4
D-8046 GARCHING
F.R.G.

Prof. M. ICHIKAWA
The Research Institute for
Catalysis
Hokkaido University
SAPPORO, 060
JAPAN

Prof. H. D. KAESZ
Department of Chemistry and
Biochemistry
University of California
LOS ANGELES, CA 90024
U.S.A.

Prof. W. G. KLEMPERER
University of Illinois
Department of Chemistry
159 NL BOX 8
505 South Mathews Avenue
URBANA, IL 61801
U.S.A.

Prof. H. KNÖZINGER
Institut für Physikalische Chemie
Universität München
Sophienstrasse 11
8000 MÜNCHEN 2
F.R.G.

Prof. G. LONGONI
Dipartimento di Chimica
Inorganica e Metallorganica
Università di Milano
21 Via Venezian
20133 MILANO
ITALY

Dr. J. E. LYONS
SUN OIL Inc.
P.O. Box 1135
MARCUS HOOK, PA 19061-0835
U.S.A.

Dr. G. MAIRE
Université Louis Pasteur
Strasbourg I
Institut de Chimie - UA 423
4 rue Blaise Pascal
67070 STRASBOURG CEDEX
FRANCE

Prof. R. MAUREL
CNRS - Institut de Recherches sur
la Catalyse
2 avenue Albert Einstein
69626 VILLEURBANNE CEDEX
FRANCE

Dr. H. MIMOUN
Institut Français du Pétrole
B.P. 311
92506 RUEIL MALMAISON
FRANCE

Prof. D. OLIVIER
Laboratoire de Réactivité de
Surface et Structure
Université Pierre et Marie Curie
75252 PARIS CEDEX 05
FRANCE

Prof. J. A. OSBORN
Institut Le Bel
Université Louis Pasteur
Strasbourg I
4 rue Blaise Pascal
67070 STRASBOURG CEDEX
FRANCE

Prof. F. PETIT
E.N.S.C. Lille
B.P. 108
59652 VILLENEUVE D'ASCQ
FRANCE

Prof. T. J. PINNAVAIA
Department of Chemistry
Michigan State University
EAST LANSING, MICHIGAN 48824
U.S.A.

Prof. R. POILBLANC
CNRS - Laboratoire de Chimie de
Coordination
205 route de Narbonne
31400 TOULOUSE
FRANCE

Dr. R. PSARO
Dipartimento di Chimica
Inorganica e Metallorganica
Università di Milano
Via Venezian 21
20133 MILANO
ITALY

Dr. J. A. RABO
Union Carbide Corporation
Tarrytown Technical Center
Old Saw Mill River Road
TARRYTOWN, N.Y. 10591
U.S.A.

Dr. Y. A. RYNDIN
Institute of Catalysis
Prospekt Akademika Lavrentieva 5
NOVOSIBIRSK 630090
USSR

Dr. A. K. SMITH
Department of Inorganic,
Physical, and Industrial
Chemistry
University of Liverpool
P.O. Box 147
LIVERPOOL L69 3BX
ENGLAND

Prof. K. I. TANAKA
The Institute for Solid State
Physics
The University of Tokyo
7-22-1 Roppongi
Minato-Ku
TOKYO 106
JAPAN

Prof. R. UGO
Dipartimento di Chimica
Inorganica e Metallorganica
Università di Milano
Via Venezian 21
20133 MILANO
ITALY

Dr. R. WHYMAN
I.C.I. New Science Group
P.O. Box 11
The Heath
RUNCORN CHESHIRE WA7 4QE
ENGLAND

Dr. A. ZECCHINA
Istituto di Chimica Fisica
Corso M. D'Azeglio
10125 TORINO
ITALY

LIST OF CONTRIBUTORS

R. M. BARRER
Department of Chemistry
Imperial College
South Kensington
LONDON SW7 2AY
ENGLAND

A. CERIOTTI
Dipartimento di Chimica
Inorganica e Metallorganica
Università di Milano
21 Via Venezian
20133 MILANO
ITALY

D. M. T. CHAN
E.I. Du Pont de Nemours and Co.
Experimental Station
Imaging Systems Department
Building 352
WILMINGTON, DELAWARE 19898
U.S.A.

A. CLEARFIELD
Department of Chemistry
Texas A&M University
COLLEGE STATION, TEXAS 77843
U.S.A.

V. W. DAY
Crystalytics Company
LINCOLN, NEBRASKA 68501
U.S.A.
Department of Chemistry
University of Nebraska
LINCOLN, NEBRASKA 68588
U.S.A.

E. DEROUANE
Facultés Universitaires Notre
Dame de la Paix
Laboratoire de Catalyse
61 rue de Bruxelles
B-5000 NAMUR
BELGIUM

J. EVANS
Department of Chemistry
The University
SOUTHAMPTON SO9 5NH
ENGLAND

W. C. FULTZ
E.I. Du Pont de Nemours and Co.
Central Research and Development
Department
Experimental Station
WILMINGTON, DELAWARE 19898
U.S.A.

P. GALLEZOT
CNRS - Institut de Recherches sur
la Catalyse
2 avenue Albert Einstein
69626 VILLEURBANNE CEDEX
FRANCE

W. A. HERRMANN
Anorganisch-Chemisches Institut
Lichtenbergstrasse 4
D-8046 GARCHING
F.R.G.

W. G. KLEMPERER
University of Illinois
Department of Chemistry
159 NL BOX 8
505 South Mathews Avenue
URBANA, IL 61801
U.S.A.

H. KNÖZINGER
Institut für Physikalische Chemie
Universität München
Sophienstrasse 11
8000 MÜNCHEN 2
F.R.G.

G. LONGONI
Dipartimento di Chimica
Inorganica e Metallorganica
Università di Milano
21 Via Venezian
20133 MILANO
ITALY

J. E. LYONS
SUN OIL Inc.
P.O. Box 1135
MARCUS HOOK, PA 19061-0835
U.S.A.

M. MARCHIONNA
Dipartimento di Chimica
Inorganica e Metallorganica
Università di Milano
21 Via Venezian
20133 MILANO
ITALY

W. A. NUGENT
E.I. Du Pont de Nemours and Co.
Central Research and Development
Department
Experimental Station
WILMINGTON, DELAWARE 19898
U.S.A.

G. PIRO
Dipartimento di Chimica
Inorganica e Metallorganica
Università di Milano
21 Via Venezian
20133 MILANO
ITALY

J. A. RABO
Union Carbide Corporation
Tarrytown Technical Center
Old Saw Mill River Road
TARRYTOWN, N.Y. 10591
U.S.A.

REN-CHAIN WANG
Department of Chemistry
University of Illinois
URBANA, ILLINOIS 61801
U.S.A.

D. C. ROE
E.I. Du Pont de Nemours and Co.
Central Research and Development
Department
Experimental Station
WILMINGTON, DELAWARE 19898
U.S.A.

Y. A. RYNDIN
Institute of Catalysis
Prospekt Akademika Lavrentieva 5
NOVOSIBIRSK 630090
USSR

C. SCHWARTZ
Department of Chemistry
University of Illinois
URBANA, ILLINOIS 61801
U.S.A.

T. H. TULIP
E.I. Du Pont de Nemours and Co.
Central Research and Development
Department
Experimental Station
WILMINGTON, DELAWARE 19898
U.S.A.

R. WHYMAN
I.C.I. New Science Group
P.O. Box 11
The Heath
RUNCORN CHESHIRE WA7 4QE
ENGLAND

Y. I. YERMAKOV
Institute of Catalysis
Prospekt Akademika Lavrentieva 5
NOVOSIBIRSK 630090
USSR

REPORT OF THE NATO WORKSHOP:

"SURFACE ORGANOMETALLIC CHEMISTRY:
MOLECULAR APPROACHES TO SURFACE CATALYSIS"

- . Summary of conclusions and recommendations
- . Reports on the following topics:
 - 1 - Reaction of organometallics with oxides, zeolites, and metals
 - 2 - Molecular models of oxides, metals, and surface complexes
 - 3 - Synthesis of new porous supports
 - 4 - The molecular approach to mechanisms of surface reactions
 - 5 - Catalysis

SUMMARY OF CONCLUSIONS AND RECOMMENDATIONS

Knowledge of the mechanisms of action of most solid catalysts remains extremely limited. Often the overall product distribution of a catalytic reaction is known, but the nature of the catalyst-reactant interactions remains obscure. In a few cases, a more detailed model can be advanced, but the models are modest in comparison with structural and mechanistic details that have been developed in molecular chemistry. The difficulty is that by comparison with strictly molecular systems, the surfaces of solid catalysts are extremely complicated, and the structures of the so-called "active sites" are almost always unknown at an atomic level.

Mechanistic progress will be closely connected with the preparation of well-defined surface catalysts, which can be achieved with organometallic compounds on surfaces. It is now evident that the systematic study of the reactivity of organometallic compounds on surfaces will have an impact on surface catalysis rivaling that of organometallic chemistry on homogeneous catalysis. This approach offers many advantages, including (i) the preparation of well-defined "active sites", (ii) establishment of elementary reaction steps, and (iii) development of a fundamental basis for the synthesis of tailor-made catalysts.

For example, surface organometallic chemistry may permit formation of well-defined species (molecular analogues) on high-surface-area solids such as silica, alumina, and magnesia. These offer the prospect of new catalysts in their own right, including, for example, supported analogues of known molecular (homogeneous) catalysts, metal centers stabilized in low or high oxidation states, and multifunctional tailor-made sites such as metal-promoter combinations. Surface-bound organometallics can also be used as precursors of small, uniform metal particles, including compositionally uniform bimetallic particles.

Understanding of surface structures (including those of the highly nonuniform surfaces of industrial catalysts), as well as understanding of elementary steps, can be developed by investigating molecular analogues. Spectroscopic characterization of surfaces and their analogues, combined with theory, can lead to much-improved structural and electronic characterization of reactive surface groups. Effort is required in the synthesis of appropriate models, such as complexes with both metal-carbon and metal-oxygen bonds, molecular metal oxide models of surface defects and low-coordination surface sites, and models of highly basic oxides. The work should be extended to analogues of metal sulfides.

Crystalline porous solids such as zeolites also offer excellent opportunities for novel supported organometallic complexes and metal particles. The molecular chemistry of the synthesis of zeolites and related molecular sieves is still obscure; the expansion of the class of molecular sieves is proceeding rapidly on an empirical basis with

little influence of molecular chemistry. The development of stable, new pillared layer structures is also anticipated, including the molecular design of functionalized bridges and methods to achieve controlled pillar distributions. The nature of the acidity that influences the catalytic character of oxide surfaces and cages continues to be elusive. The concept of acidity requires scrutiny and more careful definition.

1. REACTION OF ORGANOMETALLICS WITH OXIDES, ZEOLITES, AND METALS

The development of homogeneous catalysts in the preceding thirty years has been based on the conceptual advances in molecular organometallic chemistry. The strategy for developing new homogeneous catalysts is based on the catenation of successive elementary steps. This governs the choice of the central metal element, oxidation state, ancillary ligands, and reaction conditions.

In contrast, the development of new surface catalysts in recent years has been mostly empirical. The number of well-established elementary steps is limited, and the precise structure of the so-called "active site" is often unknown at a molecular or atomic level.

The systematic study of the reactivity of organometallic compounds with surfaces (e.g., of oxides, sulfides, zeolites, and metals) is expected to have the same impact on surface catalysis that organometallic chemistry has had on homogeneous catalysis.

This approach offers many possible advantages:

- preparation of well-defined "active sites";
- establishment of elementary reaction steps;
- development of a fundamental basis for the synthesis of tailor-made catalysts.

1.1. State of the art

Surface organometallic chemistry faces an imbalance between, on the one hand, well-defined precursor molecular complexes and, on the other, relatively poorly characterized surface-active sites to which these complexes are to be attached. It is extremely important to characterize and define the available surface sites. This subject is covered in a subsequent section of this report.

Although surface organometallic chemistry is still in its infancy, there are already several examples of surface reactions leading to well-defined surface complexes (Table 1-I). It appears that these reactions obey the same principles as those encountered in molecular chemistry: nucleophilic attack at the ligands, electrophilic attack of the metal-carbon bond, oxidative addition, Lewis acid-base adduct formation, redox reactions, disproportionation, and the cooperative effect of dual acid-base sites in an insertion reaction.

Although the resulting surface-supported complexes have not been characterized as completely as have the molecular analogues by single-crystal, X-ray diffraction, there is strong evidence in support of such structures, based upon application of the 16-18 electron rules for late transition metals and upon results of multiple analytical and spectroscopic techniques (Table 1-I).

The development of surface organometallic chemistry has been retarded by the requirement for a combination of expertise in the experimental techniques and concepts of both surface and organometallic

Table 1-I: Examples of Support-Complex Interactions

Class	Precursor Complex	Support	Surface Species	Characterization Techniques
Nucleophilic attack on coordination CO	$\text{Fe}_3(\text{CO})_{12}$	hydroxylated $[\text{HFe}_3(\text{CO})_{11}]^-$ MgO		IR; $^{1\text{H}}$ NMR; UV-vis; Ion extraction; Gas evolution.
	$\text{Fe}(\text{CO})_5$	dehydrated $[\text{Fe}(\text{CO})_4\text{CO}_2]^{2-}\text{Mg}^{2+}$ MgO		IR; UV-vis; $^{12\text{C}}\text{O}-^{13\text{C}}\text{O}$ isotopic exchange.
Electrophilic cleavage of M-C bonds	$\text{Rh}(\eta^3\text{-C}_3\text{H}_5)_3^*$	SiO_2	($\text{-SiO})\text{Rh}(\eta^3\text{-C}_3\text{H}_5)_2$	Gas analysis; IR; XPS; $^{1\text{H}}$ NMR.
Oxidative addition	$\text{M}_3(\text{CO})_{12}$ M = Ru, Os	SiO_2 Al_2O_3	($\text{-SiO})\text{M}_3(\text{H})(\text{CO})_{10}$	IR; UV-vis; EXAFS; gas analysis; molecular models; IETS; Raman; TEM.
Bronsted acid-base	$\text{H}_2\text{Os}(\text{CO})_4$	MgO	$[\text{HO}(\text{CO})_4]^-$	IR; UV-vis; ion extraction.
Lewis acid-base	$[\text{HFe}_3(\text{CO})_{11}]^-$	MgO	$\text{HFe}_3(\text{CO})_{11}(\text{μ-CO}\rightarrow[\text{Mg}])$	IR; ion extraction.
Redox reactions	$\text{Rh}_6(\text{CO})_{16}$	Al_2O_3	$(\text{Al}_10)\text{Rh}(\text{CO})_2(\text{OH}[\text{Al}])_2$	$^{13}\text{C}(^{12}\text{C})$; gas analysis; EXAFS
Disproportionation	$\text{Co}_2(\text{CO})_8$	NaY	$[\text{Co}(\text{CO})_4]_2(\text{OH}[\text{Al}])_2$	IR; UV-vis; TPD; gas analysis.
Promoted insertion	$\text{MeMn}(\text{CO})_5/\text{CO}$	Al_2O_3	$(\text{OC})_5\text{Mn}(\text{C}(\text{Me})=\text{O})\text{Al}$	IR; model studies.

*This is but one example; mention should be made of the pioneering work covering a multitude of pi-allyl metal complexes of Yermakov and Ballard and their coworkers.

chemistry. In particular, organometallic chemistry requires the determination of the stoichiometry of the surface reaction, for example, determined by quantitative analysis of gaseous products, of surface metal concentration, and quantitative extraction of surface complexes.

Some of the surface complexes, intact, are found to exhibit catalytic properties. However, complete evidence for reaction mechanisms is still lacking in almost every case.

1.1.1. Elementary steps. The reactivity of the anchored complexes has been studied in only a few cases. Evidence for a few elementary steps on surfaces has been obtained, including ligand association and dissociation reactions, oxidative addition, and insertion. Understanding of these will be a prerequisite to the fundamental understanding of the elementary steps of catalysis. At this point, these can at best be inferred by analogy to molecular chemistry in solution. Therefore, a systematic approach to the chemistry of these elementary steps on surfaces is recommended.

1.1.2. Organometallic probes of surfaces. So far the chemical means to characterize surfaces at a molecular level have been based mainly on the spectroscopic methods used with molecular probes, including CO, NO, O₂, CO₂, and organic bases. These molecules give information concerning the acid-base and redox properties of the surfaces of oxides and sulfides. They also probe the coordination properties of ensembles of metal atoms at the surfaces of monometallic or bimetallic particles.

The chemisorption of an organometallic molecule at the surface of an oxide is a new tool to chemically characterize the reactivity of the functional groups of the surface towards the metal and its ligands. These probe molecules allow evaluation, for example, of the acid-base (nucleophilic) character of the O²⁻ or OH⁻ groups, the electrophilic character of cations or surface OH groups, the redox properties of the surface, etc.

Organometallic probe molecules possessing bifunctional character (i.e., both basic and acidic functional groups) provide means of probing bifunctional surface sites; see Table 1-I. Hydrido-metal carbonyls are an example of such bifunctional complexes which also provide convenient spectroscopic means of characterization.

1.1.3. Synthesis of supported homometallic particles. Supported metal particles have been obtained by the controlled chemisorption of mono- or poly-nuclear complexes followed by their thermal decomposition. This method offers technical advantages over the preparation of heterogeneous metal catalysts by the reduction of metal salts. First, it is advantageous to eliminate the ligands and counter ions from the original salt, which can be difficult to remove during catalyst activation and which can often modify the chemical properties of the final material. Second, only coarse control of the processes occurring during high-temperature hydrogen reduction is attainable. By contrast, ligand disengagement from supported organometallics may be monitored spectroscopically and carried out under mild, controlled conditions.

1.1.4. Synthesis of supported bimetallic and multimetallic particles. Supported bimetallics have been prepared from combinations of monometallic or from bimetallic cluster precursors. In the ideal case, the resulting metals are segregated on an oxide surface, sometimes with one metal present as zerovalent aggregates and the other present as ionic complexes. Occasionally, the metals are found in small bimetallic clusters, whereas the product formed from separate monometallic precursors may yield aggregates of segregated metals.

1.1.5. Reaction of organometallics with metals. The reaction of organometallics with metals, which is still an underdeveloped area, appears to be a promising aspect of surface organometallic chemistry.

So far only organometallics of group IVA and VIII have been reacted with the surfaces of group VIII metals. The understanding of such chemistry is fragmentary and requires a precise determination of the oxidation state of the original supported metal and the nature of the resulting intermetallic materials.

New classes of metal-support interaction may be obtained by interaction of group IVB and group VIII organometallic complexes with silica. In the same vein, bimetallic catalysts selective for alcohol formation from synthesis gas can be prepared, and these merit further investigation.

1.1.6. Reaction of organometallic complexes with zeolites. The introduction of transition metals into zeolite structures is achieved by two principal routes.

The first takes place through a conventional ion exchange reaction with high-valent complexes. Low-valent organometallic species (mono-nuclear or polynuclear) can subsequently be formed with appropriate co-reagents (CO , $\text{CO} + \text{H}_2\text{O}$, H_2) and ligands (CO , NO , NR_3 , PR_3 , ...). These studies have been mainly conducted with a faujasite zeolite (having large pores).

The second route which has recently been developed (essentially with faujasite zeolites) is the reaction with low-valent metal complexes, mainly zerovalent carbonyl complexes. Different reaction pathways have been characterized according to the chemical properties of the zeolite (acidic or non-acidic) and the nature of the complexes (metal, nuclearity):

- the electrophilic centers of the zeolite (cations) interact with the complexes through acid-basic interaction with the bridging carbonyls;
- the nucleophilic centers (OH groups) react with CO ligands, leading to decarbonylation with concomitant CO_2 formation;
- the oxidizing centers (protons) lead to metal ion formation; and
- the electrical field in the zeolite induces a chemistry comparable to that in alcohol solutions, with disproportionation of neutral carbonyl clusters into cationic species.

1.1.7. Stabilization of catalytically active metal centers in high or in unusual oxidation states. Some reactions may involve oxidation of organometallics by surface hydroxyl groups, affording coordination

sites in non-zero oxidation states. Much of this chemistry has not yet been reproduced on molecular analogues since the chemistry of potential model ligands has not been developed. Nevertheless, the chemistry of these new sites is of intrinsic interest and their novel reactivity and catalytic behavior (e.g., alkene metathesis with catalysts derived from $[Re(OH)(CO)_3]_4$ on silica) may be of utility and also provide an impetus to programs aimed at devising replicatory models.

Immobilization of ions on supports may be an elegant way to stabilize unusual oxidation states and/or coordination numbers. A particular system to mention here is the preparation of a well-defined Ni(I) complex coordinated to two surface oxygen atoms on silica, for the selective dimerization of ethylene to 1-butene. In this system it is possible to control the selectivity to 1-butene by coordination of two alkylphosphine ligands at a Ni(I) center which has been smoothly reduced from a Ni(II) precursor complex.

Further studies in this area of unusual oxidation state seem to be promising.

1.1.8. Characterization techniques. Identification of surface organometallic species is a demanding procedure which is successful only when a combination of techniques is employed (Table 1-I). In recent years, high-resolution solid-state NMR, SIMS, FAMS-MS, diffuse reflectance FTIR, EXAFS, and wide-angle X-ray scattering have greatly increased the detail and reliability of structural assignments. The synchrotron-based techniques of X-ray diffraction of microscopic single crystals and anomalous X-ray scattering provide further opportunities for structural characterization.

An alternate approach to characterize grafted surface species has been the chemical cleavage of the bond of the species to the support and characterization of the species released into solution.

Some problems, such as the determination of the support sites adopted by organometallics, may be tackled definitively only by recourse to single crystal surface science techniques. Many electron spectroscopies are inappropriate to the study of metal species on insulating or semiconductor supports. Recent results using specular reflectance FTIR and SEXAFS techniques, however, are encouraging and may be applied to oxide surfaces. These experiments also give data which can be directly compared with results obtained on high-surface-area supports and therefore provide a fruitful interrelationship.

1.1.9. Tailor-made catalysts. The goal of the synthesis of tailor-made catalysts is to achieve the stabilization of the active site by control of (i) the nature and number of the metal ions, (ii) the oxidation state, (iii) the appropriate coordination number, and (iv) the nature of the ligands for a given catalytic reaction. A favorable case is one for which the reaction mechanism is understood in molecular chemistry. In the other cases it will be necessary to model the proposed intermediates in order to determine the factors which influence the elementary steps. For supported tailor-made catalysts the choice of a support is

made according to the role it has to play in the stabilization of the active site:

- to generate the active site through a redox process;
- to act as ligand in the coordination sphere (L and/or X types);
- to stabilize unusual oxidation states;
- to stabilize unusual coordination geometries; and/or
- to avoid the formation of inactive compounds, e.g., coupling of mononuclear entities.

Such catalysts have various purposes:

- to carry out surface reactions which are already known in homogeneous catalysis: olefin dimerization and metathesis, hydroformylation, methanol carbonylation, ethylene oxidation, etc.; and
- to carry out sequential reaction steps on a surface which may be incompatible in solution, such as bifunctional catalysis.

1.2. Recommendations

Surface organometallic chemistry provides a major opportunity for unifying the hitherto disparate fields of organometallic chemistry and heterogeneous catalysis. In particular, the appreciation of reactivity and fluxionality on a molecular level of the former field may be blended with the ensemble aspects of the latter.

1) The development of surface organometallic chemistry requires expertise in the experimental techniques and concepts of both surface and organometallic chemistry. For future success in this field, interdisciplinary collaborations should be encouraged.

2) Methods should be developed for preparation of well-defined surface species by deposition of organometallic complexes.

3) Stoichiometry of surface reactions between organometallic complexes and surfaces should be determined, *inter alia*, by quantitative analysis of gaseous products, surface metal concentration, and quantitative extraction of surface complexes.

4) Research with well-defined supported species should be carried out to establish elementary reaction steps.

5) Surface functionalities should be probed with suitable mono- or polyfunctional organometallic complexes, opening the possibility of using spectroscopic tools otherwise not applicable to the inorganic support.

6) Techniques should be developed for the use of organometallic precursors to produce supported metal particles smaller than 10 Å in diameter and having narrow particle size distributions in systems for which these have been previously unobtainable.

7) Procedures should be refined for formation of mixed metal particles by controlled decomposition of deposited heterometallic clusters.

8) Reactions of organometallic complexes with supported metal particles should be used to extend the range of preparation of mixed metal particles.

9) Only a restricted range of metal oxides has thus far been investigated fully as supports. The range of supports should be

extended to include, for example, basic oxides, metal sulfides and carbides, and carbons.

10) Porous crystalline materials should be investigated as supports because they offer special advantages through their well-defined geometrical sites for the attachment of metal complexes.

11) Molecular analogues of proposed catalytically active sites should be prepared and characterized.

12) Molecular complexes of different catalytic functions should be placed on supports to provide sequential reactivity when the functions would be incompatible in solution.

13) Tailor-made surface catalysts are required to improve the technical performance of known homogeneous processes as in alkene dimerization, alcohol homologation, and methanol carbonylation.

14) Molecular complexes of biomimetic character should be investigated, with the goal of bringing entirely new stereo- and regio-selective capabilities to supported catalysts.

2. MOLECULAR MODELS OF OXIDES, METALS, AND SURFACE COMPLEXES

A wide variety of extremely useful physical and chemical techniques are available today for surface characterization of catalysts at the atomic or molecular level. However, since in many cases the reactions occur on a limited fraction of the surface, other approaches are helpful in clarifying the nature of the active site, including modelling the active site. Modelling has proved to be extremely useful for understanding the surface structure of metal particles or metal oxides at a molecular level. Besides providing structural information, molecular models can also mimic elementary steps of surface reactions. Modelling of the active site could also eventually help in the design of catalysts when well-defined structures and coordination spheres are required.

2.1. State of the art

2.1.1. Metal surfaces and metal particles

2.1.1.1. Local structure of adsorbate species. The structures of adsorbates chemisorbed on metals are traditionally assigned by analogy to structurally well-characterized low-valent metal complexes. The description of CO adsorption sites based on the available metal carbonyl structures is the most obvious example. Molecular clusters which can accommodate monodentate ligands as well as multiply bonded species play an important role here. Almost all conceivable forms of bonding modes have been exemplified by molecular clusters. Recent examples included μ - η^2 -coordination modes of CO, which were suggested as models for the chemisorption on sites of threefold symmetry or on step sites of metal surfaces. Hydrocarbon fragments on small metal ensembles also have their analogues in cluster structures. C₁ fragments, terminal and μ_2 -bridged alkyl and carbene groups, terminal, μ_2 - and μ_3 -bridged carbynes, exposed and non-exposed carbides (μ_4 , μ_5 , μ_6), vinyl and vinylidene or alkyne cluster derivatives are all known. Examples of clusters containing single heteroatoms (N, O, S, P) or diatomic ligands (S₂, μ_3 -SO, μ_6 -C₂) exist. Hydride ligands are also found in a series of characteristic environments, e.g., in terminal, μ_2 - or μ_3 -bridged, and in interstitial positions. Transformations of these species coordinated to cluster frameworks have been studied, e.g., the coupling of unsaturated hydrocarbons and C-H, C-C, and in some cases C-O bond cleavage.

2.1.1.2. Models of small particles. Structural information characterizing metal particles is lacking; the particles are often considered as small, rigid pieces of bulk metal. Large molecular carbonyl clusters are electronically saturated by ligands, but information regarding

their structural and physical behavior appears to be relevant for a better understanding of highly dispersed metals.

a) Structural information. Metal carbonyl clusters have provided molecular models for metal particles with fivefold symmetry. They can also serve as models for metal particles which are spread over supports forming rafts (e.g., $Og_6(CO)_{21-x}L_x$, which form a plane triangular array of metal atoms). Rearrangement of atoms in the metal skeleton brought about by ligand substitution may be related to the phenomenon of surface reconstruction. Large molecular clusters are good models of very small particles containing less than 100 atoms. Most atoms are then at the surface and can coordinate surface ligands. The atomic packing and bond lengths should therefore depend upon the nature of surface ligands, as in molecular clusters.

b) Magnetic behavior. Physicists predict peculiar behavior of small particles as a result of the shift from continuum to discrete energy levels (e.g., a shift from Pauli to Curie type behavior). Interestingly, a change from temperature-independent to temperature-dependent magnetic susceptibility has been observed in osmium carbonyl clusters on increasing the nuclearity.

c) Surface vs. bulk composition in bimetallic particles. The surface composition of bimetallic particles, which affects the chemisorption and catalytic properties, may differ from bulk composition. The surface and bulk compositions are determined both by the nature of the atoms and by the presence of adsorbates preferentially bonded to one of the components. Heteronuclear clusters have provided models for the cherry-like structures of small particles or solid solutions.

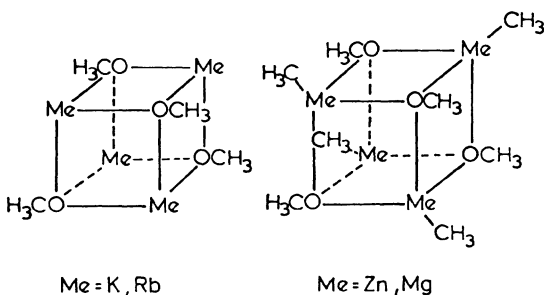
2.1.1.3. Ligand and metal dynamics. After reactant adsorption, the next step of a catalytic reaction on a surface is the migration of adsorbed species. There are very few data characterizing this important step which allows chemisorbed species to be close enough to react. Molecular clusters may provide good models, since the mobility of ligands is well documented, especially by NMR experiments. The packing of atoms itself is also dynamic, and there are some examples of metal atom frameworks in clusters themselves being non-rigid. These concepts could probably be extended to small particles. As a result of this dynamic behavior of both ligands and metal atoms, the number and type of adsorption sites on metal particles are expected to change according to the conditions.

2.1.2. Oxide surfaces and surfaces complexes

2.1.2.1. Structure and spectroscopy. The structure of a high-surface area oxide is traditionally described on the basis of spectroscopic information and by the application of models derived from structures of perfect or defective crystallographic planes. Vibrational and optical spectroscopies are employed to detect hydroxyl groups and low coordination oxide ions, respectively, on pure oxide surfaces. When

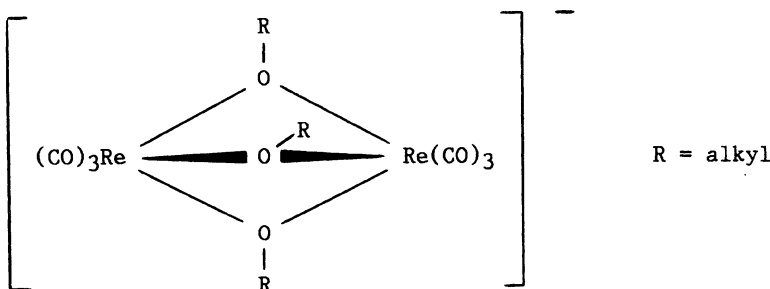
oxo compounds are supported on oxide surfaces, again vibrational (Raman in particular) and optical spectroscopies provided significant information for structural assignments. OH groups, oxide ions and oxo-species may thus be considered as intrinsic probes. The characterization of anion vacancies (Lewis acid sites) can be performed using probe molecules (CO, NH₃, pyridine, etc.). The use of model molecular compounds has almost completely been confined to their application as reference compounds (alcohols, carbonates, bicarbonates, carbonyls, carboxylates, Lewis acid-base adducts, oxo-compounds, etc.) for the interpretation of spectroscopic data.

Molecular models of oxide surfaces or low coordination sites on oxide surface are scarce. Compounds such as



have been suggested to mimic low coordination sites at corners or edges of cubic oxide structures (alkaline earth oxides) with suitable ligands attached to them.

Model molecular compounds have been synthesized as analogues of polynuclear transition metal carbonyl clusters grafted onto oxide surfaces. An example is Ph₃Si(u₂-O)Os₃(CO)₁₀. The dichloro-dirhodium complex Rh₂(CO)₄Cl₂ has been considered to serve as a molecular model for the assignment of vibrational spectra of RhI(CO)₂ surface complexes. The anions



or $[(\text{CO})_3\text{Re}(\text{cis-Nb}_2\text{W}_4\text{O}_{19})]^{3-}$ may even better mimic the coordination of such carbonyl complexes onto oxide surfaces. Also, transition metal-Lewis acid adducts find surface analogues which might be considered to

be important intermediates in higher alcohol synthesis from CO + H₂. Surface analogues of Lewis-acid-bound acyl complexes have also been encountered.

Besides these direct applications of model compounds for the identification of surface sites, surface groups, or surface complexes, there are a variety of compounds available today which provide potential to mimic certain aspects of oxide surfaces at a molecular level. These include extended oxide structures (models of oxide layers or silicate cages), (CpM)_nO_m (models of M-O arrangements on oxide surfaces, defect sites), and complexes with bulky alkoxide ligands (steric hindrance at surfaces). The usefulness of these materials as model compounds has not been fully exploited.

2.1.2.2. Reactivity. While it is perhaps true that the main role of molecular models of oxides and surface complexes is to provide an aid for characterization in terms of oxide structure and the nature of surface species, it is also important to investigate the reactivity of the molecular models for comparison purposes and to provide guidelines for mechanistic studies. A few examples are given below.

There have been several studies of the reactivity of complexes (for example, the many molybdenum-oxo complexes) in relation to oxidation reactions and of metal-imine complexes in relation to ammonoxidation reactions. For the latter case, the reactivity of $M(=NR)_2(OR')_2$ ($M = Cr, Mo$; $R' = SiMe_3$) and $W(=NR)_2(NH_2R)(OCX_2CX_2O)$ ($X = Me, Ph, CF_3$) has been studied to provide support for the proposed reaction mechanism.

With respect to the alkene metathesis reaction, complexes of the type $[W(CHR)(OR)_2X_2AlX_3]$, which are excellent homogeneous catalysts in their own right, could be regarded as molecular models of the heterogeneous catalytic system.

With oxide-supported cluster complexes, models have been made to mimic the cluster-support interaction, but their reactivity has not been studied. For example, the silica-supported cluster $\geq SiCH_2CH_2PPh_2Os_3H_2(CO)_{10}$ undergoes a decarbonylation reaction, not to give the $Os_3H_2(CO)_9(L)$ species, as occurs in solution, but to give an uncharacterized species which may be of the type $Os_3(\mu_2-O)_3(CO)_x$ (where μ_2-O represents a surface oxygen atom). It should be possible to model the reactivity of such supported complexes.

The enhancement of methyl migration to form a surface acyl complex upon reaction of, for example, $Mn(CO)_5(CH_3)$ or $Fe(Cp)(CO)_2(CH_3)$ with γ -alumina has been explained by the known reactivity of these same molecular metal-alkyl complexes in the presence of soluble Lewis acids.

A large family of polymolybdate and polytungstate structures exists, and the reactivity of some of these compounds has been studied in terms of modelling surface reactions, particularly oxidation reactions. Theoretical approaches have also been applied in this area.

2.2. Opportunities and research goals

2.2.1. Metal particles. In the field of cluster complexes, one of the general goals is the synthesis of high-nuclearity clusters for the

purpose of making a comparison with metal particles. Increasing the nuclearity of clusters in order to decrease the relative stabilizing influence of ligands is of fundamental importance.

More elaborate models to mimic different kinds of supports considered as ligands are obviously needed. Both the geometric and electronic structures of oxide-supported species could be modelled using appropriate ligands containing Si—O—Si and Al—O—Al groups. In this context, the synthesis of molecular macrocage compounds warrants special consideration. Although very large oxide cages of the type found in zeolites are in principle stable as molecular species, none has been synthesized to date.

Clusters involving several hydrocarbon fragments located at contiguous metal atoms are of interest to provide models for surface adsorption sites known as ensembles or multiplets. In addition, their dynamic properties and intramolecular transformations could provide valuable information concerning the numerous steps of the catalytic conversion or synthesis of hydrocarbons. Finally, improved model compounds for the dissociative chemisorption of CO and possibly N₂ are required.

Effects of promoters on adsorption and catalysis should be modelled by bimetallic clusters which contain more easily oxidizable non-noble metal elements. Also, the structural arrangements of metal within the framework of bimetallic carbonyl clusters might be useful models for the segregation phenomena occurring in small metal particles in the presence of adsorbed CO.

In order to allow the molecular species to be fully used as models of metal particles, spectroscopic data using techniques available for surface characterization should be reported, in addition to complete crystallographic data.

2.2.2. Oxide surfaces and surface complexes. For oxide surfaces to be terminated by faces of stoichiometric composition, coordinative unsaturation is a necessary consequence. Oxide surfaces derived from layer structures (MoO₃) can expose stoichiometric and coordinatively saturated faces, but even there coordinative unsaturation must occur at edge areas. Oxide surfaces are terminated by hydroxyl groups, oxygen atoms and metal atoms in many possible coordination and bonding situations. The possibilities for changes of coordination numbers of metal atoms at surfaces are not well established at present. As these constitute the sites which are involved in surface chemistry and catalysis, in-depth information regarding their structural and electronic properties and their reactivities is required. Characterization beyond the existing spectroscopic information is inevitably needed, whereby all available methods should be applied with both the surfaces and molecular analogues.

Opportunities for research include both the development of entirely new types of models that mimic features of oxide surfaces that have not yet been addressed, and the refinement of existing types of models in order to more closely mimic solid surface behavior. In the former area, a high priority should be placed on developing molecular models of lanthanum, zinc, magnesium, aluminum, and silicon oxides.

Features of particular interest include low-coordinate surface oxygen and metal sites, and hydroxyl groups in different coordinations.

Concerning the further development of existing types of model systems, several areas should be mentioned. First, models for selective hydrocarbon oxidation reactions, although they have served well as structural models and substrate bonding models, have been relatively ineffective as models for the actual oxidation event itself. Specific oxidations lacking good model systems include, for example, the molybdate-catalyzed oxidations of hydrocarbons to alcohols, of alcohols to aldehydes, and of aldehydes to carboxylates. Second, sophisticated polydentate oxide ligands having good thermal stability are needed to model the metal and metal cluster binding sites in solid-oxide-supported organometallic complexes such as metal carbonyl units. Third, hybrid metal-cluster oxide-cluster species containing metal-metal plus metal-oxygen bonds, species such as $\text{Os}_6(\text{CO})_{16}(\mu_3\text{-O})$, should be further investigated, since these may be good models for reduction catalysis on oxide surfaces, oxidation catalysis on metal surfaces, and C-O cleavage reactions on both metal and metal-oxide surfaces. Finally, emphasis should be placed on molecular modelling of the reactivity of traditional, extremely reactive solid-oxide-supported olefin polymerization catalysts. This may involve combining several of the efforts outlined above, such as incorporating oxide subunits and preparing new polydentate oxide ligand systems.

Besides attempting to prepare specific models for specific chemistry occurring on oxide surfaces, there is a great need for molecular systems designed to model more fundamental aspects of surface chemistry. First, further structural studies of polynuclear oxides and alkoxides must be carried out in order to better establish structural principles governing surface reconstruction. Second, proton and cation binding studies must be performed in order to delineate the factors controlling the relative basicities of different types of surface oxygens. Similarly, the factors influencing the acidity and redox abilities of metal centers in oxide environments should be clarified through systematic investigations. Finally, oxide mobility in solid oxides could be modelled through solution NMR studies of oxide mobility in species such as polymolybdates.

2.3. Recommendations

- 1) Improve structural and electronic characterization of surface groups by spectroscopic and chemical approaches.
- 2) Provide well-designed molecular analogues for interpretation of spectra.
- 3) Provide spectroscopic data for molecular analogues using techniques applicable to surfaces (e.g., EXAFS, IR, etc.).
- 4) Study chemical reactivity of surface groups (coordination sites).
- 5) Rationalize the chemistry of high-nucularity clusters.
- 6) Develop chemistry of hydrocarbon interactions with high-nucularity clusters.

- 7) Model promoter effects by using non-noble metals in cluster frameworks.
- 8) Improve the knowledge of intramolecular reactivity and ligand and metal dynamics in high-nuclearity clusters.
- 9) Use homo- and heterometallic clusters to model restructuring and segregation phenomena.
- 10) Model metal-support interactions by using reactions of high-nuclearity clusters with specific ligands.
- 11) Synthesize models for very basic oxides such as magnesium, lanthanum, and zinc oxides.
- 12) Design and synthesize molecular oxide models of surface defects and low coordination sites.
- 13) Develop synthetic strategies for polydentate oxide ligands with high thermal stability.
- 14) Synthesize molecular oxide macrocage ligands to model entrapment and anchoring of metal complexes therein.
- 15) Study hybrid metal cluster/molecular oxide systems.
- 16) Synthesize and extend the study of reactivity of complexes containing M-C and M-O bonds.
- 17) Investigate large molecular oxides to establish structural principles governing surface reconstruction.
- 18) Study dynamics of molecular oxides in solution to model oxide and cation mobility in solids.
- 19) Investigate binding of Lewis acids and bases to molecular oxide surfaces to delineate factors controlling surface basicity.
- 20) Perform analogous characterization and modelling studies for important catalytic and support materials other than oxides, e.g., sulfides, carbides, carbon, etc.

3. SYNTHESIS OF NEW POROUS SUPPORTS

Microporous materials possess pore structures in which the major fraction of the total void volume is contained in the pore size region below 20 Å. The structures of microporous materials can span the entire range from X-ray amorphous compounds (e.g., small pore oxides, xerogels) and highly disordered materials (e.g., carbon molecular sieves) to quasi-crystalline compounds (e.g., pillared clays) and regular, 3-dimensional crystalline structures (e.g., zeolites).

These materials have pore sizes comparable to molecular dimensions and allow an approach at the molecular level for understanding of active site action. The electric field strengths and symmetries associated with such structures can induce chemical reactivity in adsorbed species and influence the behavior of surface functional groups (e.g., the acidity of surface silanol groups).

The great influence of microporous materials, particularly of zeolites, on the molecular pathways of catalytic reactions is well-explored and broadly utilized in practical applications. However, the molecular approach to the synthesis of 3-dimensional microporous crystals is still in an embryonic state because of the great complexity of the reaction systems and the dominance of kinetic control in structure formation.

3.1. State of the art

3.1.1. Synthesis and structure of 3-dimensional porous materials. In the zeolite family, nearly 50 different zeolites framework topologies are known, together with variants of a number of these topologies brought about by isomorphous substitution in their frameworks (e.g., changing Si/Al ratios), by substituting elements other than Si or Al in the framework, or by exchange of interstitial cations. Ways have also been found for producing variants after the synthesis of the zeolite, again by changing Si/Al ratios. Methods have been proposed to promote the thermal and hydrothermal stability of zeolite-based catalysts.

The range of structures and compositions has recently been greatly expanded into a new generation of microporous crystals. These materials, representing about 200 new species, may consist only of Al, P, and O atoms. However, their compositions may include additional atoms comprising more than a dozen elements, forming compositions consisting of up to six different framework cations. These crystals show numerous new structures and have pore dimensions covering the whole range known for zeolites. The aluminophosphates themselves are stoichiometric, with one Al for each P atom, and thus they have no net electrical framework charge, nor extra-framework cations. In contrast, the crystals containing additional elements such as Si, Co, Mg, Ti, etc., usually develop a net electrical framework charge, balanced by extra cations such as H⁺; these display weak to strong acidity as catalysts.

3.1.2. Synthesis and structures of intercalated porous compounds. The two most widely investigated classes of pillared layer compounds are derivatives of the smectite clays and the group IV metal phosphates. The smectite clays have 2:1 layer structures in which the silicate layers are separated by sheets of hydrated cations. The cations in the parent structures (Na^+ , Ca^{++}) are easily replaced by complex cations of molecular size, through intercalative ion-exchange reactions. The early work made use of tetraalkylammonium ions as pillaring reagents. More recent work has utilized bicyclic amine cations, tris-metal chelates, and metal cluster cations as pillaring agents. Clays interlayered with polyoxocations are especially attractive. At elevated temperatures, these derivatives are transformed into structures in which molecular-sized oxide aggregates are formed in the interlamellar spaces. In addition, Brønsted acidity is introduced in the thermolysis process, and this property leads to acid catalytic properties.

The group IV metal phosphates have layered structures in which an octahedrally coordinated metal sheet is sandwiched between phosphate tetrahedra. In these structures the PO_4 tetrahedra are inverted relative to the position of the SiO_4 units in smectite clays. The pillared derivatives are formed by replacing phosphate groups with organic phosphates or phosphonates. In order to create porosity, a spacer compound such as H_3PO_4 or H_3PO_3 is added to the organic phosphonate. Disphosphonic acids are used to bridge across layers so that they are held rigidly in place. The porosity is then created by the inorganic groups which space the bridges of pillars. A whole series of microporous derivatives has been produced in this way. Incorporating molecular-sized cations in place of interlamellar protons offers another route to pillared phosphates.

3.2. Opportunities and goals

3.2.1. 3-dimensional porous materials.

1) The number of zeolites so far synthesized, although large, is only a fraction of the hundreds of frameworks which have been built as models. There is a clear interest in seeking ways to synthesize more of these hypothetical structures. This interest is of both fundamental and industrial significance. Some of the hypothetical structures have pore openings governed by rings larger in diameter than the 12-ring, e.g., 18-membered rings of ~ 15 Å free diameter. If such zeolites could be made, they would be available as matrices for carrying enzyme catalysts and metal clusters, or as catalysts in their own right. It is noted that larger rings exist in nature.

2) The host lattice-guest molecule relationship, which is so important both in clathration and zeolite formation, has already been further extended to the preparation of porous crystalline silicas. This area is capable of further development, and the number of such phases could be comparable to the number of zeolites. The framework topologies of these "porosils" are sometimes different from those of zeolites.

3) Synthesis of zeolites and porosils in non-aqueous media seems possible, an example being the preparation of silica-sodalite in a

glycol medium. For this purpose, means should be sought of enhancing the solubility of the sources of Si and Al in non-aqueous media. For example, it might be possible to do this by the use of crown ethers, which serve to dissolve inorganic salts in organic liquids. They might do this also for aluminates and silicates that are soluble in water but not in the organic liquid.

Synthesis media in which two immiscible liquid phases co-exist are of interest. One of the liquids gives a controlled release of one or more reactants to the second, within which the synthesis takes place.

Another area in which further exploration is of interest involves the use of non-volatile substances such as salts for space fillers and stabilizers of porous tectosilicates. Synthesis by cooling of anhydrous melts could also be relevant.

4) In the area of isomorphous replacement, there is need to measure quantitatively the extent to which such elements as B, Fe, Cr, Be, and the like can replace Al, P, and Si in 3-dimensional frameworks and the extent to which they are present merely as detrital material. It should also be established how such framework substitutions vary with temperature, according to the physicochemical background theory, and whether pH and other factors can also influence the extent of genuine framework substitution.

In order to try to obtain information at the molecular level characterizing how zeolites nucleate and grow, more study of the chemistry of solutions containing dissolved silicate, aluminate, and aluminosilicate species is essential. It is important to know what anionic species are present as a function of temperature, pH, and concentrations of dissolved Si, Al, or other elements. Such work, carried out with the best available physical methods, is already in progress.

5) For porosils and high-silica zeolites, the possibility of growing very large crystals in systems embodying a temperature gradient should be explored. Massive optical-quality quartz has been grown by this method. Such porosil and zeolite crystals can then be sectioned to provide true molecule-sieving membranes for separation and catalytic processes.

6) In the synthesis of non-zeolitic 3-dimensional microporous materials, the investigation of the structure-directing role of the templating agent and the effect of aqueous versus non-aqueous synthesis media offer opportunities for the discovery of new microporous crystals, particularly with the added goal of the formation of larger pores.

7) For aluminophosphate-type materials, their demonstrated ability to contain several substituted framework cations chosen from a dozen elements opens opportunities to introduce transition metals in tetrahedral environments accessible to reactant molecules. Thus these materials may contribute to catalysis by direct interaction with reactant molecules, providing catalytic paths in chemical reactions similar to those in homogeneous catalysis. The prevailing steric restrictions may help to carry out new and even novel reaction steps such as the formation of optically active molecules.

3.2.2. Intercalated porous compounds.

1) A major goal is the production of pillared compounds with uniform pore sizes in the range 5-20 Å. Additional synthesis methods for pillarizing have to be developed.

2) The mechanism of pillarizing of smectite clays is beginning to be elucidated. Such understanding could lead to the synthesis of derivatives with improved thermal stability.

3) Mainly acid-catalyzed reactions have been studied in pillared clays. There is a need to investigate metal-catalyzed reactions which might be structure-sensitive or shape-selective. Synthetic methods are needed to design molecular and molecular ion pillarizing agents containing catalytically active metals. In particular, metal complexes and organometallic complexes should be investigated as pillarizing agents. The range of potential products for catalytic purposes can be enlarged by functionalizing pillars.

4) The concepts developed through the pillarizing of layered silicate clays and group-IV metal phosphates should be extended to other classes of layered host structures. Some work has been initiated in the area of related layered phosphates (e.g., vanadyl and uranyl phosphates), and this approach should be extended. Layered compounds with well-defined structures should receive first priority because they present the best possibilities for a molecular design approach.

3.2.3. Other porous crystalline materials. Crystals other than those already mentioned have permanent microporosity. These include some cyanometallates in which the porous framework is based upon linked octahedral rather than tetrahedral units, and also certain Werner-type compounds. Such materials merit further study.

3.3. Recommendations

1) The size and shape of the intracrystalline pore/cavity system are critical for the utility of microporous crystals. Thus, the ability to direct the synthesis towards crystals of desirable pore structure, particularly of large-pore 3-dimensional networks, is of great importance. Therefore, new studies should be directed to the characterization of structural precursors at the molecular level. In particular, emphasis should be placed on synthesis media incorporating cations, molecular species, and/or templates that are structure-directing. These factors may ultimately determine the nature of the pores as well as the crystal lattice. Chemical studies coupled with NMR and other in-situ methods of characterization may provide information leading to predictable structure-directing synthesis methods.

2) In order to provide a foundation for the structural precursor studies, the solution chemistry should be investigated, including that of relevant organometallic compounds of framework elements occurring in microporous materials.

3) New routes to the development of stable, pillared layer structures should be looked for, including molecular design of func-

tionalized bridges and methods to achieve controlled pillar distributions.

4) The presence of structural Al in porous aluminosilicates determines their polarization and their acidity, which control the molecular pathways in practical catalysis. The structural and theoretical origins of strong acidity in zeolites need further exploration.

5) Studies should be directed at investigating those molecular interactions between reactants and crystalline materials which influence pore size and accessibility.

6) Microporous crystals containing framework transition metal ions should be studied both in the as-synthesized state and in modified states to try to affect catalytic behavior, as in homogeneous catalysis.

7) Guidelines and methods (experimental and theoretical) should be developed to quantify the relative and absolute chemical and structural stabilities of microporous materials. Such studies should focus on both chemical (localized) and structural (longer range) factors.

4. THE MOLECULAR APPROACH TO MECHANISMS OF SURFACE REACTIONS

4.1. State of the art

The knowledge of the mechanism of action of most heterogeneous catalysts remains extremely limited. At the most primitive level, often only the overall product distribution is known, the nature of the catalyst-reactant(s) interactions remaining mysterious. In a few cases a more detailed proposition of mechanism can be advanced, but these propositions remain modest and ineffective in comparison with mechanistic details that have been developed in molecular organic chemistry, and more recently, in organometallic chemistry. Indeed, even the apparently well-established catalytic mechanisms (e.g., hydrogenation of olefins) are sometimes contested, an indication of the fragility of evidence on which these mechanistic proposals are based. It must be recognized, however, that by comparison with strictly molecular systems, heterogeneous catalysts are intrinsically much more complicated. In addition, their study by physical methods is difficult and interpretations nearly always ambiguous. The status of the art can best be illustrated by the following examples.

4.1.1. Acid catalysis in hydrocarbon conversion. In terms of the transformation of substrates, our mechanistic understanding has reached a high level, mainly because the systems can be largely (but not totally) explained in terms of classical organic chemistry. Many mechanistic details remain to be elucidated, however, such as how the first C-C bond is formed in the methanol-to-hydrocarbon conversion on zeolites and other solid acids. The steric and topologic constraints that are specific to zeolites have been identified and used to predict catalytic properties. Much more needs to be understood about how structure and composition at the surface sites control the chemistry.

4.1.2. Metal catalysis. The making and breaking of C-H and C-C bonds by metal catalysts is a domain where our knowledge appears to be rather good (e.g., hydrogenation of olefins, skeletal rearrangements of hydrocarbons). Here confidence in such mechanisms has been reinforced by the existence not only of equivalent mechanistic proposals (analogous elementary steps) in homogeneous systems (e.g., hydrogenation), but also by established structural and reactivity models (metallocarbenes, metallacycles) in organometallic chemistry. This concentration of forces allows a unifying picture of catalytic action and permits us to question mechanistic proposals which do not have a firm basis in molecular chemistry.

4.1.3. Selective oxidation catalysts. This area presents a situation where an exemplary concertation of forces is under development. The identification of the probable active site in MoO_3 , coupled with

efforts to model the structure and reactivity of such a site, along with theoretical calculations, presents us with an increasingly intimate picture of the catalytic events.

4.1.4. Hydrodesulfurization and hydrodenitrogenation catalysis. The supported metal sulfides used as catalysts for hydroprocessing reactions have been characterized by many techniques, but the nature of the catalytically active sites is still a matter of controversy which makes it difficult to understand the mechanisms, and relevant organometallic models need to be developed.

4.2. Opportunities and research goals

1) For both homogeneous and heterogeneous catalysis it is essential to extract an atomic level understanding of the catalytic processes. That is, we want to follow the atoms of catalyst and substrate from reactants to products. As this atomic level of understanding evolves, we will come to view the surface of the heterogeneous catalyst along with the substrate as a supermolecule.

There is in fact a hierarchy of levels of understanding. Initially we obtain a relatively coarse view involving reactants and products but little about intermediates or elementary steps. As experiment and theory progress we obtain successively more refined views involving more precise information characterizing the critical compounds and critical steps.

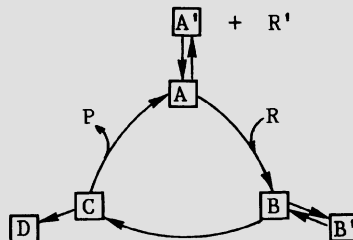
2) To obtain this atomic-level understanding we must identify and characterize various intermediates formed in converting from reactants to products. In doing this we develop models embodying both structural and electronic characteristics.

3) Given these structures, we must determine the rates of transformations between various intermediates; in doing this we endeavor to break complicated transformations into the fundamental or elementary steps that can be used in constructing reactivity models.

It is important to emphasize that elementary steps established for one reaction will form useful concepts for analyzing many other reactions.

4) The goal in these studies is to construct a mechanism, i.e., a set of hypotheses to explain the observations and to suggest predictions of how to modify the rates and products and design new catalysts and new processes.

5) Consider the generalized mechanism:



The sequence of steps $A + R \rightarrow B \rightarrow C \rightarrow A + P$, including the detailed structures (geometric and electronic) of intermediates A, B, and C plus the rates of transformation between them constitute the mechanism. The starting point may be A' , which must be transformed into the active catalyst A.

Prominent species in a reacting system may include B' and D, which are not involved in the direct catalytic process. Even so B' and D may be the dominant species observed in spectroscopic and structural experiments. The various species A' , A, B, B' , C, and D may affect the rates and structures of each other so that this concept of the reaction in terms of independent species and transformations is an idealization. Even so, such idealizations are crucial to extracting concepts used in designing experiments and new catalysts.

6) The hypotheses concerning mechanism are often based on molecular or theoretical models and often arise from imaginative interpolation. They are used to define the catalyst and to design the structural and kinetics tests of mechanisms based on expected intermediates and kinetics.

7) Detailed mechanistic understanding often occurs more quickly from homogeneous studies because (i) the systems are intrinsically simpler, (ii) such techniques as NMR and X-ray crystallography lead to more precise detail about molecular structures, (iii) the kinetics schemes are simpler and NMR can provide detailed reactivity models with information about the sequence of intermediates and rates connecting them, and (iv) synthetic techniques can be more precisely directed.

8) Surface spectroscopies generally lead to fingerprints for adsorbed species which rely on well-established molecular models for their interpretation.

9) Problems in surface catalysis such as the function of alloy catalysts, modifiers, promoters, and poisons may be understood by a molecular approach, and such terms as substituent, ligand, steric, and electronic may find their equivalence in heterogeneous systems.

10) Theory plays three important roles in elucidating the atomic-level mechanisms: one role is establishing the general qualitative concepts concerning various elementary steps. This conceptual understanding which is used to design or predict new catalysts is ultimately the most important role of theory. The second role is establishing quantitative data characterizing structures and barriers for intermediates too ephemeral for detailed experimental study. Because of the complexities with surface processes and the limitations of experimental techniques, such quantitative theory will remain essential. The third role is to extract force fields from detailed molecular cluster calculations which are used in molecular dynamics and statistical simulations of complex models including all known intermediates and mechanistic steps. Such simulations involving the dynamics of thousands of atoms will provide a strenuous test for the completeness of our molecular understanding of heterogeneous processes.

It is important to emphasize that the ultimate test for the usefulness and correctness of this theoretical understanding is whether the theory suggests new approaches to improving a particular catalyst, or better, entirely new strategies to developing catalysts.

11) Some barriers in communication between molecular and heterogeneous catalysis chemists involve language (oxidative addition vs. dissociative chemisorption, reductive elimination vs. associative desorption, ligand effects vs. promoters and poisons). A new language will probably arise as these groups come together.

12) Ultimately a sufficiently clear understanding of mechanism will allow the design of better catalysts (more selective, faster, less sensitive to poisons), much as a full understanding of mechanism led synthetic organic chemists to design strategies for synthesizing very complicated molecules (e.g., vitamin B₁₂).

13) In order to illustrate how concepts shared between molecular and homogeneous chemists help enrich both fields, we consider the evolution of the role that CH₂ plays in both homogeneous and surface reactions. In Fischer-Tropsch catalysis, the original mechanism, proposed in about 1926, involved surface CH₂ complexes. This mechanism fell out of favor and was replaced by other, more complicated mechanisms involving formyl complexes and hydroxy-carbene. Subsequent studies of soluble models and more precise surface studies did not support these new proposals. However, during this period, synthetic organometallic chemistry and studies of soluble catalysts resulted in the discovery that CH₂ complexes are much more stable and prevalent than originally thought. Indeed, intermediates involving bonds of CH₂ to transition metals were isolated, and the role of such species in metathesis was established. This led Pettit, a developer of molecular models, to carry out the experiments with solid catalysts that established CH₂ complexes as the accepted intermediates in Fischer-Tropsch catalysis. The CH₂ fragment now appears to be a key intermediate in a variety of other reactions of hydrocarbons on surfaces.

Using labelling, substituent effects, synthesis of well-defined catalysts, and isolation and characterization of proposed intermediates, the mechanism for olefin metathesis in soluble systems has been firmly established to involve carbene complexes. Corresponding labeling studies suggest that the solid catalysts act by a similar mechanism. The definition of the role of carbene in these reactions has led to the development of effective new catalysts for the metathesis of functionalized olefins and the design of controlled ring-opening polymerization catalysts.

4.3. Recommendations

1) Encourage workers in the organometallic community to direct greater creative energies toward developing new models relevant to the elementary steps in heterogeneous catalysis.

2) Encourage theorists toward developing methods applicable to extracting qualitative concepts concerning elementary steps of homogeneous and heterogeneous catalytic reactions.

3) Encourage workers in heterogeneous catalysis and surface science to actively explore the applicability of new molecular concepts being developed in the theoretical and organometallic communities and

to utilize the elementary molecular steps in analyzing surface reactions.

4) For designing effective catalysts and effective combinations of multifunctional sites, the following emphasis is particularly recommended:

- define the elementary steps of surface reactions and their dependance upon surface site and surface composition;
- study the energy redistribution associated with adsorption/desorption and reaction processes; and
- examine the mobility of adsorbed molecules and intermediates on solid surfaces.

5) Develop and refine physical characterization methods capable of yielding structural information about surfaces and intermediates. Particularly important are in-situ and non-destructive techniques.

6) Develop chemical characterization methods designed to yield molecular-level information. This involves new substrates capable of distinguishing the chemical character at various sites. Also included is the study of isotopically labeled reactants and molecules that are complex enough to yield information about stereochemical and substituent effects. Transient kinetics methods will be particularly valuable in these investigations.

5. CATALYSIS

5.1. State of the art

Although chemical technology is dominated by surface catalytic processes, the greater depth of understanding of the molecular chemistry of catalysis has had a tremendous impact on the development of homogeneous catalytic processes. The principles of oxidative addition, reductive elimination, migratory insertion, etc. have provided guidelines for the practitioner to design and test new catalysts for such processes. The principles learned from molecular chemistry and homogeneous catalysis can be applied to surfaces and will greatly aid the development of this field.

5.2. Opportunities and research goals

5.2.1. Reactions of interest. Table 5-I is a summary of some opportunities to produce more active, selective, and efficient catalysts by applying principles of molecular catalysis to surfaces. Examples in the table are concerned with (1) homogeneous processes that might more profitably be run using properly designed surface catalysts and (2) new reactions for which neither soluble nor surface catalysts currently exist.

5.2.2. Understanding catalytic cycles. Surface catalysis is a dynamic, molecular phenomenon, and attempts to understand catalytic cycles can benefit greatly from the application of in-situ physical techniques and of chemical reaction probes. Such studies are unlikely to identify an active site (unless it is very inactive!), but they can provide valuable pointers in terms of the immediate catalyst precursors.

5.2.2.1. In-situ physical techniques. In-situ spectroscopic methods (particularly infrared spectroscopy) are now almost routine, but no single analytical technique is sufficient to solve the problem of ambiguity of structure and reactivity; a combination of techniques should be applied. The use of EXAFS has developed rapidly, and a similar advance in solid-state NMR is anticipated. Both are amenable to in-situ studies, in contrast to the majority of surface-science techniques.

5.2.2.2. Use of catalytic probe reactions. Chemical probes of surface structure have been underutilized. The ideal catalytic probe reaction would be gentle (operate at low temperature) and would be sufficiently well understood to provide information characterizing the catalytic site. Reaction probes which have been widely used are olefin hydrogenation, olefin and paraffin isomerization, and paraffin hydroge-

Table 5-I : Examples of potential process applications of molecular catalysis at surface.

CATALYTIC REACTION	CURRENT STATUS	PROBLEM AREAS	MOLECULAR CATALYSIS ON SURFACES
1) PARAFFIN ACTIVATION			
a) Methane to methanol or formaldehyde	no high-yield catalytic reaction		Coordinative unsaturation to allow reaction under mild conditions and give high selectivity
b) Oxidative coupling to ethylene or ethane	no commercial process; low yield, high temperature, low selectivity	Activity and Selectivity	Cooperativity of catalyst components to increase rate and to influence product profile
c) Methane-ethane to high-octane liquids	patented process (cyclar) needs improvement		Vapor phase-remove product as formed
2) DIRECT FUNCTIONALIZATION OF AROMATICS			
a) Acetoxylation for phenol production	low yields and selectivity in liquid phase with O ₂ ; good yields with strong oxidant but uneconomical	Activity and Selectivity	Stabilize Pd(II) hydridic intermediate Promote high oxidation states by strongly oxidizing supports (V ₂ O ₅) to promote selective acetoxylation over coupling
b) Selective hydrogenation to cyclohexene	heterogeneous ruthenium catalysts give fair yields, but improvement needed (> 80%)	Activity and Selectivity	Multimetallic systems on basic supports will benefit from enhanced cooperativity and organization; removal of reactive product will aid selectivity
c) Amination of benzene to aniline	poor rate and yields; poisoning by product	Not catalytic	Multimetallic catalyst having redox function

(continued)

3) OLEFIN REACTIONS

a) Wacker oxidation	efficient industrial homogeneous processes; some becoming obsolete (new CO chemistry)	Catalyst instability	Supported Pd system; redox function required
b) Oxycarbonylation to acrylates and similar materials or oxycarbonylation of amines to isocyanates	good rates and selectivity in lab; recovery not suitable for industrial use	Catalyst	As above Inhibition by water
c) Epoxidation	no efficient catalytic reaction at present	Selectivity	Formation and stabilization of reactive surface oxo

4) ACTIVATION OF CO/H ₂ to organic oxygenates, especially heavy products: glycol, anhydride, heavy alcohol	efficient homogeneous catalytic processes; some practiced	Product and catalyst separation	Supported catalyst provides ease of separation of catalyst from heavy organic products
--	---	---------------------------------	--

5) N ₂ ACTIVATION	commercial reaction	High temperature, adverse equilibrium	More active catalyst for use at lower temperature
------------------------------	---------------------	---------------------------------------	---

nolysis. These probes are widely used to assess site congestion and its effect on the selectivity and activity of metals.

Of these, only olefin hydrogenation and olefin isomerization are sufficiently gentle to probe molecular model catalysts and surface catalysts without modification of their structures. Additional probe reactions should be developed and used. In particular, probe reactions should be developed for and applied to oxidation catalysts. Potential oxidation probe reactions include $H_2 + O_2 \rightarrow H_2O$, CO oxidation, and simple hydrocarbon oxidations.

5.2.2.3. Comparison with model systems. Extrapolation from homogeneous chemistry to surfaces, although risky, provides a basis for molecular-level understanding. For example, crystallographic studies of transition metal clusters containing hydrocarbon ligands have demonstrated the existence of many of the possible C-, H-, and O-containing fragments postulated as catalytic surface intermediates in CO hydrogenation and hydrocarbon conversion. It is important to develop well-defined models of metals, ranging from single atoms, through clusters, to single crystals, to provide the basic concepts upon which the relationships between structure and activity rely. Intermediates in homogeneous catalytic oxidation, including superoxo, peroxy, oxo, and peroxy metallacyclic species, are known and their roles are partially understood. The surface analogues of these species are poorly understood and in need of investigation; model structures incorporating organic reactant ligands such as metal alkoxy, alkylperoxy or dioxo-metallacyclopentanes, and oxometallacyclobutane are also worthy of investigation.

5.2.3. Novel supported metal catalysts. Homogeneous catalysis is molecular catalysis in solution; analogous catalysis is carried out on surfaces with analogues of the molecular species. In general, work on such materials must confront the problems of stability and regenerability. A unique example is the molecular metal complexes of Ti, Zr, and Cr on inorganic supports used commercially as Ziegler polymerization catalysts. These are extremely effective and offer the advantage of not requiring regeneration since the catalyst in the polymer product is retained as a trace impurity.

This section is concerned with the use of molecular species as:

- molecular models of surface catalytic systems and
- precursors of supported catalysts.

The unique problems associated with such approaches are also considered.

5.2.3.1. Supported molecular species. Although there are several examples of intact oxide-supported metal clusters acting as catalysts at relatively low temperatures, e.g., alkene isomerization at $< 100^\circ C$, there is at least one example whereby, for specific combinations of metal, support, pre-treatment, reaction conditions, etc., catalysis can be carried out at up to $275^\circ C$. At this temperature, on the basis of the structural characterization at present available, the structure of the cluster is maintained. The catalytic properties of such stable support-

ed clusters are virtually unexplored and worthy of further investigation, in the expectation that new selectivities or activities will emerge. It is of paramount importance that these clusters be adequately characterized by a range of physical techniques to demonstrate that the cluster is preserved intact under such reaction conditions.

In general, however, supported metal clusters suffer from problems of instability at higher temperatures, which seriously limits their potential exploitation in chemical technology. These materials appear to be of greater value as model catalysts and as precursors of supported metal catalysts with unique structures.

A wider range of metal clusters should be studied. For example, the M_xL_y clusters used to date are largely limited to M = transition metal and L = CO. Not only should other types of L be investigated, e.g., hydrocarbon-, sulfur-, and oxygen-containing ligands, but also the range of metals should be extended to include the lanthanide and actinide series. Metal clusters with hydrocarbon ligands are readily available by metal vapor synthesis routes, and only recently has interest developed in this approach to catalyst preparation.

Metal-oxide clusters such as polyoxometallates offer attractive prospects as catalysts, since these oxide clusters are robust, their structures can be systematically varied, sites of stable coordinative unsaturation can be created, and catalytically active metal centers can be incorporated at the cluster surfaces or within the cluster framework. Structures approximated as $Cs_2H_2(PVMo_{11}O_{40})$ are selective methacrolein oxidation catalysts. Further research is recommended: it should include synthesis and development of methods for stable molecular dispersion on supports and systematic investigation of structure, reactivity, and catalytic activity.

Metal sulfides such as molybdenum sulfides occur in a wide range of "cluster" structures with properties akin to those of MoS_2 crystallites, which are used in industrial hydroprocessing catalysts. Stable molecular metal sulfides have scarcely been investigated as supported catalysts, and they are worthy of attention.

5.2.3.2. Supported clusters as catalyst precursors. These various supported molecular clusters may be far more important as precursors of novel catalysts than as catalysts themselves. For example, supported molecular clusters may be used to form intricate new surface species with specific catalytic properties. Some may be stable and regenerable and may be activated for structure-sensitive reactions such as C-C bond breaking. It is evident how one can use metal clusters to tailor make catalytic sites with various numbers of metal centers on a support for particular structure-sensitive reactions. Multimetallic clusters give multimetallic sites, potentially incorporating the bifunctional promotion and redox cycle for the particular reactions, e.g., a selective $CO + H_2$ conversion to give oxygenates and oxidation of hydrocarbons to give functionalized organics. When the metals are strongly bonded to the support, the catalysts may be stable and regenerable; however, it is doubtful whether zerovalent metals in this form would be stable.

Metal clusters may also be used to prepare supported metal particles of unique nuclearities, but, again, the issues of stability intrude with these supported particles.

The structures referred to above, by virtue of their simplicity, may be of greatest value for the fundamental understanding of surface reactivity of catalysts. We have the opportunity to understand:

- structure sensitivity in catalysis on a molecular basis;
- the exact nature of metal-surface bonds (from characterization such as EXAFS combined with other spectroscopic methods); and
- the role of systematically varied metal oxidation state and ligand environment of the metal.

5.3. Recommendations

- 1) Develop in-situ catalyst characterization methods for elucidation of catalytic cycles, including metal oxidation states and coordination.
- 2) Develop new catalytic probe reactions, in particular for oxidation catalysis.
- 3) Develop stable supports with properties such as hydrophobicity, resistance to metal sintering, and ability to stabilize low-valent metals.
- 4) Investigate stable supported molecular catalysts (metal clusters, polyoxometallates, and metal sulfide clusters) as models for metals, oxides and sulfides.
- 5) Carry out catalytic studies of supported molecular catalysts with in-situ characterization to establish retention of structure.
- 6) Design stable multicenter catalytic sites on surfaces (e.g., by use of metal cluster precursors) for bifunctional and promoted catalysts.
- 7) Develop molecular surface catalysts for use in selective paraffin C-H bond activation.
- 8) Generate group VIII metal centers which can be maintained in high oxidation states by strong bonds to strongly oxidizing early transition metal oxide surfaces, to be used for catalytic oxidation, oxidative carbonylation, and similar reactions.

THE SURFACES OF OXIDES AT A MOLECULAR LEVEL

Helmut Knözinger
Institut für Physikalische Chemie
Universität München
Sophienstr. 11
8000 München 2
W.-Germany

ABSTRACT. A description of the surfaces of oxides at a molecular level requires information about the surface at an atomic level. The surfaces can be described only in terms of models based on the structures of well-defined crystal planes. As examples, geometric and electronic properties of MgO and TiO₂ (rutile) single crystal planes are discussed. The surfaces of high-surface-area oxides can conveniently be studied by using surface OH groups as intrinsic probes. The O-H stretching frequencies and the chemical properties of OH groups are determined predominantly by their coordination to surface cations and the nearest oxygen environment of the cations. The interaction of probe molecules with aprotic surface sites is discussed, and special emphasis is placed on adsorption interactions of CO with surface sites on oxides. It is concluded that surface chemistry of oxides at a molecular level can be considered as essentially equivalent to surface coordination chemistry of oxides.

1. INTRODUCTION

The surface of a metal oxide consists of exposed cations, oxide ions, and hydroxyl groups. It is clear that these cations and anions in the surface of an oxide cannot be coordinatively saturated and, hence, that they must develop characteristic properties. The degree of unsaturation of individual surface atoms will be determined by the requirement for retaining stoichiometry in the crystal, and the type of crystal lattice will determine the local symmetry of surface vacancies. A detailed knowledge of the properties, structural and electronic, at an atomic level would be required for an in-depth understanding of the surface chemistry of oxides at a molecular level. This information, however, is almost impossible to obtain experimentally for high-surface-area materials of practical importance in adsorption and catalysis. The descriptions of these surfaces at an atomic level are based almost exclusively on model surfaces and the assumption that certain well-defined crystal planes (preferentially those providing the lowest

surface energy) terminate the crystals in such a way that stoichiometry of the crystal is preserved. This approach towards a model description of oxide surfaces has been discussed by Farragher [1] for the majority of possible oxide lattices.

Since regular crystal planes are considered as models of oxide surfaces, it is tempting to study structural and electronic properties of oxide single-crystal surfaces of known orientation, as these are accessible to a variety of modern surface physics techniques which are not applicable to the study of high-surface-area materials. Unfortunately investigations of this type are still rather scarce in comparison with investigations of the surface physics of metals. A recent review by Henrich [2] summarizes the state of surface science as regards single-crystal oxide surfaces.

It is not intended to discuss surface properties of oxides comprehensively here. Instead, some important aspects will be considered in a selective way, and the reader is referred to the above-mentioned [1,2] and additional [3-10] reviews for further information. The first part of this article is focused on single-crystal oxide surfaces, with MgO and TiO₂ (rutile) chosen as representative examples. In the second part, surface chemistry of disperse, high-surface-area materials is described, the surfaces of aluminas playing a central role.

2. WELL-DEFINED SURFACES

As a representative example, the surface of MgO is discussed in some detail. This oxide crystallizes in the rock salt structure, in which the oxide ions form a ccp sublattice with the Mg²⁺ ions occupying all the octahedral holes. Both anions and cations are octahedrally coordinated in the bulk. The structure of a perfect surface of such a crystal can be described by the structure of the crystallographic plane which is considered to be exposed. Fig. 1 shows a perfect MgO/(100) surface, which can be obtained by cleavage along the corresponding crystallographic orientation. This surface is stoichiometric. As a result of the cleavage of the crystal, bonds are broken and coordinative unsaturation created. In the (100) MgO surface — the energetically most favorable surface [11] — both the cations and anions occupy so-called O₅ sites¹, and all the available sites are occupied in a perfect surface. Due to the equivalency of the bonds in the surface plane which differ from the bond perpendicular to the surface, the site symmetry is exactly C_{4v}.

Sites of different coordination and site symmetry can be envisaged

¹The terminology for surface sites is derived from the coordination of the bulk ions; thus C, O, P, and T indicate that the surface site is derived from cubic, octahedral, trigonal prismatic or tetrahedral sites in the bulk, respectively. The subscript refers to the coordination number of the surface atom or ion.

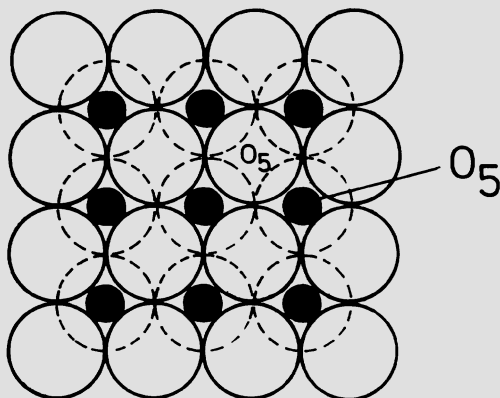


Figure 1. Stoichiometric (100) MgO surface.

Large circles and filled, small circles are O^{2-} and Mg^{2+} ions, respectively, in the plane of the paper; dashed large circles are O^{2-} ions in the next lower layer.

when other cleavage planes are considered. Thus, the stoichiometric MgO (110) surface is expected to expose anions and cations in O_4 sites of C_{2v} symmetry. The (111) surface is more complex: the cations are expected to occupy O_3 sites in parallel rows, while there must be two crystallographically distinct oxide ions which are 4- and 5-coordinated, respectively.

Such stoichiometrically perfect surfaces need not necessarily provide the energetically most favourable arrangement. The anisotropic distribution of bonds of a central ion with nearest neighbours will produce forces which can lead to drastic relaxation and reorganization of the surface layers [1,11]. These surface relaxation phenomena are less pronounced in ionic solids than they are in covalently bonded ones. However, small but clearly detectable changes in the interplanar spacings (typically of the order of a few percent) of MgO are known to occur in the three surfaces mentioned above, namely the (100), (110), and (111) surfaces. The occurrence of a finite rumpling of the MgO (100) face was unambiguously demonstrated by LEED [12].

Due to the surface bonding characteristics which deviate from those of the bulk, surface vibrational modes are different from those of the bulk. Phonon density of states measurements have been obtained for the (100) surface of MgO [13].

Even allowing for relaxation at the surface, the description of a surface as given above is an extreme idealization, since the existence of defects has been ignored. The surface may indeed be built up of regions of terraces of a distinct crystallographic orientation, these terraces being interrupted by crystal facets [14]. Moreover, on the

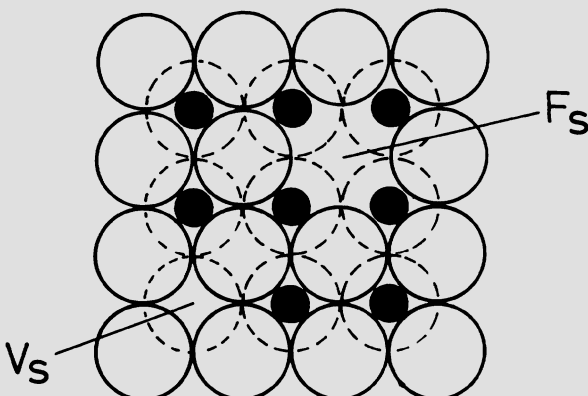


Figure 2. (100) MgO surface anion (F_s center) and cation (V_s center) vacancies.

terraces themselves both point and extended defects can occur. Fig. 2 shows schematically a (100) surface of MgO containing an anion vacancy (F_s center) and a cation vacancy (V_s center). It is clear that the ions located at defects are coordinatively more highly unsaturated than those forming the perfect surface. Due to the coordinative unsaturation of surfaces — even if they were perfect — adsorption phenomena will occur with a tendency to reduce the coordinative unsaturation of surface ions. In addition to the regular surface sites, defects must be considered as specific sites developing coordination properties which will be determined by the reduced coordination number and the site symmetry, these being dependent on the type of defect and the nature of the underlying structure.

Besides structural properties, the electronic properties of surfaces and of surface sites determine the surface chemistry at a molecular level. Though scarcely available to date, a variety of surface spectroscopies can provide information about electronic surface properties. Electron energy loss spectroscopy (EELS) was applied in a study of the (100) surface of MgO [15]. The observed loss peaks could be identified with known inter- and intra-atomic electronic transitions of bulk MgO. In addition, two features were detected at lower energies (near 6 eV and 2.3 eV) which proved to be characteristic of surface states since their relative intensities strongly increased with decreasing primary electron energy. The loss feature at 6 eV was identified as an intrinsic feature of a perfect surface, whereas the feature at 2.3 eV must be attributed to a defect. Its assignment, however, is not yet clear. Its energy is too low for it to be assigned as a F_s center, but it may be attributed to a cation vacancy (V_s center). Data of this kind can be related to optical spectra (diffuse reflectance) obtained with high-surface-area materials [16]. Zecchina

et al. [17] have studied MgO and attributed transitions observed below the bulk optical band gap (7.8 eV) to surface states involving interatomic transitions between atoms with low coordination numbers. No electronic transitions at 2.3 eV have been detected by reflectance spectroscopy.

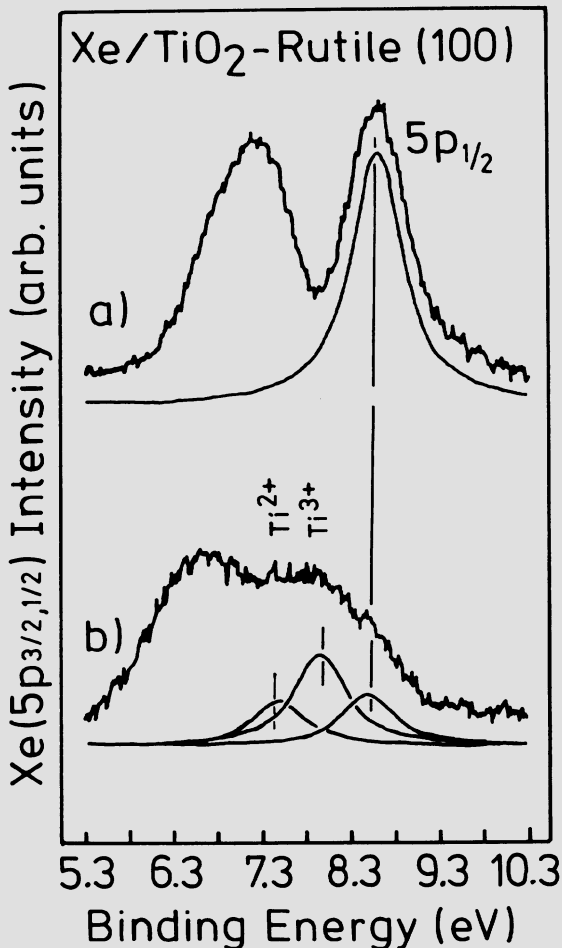


Figure 3. $5p_{3/2,1/2}$ UV photoemission spectra of xenon adsorbed on a) stoichiometric rutile (100) plane and b) the same rutile plane annealed at 1123 K in UHV.

Another method providing information about structural and electronic properties of well-defined oxide surfaces is photoemission of adsorbed xenon (PAX). Xenon is adsorbed at low temperature, and the UV-photoemission from Xe 5p_{3/2,1/2} levels is measured. The corresponding binding energies are a measure of local work function changes at a spatial resolution of approximately 1 nm. The physical principles of the method have been discussed by Wandelt [18]. This technique, although very promising, has hitherto been used for only one study of an oxide surface, namely the (100) surface of TiO₂ (rutile) [19]. Fig. 3a shows the spectrum obtained for a stoichiometric surface. A Xe 5p_{1/2} binding energy of 8.5 eV (below the Fermi level) is characteristic of this surface. Annealing at high temperatures (1120 K) in UHV leads to defect formation by oxygen loss. The surface defects lead to a dramatic change of the UV-photoemission spectrum in the Xe 5p_{1/2} region (Fig. 3b). The broad feature can be fitted by three Lorentzian functions, as shown in Fig. 3b, indicating the presence of the original feature at 8.5 eV with significantly reduced intensity and, in addition, two new features at lower energy, namely ~ 8 and ~ 7.5 eV. The corresponding defect sites were identified as oxygen-deficient sites, since the shift in Xe 5p_{1/2} binding energy to lower values is compatible with an increased charge density at the corresponding Ti^{x+} sites ($x < 4$). It may be suggested that the defect sites would expose Ti³⁺ and Ti²⁺ ions, respectively.

These results can again be related to studies of high-surface-area materials. When CO is adsorbed on TiO₂ after thermoevacuation at elevated temperatures (>770 K), a carbonyl stretching frequency is observed near 2180 cm⁻¹. Calculations based on an electrostatic model suggest that the frequency must arise from a CO ligand coordinated to Ti³⁺ sites [20,21].

3. HIGH-SURFACE-AREA OXIDES

For practical purposes such as adsorption and catalysis, oxide materials having high surface areas of the order of magnitude of typically 100 m²g⁻¹ are required. The determination of the surface structures of such materials is almost impossible and model considerations are based on the assumption that the crystallites and particles of these materials are terminated by the more energetically favourable low-index crystal planes, as was discussed above for extended single-crystal planes. In this way it is possible to describe surface properties on the basis of models at an atomic or molecular level. However, in reality, the surfaces of such disperse materials are expected to be highly irregular and defective, so that simple models provide only a rough approximation, the more so as the surface properties may be dominated by some particularly energetic and reactive minority defect sites.

Experimentally, almost the only approach towards a characterization of high-surface-area oxides is the use of surface probes (e.g., adsorption of probe molecules) and their spectroscopy. Oxide surfaces are usually terminated by OH groups unless they are treated at elevated

temperatures. These OH groups are formed as a result of dissociative H₂O adsorption on adjacent cation/anion pairs. Molecular water adsorption reduces the coordinative unsaturation of exposed cations. However, a surface being terminated by neutral H₂O molecules and negatively charged O²⁻ ions is energetically less favourable than a surface which is uniformly terminated by OH⁻ ions [3,4]. Therefore, dissociation of H₂O will occur except when this process is kinetically hindered. These surface OH groups are sensitive intrinsic probes, the behaviour and properties of which can conveniently be studied by IR spectroscopy.

Aprotic sites are produced during thermal dehydroxylation in the form of Lewis acid (coordinatively unsaturated, cus, cations) and base (O²⁻ ions) sites. These sites can be studied only by adsorption of probe molecules. This has been an area of extensive research activities [4-7, 22, 31].

In the following, the IR spectroscopy of intrinsic OH probes is briefly discussed, and then an overview of the use of CO as a surface probe is presented. Regarding other surface probes the reader is referred to the above-mentioned review articles. Finally, a short description of surface reactivities is given, with emphasis placed on alumina surfaces.

3.1. Surface Hydroxyl Groups

It has been shown theoretically that the frequency of an O-H oscillator decreases with increasing electronegativity of the central cation X to which it is coordinated [23]. Fink *et al.* [24] experimentally demonstrated this tendency in a study of the hydroxyl IR spectra of X-OH groups (X = B, P, Ge, Sn) which were grafted onto silica surfaces. It is important to note that this correlation can hold only if the coordination of the OH group to the cation X is the same for all X-OH groups being compared. In the example mentioned above, the OH groups were terminal. However, the coordination of surface OH groups will depend on the crystal structure of the oxide and on the geometry of the particular crystal plane under consideration. This means that bridging (doubly, triply,...) OH groups must in principle be expected to occur in addition to terminal OH groups. These various groups should be distinguishable by their O-H stretching frequencies, and they should develop distinct chemical properties and reactivities [4]. As will be discussed later (for Al₂O₃), the coordination of the cations to O²⁻ in the oxide matrix also has an additional effect on the properties of the surface OH groups. Table I is a summary of a few examples of O-H stretching frequencies and their assignments for several oxides. The hydroxyls are distinguished by their coordination numbers and accordingly designated type I (-OH), type II (=OH), type III (\equiv OH), type IV (\equiv OH), etc. The assignments given in Table I are consistent with possible coordinations based on the crystal structures of the particular oxide.

The situation becomes very complex for the surfaces of transition aluminas. These oxides, namely the γ - and η -modifications, have a cubic oxygen sublattice with the Al³⁺ cations being distributed over tetrahedral and octahedral interstices. The cation distributions are

Table I. Vibrational frequencies of free surface hydroxyls on oxides with different crystal structures.^a

Oxide	Frequency/cm ⁻¹			
	Type I	Type II	Type III	Type V
SiO ₂	3750			
ZnO		3675		3622
ThO ₂	3745			3655
ZrO ₂	3770			3670
MgO	3750			3630
CaO	3700			3610

^a Data from ref. [25].

different for the two modifications, and they are temperature dependent [26]. Surface models of aluminas usually consider the (111), (110), and/or (100) planes as terminating the particles [27]. Among these planes, the close-packed (111) plane is energetically the most favourable. Considering the geometry of this plane and the two possible coordinations of Al³⁺ cations, one can anticipate five different types of surface OH groups, which have been designated types Ia, Ib, IIa, IIb, and III [27]. On the (110) plane, types Ia, Ib, and IIb are possible, whereas the (100) plane would permit only type Ib. Assuming, again, that the coordination of the OH group would primarily determine the O-H stretching frequency, with some additional influence of the Al³⁺ coordination in the oxide matrix, one would expect the occurrence of five O-H stretching bands in the IR spectra, as observed. The observed frequencies and band assignments are given in Table II.

Table II. Hydroxyl group configurations and O-H stretching frequencies of transition aluminas.^a

OH-type	Coordination number			$\tilde{\nu}_{\text{OH}}/\text{cm}^{-1}$	Net charge at OH
	Al ³⁺ total	Al ³⁺ oct	Al ³⁺ tet		
Ia	1	-	1	3760-3780	-0.25
Ib	1	1	-	3785-3800	-0.50
IIa	2	1	1	3730-3735	+0.25
IIb	2	2	-	3740-3745	0
III	3	3	-	3700-3710	+0.50

^a Data from ref. [27].

Also included in Table II are the net charges at the OH groups in different configurations, as estimated by means of Pauling's electrostatic valence rule. As can be seen from Table II, the O-H stretching frequencies decrease with increasing positive charge of the OH group. Hence it is expected that the acidity of the OH groups should increase with decreasing frequency while the basicity should follow the opposite trend. In fact, the OH groups of configurations Ia and Ib act as basic sites or nucleophiles [5,28], while OH groups of configurations IIa, IIb, and III engage in H-bonding interactions. Also, when surface OH groups are reacted with $\text{Mo}_2(\text{acac})_2$ (acac = acetylacetone) only the type I configurations are removed, while the low frequency groups remain unaffected [29]. When CO is adsorbed on $\gamma\text{-Al}_2\text{O}_3$ (pretreated at 770 K and at 80 K), the two high-frequency configurations Ia and Ib remain unaffected, whereas the three other O-H bands are shifted to lower frequencies by approximately 100 cm^{-1} [30].

These results can in principle be interpreted by the assumption that the (111) planes of the spinel matrix preferentially terminate the Al_2O_3 particles. However, one can hardly anticipate that these highly dispersed materials develop extended regions of well-defined crystallographic planes. For a description of the surface structure at a molecular level it is sufficient to assume that the by far predominant OH configurations are the ones summarized in Table II. All experimental evidence available to date supports this view.

3.2. Aprotic Surface Sites

When oxide surfaces are evacuated at elevated temperatures, condensation of neighbouring OH groups and loss of water create coordinatively unsaturated surface atoms. This dehydroxylation process may be accompanied by oxygen loss from reducible oxides and the formation of low-valent surface cations as has discussed in section 2. The study of such partially or fully dehydroxylated oxide surfaces by means of probe molecules involves a wide area of surface chemistry at a molecular level [4,5,22,31]. Here we discuss only the use of CO adsorption on aluminas in the temperature range $80 < T \leq 300 \text{ K}$ as a typical example. CO is a rather soft molecule and therefore interacts weakly with the hard cus surface cations, provided that these are main group elements or high-valent transition metal ions with low d-electron density, so that π -back donation does not play a role. Under these circumstances, the carbonyl stretching frequency of adsorbed CO typically is shifted to higher energies relative to the gas-phase frequency at 2143 cm^{-1} , and the frequency shift can be interpreted on the basis of simple electrostatic models [20,21]. The advantage of the soft CO probe is the fact that it adsorbs more selectively than hard probe molecules [5,6].

When CO is adsorbed on an Al_2O_3 surface that has been thermally pretreated at 770 K, a single band of coordinated CO is observed at $2190\text{-}2200 \text{ cm}^{-1}$ [20,21,32]. This band must be attributed to an $\text{Al}^{3+}\leftarrow\text{CO}$ species. When the thermal pretreatment is carried out at higher temperatures ($T > 870 \text{ K}$), a second carbonyl band is recorded near 2240 cm^{-1} [32]. The corresponding adsorption complex is thermally more stable and has a significantly higher heat of adsorption [32]. It is

known [27] that surface defect sites (adjacent anion vacancies) are produced on the alumina surface under these high-temperature conditions, and hence it is plausible to attribute the high-frequency carbonyl species to CO adsorbed on such defect sites. It is interesting to note that this strongly held CO perturbs the type Ia OH groups, this interaction obviously being an indirect weak interaction. The type Ia OH groups must therefore be located close to the defect coordination site for the CO molecule. Such acid-base pair sites on alumina surfaces have been called X-sites [33], and they provide special reactivities in that the Lewis acid center (anion vacancy) can accommodate molecules in the immediate vicinity of a nucleophilic OH group. The coordination bond to the Lewis acid site will activate the adsorbed molecule (e.g., CO₂, CH₃CN, ketones, etc.) for nucleophilic attack by the OH group, which most probably proceeds in a cooperative manner [5,28].

The defect sites mentioned above are to be considered as charge defects, so that significant forces should act on the neighbouring anions, which would lead to a relaxation of the surface site. The adsorption of pyridine on aluminas provided experimental evidence of this phenomenon [34]. Two types of coordinated pyridine were detected, a low-temperature species and a high-temperature species, the latter being formed from the former by an activated process. This observation was interpreted by assuming that a so-called outer complex was formed on a relaxed site at low temperature. This complex should be characterized by a comparatively long Al-N bond due to steric hindrance. It was suggested that as the temperature increases, an inner complex having a shorter Al-N bond could be formed by pushing the anions back towards their unrelaxed positions. Analogous situations have been reported for molecular adducts in which there was steric hindrance [35]. The importance of steric hindrance at surfaces has been demonstrated by use of substituted pyridines as surface probes [36,37].

4. CONCLUSIONS

The geometric structures of oxide surfaces, particularly of high-surface-area materials, can at present be described only in terms of models, where well-defined crystallographic planes are considered as terminating the crystallites or particles. Studies of single-crystal planes are advantageous in this context. Spectroscopy of surface hydroxyl groups as intrinsic surface probes and of suitably selected adsorbed probe molecules gives detailed information concerning the geometric nature, energetics, electronic properties, and reactivities of surface groups and sites at a molecular level. Bonding in most oxides, namely, the more ionic oxides, can be considered to be localized so that long-range effects play a minor role. In fact, properties of surface groups and sites can be interpreted by considering the central cation and its nearest oxygen environment only. Thus, the discussion throughout this paper was primarily based on a consideration of surface cations and their ligands, the latter being surface species (OH, O, adsorbed molecules) and bulk oxygen ions.

Hence, surface chemistry of oxides at a molecular level is to be considered as surface coordination chemistry of oxides.

5. ACKNOWLEDGMENTS

Financial support for the work done in the author's laboratory was provided by the Deutsche Forschungsgemeinschaft and the Fond der Chemischen Industrie.

6. REFERENCES

1. A.L. Farragher, Adv. Colloid Interface Sci. 11, 3 (1979).
2. V.E. Henrich, Reports Progr. Phys. 48, 1481 (1985).
3. H.P. Boehm, Adv. Catal. 16, 179 (1966).
4. H.P. Boehm and H. Knözinger, in Catalysis - Science and Technology, (Eds. J.R. Anderson and M. Boudart), v. 4, p. 39 (1983).
5. H. Knözinger, Adv. Catal. 25, 184 (1976).
6. J.B. Peri, in Catalysis - Science and Technology, (Eds. J.R. Anderson and M. Boudart), v. 5, p. 171 (1984).
7. A. Zecchina, E. Garrone, and E. Guglielminotti, Specialist Period. Rep., Catalysis, v. 6, p. 90 (1983).
8. J.P. Bonnelle, B. Delmon, and E. Derouane, Eds., Surface Properties and Catalysis by Non-Metals, NATO ASI Series, Reidel, Dordrecht, Boston, Lancaster (1983).
9. J. Haber, in Catalysis - Science and Technology, (Eds. J.R. Anderson and M. Boudart), v. 2, p. 13 (1981).
10. V.F. Kiselev and O.V. Krylov, Adsorption Processes on Semiconductor and Dielectric Surfaces I, Springer, Berlin, Heidelberg, New York, Tokyo (1985).
11. W.C. Mackrodt and P.W. Tasker, Chemistry in Britain 21, 366 (1985).
12. M.R. Welton-Cook and W. Berndt, J. Phys. C: Solid State Phys. 15, 5691 (1982).
13. P. Masri and P.W. Tasker, Surf. Sci. 149, 209 (1985).
14. A.G. Shastri, H.B. Chae, M. Bretz, and J. Schwank, J. Phys. Chem. 89, 3761 (1985).
15. V.E. Henrich, G. Dresselhans, and H.J. Zeiger, Phys. Rev. B22, 4764 (1980).
16. S. Coluccia, A. Barton, and A.J. Tench, J. Chem. Soc., Faraday Trans. 1 77, 2203 (1981).
17. A. Zecchina, M.G. Lofthouse, and F.S. Stone, J. Chem. Soc., Faraday Trans. 1 71, 1476 (1975).
18. K. Wandelt, J. Vac. Sci. Technol. A2, 802 (1984).
19. P. Dolle, K. Markert, W. Heichler, N.R. Armstrong, and K. Wandelt, J. Vac. Sci. Technol. 4, 1465 (1986).
20. M.I. Zaki, B. Vielhaber, and H. Knözinger, J. Phys. Chem. 90, 3176 (1986).
21. M.I. Zaki and H. Knözinger, Spectrochim. Acta, Part A, in press.
22. M.C. Kung and H.H. Kung, Catal. Rev.-Sci. Eng. 27, 425 (1985).

23. E.P. Smirnov and A.A. Tsyganenko, React. Kinet. Catal. Lett. 7, 425 (1977).
24. P. Fink, B. Camara, E. Welz, and Ty Pham Dinh, Z. Chem. 11, 473 (1971).
25. A.A. Tsyganenko and V.N. Filimonov, J. Mol. Struct. 19, 579 (1973).
26. C.S. John, N.C.M. Alma, and G.R. Hays, Appl. Catal. 6, 341 (1983).
27. H. Knözinger and P. Ratnasamy, Catal. Rev.-Sci. Eng. 17, 31 (1978).
28. H. Knözinger, H. Krietenbrink, H.-D. Müller, and W. Schulz, Proc. 6th Intern. Congr. Catal., London, 1976, v. 1, 183 (1977).
29. J.A.R. Van Veen, J. Colloid Interface Sci., in press.
30. M.I. Zaki and H. Knözinger, Mater. Chem. Phys. 17, 201 (1987).
31. E.A. Paukshtis and E.N. Yurchenko, Russ. Chem. Rev. 52, 242 (1983).
32. G. Della Gatta, B. Fubini, G. Ghiotti, and C. Morterra, J. Catal. 43, 90 (1976).
33. P. Fink, Z. Chem. 7, 324 (1967); and Rev. Roum. Chim. 14, 811 (1969).
34. H. Knözinger and H. Stoltz, Fortschr. Kolloide Polym. 55, 16 (1971).
35. R.S. Mulliken, J. Phys. Chem. 56, 801 (1952).
36. H. Knözinger and H. Stoltz, Ber. Bunsenges. Phys. Chem. 75, 1055 (1971).
37. P.A. Jacobs and C.F. Heylen, J. Catal. 34, 267 (1974).

REACTION OF ORGANOMETALLICS WITH SURFACES OF METAL OXIDES

John Evans
Department of Chemistry
The University
Southampton SO9 5NH
England

ABSTRACT. Organometallic complexes can be introduced onto metal oxide supports either by direct bonding or via an intervening ligand. The former method uses the diverse reaction sites available on oxide surfaces. The chemisorption processes may be considered in the same way as reactions of organometallic complexes in solution. For example, interaction of $\text{Rh}(\text{allyl})_3$ with silica causes an electrophilic cleavage of one metal-allyl bond to generate a new metal centre, viz. $[\text{Si}-\text{ORh}(\text{allyl})_2]$. Alternatively, interaction of $\text{Ru}_3(\text{CO})_{12}$ with silica proceeds via an oxidative addition reaction of a silanol group across one of the metal-metal bonds. Nuclearity is not always maintained during anchoring procedures, as in the case of the interaction of $\text{Rh}_4(\text{CO})_{12}$ with alumina, in which mononuclear metal centres are produced. Some of the coordination centres derived from these grafted organometallic complexes have close analogues in mainstream organometallic chemistry; others appear to have no discrete counterpart at present and offer a challenge to the synthetic chemist. Organometallics also provide alternative routes to supported metal particles. In some instances these may be formed under much milder conditions than conventional reductions of metal salts. By virtue of the differing kinetics involved, different (often smaller) particle sizes, compositions, and size distributions become available. Ligand-tethered complexes may be synthesised with high specificity. However, subsequent surface reactions occur to give new coordination centres. If the aim is to anchor a known homogeneous catalyst, then precautions must be taken to avoid these, either by protective silylation or by design of a stabilising tethering ligand. But the original tethered complex may be used as a catalyst precursor, and so these surface reactions may be of interest. Many new catalysts have been prepared by supporting organometallic complexes on oxide supports. Establishing the metal coordination site requires a combination of total product analysis and direct spectroscopic measurements characterizing the supported complex, preferably aided by reference to close model compounds. This is now considerably easier with the range of techniques presently available. For a high proportion of materials, the oxide surface binding site is not understood. Progress in this is necessary

to understand catalytic activity and selectivity on a molecular level. Nevertheless, the relatively homogeneous dispersion of metal centres as compared to conventional heterogeneous catalysts gives some prospect of this being achieved.

1. INTRODUCTION

The drive for studying the interaction of organometallics with oxide supports has been primarily related to the synthesis of new heterogeneous catalysts [1,2]. Two main approaches have been adopted, involving either the direct interaction of the complex with the oxide surface or using an intervening functionalisation at the oxide surface with the chosen binding ligand. These alternatives have generally been guided by differing philosophies.

In the latter approach the principal aim has been to immobilize a homogeneous catalyst to eliminate the necessity of separating the catalyst from the reaction products; oxides have considerable advantages over organic polymers in this regard by virtue of their higher thermal stability, rigidity, and physical strength. Any direct reaction between the tethered complex and the surface of the oxide is, unless adventitiously advantageous, to be avoided to maintain the catalyst's activity.

However, the former methodology of direct reaction of the organometallic with the surface aims to use the oxide as a reagent to generate new metal centres. These may or may not have close analogues in organometallic chemistry, but the history of conventional oxide-supported metals as heterogeneous catalysts [3] would indicate that novel heterogeneous catalysts could be prepared in this way. Indeed, by applying the synthetic techniques of organometallic chemistry it is hoped that specific metal centres can be produced. This uniformity and control is generally in marked contrast to heterogeneous catalysis and, in principle, should provide two advantages. Firstly, there is more likelihood of understanding the chemistry at these centres on a molecular level since all measurements are performed on a single, rather than a multiplicity, of potentially active sites. Secondly, the control of catalytic selectivity should be greatly enhanced, both by the simpler nature of the materials concerned and by the more detailed understanding of their chemistry. In this review the chemistry relating to the two supporting methods will be outlined and views presented about the current level of understanding and future opportunities.

2. THE NATURE OF OXIDE SURFACES AS REAGENTS

2.1. Oxide Surfaces

Oxide surfaces are generally thought to consist of Brønsted acid (hydroxyl) and basic (oxide and hydroxyl) sites as well as Lewis acid (metal cation) and basic (oxide) centres [3]. Probably the four high-surface-area oxides which have been used most in surface organometallic

chemistry have been silica, alumina, titania, and magnesia. The nature of these surfaces is the subject of an accompanying chapter by Knözinger, and so this section will just outline the likely sites that will be available to an interacting organometallic complex.

Silica is probably the most widely employed oxide; two forms, gels and sils, differ in their morphology [3]. The former are highly porous materials, and probably are less suitable for surface organometallic chemistry. There is a doubt over the accessibility of large organometallics to pores (indeed pore size distributions for these supports would have to be known) and also some metal cations can be present as contaminants from the hydrolysis procedures used in their production. Sils, on the other hand, are essentially non-porous and derive their high surface areas from small particle sizes (5-40 nm diameter); generally they are also of higher purity, with some residual chloride (from the SiCl_4 precursor) being the most likely contaminant. The degree of hydroxylation of the surface of silicas has been much studied by infrared spectroscopy [4,5]; more recently high resolution ^{29}Si nmr, which derives surface selectivity by the cross-polarisation of proton to silicon spins, has added further detail [6]. The loss of the physically adsorbed water present under ambient conditions is the predominant dehydration process at temperatures below 150°C, but is incomplete below 300°C. At temperatures above 150°C, however, the condensation of surface hydroxyls is the principal route to the elimination of water. So at a moderate drying temperature, adsorbed water, silanol groups, and siloxane linkages provide possible reactive sites to an organometallic. Some hydroxyl content is still evident after drying at 1100°C. The silanol groups themselves will have different spatial distributions. Considering the silica surface in more detail, on an ideal (111) crystal face of β -cristobalite the silanols are $\sim 5 \text{ \AA}$ apart and are virtually isolated. Vicinal pairs separated by 3.3 Å occur on a (110) face. There is also evidence of gem silanediols which may represent 10-20% of the total silanol population depending upon the pretreatment regime adopted. This spatial distribution is important for adsorption sites. For example, water is chemisorbed preferentially on neighbouring silanol pairs whereas amines bind to isolated groups [4]. When the silica is pure, these silanol groups act as weak Brønsted acid sites, but Lewis acidity is not evident.

The chemistry of alumina is more complex. There are several modifications of the defect spinel structure adopted. Aluminium ions reside in both octahedral and tetrahedral sites, and these are in different relationships in these various phases [1,3,7]. This provides a substantial range of potential surface sites, and indeed five hydroxyl types have been classified according to their O-H stretching frequencies. Some hydroxyl content is present after treatment at temperatures below 1200°C, and the strength and quantity of their acidity is highly dependent upon the pretreatment temperature. Surface oxide or hydroxyl groups can act as electron transfer reagents to an acceptor such as TCNE [8]. However, the reactivity of dehydrated aluminas is not primarily due to Brønsted acidity, but to the Lewis acid sites at exposed aluminium ions.

Titania also contains surface hydroxyl groups, even when dried at temperatures exceeding 1000°C; at ~1300°C oxygen loss occurs to form a non-stoichiometric oxide [3,9,10]. There are both acidic and basic Brønsted sites among these hydroxyls, and a method of estimating these has recently been reported [11]. The acid sites, however, are relatively weak and do not protonate pyridine or ammonia. As for alumina, surface sites can act as electron donors and, for example, can generate the radical anion of trinitrobenzene [12]. Dehydration of a hydrated sample, as for alumina, forms Lewis acid sites; relatively weak ones become evident after heating to 250°C, and stronger sites form at 400°C. It is also relevant that surface Ti^{IV} centres can be readily reduced to Ti^{III}.

The surface of magnesia also contains hydroxyl groups, at temperatures up to ~900°C [3]. As the pretreatment temperature is raised, there is an increasing tendency for magnesia to act as an electron donor to TCNE [12]. Adsorption of water (or CO₂) onto a dehydrated sample inhibits radical anion formation [13]. Hydration decreases the surface exciton bands in the ultraviolet, with the lowest-frequency bands being first affected [14]. These bands (and probably the electron donor properties) have been associated with low coordination oxide sites (to 3 and 4 cations) [14,15]. The proportion of three- and four-coordinate sites varies considerably with sample history [15]. CO itself undergoes complex disproportionation reactions following attack by the highly reactive surface oxide groups; both oligomeric carbanions and carbonate are formed [16].

2.2. Ligand-Functionalised Oxides

Of the many alternatives, the prevalent method of tethering a ligand to an oxide surface is to employ a bifunctional reagent of the type X₃Si(CH₂)_nL (X = halide, OAc, or OR; L = PR₂, NR₂, -NC, etc.). Both the Si-O and Si-C bond strengths are high, so this is expected to give a durable unit on an oxide surface. Also the silicon is a kinetically labile centre, so hydrolysis of the Si-X bond can proceed under reasonable conditions [1,2]. Virtually all detailed studies have been carried out on silica. From these it is apparent that higher ligand surface concentrations are possible for X being Cl, rather than OMe, OAc, or OEt [17]. The concentration of (EtO)₃SiCH₂CH₂PR₂ also decreases with the steric bulk of the phosphine substituent, R, and the silica dehydration temperature [1]. This reaction is accompanied by the reduction in intensity of the high-frequency O-H stretching vibration in the infrared and an increase in the band at 3650 cm⁻¹ characteristic of hydrogen-bonded hydroxyl groups; this is attributed to secondary reactions of the liberated EtOH.

A recent ²⁹Si and ¹³C nmr study of the reaction of (EtO)₃Si-(CH₂)₃NH₂ with silica shows that the residual content of ethoxy groups decreases with decreasing surface hydroxyl concentration [18]. ²⁹Si resonances due to silicon centres of the silica framework and those with 3 siloxane bonds and one silanol were observed from the support; no geminal sites were observable in the functionalised silicas. Three further resonances emanating from the functionalising ligand could be

assigned to differing degrees of substitution at the silane centre, i.e., $\text{RSi(OEt)}_2\text{O-[Si]}$, $\text{RSi(OEt)(O-[Si])}_2$, and RSi(O-[Si])_3 .

Interestingly, ^{13}C resonances attributable to a quaternised amino species were also observable, the amount of which increase with the water content of the original silica; so the intended ligand in these bifunctional reagents may also interact with the support. A further example of this is provided by ^{31}P work on phosphinated silicas [19]. As well as the resonance expected for a $[\text{Si}]\text{-(CH}_2\text{)}_2\text{PPh}_2$ species, a second signal further downfield has been assigned to oxidation of the phosphorus.

Even on the relatively simple surface provided by silica, several reaction types can occur with these bifunctional reagents. Nevertheless, the majority of the functionalising groups provide the intended ligand sites even though there may be a distribution of binding modes of the silane centre to the silica surface. Similar studies to these on oxides with different chemical reactivity would be seem to be potentially fruitful.

3. DIRECT INTERACTION OF ORGANOMETALLICS WITH OXIDE SUPPORTS

3.1. Metal Carbonyl Complexes

There are several classes of reaction that might be anticipated for transition metal carbonyls on an oxide surface, based on precedents in solution. Two ligand-centred interactions might be nucleophilic attack on the carbon atom or coordination of the oxygen to a surface Lewis acid site. The most likely alternatives for metal-centred attack involve a CO dissociation followed by either coordination by a surface Lewis base site (effecting CO substitution) or oxidative addition of a hydroxyl group. Only on strongly acidic substrates is direct protonation of a neutral metal carbonyl to form a hydrido complex probable; protonation of carbonylate anions, however, might be more general. Subsequent reactions may then ensue which may effect redox reactions on the original complex, or, possibly, the liberated CO.

The reactions between the Group VI metal hexacarbonyls, representing relatively simple binary carbonyl complexes, and a variety of oxides is illustrative and also derives interest from the active alkene metathesis catalysts provided [20,21]. The initial interaction of $\text{Mo}(\text{CO})_6$ with silica has been monitored by infrared [22] and Raman [23] spectroscopies. The complex has been shown to be physisorbed in a similar environment to that adopted in a polar solvent and to have its symmetry lowered. At 44°C , in vacuo, this species is converted to a chemically bound carbonyl which itself is apparently decarbonylated. This is complete by 100°C , giving rise to an active propene metathesis catalyst [22]. Although no C-O infrared absorptions are evident, only 3 CO groups per metal atom have been released [21], but the nature of the molybdenum in this yellow material is unclear. Some of the metal is EPR active, and this signal indicates a Mo^{V} site in an axially symmetric site, possibly square pyramidal [24]. The proportion of Mo^{V} increases to a maximum with an activation temperature of 200°C [25]. At that

temperature the material is again white, and TPD experiments indicate the following equation for an irreversible decomposition:



The chemistry of the chromium and tungsten analogues on silica appears to be broadly similar to that of molybdenum [25].

The initial physisorption of $\text{Mo}(\text{CO})_6$ on alumina is similar to that on silica, although if the alumina has been activated at 450°C , low-frequency C-O infrared bands suggest chemisorption via a carbonyl oxygen to an exposed Al^{III} site [26]. Unlike the situation on silica, there is clear evidence of stepwise decarbonylation [22]. The adsorbed carbonyl reacts at -10°C [27], and the species formed exhibits a similar infrared spectrum in the M-C-O region [22] to those of $\text{Mo}(\text{CO})_5$ centres solvated by alcohols or ethers [28]; there has effectively been a monosubstitution reaction of a CO ligand by a surface Lewis base site (Fig. 1).

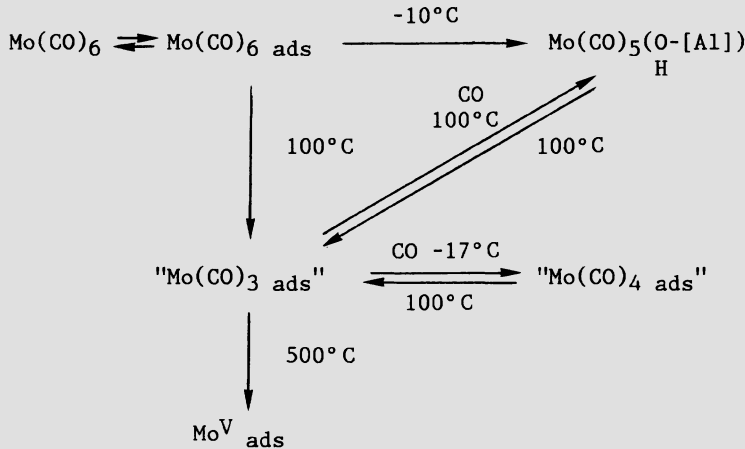


Figure 1. Reactions of $\text{Mo}(\text{CO})_6$ on alumina.

Thermolysis at 100°C causes the loss of a further 2 CO groups, and the re-coordination of one and two CO ligands occurs at different temperatures [29,30]. So there appear to be two more materials of apparent composition $\text{Mo}^{\text{o}}(\text{CO})_n \text{ ads}$ ($n = 4$ and 5). The infrared spectra are complex and each seems to be a mixture of sites [26]. Low-frequency C-O infrared bands are evident and suggest the presence of either bridging carbonyls or interaction of a CO oxygen with a Lewis acid site. Temperature-programmed decomposition studies indicate further CO loss at $>200^\circ\text{C}$; by 400°C this is complete [31]. This higher-temperature CO loss is accompanied by the evolution of H_2 and CH_4 . Oxidation of the molybdenum centres is apparent, giving an average oxidation state of ~ 5 by $500\text{-}600^\circ\text{C}$ [30,32]. EPR signals due to Mo^{V} centres increase in magnitude with this oxidation, but only represent a

maximum of ~8 % of the total metal content [26]. So the nature of the metal sites in this regime is still ill-defined. Nevertheless, their varied catalytic activity gives them considerable interest [33].

The chemistry of $\text{Cr}(\text{CO})_6$ on alumina appears to be rather simpler [34]. Infrared bands are attributable to the physisorbed complex, as well as chemically bound versions of $\text{Cr}(\text{CO})_5$ and $\text{Cr}(\text{CO})_4$ in which one CO group is thought to interact with an Al^{3+} centre. Decarbonylation is essentially complete by $\sim 100^\circ\text{C}$, and further heating eventually gives an average oxidation state of ~ 4.5 [32]. The tungsten analogue, however, gives rise to even more complex behaviour, with many infrared bands due to partially decarbonylated species being observed [34]. Three CO groups are reversibly lost after heating to $\sim 135^\circ\text{C}$ [35]. A second, higher-temperature CO loss is accompanied by H_2 evolution, except on highly dehydroxylated surfaces. The eventual oxidation state of the metal is estimated as $\sim 5.1\text{-}5.8$ [32,35]. These materials are EPR silent, indicating strong spin pairing interactions.

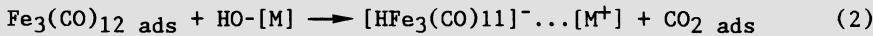
Chemisorption of $\text{Mo}(\text{CO})_6$ on magnesia is also considered to afford a $\text{Mo}(\text{CO})_5$ species initially [22]; the binding of this fragment has been proposed to be via nucleophilic addition of a surface oxide to yield $[(\text{OC})_5\text{Mo}(\text{CO}_2)]^{2-}$ which then forms a close ion pair with a magnesium ion [36]. Other, possibly oligomeric, metal carbonyl species are formed after heating to higher temperatures, while thermolysis at $\sim 250^\circ\text{C}$ results in complete decarbonylation.

A comparison may be made with $\text{Fe}(\text{CO})_5$, representing a rather less oxophilic metal. When a solution interacts with alumina at room temperature, an anionic cluster complex, $[\text{HFe}_3(\text{CO})_{11}]^-$, is formed on the surface [37]; this reaction is well known in basic solutions. At higher temperatures (120°C), 3 CO groups/Fe atom are evolved, but the metal is considered to retain a zero oxidation state, as indicated by temperature-programmed decomposition measurements [38]. (It must be added that oxidative addition reactions may occur at these partially decarbonylated centres which do not cause the evolution of a volatile product. In these circumstances, temperature-programmed decomposition experiments would not indicate the true oxidation state). At higher temperatures again ($>200^\circ\text{C}$), the remaining CO ligands are evolved, and the metal centres attain a mean oxidation number of 2. A similar reaction was observed on magnesia [37]. However, rather different chemistry seems to pertain when this oxide has been activated at high temperature. On this dehydroxylated surface, the addition of an oxide ion to a CO ligand to form $[(\text{CO})_4\text{Fe}(\text{CO}_2)]^{2-}$ has been proposed [39]. Decarbonylation is then not accompanied by oxidation, and instead aggregation to small metallic particles (diameter 1.2-1.4 nm) is observed [40].

3.2. Metal Carbonyl Cluster Complexes

The reactions of the trinuclear clusters $\text{M}_3(\text{CO})_{12}$, $\text{M} = \text{Fe}$, Ru , and Os , have been extensively studied and demonstrate a range of basic reactions. Taking the iron complex first, on contact with hydroxylated alumina or magnesia the cluster affords the same product as iron pentacarbonyl [37]; in this case nucleophilic addition to a CO ligand

will be initially involved prior to elimination of CO₂ resulting in Eq. (2).



The adsorbed complex interacts via the oxygen of the bridging CO group to a surface Lewis acid site. CO evolution proceeds at >40°C [38,41], and oxidation is evident (by H₂ evolution) at temperatures above 100°C. In contrast, Fe₃(CO)₁₂ is adsorbed as such on silica at room temperature [41]. Two species are apparent — one very similar to the molecular form and a second showing stronger interactions between the bridging CO ligands and the surface hydroxyl groups. Decarbonylation at up to 100°C is reversible, but at temperatures above 150°C, it appears that oxidation to Fe²⁺ occurs [40].

The chemisorption of the ruthenium and osmium analogues on silica follows a common, but different, pathway. The chemisorption of Ru₃(CO)₁₂ on silica was one of the first cluster systems investigated [42], but it was some years later before the initially formed species was identified as being due to the oxidative addition of a silanol group as in Fig. 2 [43,44].

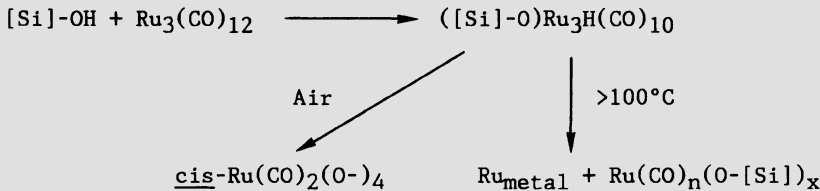


Figure 2. Reactions of Ru₃(CO)₁₂ on silica.

The bridging hydride has been confirmed by infrared spectroscopy, and analysis of the Ru K-edge EXAFS of the grafted cluster HRu₃(CO)₁₀(O-[Si]) indicates an essentially equilateral metal triangle with Ru-C, Ru-O, and Ru-Ru bond lengths of 1.90, 2.06, and 2.79 Å respectively [45]. Although the nuclearity of the cluster is maintained during the initial binding to the surface, this appears to be disturbed during subsequent thermal reactions [46]. Exposure to air causes decomposition to a new carbonyl-containing species; infrared and EXAFS results suggest that this has a cis-Ru(CO)₂(O-)₄ ligand arrangement. This is EPR silent and is probably a Ru^{II} centre, although the nature of the oxygen ligands is unclear. Heating to 200°C in vacuo affords 3-dimensional metal particles with the hcp structure of bulk ruthenium. There is some evidence for the coexistence of higher oxidation state centres in some of these materials.

This surface chemistry is oxide dependent. For example, the initial attack of the surface hydroxyl groups on magnesia has been shown to be on a carbonyl ligand [44]. Subsequent elimination of CO₂ from the complex affords [HRu₃(CO)₁₁]⁻. The oxygen atom of the bridging CO is electron rich in this complex and seems to engage in ion pair formation with an exposed magnesium cation. Another of the reaction

products from ruthenium carbonyl in basic solutions, namely, $[\text{Ru}_6(\text{CO})_{18}]^{2-}$, has also been observed on magnesia [47]. Trinuclear clusters (other than the unmodified adsorbed cluster) are not observed on alumina or titania [46,48]; rather the initially observed species are two $\text{Ru}(\text{CO})_2$ units together with a possible $\text{Ru}^{\text{IV}}\text{-CO}$ centre.

The chemisorption of $\text{Os}_3(\text{CO})_{12}$ on silica follows the same initial process as its ruthenium counterpart (Fig. 3) [49,50]; spectroscopic data obtained on this metal centre agree closely with those obtained for model complexes [45,49,50], one of which, $[\text{HOs}(\text{CO})_{10}(\text{OSiEt}_3)]$, represents a particularly close relationship to the grafted cluster and has been characterised by X-ray diffraction [51]. This material is stable up to $\sim 150^\circ\text{C}$, at which point further oxidation occurs to form a mixture of $\text{Os}^{\text{II}}(\text{CO})_n$ centres where $n = 2$ and 3 [50,52]. The chemistry on alumina is similar. The grafted sample " $\text{HOs}_3(\text{CO})_{10}(0\text{-[Al]})$ " [49,50,52] has been the subject of much study. Direct observation of the hydride by infrared spectroscopy was not possible due to absorptions of the support itself [45]. However, the Raman spectrum of this cluster [54] exhibits bands attributable to Os-Os stretching modes at frequencies most closely comparable to those of model compounds with bidentate oxygen ligands [45]. So an alternative structure for this species has been proposed (Fig. 3).

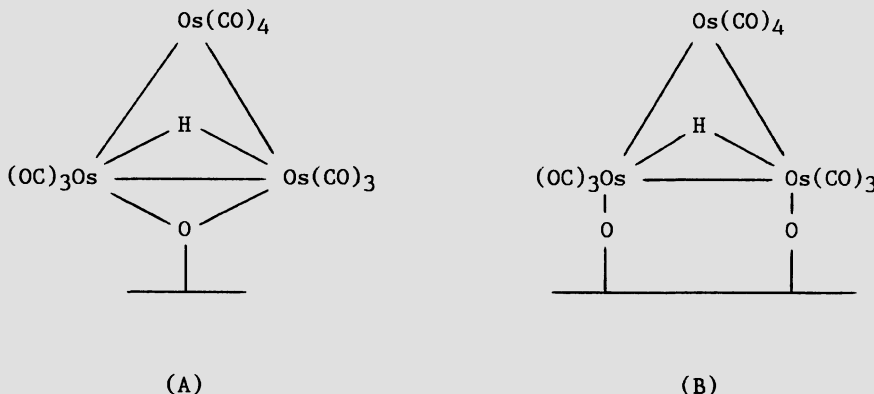


Figure 3. Structures proposed for the chemisorption products of $\text{Os}_3(\text{CO})_{12}$, (A) on silica and (B) on alumina.

Os L(III) edge EXAFS results on it could be interpreted on this model, which would also give a virtually equilateral metal triangle. Oxidation of the cluster by the support occurs more readily on alumina than silica and also affords $\text{Os}^{\text{II}}(\text{CO})_n$ [$n = 2$ and 3] centres [49,50,52]. There have been widely differing proposals concerning the nature of these metal sites, but the balance clearly indicates a coordination site containing only oxygen and the CO ligands with no direct osmium-osmium bonding [49,50,55-57]; these units are detectable by electron diffraction [53,58] and may well form some sort of aggregate. Weak EPR signals are also displayed (due to 1-2 % of the metal content) which

may be due to small proportions of Os^I and Os^{III} fragments [59]. The chemistry of osmium carbonyl has been less intensively studied on titania, but appears to follow a similar pattern to that on alumina, although the grafted cluster is less stable [51,52]; published evidence for the existence of such a cluster on magnesia is rather less clear [60]. The chemisorbed form is very probably highly dependent upon the pretreatment of the magnesia, and indeed, an alternative report of the presence of $[Os_3(CO)_{11}]^{2-}$ seems in keeping with the basicity of this support [61]. Reaction with oxygen affords a stable cis-Os^{II}(CO)₂(O-[Mg])₄ site.

Rather different chemistry is displayed by small rhodium carbonyl clusters on the surfaces of these oxides. Much of this is dominated by the same equilibria as in solution, between $[Rh(CO)_2X]_2$, $Rh_4(CO)_{12}$, and $Rh_6(CO)_{16}$. As in solution, the species observed are very sensitive to the acidity and water content of the reaction media. $Rh_4(CO)_{12}$ is substantially converted to $Rh_6(CO)_{16}$ on a dried silica surface [62]; this can be inhibited by a CO atmosphere. Treatment with water and air affords metallic particles and Rh^I sites, respectively [62,63]. A similar sensitivity to pretreatment is observed on an alumina surface. The proportions of the initially observed species also vary with the degree of hydroxylation of the alumina, with these being principally $Rh_6(CO)_{16}$ and Rh^I(CO)₂ sites (Fig. 4) [62,64-66]; this provides an active water gas shift catalyst [44].

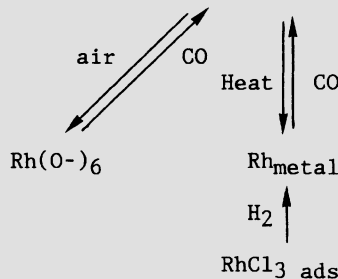


Figure 4. Reaction scheme for rhodium carbonyls on alumina.

As on silica, there is no clear evidence at present of direct Rh-O binding in a chemisorbed rhodium cluster similar to that observed for $M_3(CO)_{12}$ ($M = Ru, Os$) on silica. Two different $[Al]-ORh^I(CO)_2$ sites have been proposed, with a fourth coordination site in a typical $4d^8$ square planar complex being occupied by either a surface hydroxyl group or by a water molecule [44]. Exposure of these species to air causes a (reversible) decarbonylation [66-68]. Several polynuclear species have been proposed for this decarbonylated material [67,68] but Rh K-edge EXAFS and diffuse reflectance ultraviolet-visible data indicate only oxygen atoms as near neighbours, with no metal-metal bonds being retained; there may, however, be more remote ($>3.5 \text{ \AA}$) intermetallic

distances [66]. These clusters therefore provide a route to surface coordination chemistry without any complications due to halide ions.

Thermolysis of the grafted Rh(I) centres gives rise to metallic rhodium particles. Indeed, there is a direct connection with the chemistry of conventionally prepared heterogeneous catalysts. Small 3-dimensional metal particles have been identified after hydrogen reduction of adsorbed rhodium trichloride, but chemisorption of CO causes the formation of $\text{Rh}^{\text{I}}(\text{CO})_2$ centres [69]. This disruption of the metal particles is of clear consequence to the use of such chemisorption measurements in surface area estimations, but also demonstrates that the same coordination sites can be generated from conventional catalyst preparation procedures as are obtainable from metal carbonyl clusters. A slightly different $\text{Rh}^{\text{I}}(\text{CO})_2$ site was proposed on the basis of EXAFS results from the conventional catalyst [69]. This was a five-coordinate complex bound to three surface sites. Similar analysis on the cluster-derived analogue had considerable uncertainty in the Rh-O coordination number estimation [66]. There may be a variety of four- and five-coordinate centres formed after different sample histories.

3.3. Heterometallic Carbonyl Cluster Complexes

Recently there has been considerable interest in the reactions of mixed-metal cluster complexes with oxide supports. To a large extent this emanates from the established phenomena within the field of heterogeneous catalysis which show that unusual activities and selectivities can be observed for supported "alloy" catalysts [70]. The development of the solution chemistry of heterometallic cluster complexes has reached the stage of providing several series of related complexes which can be used as the basis of systematic studies. Indeed, the complexes $\text{Co}_2\text{Rh}_2(\text{CO})_{12}$ and $\text{Co}_3\text{Rh}(\text{CO})_{12}$ were reacted with silica and alumina some years ago with the aim of generating new alloy catalysts [71]. For the former complex in particular, higher dispersions were obtained than for the conventional preparation from hydrated cobalt(II) nitrate and rhodium(III) chloride.

One of the series of related clusters is provided by some bimetallic tetranuclear derivatives of $\text{Ru}_4\text{H}_{n+2}(\text{CO})_{13-0.5n}$ ($n = 0$ and 2). The chemistry of $\text{RuOs}_3\text{H}_2(\text{CO})_{13}$ on alumina is presented in Fig. 5 [72]. In the initial reaction the oxide acts as a Brønsted base to generate the conjugate base of the cluster. Treatment with synthesis gas at elevated temperatures causes the transformation to a second tetranuclear cluster which can be extracted into solution and identified. This trihydrido cluster is quite stable on the alumina surface, decomposing at temperatures above 100°C in vacuo and only at 200°C under CO/H_2 .

The same Brønsted base behaviour has been observed on magnesia using the hydrido clusters $\text{FeM}_3\text{H}_2(\text{CO})_{13}$ ($M = \text{Ru}$ and Os) and $\text{FeCo}_3\text{H}(\text{CO})_{12}$ [73]. At room temperature the corresponding mono-anionic clusters were observed with essentially no disproportionation to other cluster species. No evidence of a strong Lewis acid-base interaction between the anions and the support was detectable by infrared

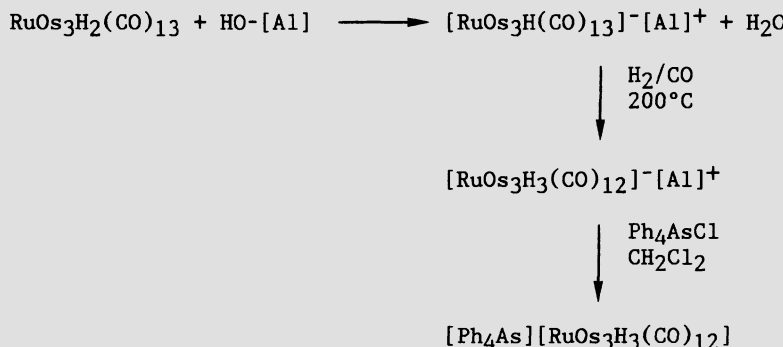


Figure 5. Chemistry of $\text{RuOs}_3\text{H}_2(\text{CO})_{13}$ on alumina.

spectroscopy. Generally interaction with the oxygen of a CO group causes the C-O stretching frequency of that group to be lowered; direct interaction with the metal centre results in a general increase in the frequencies of all the C-O stretching modes. Thermal decomposition of the adsorbed $[\text{Fe}_3\text{Co}(\text{CO})_{12}]^-$ at 50°C causes evolution of CO and H_2 . The hydrogen is thought to result from a stoichiometric water gas shift reaction with the CO_2 being adsorbed as carbonate on the surface of the basic support. Methane is evolved at temperatures above 200°C . The thermal decomposition of the supported $[\text{FeM}_3\text{H}(\text{CO})_{13}]^-$ ions differs in that little, or no, CO is evolved. These two species are more stable, but at temperatures above 100°C only hydrogen is lost from these materials. Again, at temperatures above 200°C methane is also formed. Metal particles are observed in the resulting materials, again indicating that evolution of hydrogen may not always be equated with oxidation of the metal centres.

The nature of the metal particles produced by the hydrogenation (at 400°C) of these supported anions has been compared with those using mixtures of homometallic clusters as precursors [74]. Co-adsorption of $\text{Fe}_3(\text{CO})_{12}$ and $\text{M}_3(\text{CO})_{12}$ ($\text{M} = \text{Ru}$ and Os; Fe/M ratio 1:3) onto magnesia, followed by hydrogen reduction resulted in small particles of the heavier element (ruthenium or osmium). The iron was probably dispersed in an oxidised form. In contrast, parallel treatment of adsorbed $[\text{FeM}_3\text{H}(\text{CO})_{13}]^-$ gave rise to bimetallic particles of a narrow size distribution ($10\text{-}15$ Å) and of the same metal composition as the precursor cluster. Similarly, hydrogenation of $\text{HFeCo}_3(\text{CO})_{12}/\text{MgO}$ also gave rise to bimetallic particles. Evidently, the preexistence of the heterometallic unit favours the formation of true alloy particles.

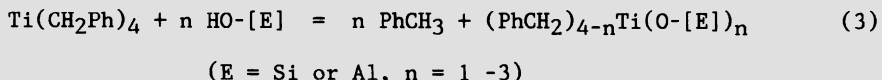
This effect is probably not universal and may depend upon the support and reaction conditions employed. The chemistry of $\text{FeOs}_3\text{H}_2(\text{CO})_{13}$ on alumina may be used as an illustration of this [75]. As cited above for the analogous RuOs₃ derivative (Fig. 5), treatment with CO/H₂ appears to form adsorbed $[\text{FeOs}_3\text{H}_3(\text{CO})_{12}]^-$. Thermolysis at 270°C then causes disruption of the cluster units into separated oxidised centres. The reactions of $\text{RhOs}_3\text{H}_2(\text{CO})_{10}(\text{acac})$ on alumina are also instructive. This cluster is known to fragment on treatment with

CO {affording $\text{Rh}(\text{CO})_2(\text{acac})$ and $\text{Os}_3\text{H}_2(\text{CO})_{10}$ }, and a similar effect is observed on alumina after exposure to synthesis gas at 100°C; the species characteristic of these separated units on alumina, viz. " $\text{Os}_3\text{H}(\text{CO})_{10}\{\text{O}-[\text{Al}]\}$ " and $\text{Rh}^{\text{I}}(\text{CO})_2$ centres (Figs. 3 and 4) were observed. [A parallel effect has also been reported for the reaction of $\text{FeOs}_3\text{H}_2(\text{CO})_{13}$ with silica with $\text{Os}_3\text{H}(\text{CO})_{10}\{\text{O}-[\text{Si}]\}$ being formed [76]]. Treatment at higher temperatures causes the formation of the oxidised $\text{Os}(\text{CO})_n$ ($n = 2$ and 3) centres and also rhodium particles. The catalytic activity displayed by this material for synthesis gas conversion seems to be entirely due to the rhodium particles.

3.4. Transition Metal Hydrocarbyl Complexes

The basic reaction between a metal-alkyl or -allyl complex is an electrophilic cleavage by a hydroxyl group causing elimination of the corresponding alkane or alkene, with this coordination site being replaced by the metal-surface link. This would suggest that the chemistry might be relatively simple by comparison to the more varied reaction classes by which a metal carbonyl might be chemisorbed. However, there may also be subsequent reactions at what may well be coordinatively unsaturated centre which give rise to some divergences in behaviour and difficulties in interpretation.

The earliest chemistry of the type has been connected with alkene polymerisation catalysis and has been reviewed [1,2]. To form derivatives of original Ziegler-Natta catalysts, hydrolysis of complexes such as $\text{Ti}(\text{CH}_2\text{Ph})_4$ on several hydroxylated surfaces has been employed [77,79]:



The mean degree of hydrolysis is dependent upon the degree of hydroxylation of the surface. Higher support dehydration temperatures reduce both the quantity of complex bound on the surface and also the degree of hydrolysis for those titanium centres bound. Titanium(III) centres can be produced in a variety of ways, most effectively by ultraviolet photolysis under hydrogen. However, these reduced metal ions seem to adopt a range of coordination spheres.

Many materials have been prepared by general reaction processes of the same type as Eq. 3, which display interesting catalytic activity. As an example of this, active propene metathesis catalysts may be derived from the interaction of $\text{M}_2(\text{CH}_2\text{SiMe}_3)_6$, $\text{M}_2(\text{CH}_2\text{CMe}_3)_6$ ($\text{M} = \text{Mo}$ and W), and WMe_6 with silica and alumina [80]. However, the nature of the metal centres in the activated catalysts remains uncertain.

Indeed, considerable effort is required to obtain a reasonably precise description of such sites. This may be illustrated by the reported work on the interaction of $\text{Rh}(\text{allyl})_3$ with silica [81,82] (Fig. 6). The initial chemisorptive reaction involves the (probable) electrophilic cleavage of one Rh-allyl linkage to afford a yellow material containing the coordination sphere $(\text{allyl})_2\text{RhO-[Si]}$, as

indicated by chemical degradation and spectroscopic results [81-84]. Although there is general agreement over the formulation of this species (allowing for the doubt in the number of surface atoms coordinated to the rhodium centre), there are wide divergences of view over the subsequent reaction products. The scheme in Fig. 6 presents a possible assessment of the published evidence. Exposure of such a material to CO bleaches the silica and results in a new Rh(CO)₂ unit [84].

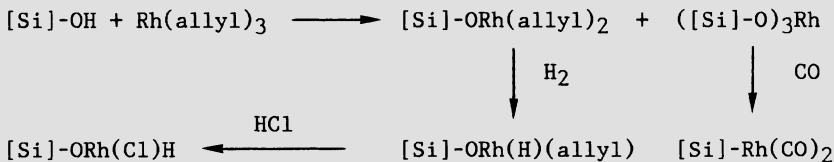


Figure 6. Some chemistry of Rh(allyl)₃ on silica.

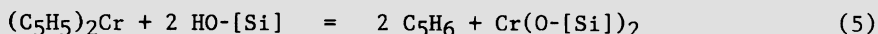
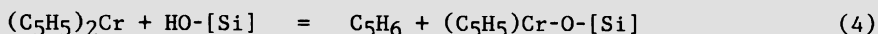
It is suggested that a proportion of the rhodium sites undergo total hydrolysis to afford a centre formulated as ([Si]-O)₃Rh and that it is this which reacts with CO to form the rhodium(I) dicarbonyl centre. The implication of this would be that it the total hydrolysis product, rather than ([Si]-O)Rh(allyl)₂ which exhibits the chromophore in the visible region.

Hydrogenation of the first silica-bound complex proceeds at room temperature to give a second complex variously reported as (allyl)RhH(O-[Si]) [81-83] and supported rhodium metal [84]. It appears that mixtures of rhodium species can be generated and that these are strongly dependent upon the mode of preparation. Any adventitious Rh(allyl)₃ seems to be more readily reducible and this may account for these divergences in interpretation. The species (allyl)RhH(O-[Si]) exhibits infrared vibrations at 2010 and 1800 cm⁻¹, which have been assigned to rhodium-hydride stretching modes. The intensity of the higher-frequency band decreases less rapidly when this material is exposed to an atmosphere of carbon monoxide [85], but the ramifications of this are uncertain. Exposure of this material to HCl gas is generally considered to result in a new rhodium(III) centre, formulated as Rh(H)Cl(O-[Si]). Several of these materials have interesting catalytic properties including alkane/D₂ exchange and methane chlorination, but the natures of the rhodium coordination spheres are still incompletely described.

Hydrolysis of metal-allyls has been widely employed as a means of introducing transition elements onto oxide surfaces [1]. There has been an extensive study of the use of chromium derivatives as precursors to alkene polymerisation catalysts. For example, both Cr(allyl)₃ and Cr₂(allyl)₄ are rapidly adsorbed on silica and silica-alumina and have afforded active catalysts [86]. The materials from each complex behaved in a similar way, as expected by the ready conversion of the Cr(III) species to the Cr(II) dimer. When the chemisorbed Cr(allyl)₃ on silica is exposed to CO, infrared bands attributable to Cr(CO)₆ are rapidly formed [87]. This suggests that a proportion of the metal is in a

highly reactive, low oxidation state form. Low-temperature adsorption of CO was also used to probe the presence of Cr(II) sites. The interactions of $\text{Cr}_2(\text{allyl})_4$ and $\text{Cr}(\text{allyl})_3$ with silica and alumina have been studied by a range of analytical and spectroscopic techniques [88]. There were significant differences in behaviour of different samples. For example, reaction of the chromium(II) dimer with both partially dehydroxylated alumina and silica resulted in the loss of two allyl groups per chromium; subsequent temperature-programmed decomposition experiments under hydrogen gave a single main peak at 326°C for the elimination of the majority of the remaining organic ligands as propene and propane, with small amounts of apparent hydrogenolysis also occurring. It appears though that the resulting $\text{Cr}(\text{allyl})(\text{O}-[\text{E}])_x$ species are support dependent. The alumina version exhibits electronic absorptions at 470 and 610 nm (it is also EPR active), whereas a single absorption between 800 and 200 nm is observed for the silica-supported complex at 553 nm. This was explained in terms of the latter material maintaining Cr(II) sites still in a strongly bonded dimer. On alumina, however, oxidation to weakly interacting Cr(III) centres was proposed.

Polymerisation catalysts were also prepared using chromocene as the precursor [89]. There appear to be two sequential hydrolysis processes on silica [89,90]:



Higher degrees of hydroxylation allow the presence of adjacent hydroxyl sites, and so the hydrolysis of both cyclopentadienyl groups (liberating cyclopentadiene) becomes possible. It appears though that having closely spaced (vicinal or geminal) silanols has a deleterious effect on the catalytic performance. The catalysts derived from chromocene are more thermally stable than those formed from chromium allyls, and this may explain their greater observed catalytic activity [86]. Polymerisation catalysts may also be prepared from bis(indenyl)- and bis(fluorenyl)-chromium(II) [91]. The ligands in these benzocyclopentadienyl derivatives are poorer electron donors and sterically more crowded. The latter feature may account for their still higher thermal stability; the reduction in catalytic activity may be due to both factors.

The stoichiometry of the reaction between alumina and $\text{Mo}(\text{allyl})_4$ at 0°C is as follows [92,93]:



This species acts as a propene metathesis catalyst even at 0°C. Apparently clean oxidation, hydrogenation, and chlorination processes can be achieved from this material to afford new metal sites. The same coordination centre as shown in Eq. 6 can also be formed from $\text{Mo}_2(\text{allyl})_4$ [94]. In that case adsorption at 0°C did not cause loss of propene; rather the molybdenum-molybdenum quadruple bond is considered

to be broken with each metal being oxidised to Mo(IV). Under hydrogen this material shows a temperature-programmed decomposition maximum at 235°C, with ethylene being the predominant product; this differs markedly from the chemistry shown by the chromium containing materials (v.s.). The molybdenum dimer also reacts with the hydroxyl groups (rather than the siloxane units) on a silica surface at 0°C [95]. In this report, the stoichiometry of the grafting reaction was found to vary between silica preparations. On a higher-surface-area support (285 m²/g), an analogous reaction to that observed on alumina was noted (Fig. 7). However, on another sample, one allyl ligand per molybdenum is also lost, apparently forming an intermediate oxidation state in (allyl)Mo(III)(O-[Si])₂; the oxidation of the metal was accompanied by the evolution of hydrogen gas. Under hydrogen, the temperature-programmed desorption of the Mo(III) species gives a peak at 235°C, with propane and ethane now the major components; much less propane was derived from the Mo(IV) species, indicating a different reactivity towards hydrogen. This latter material has been hydrogenated at higher temperatures (580°C) to yield molybdenum(II) sites, a proportion of which (~0.6) have other molybdenum in close proximity, as indicated by analysis of the Mo K-edge EXAFS data recorded at a synchrotron radiation source (Fig. 7) [96]. Oxidation products of these materials act as selective propene oxidation catalysts (to acraldehyde and acetaldehyde).

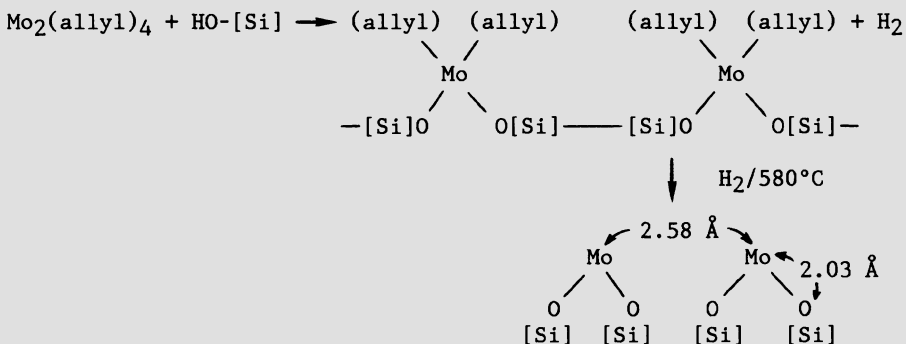
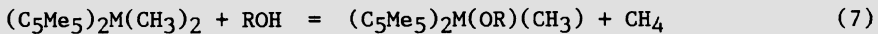


Figure 7. Structures proposed for metal centres derived from Mo₂(allyl)₄.

An interesting chemistry is displayed by the highly active propene hydrogenation and ethylene polymerisation catalysts prepared by supporting the organoactinide complexes, (C₅Me₅)₂MMe₂ (M = U or Th) on alumina [97]. In solution these complexes undergo a ready alcoholysis as follows:



and this might seem to represent a good model for an electrophilic cleavage reaction at a surface hydroxyl group. However, careful ^2H labelling experiments demonstrated that the equivalent surface reaction was only one of three alternative mechanisms for the elimination of methane on interaction with the surface (Fig. 8) [98,99]. The other two are essentially intramolecular processes occurring on the alumina surface in which the metal-bound methyl group abstracts an extra hydrogen either from a ring methyl group or from the other metal-methyl.

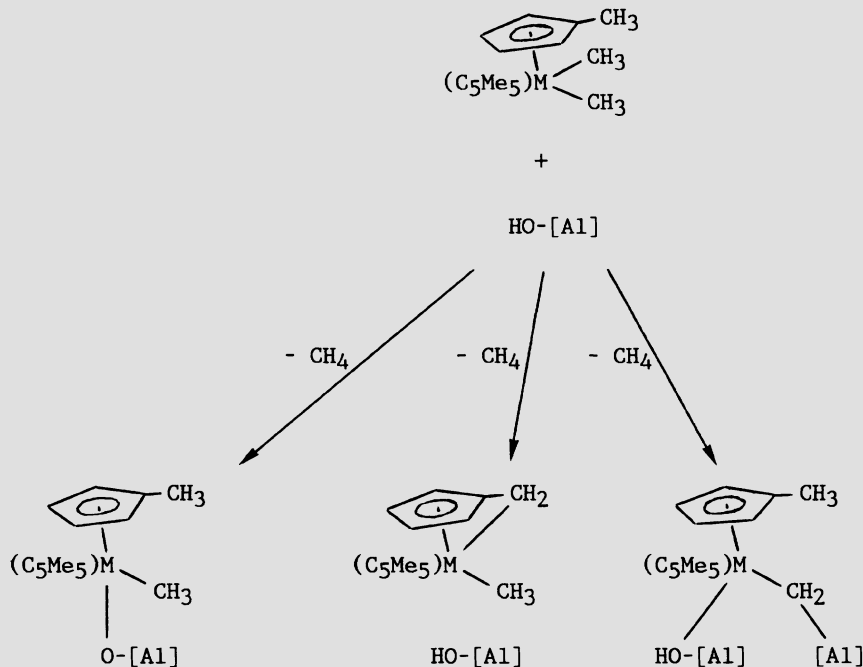


Figure 8. Adsorption processes for $(\text{C}_5\text{Me}_5)_2\text{MMe}_2$ ($\text{M} = \text{Th}$ and U) on alumina.

In the latter case this leads to the formation of an alkylidene complex; the methylene group is thought to bridge between the actinide and aluminium.

However not all the available methyl groups evolve methane; this is especially so on a dehydroxylated alumina. The diamagnetic thorium species were studied by ^{13}C CP-MAS NMR to provide further evidence about the surface organometallic centres [100]. Only the major species could be observed due to sensitivity limitations, but the results clearly demonstrated that on the dehydroxylated alumina there is a transfer of a methyl group from thorium to aluminium. The chemical

shift observed for this carbon indicates that in all probability the transfer is complete, and does not result in a Th-Me-Al bridge. One of the possible structures for the surface complexes is presented in Fig. 9a.

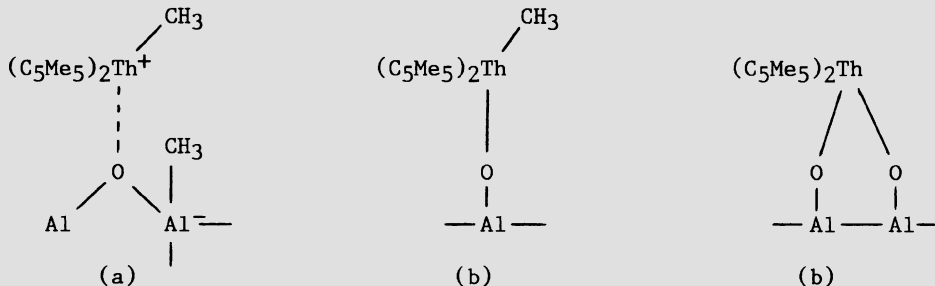


Figure 9. The probable major surface complexes formed by $(C_5Me_5)_2ThMe_2$ on (a) essentially and (b) partially dehydroxylated alumina.

This result is of considerable significance and suggests that, particularly on supports activated at relatively high temperatures (perhaps $>500^\circ C$), transfer of a hydrocarbyl group from electropositive transition metal centres to exposed support cations must be considered. Certainly these reactions have their counterparts in solution organometallic chemistry. Ignoring them may lead to erroneous conclusions based upon the sole expectation of protonolysis of M-C bonds as the surface reaction. A further point is the clear distinction between the major species formed on dehydroxylated and partially dehydroxylated surfaces (Fig. 9).

4. LIGAND-TETHERED ORGANOMETALLIC COMPLEXES

In many instances the tethering of metal complexes to ligand-functionalised oxides is approached solely as a means of transferring the phase of the catalytic species from a homogeneous to a heterogeneous system. There is a substantial literature in this regard, much of which has been reviewed in the monographs by Yermakov *et al.* [1] and Hartley [2]. For our purposes, this approach will be only outlined with more attention being paid to the special chemistry of a ligand-functionalised oxide.

Tethering of analogues of homogeneous rhodium(I) catalysts can be achieved by either of the two routes indicated in Fig. 10 [101]. In principle, each method involves competition reactions. If the surface is prefunctionalised then the complex has both the hydroxylated surface and the pendant ligand available for reaction. (The concentration of the former may be reduced by subsequent silylation with, e.g., Me_3SiCl). When the reverse sequence is adopted then the precursor complex may react with the surface either at the silicon centre or at the metal coordination sphere. The chemistry of such systems however

may be controlled to afford working heterogeneous catalysts [17] for reactions including alkene hydrogenation [102] and hydroformylation [103]. Rhodium(I) complexes tethered by phosphines with varying alkyl chain length [ligands of type such as $(EtO)_3Si(CH_2)_nPPh_2$, $n = 1 - 6$] were prepared and tested for their activity towards alkene hydrogenation [104] and hydrosilylation [105]. In both cases complexes tethered by ligands with only one methylene group between phosphorus and silicon were the most active. This was thought to be due to the reduction in the tortional mobility of the tethered complex on the surface due to the very short chain length which may prevent coordinatively unsaturated rhodium centres from forming an inactive dimer. This site isolation effect has also been used to engineer a Rh(I)-Cu(II) based heterogeneous catalyst for the oxidation of hex-1-ene to hex-2-one [106]. At high coverages of thiol groups on silica prepared using $(MeO)_3Si(CH_2)_3SH$ as the functionalising reagent, reaction with $[Rh(CO)_2(solv)]_2BF_4$ afforded dimers of the form $[(OC)_2Rh(SR)_2Rh(CO)_2]$; analogues in solution were catalytically inactive for the process in question. However at low surface concentrations of thiol groups infrared bands attributable to a monomeric complex, formulated as $[Rh(CO)_2(solv)(SR)]$, were prevalent, and under these conditions the materials so formed provided heterogeneous catalysts. This seems to be a good example of the possible benefits of using tethered complexes since no homogeneous analogue of this monomeric Rh(I)-thiolate complex had been prepared.

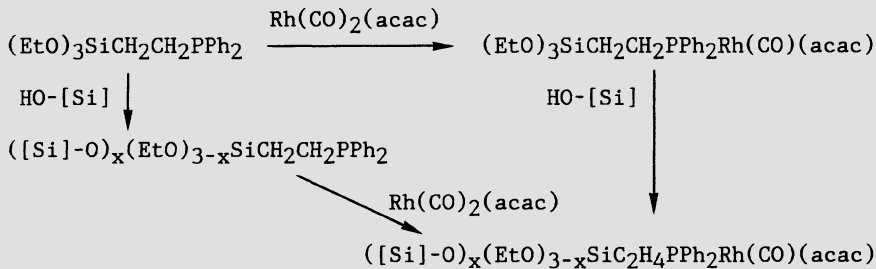


Figure 10. Typical methods for the tethering of transition metal complexes via pendant ligands to oxide surfaces.

This isolation aspect has also been utilised in the chemistry of tethered ruthenium clusters [107,108]. Both $Ru(CO)_4L$ and $Ru_3(CO)_9L_3$, $L = PPh_2CH_2CH_2Si(OEt)_3$, were prepared and reacted with a high-surface-area silica. The tethered complexes were thoroughly characterised and an important part of this process was the recording of ^{13}C , ^{29}Si and ^{31}P NMR spectra [108]; these were quite consistent with the coordination centre remaining unchanged as the silicon centre was hydrolysed by silanol groups. Irradiation of the anchored trimeric complex under CO resulted in the formation of $Ru(CO)_4\{PPh_2CH_2CH_2-[Si]\}$, spectroscopically indistinguishable from that prepared from $Ru(CO)_4L$. However, the two different preparations of the tetracarbonyl complex lead to different distributions on the surface. Irradiation of the

photochemically derived complex causes the reconstitution of the trinuclear complex $\text{Ru}_3(\text{CO})_9\{\text{PPh}_2\text{CH}_2\text{CH}_2\text{-[Si]}\}_3$, indicating that the three mononuclear centres were still in close proximity. However, irradiation of the material prepared from $\text{Ru}(\text{CO})_4\text{L}$ (unlike solution chemistry) does not afford the cluster. Here the complexes are isolated and immobilised and so cannot aggregate at least at low temperatures.

However, interaction of complexes with functionalised oxides does not always occur without involvement of surface sites in the metal coordination chemistry. For example, the interaction of $\text{Rh}_6(\text{CO})_{16}$ with phosphinated silica at ambient temperatures can result in the tethering of hexanuclear units [109]. Indeed, the complex $\text{Rh}_6(\text{CO})_{15}\text{L}$ ($\text{L} = \text{PPh}_2\text{C}_2\text{H}_4\text{Si(OEt)}_3$) can be specifically bound to a silica surface [110]. But in the presence of oxygen the cluster fragments to form Rh(I)(CO)_2 sites in which there may be a direct Rh-O surface link [111].

The chemistry of one such interaction has been monitored by a combination of spectroscopic methods. Interaction of the unsaturated cluster $\text{Os}_3\text{H}_2(\text{CO})_{10}$, with $\text{PPh}_2\text{C}_2\text{H}_4\text{-[Si]}$ gives an adduct with high specificity (Fig. 11) [112,113]. Mild thermolysis causes the loss of one CO group to yield a material considered to be a derivative of the original unsaturated cluster, viz. $\text{Os}_3\text{H}_2(\text{CO})_9\{\text{PPh}_2\text{C}_2\text{H}_4\text{-[Si]}\}$. This material acts as a catalyst for alkene hydrogenation and isomerisation [114,115]. Formulation of this structure was largely based upon infrared comparisons with analogues of the type $\text{Os}_3\text{H}_2(\text{CO})_9\{\text{PPh}_2\text{R}\}$.

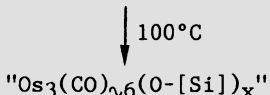
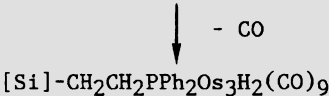
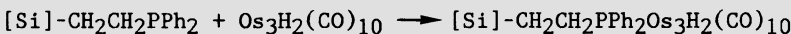


Figure 11. Reactions of $\text{Os}_3\text{H}_2(\text{CO})_{10}$ with phosphinated silica.

These models have ^{31}P chemical shifts which are 20 ppm downfield of that recorded for the surface-bound material [116]. It appears that the nonacarbonyl complex is formed but rapidly undergoes some reaction with the support to alleviate its unsaturation. Evidence for this comes from analysis of its Os L(III) EXAFS data which shows coordination to carbon (1.87 Å), oxygen (2.23 Å), phosphorus (2.36 Å), as well as the metal-metal bonds (2.82 Å) [117]. Of several models synthesised, only one at present provides similar infrared and ^{31}P NMR data to that observed for the surface species. This was one isomer of the complex $\text{Os}_3\text{H}_2(\text{CO})_9(\text{OAc})(\text{PPh}_3)$ (Fig. 12a) [118]. Although an alternative with only one oxygen atom involved in the new link to the oxide cannot be

eliminated, the structure in Fig. 12a represents the closest spectroscopic match with currently available model compounds.

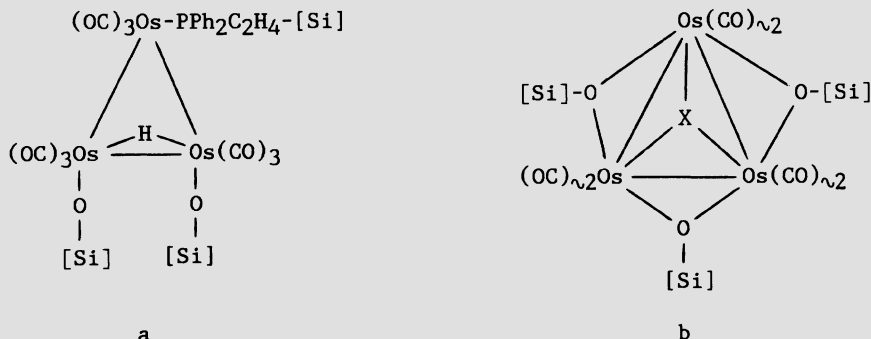


Figure 12. Structure proposed for a) the species $\text{Os}_3\text{H}_2(\text{CO})_9(0-\text{[Si]})(\text{PPh}_2\text{C}_2\text{H}_4-\text{[Si]})$ and b) the thermolysis product at 100°, X is vacant. On $[\text{Si}]-\text{C}_3\text{H}_6\text{SH}$, X = S.

This surface interaction is one stage in the transfer of the cluster from the initial attachment site of the phosphine onto the surface [119]. The EXAFS data obtained at the Os L(III) edge of the thermolysis product indicated an absence of phosphorus coordination. An approximate coordination sphere at osmium of $(\text{CO})_2(0)_2\text{Os}_2$ was derived. Two possible arrays maintain a metal connexity of 2 are chains and triangles. A structure based on the latter is presented in Fig. 12b. In that structure the site "X" is largely vacant. It is interesting to compare this with the situation for the pyrolysis product of $\text{Os}_3\text{H}(\text{CO})_{10}\{\text{SC}_3\text{H}_6-\text{[Si]}\}$. In that material the site "X" is adopted by sulphur. Hence in the latter material at least the surface functionalisation has modified the chemistry of the cluster even during the interaction with the surface.

Retarding such reactions with the surface can be achieved by use of cluster-stabilising bridging ligands. Phosphinidene ligands have been widely used in this regard, and one such complex, $\text{Ru}_3\text{H}_2(\text{CO})_9\{\text{PCH}_2\text{CH}_2\text{Si}(\text{OEt})_3\}$ has been tethered to several oxide supports [120] and its structure before and after tethering established by Ru K-edge EXAFS [121]. This showed the metal triangle on the anchored complex to be isocean in nature with one shorter Ru-Ru bond (2.75 Å) and a pair of longer hydride-bridged metal-metal distances (2.94 Å). The cluster centre is stable at 70°C on the alumina surface.

5. DISCUSSION

It is clear from these results that a great variety of new coordination sites can be generated by the interaction of organotransition metal complexes with oxide supports. Under some conditions this may also be used as a method of preparing small metal particles with a topology and

composition not attainable with conventionally prepared heterogeneous catalysts; the production of true alloy particles of narrow size distribution from heterometallic clusters is good evidence of this [74].

Indeed, there is a unity with the field of heterogeneous catalysis. As evidence of this, similar (or identical) Rh^I(CO)₂ sites can be prepared either by CO chemisorption on preformed metal particles [69] or by decomposition of rhodium carbonyl clusters on the oxide surface [62-66]. Further evidence for this can be seen from the observation of metal carbonyl clusters under operating supported metal catalysts. For example, ruthenium catalysts for the conversion of synthesis gas to polymethylene [122] afford mixtures of cluster species at elevated temperatures (120°C) and pressures (1000 atm) [123]. One of these was Ru₃(CO)₁₂, but the others appear to be ill-characterised. A similar observation has been recently reported for Ru/MgO and Os/MgO synthesis gas conversion catalysts [124]. On this basic support, two anionic clusters were isolated, viz. [Ru₆C(CO)₁₆]²⁻ and [Os₁₀C(CO)₂₄]²⁻, which may be synthesised in solution by thermolysis in basic or reducing media. It is unclear whether these clusters are actually effecting the catalysis. They may instead, as highly stable species, be formed in a side reaction.

The schemes in the Figures also indicate some uncertainty concerning the precise nature of most of the coordination sites of the supported complexes. This can only be approached when a total product analysis is combined with detailed spectroscopic studies of the reaction at the surface. A good example of this is the ¹³C nmr study of the binding of (C₅Me₅)₂ThMe₂ on dehydroxylated alumina [100]. This revealed the transmethylation reaction between thorium and aluminium which accounted for the "missing" methyl groups in the supported complex. However, the techniques now available, e.g., FTIR, CP-MAS NMR, EXAFS, and HREM make it possible to tackle what were hitherto intractable problems. Even so it is, at the least, extremely difficult to establish the precise surface sites which bind the surface organometallic complex, due largely to the heterogeneity of the surfaces of the high-surface-area oxides generally used in studies so far. This can only be improved by carrying out parallel experiments on supports of a high degree of crystallinity, such as clean single crystals.

Surface organometallic chemistry is a relatively new field. Presently we are establishing the ground rules and as they are being established they appear to be very similar to those already delineated in mainstream organometallic chemistry. This gives a confidence that synthetic strategies devised with that background (albeit modified to account for the chemistry of the oxide surface) will continue to provide new materials with diverse catalytic properties. The controlled synthesis of such catalysts should allow the reaction processes to be understood at a molecular level which should ultimately result in precise prescriptions for catalytic sites.

6. REFERENCES

1. Yu.I. Yermakov, B.N. Kuznetsov, and V.A. Zakharov, Catalysis by Supported Metal Complexes, Elsevier (1981).
2. F.R. Hartley, Supported Metal Complexes, Reidel (1985).
3. J.R. Anderson, Structure of Metallic Catalysts, Academic (1975).
4. M.L. Hair, p. 25 in reference 5, and references therein.
5. Silanes, Surfaces and Interfaces, (Ed. D.E. Leyden), Gordon and Breach (1986).
6. D.W. Sindorf and G.E. Maciel, J. Am. Chem. Soc. 105, 1487 (1983); J. Phys. Chem. 87, 5576 (1983).
7. H. Knözinger and P. Ratnasamy, Catal. Rev. Sci. Eng. 17, 31 (1978).
8. C. Naccache, Y. Kondratoff, R.C. Pink, and B. Imelik, J. Chim. Phys. 63, 341 (1966).
9. M.L. Myers and P.G. Wahlbeck, J. Phys. Chem. 87, 1008 (1983).
10. H.P. Boehm, Discuss. Faraday Soc. 52, 264 (1971).
11. J.A.R. van Veen, F.T.G. Veltmaat, and G. Jonkers, J. Chem. Soc., Chem. Commun., 1656 (1985).
12. M. Che, C. Naccache, and B. Imelik, J. Catal. 24, 328 (1972).
13. A.J. Tench and R.L. Nixon, Trans. Faraday Soc. 63, 2254 (1967).
14. A. Zecchina, M.G. Lofthouse, and F.S. Stone, J. Chem. Soc., Faraday Trans. 1 71, 1476 (1975).
15. S. Coluccio, A.J. Tench, and R.L. Segall, J. Chem. Soc., Faraday Trans. 1 75, 1769 (1979).
16. E. Guglielminotti, S. Coluccia, E. Garrone, L. Cerroti, and A. Zecchina, J. Chem. Soc., Faraday Trans. 1 75, 96 (1979).
17. L.L. Murrell, in Advanced Materials in Catalysis, (Eds. J.J. Burton and R.L. Garten), p. 236, Academic (1977).
18. G.S. Caravajal, D.E. Leyden, and G.E. Maciel, p. 283 in reference 5.
19. L. Bemi, H.C. Clark, J.A. Davies, C.A. Fyfe, and R.E. Wasylishen, J. Am. Chem. Soc. 104, 438 (1982).
20. E.S. Davie, D.A. Whan, and C. Kemball, J. Catal. 24, 272 (1972), and references therein.
21. A. Brenner and R.L. Burwell, Jr., J. Catal. 52, 364 (1978).
22. R.F. Howe, D.E. Davidson, and D.A. Whan, J. Chem. Soc., Faraday Trans 1 68, 2266 (1972).
23. D.M. Adams, I.R. Gardner, and N.D. Parkyns, J. Catal. 45, 145 (1976).
24. R.F. Howe and I.R. Leith, J. Chem. Soc., Faraday Trans. 1 69, 1967 (1973).
25. A. Brenner, D.A. Hucul, and S.J. Hardwick, Inorg. Chem. 18, 1478 (1979).
26. A. Kazusaka and R.F. Howe, J. Mol. Catal. 9, 183 (1980).
27. R.F. Howe, Inorg. Chem. 15, 486 (1976).
28. I.W. Stoltz, G.R. Dobson, and R.K. Sheline, Inorg. Chem. 2, 323 (1963).
29. A. Brenner and R.L. Burwell, Jr., J. Am. Chem. Soc. 97, 2565 (1975).
30. A. Brenner and R.L. Burwell, Jr., J. Catal. 52, 353 (1978).

31. A. Brenner and D.A. Hucul, J. Am. Chem. Soc. **102**, 2484 (1980).
32. D.A. Hucul and A. Brenner, J. Phys. Chem. **85**, 496 (1981).
33. R.L. Burwell, Jr., J. Catal. **86**, 301 (1984).
34. A. Kazusaka and R.F. Howe, J. Mol. Catal. **9**, 199 (1980).
35. A. Brenner and D.A. Hucul, J. Catal. **61**, 216 (1980).
36. E. Guglielminotti and A. Zecchina, J. Chim. Phys. **78**, 89 (1981).
37. F. Hugues, A.K. Smith, Y. Ben Taarit, J.M. Basset, D. Commereuc, and Y. Chauvin, J. Chem. Soc., Chem. Commun., 69 (1980).
38. A. Brenner and D.A. Hucul, Inorg. Chem. **18**, 2836 (1979).
39. E. Guglielminotti, A. Zecchina, F. Bocuzzi, and E. Bonello, in Growth and Properties of Metal Clusters, (Ed. J. Bourdon), p. 165, Elsevier (1980); A. Zecchina, E. Garrone, and E. Guglielminotti, in Catalysis, (Eds. G.C. Bond and G. Webb), vol.6, p. 128, Royal Society of Chemistry (1983).
40. F. Hugues, J.A. Dalmon, P. Bussiere, A.K. Smith, J.M. Basset, and D. Olivier, J. Phys. Chem. **86**, 5136 (1982).
41. K. Lazar, K. Malusek, J. Mink, S. Dubos, L. Guczi, A. Vizi-Orosz, L. Marko, and W.M. Reiff, J. Catal. **87**, 163 (1984).
42. J. Robertson and G. Webb, Proc. R. Soc. London, A **341**, 383 (1974).
43. A. Theolier, A. Choplin, L. D'Ornelas, J.M. Basset, G.M. Zanderighi, R. Ugo, R. Psaro, and C. Sourisseau, Polyhedron **2**, 95 (1983).
44. J.M. Basset and A. Choplin, J. Mol. Catal. **21**, 95 (1983).
45. V.D. Alexiev, N. Binsted, J. Evans, G.N. Greaves, and R.J. Price, J. Chem. Soc., Chem. Commun., 395 (1987).
46. J. Evans and G.S. McNulty, J. Chem. Soc., Dalton Trans., 1123 (1984); N. Binsted, J. Evans, G.N. Greaves, and R.J. Price, unpublished results.
47. R. Pierantozzi, E.G. Valagene, A.F. Nordquist, and P.N. Dyer, J. Mol. Catal. **21**, 189 (1983).
48. A. Zecchina, E. Guglielminotti, A. Bossi, and M. Camia, J. Catal. **74**, 225, 240, 252 (1982); V.L. Kuznetsov, A.T. Bell, and Y.I. Yermakov, J. Catal. **65**, 374 (1980).
49. B. Besson, B. Moraweck, A.K. Smith, J.M. Basset, R. Psaro, A. Fusi, and R. Ugo, J. Chem. Soc., Chem. Commun., 569 (1980).
50. R. Psaro, R. Ugo, G.M. Zanderighi, B. Besson, A.K. Smith, and J.M. Basset, J. Organomet. Chem. **213**, 215 (1981).
51. L. D'Ornelas, A. Choplin, J.M. Basset, L.-Y. Hsu, and S.G. Shore, Nouv. J. Chim. **9**, 155 (1985).
52. S.L. Cook, J. Evans, G.S. McNulty, and G.N. Greaves, J. Chem. Soc., Dalton Trans., 7 (1986).
53. G. Collier, D.J. Hunt, S.D. Jackson, R.B. Moyes, I.A. Pickering, P.B. Wells, A.F. Simpson, and R. Whyman, J. Catal. **80**, 154 (1983).
54. M. Deeba, B.J. Streusand, G.L. Schrader, and B.C. Gates, J. Catal. **69**, 218 (1981).
55. F.B.M. Duivenvoorden, D.C. Koningsberger, Y.S. Uh, and B.C. Gates, J. Am. Chem. Soc. **108**, 6254 (1986).
56. H. Knözinger and Y. Zhao, J. Catal. **71**, 337 (1981).
57. H. Knözinger, Y. Zhao, B. Tesche, R. Barth, R. Epstein, B.C. Gates, and J.P. Scott, Discuss. Faraday Soc. **72**, 53 (1981).

58. J. Schwank, L.F. Allard, M. Deeba, and B.C. Gates, J. Catal. 84, 27 (1983).
59. V.A. Shvets, A.L. Tarasov, V.B. Kazansky, and H. Knözinger, J. Catal. 86, 223 (1984).
60. M. Deeba, J.P. Scott, R. Barth, and B.C. Gates, J. Catal. 71, 373 (1981).
61. R. Psaro, C. Dossi, and R. Ugo, J. Mol. Catal. 21, 331 (1983).
62. A. Theolier, A.K. Smith, M. Leconte, J.M. Bassett, G.M. Zanderighi, R. Psaro, and R. Ugo, J. Organomet. Chem. 91, 415 (1980).
63. J.L. Bilhou, V. Bilhou-Bougnol, W.F. Graydon, J.M. Bassett, A.K. Smith, G.M. Zanderighi, and R. Ugo, J. Organomet. Chem. 153, 73 (1978).
64. G.C. Smith, T.J. Chojnacki, S.R. Dasgupta, K. Iwatake, and K.L. Watters, Inorg. Chem. 14, 1419 (1975).
65. A.K. Smith, F. Hugues, A. Theolier, J.M. Bassett, R. Ugo, G.M. Zanderighi, J.L. Bilhou, V. Bilhou-Bougnol, and W.F. Graydon, Inorg. Chem. 18, 3104 (1979).
66. J. Evans and G.S. McNulty, J. Chem. Soc., Dalton Trans., 587 (1984); N. Binsted, J. Evans, G.N. Greaves, and R.J. Price, unpublished results.
67. K.L. Watters, R.F. Howe, T.P. Chojnacki, C.-M. Fu, R.L. Schneider, and N.-B. Wong, J. Catal. 66, 424 (1980).
68. S.L.T. Anderson, K.L. Watters, and R.F. Howe, J. Catal. 69, 212 (1981).
69. J.B.A.D. van Zon, D.C. Koningsberger, H.F.J. van't Blik, and D.E. Sayers, J. Chem. Phys. 82, 5742 (1985); H.F.J. van't Blik, J.B.A.D. van Zon, T. Huizinga, J.C. Vis, D.C. Koningsberger, and R. Prins, J. Am. Chem. Soc. 107, 3139 (1985).
70. J.H. Sinfelt, Bimetallic Catalysts: Discoveries, Concepts and Applications, Wiley (1983).
71. J.R. Anderson, P.S. Elmes, R.F. Howe, and D.E. Mainwaring, J. Catal. 50, 508 (1977).
72. J.R. Budge, J.P. Scott, and B.C. Gates, J. Chem. Soc., Chem. Commun., 342 (1983).
73. A. Choplin, L. Huang, J.M. Bassett, R. Mathieu, U. Siriwardane, and S.G. Shore, Organometallics 5, 1547 (1986).
74. A. Choplin, L. Huang, A. Theolier, P. Gallezot, J.M. Bassett, U. Siriwardane, S.G. Shore, and R. Mathieu, J. Am. Chem. Soc. 108, 4224 (1986).
75. J.R. Budge, B.F. Lücke, B.C. Gates, and J. Toran, J. Catal. 91, 272 (1985).
76. A. Choplin, M. Leconte, J.M. Bassett, S.G. Shore, and W.-L. Hsu, J. Mol. Catal. 21, 389 (1983).
77. D.G.H. Ballard, Adv. Catal. 23, 267 (1973).
78. O.A. Yefimov, A.I. Minkov, V.A. Zakharov, and Yu. I. Yermakov, Kinet. Katal. 17, 995 (1976); Chem. Abs. 85, 160656 (1976).
79. G.A. Nesterov, V.A. Zakharov, Ye. A. Paukshtis, E.N. Yurchenko, and Yu. I. Yermakov, Kinet. Katal. 20, 429 (1979).
80. J. Smith, W. Mowat, D.A. Whan, and E.A.V. Ebsworth, J. Chem. Soc., Dalton Trans., 1742 (1974).

81. M.D. Ward, T.V. Harris, and J. Schwartz, J. Chem. Soc., Chem. Commun., 357 (1980).
82. M.D. Ward and J. Schwartz, J. Mol. Catal. 11, 397 (1981).
83. J. Schwartz, Acc. Chem. Res. 18, 302 (1985).
84. H.C. Foley, S.J. DeCanio, K.D. Tau, K.J. Chao, J.H. Onuferko, C. Dybowski, and B.C. Gates, J. Am. Chem. Soc. 105, 3074 (1983).
85. M.D. Ward and J. Schwartz, Organometallics 1, 1030 (1982).
86. F.J. Karol and R.N. Johnson, J. Polym. Sci. A-1 13, 1607 (1975).
87. B. Rebenstorf, B. Johnson, and R. Larsson, Acta Chem. Scand. A36, 695 (1982).
88. Y. Iwasawa, T. Chiba, and N. Ito, J. Catal. 99, 95 (1986).
89. F.J. Karol, G.L. Karapinka, C. Wu, A.W. Dow, R.N. Johnson, and W.L. Carrick, J. Polym. Sci. A-1 10, 2621 (1972).
90. F.J. Karol, C. Wu, W.T. Reichle, and N.J. Maraschin, J. Catal. 60, 68 (1979).
91. F.J. Karol, W.L. Munn, G.L. Goeke, B.E. Wagner, and N.J. Maraschin, J. Polym. Sci. A-1 16, 771 (1978).
92. Y. Iwasawa, S. Ogasawara, and M. Soma, Chem. Lett., 1039 (1987).
93. Y. Iwasawa, H. Ichinose, S. Ogasawara, and M. Soma, J. Chem. Soc., Faraday Trans. 1 77, 1763 (1981).
94. Y. Iwasawa, Y. Sato, and H. Kuroda, J. Catal. 82, 289 (1983).
95. Y. Iwasawa and M. Yamagishi, J. Catal. 82, 373 (1983).
96. Y. Iwasawa, N. Ito, H. Ishii, and H. Kuroda, J. Chem. Soc., Chem. Commun., 827 (1985).
97. R.B. Bowman, R. Nakamura, P.J. Fagan, R.L. Burwell, Jr., and T.J. Marks, J. Chem. Soc., Chem. Commun., 257 (1981).
98. M.-Y. He, R.L. Burwell, Jr., and T.J. Marks, Organometallics 2, 566 (1983).
99. M.-Y. He, G. Xiong, P.J. Toscano, R.L. Burwell, Jr., and T.J. Marks, J. Am. Chem. Soc. 107, 653 (1985).
100. P.J. Toscano and T.J. Marks, J. Am. Chem. Soc. 107, 653 (1985).
101. K.G. Allum, R.D. Hancock, I.V. Howell, S. McKenzie, R.C. Pitkethly, and P.J. Robinson, J. Organomet. Chem. 87, 203 (1975).
102. K.G. Allum, R.D. Hancock, I.V. Howell, T.E. Lester, S. McKenzie, R.C. Pitkethly, and P.J. Robinson, J. Catal. 43, 331 (1976).
103. K.G. Allum, R.D. Hancock, I.V. Howell, R.C. Pitkethly, and P.J. Robinson, J. Catal. 43, 322 (1976).
104. M. Czakova and M. Capka, J. Mol. Catal. 11, 313 (1981).
105. Z.M. Michalska, M. Capka, and J. Stoch, J. Mol. Catal. 11, 323 (1981).
106. E.D. Nyberg and R.S. Drago, J. Am. Chem. Soc. 103, 4966 (1981).
107. D.K. Liu and M.S. Wrighton, J. Am. Chem. Soc. 104, 898 (1982).
108. D.K. Lui, M.S. Wrighton, D.R. McKay, and G.E. Maciel, Inorg. Chem. 23, 212 (1984).
109. J.L. Bilhou, V. Bilhou-Bougnol, W.F. Graydon, J.M. Basset, and A.K. Smith, J. Mol. Catal. 8, 411 (1980).
110. R.J. Crowte, Ph.D. Thesis, University of Southampton, (1985).
111. H. Knözinger, E.W. Thornton, and M. Wolf, J. Chem. Soc., Faraday Trans. 1 75, 1888 (1979).
112. S.C. Brown and J. Evans, J. Chem. Soc., Chem. Commun., 1063 (1978).

113. R. Pierantozzi, K.J. McQuade, B.C. Gates, M. Wolf, H. Knözinger, and W. Ruhmann, J. Am. Chem. Soc. 101, 5436 (1979).
114. S.C. Brown and J. Evans, J. Mol. Catal. 11, 143 (1981).
115. M.B. Freeman, M.A. Patrick, and B.C. Gates, J. Catal. 73, 82 (1982).
116. V.D. Alexiev, N.J. Clayden, S.L. Cook, C.M. Dobson, J. Evans, and D.J. Smith, J. Chem. Soc., Chem. Commun., 938 (1986).
117. S.L. Cook, Ph.D. Thesis, University of Southampton, (1985).
118. V.D. Alexiev, Ph.D. Thesis, University of Southampton, (1987).
119. N. Binsted, S.L. Cook, J. Evans, and G.N. Greaves, J. Chem. Soc., Chem. Commun., 1103 (1985).
120. S.L. Cook and J. Evans, J. Chem. Soc., Chem. Commun., 713 (1983).
121. J. Evans and R.J. Price, unpublished results.
122. H. Pichler and W. Burgert, Brennst. Chem. 49, 5 (1968).
123. H. Pichler, N. Meier, W. Gabler, R. Gaertner, and D. Kiossis, Brennst. Chem. 48, 266 (1967).
124. H.H. Lamb, T.R. Krause, and B.C. Gates, J. Chem. Soc., Chem. Commun., 821 (1986).

CATALYTIC REACTIONS CARRIED OUT WITH METALS DERIVED FROM CLUSTERS

Robin Whyman
Imperial Chemical Industries plc
New Science Group
P.O. Box 11
The Heath, Runcorn, Cheshire, WA7 4QE
U.K.

ABSTRACT. This paper is a survey of recent progress in the preparation, characterisation, and catalytic properties of metals derived from molecular metal clusters. Particular emphasis is placed on the problem areas, the limitations and shortcomings of the investigations to date, and the types of systems which have not been investigated. Possible future directions and challenges facing research in the general field of cluster chemistry are also discussed.

1. INTRODUCTION

Metal clusters are of interest as potential catalysts, principally because they may be considered to represent the interface between the traditional disciplines of homogeneous and heterogeneous catalysis. Thus, on the one hand, the presence of adjacent metal sites in poly-nuclear complexes makes available coordinative, electronic, and steric situations that cannot be duplicated at the single metal site typical of most conventional homogeneous catalysts. Catalysts derived from supported metal clusters, on the other hand, can represent one extreme, namely, that of the very small particles in which almost every atom is a surface atom, characteristic of classical heterogeneous supported metal catalysts. The situation is summarised in Fig. 1. The areas 'cluster catalysis' and 'supported clusters' are of course very diffuse and may be further subdivided as indicated in Table I. For example, in addition to catalysis by molecular metal clusters, catalysis by colloidal metal particles should perhaps also be considered under the former heading. Molecular metal clusters may act either as catalysts in their own right or simply as catalyst precursors, possibly with subsequent fragmentation under reaction conditions to give highly reactive species of lower nuclearity. Distinction between these two possibilities is difficult. Under the 'supported clusters' heading, a distinction should be drawn between those materials in which most of the original attached ligands are retained (i.e., catalysis by

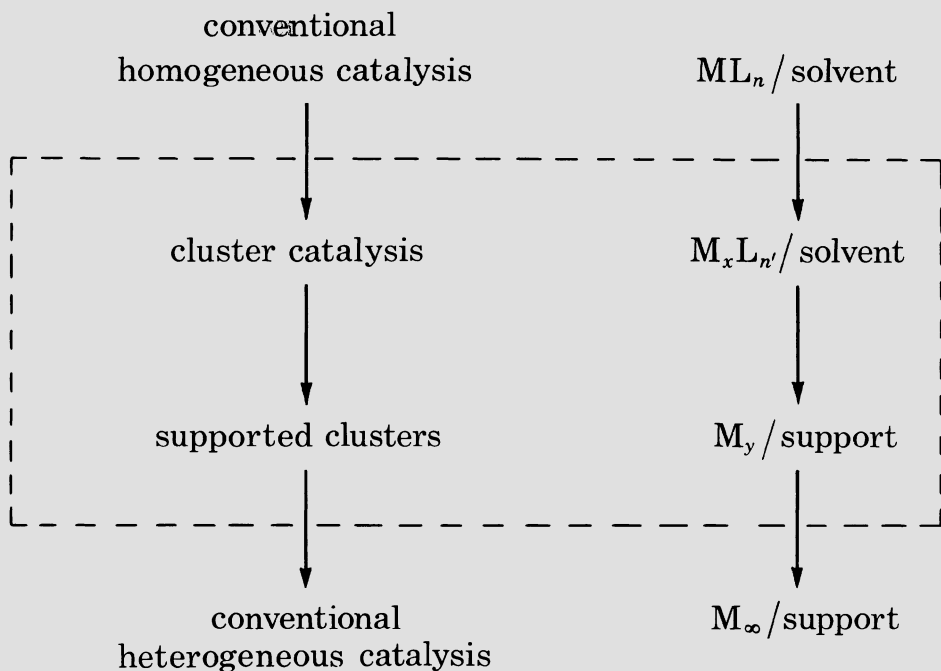


Figure 1. Relations between metal clusters, homogeneous and heterogeneous catalysis.

Table I. Molecular basis of catalysis by metals.

Homogeneous	Mononuclear organometallic complexes Molecular clusters
	Colloidal metal aggregates Slurry systems
Heterogeneous	Supported organometallics
	Anchored organometallics
	Constrained metal aggregates — Zeolites Highly dispersed supported metals Bulk metals

Mononuclear
 Metal clusters
 Mononuclear
 Metal clusters

supported molecular metal clusters) and those in which the majority of the ligands have intentionally been removed in an activation process (i.e., catalysis by very highly dispersed metal particles).

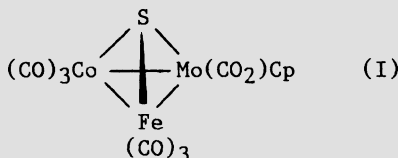
High selectivities frequently characterise homogeneously catalysed processes, whereas high activities tend to be associated with heterogeneous catalysis. It is therefore an attractive hypothesis that operation in this interfacial area between homogeneous and heterogeneous catalysis may provide a means of combining the high selectivity associated with the former with the high activity characteristic of the latter. Two simple questions, to which answers are now available, could therefore be posed at the outset of the interest in catalysis by clusters. First, do homogeneous catalysts derived from metal clusters provide catalytic activities or selectivities which are not attainable using mononuclear catalyst precursors? Second, do heterogeneous catalysts derived from metal clusters show genuinely different behaviour from that displayed by supported metal catalysts prepared by traditional routes?

The subject has been a very active area of research for almost 10 years, and some recent review articles and books [1-11] amply illustrate the range of different aspects which has been studied worldwide. The present paper is a review of some of the progress made during this period with respect to the catalytic properties of metals derived from clusters. Preparative and characterisation aspects are also considered since these should form an integral part of any comprehensive study of catalytic properties. Particular emphasis is placed on the problem areas, the limitations and shortcomings of the investigations to date, and the types of systems which have not been investigated. Possible future directions and challenges facing research in the general field of cluster chemistry are also discussed. Some of these aspects are highlighted by reference to work which has been carried out under the auspices of a Joint Research Scheme between ICI and Hull University, spanning the period 1979-1984 ([7] and references cited therein).

Before embarking on a discussion of catalysis by metal clusters, it is pertinent to quote a few cautionary comments from a recent article by Rooney [12], which are relevant to catalytic phenomena in general. First, the catalytically active intermediates involved on surfaces or in solutions are very unstable and transient, and far fewer in number than is generally realised. Second, in most cases it is therefore extremely difficult using spectroscopic techniques to identify them, especially on metal surfaces, among the much more numerous and more stable complexes which are also frequently present, but only transform, if at all, with a much lower frequency than those which are an intrinsic part of the catalytic cycle. Third, real turnover numbers are therefore far higher than estimated from surface areas or metal concentrations in solution, and may approach those for enzymes, which seem to be genuine rather than extreme models of all good catalysts. These are general points which should be borne in mind when advocating examples of cluster catalysis.

2. HOMOGENEOUS CATALYSIS BY METAL CLUSTER COMPOUNDS

Since the theme of the Workshop involves organometallic chemistry and a molecular approach to surface science and catalysis, it is appropriate to make a few comments concerning the state-of-the-art with respect to homogeneous catalysis by metal cluster compounds. There are many examples of homogeneously catalysed reactions in which metal cluster compounds have been used as catalyst precursors, and these have been the subject of several reviews [4,13-16]. However, in most cases, although the metal-cluster compound may have been present initially in solution, and may indeed have been isolated at the end of the reaction, there is little direct evidence to suggest that the integrity of the cluster itself is maintained throughout. In many instances the opposite is specifically thought to be the case; that is, the cluster compound breaks down under reaction conditions to give highly reactive mononuclear entities that are responsible for the catalysis. So, clearly, the maintenance of the cluster compound intact throughout reaction is a problem central to the establishment of cluster catalysis. Considerable effort has been expended in this area, and Laine [17] has established a useful set of criteria for the identification of homogeneous transition metal cluster-catalysed reaction. Pittman's approach, using metal cluster compounds that are bonded by stable non-fluxional bridging groups in addition to metal-metal bonds, has given some promising results in support of catalysis by intact clusters, particularly in the context of alkene hydroformylation with cobalt clusters [18] and with mixed metal tetrahedrane clusters [19] and the selective hydrogenation of alkynes to alkenes with iron clusters [18]. In more recent work, the photoinitiated hydrosilation of benzophenone in the presence of tetrahedral heterometallic clusters has also afforded strong circumstantial evidence for cluster catalysis [20]. However, the key experiment using the chiral cluster (I) unfortunately failed because the rate of



photoracemisation of the cluster was substantially higher than the rate of hydrosilation. Recent photocatalytic studies of the hydrogenation of ethylene in the presence of $\text{H}_4\text{Ru}_4(\text{CO})_{12}$ have also been interpreted in terms of catalysis by the intact tetraruthenium cluster [21].

Thus, although there is reasonable evidence for cluster-catalysed processes in a few cases, with the comments of Rooney in mind, an unequivocal demonstration of polynuclear catalysis is still awaited. Conclusive evidence does appear to require the use of a rigid chiral cluster to catalyse an asymmetric catalytic reaction with the

subsequent isolation of chiral products. This remains a desirable intellectual objective but is unlikely to be of practical significance.

The main conclusion to be drawn from the recent developments concerns the belief, initially held by leading workers in the field, that metal cluster compounds would prove to occupy a unique place in homogeneous catalysis. Early examples did indeed suggest that metal clusters could catalyse the energetically more demanding reactions, such as the reduction of carbon monoxide, nitriles, and isonitriles, which were not generally the preserve of homogeneous catalysts derived from mononuclear complexes. In particular, the reduction of carbon monoxide to ethylene glycol in the presence of the anionic rhodium cluster $[Rh_5(CO)_{15}]^-$ was, for some time, widely held as a unique example of cluster catalysis. Subsequently, however, it has been shown that mononuclear complexes can act as effective catalyst precursors of such reactions, particularly when they are used in tandem to provide bimetallic systems.

Thus the answer to the first question posed in the introduction is clear; no totally new catalytic activities or selectivities have been observed as a consequence of the use of molecular metal clusters as catalyst precursors. Indeed, in general the catalytic activity of metal clusters does appear to be rather low in reactions for which comparisons with mononuclear counterparts have been possible, e.g., alkene hydroformylation.

Finally, a potential application of molecular metal clusters which is virtually unexplored is the intentional generation of colloidal metal particles and the production of slurry phase catalysts (Table I). This may offer scope for future work.

3. HETEROGENEOUS CATALYSIS BY METAL CLUSTERS

Recent activity in this area reflects the view that supported metal clusters could form the basis of a new generation of heterogeneous catalysts. Characterisation of such materials, especially under reaction conditions, is difficult. Such catalysts will be valuable if they exhibit activities and selectivities that differ from those afforded by conventionally prepared catalysts; unfortunately, it is a deficiency of much of the extensive work so far reported that such comparisons have not been made. However, evidence has recently become available to show that cluster-derived heterogeneous catalysts do exhibit distinctive behaviour.

Any discussion of heterogeneous catalysis by supported metal clusters necessarily includes a consideration of progress with the preparative and characterisation aspects in addition to the purely catalytic properties of such materials.

3.1. Preparation of Supported Metal Clusters

Basically three different preparative approaches have been adopted, namely, the direct surface bonding of the cluster to an inorganic oxide [1], anchoring of the metal cluster to functionalised inorganic oxides

[22,23], and metal cluster entrapment in zeolites [24,25]. In many cases these processes may involve the partial or even complete destruction of the original cluster, which may ultimately lead to the formation of very small supported metal particles. Distinction between these possibilities is difficult. Possible methods which are applicable to the three approaches are listed in Table II. This table was first drawn up for a lecture given in Cambridge in 1976, and it is noteworthy that in the intervening 10 years virtually all the work with M_xL_y species has been carried out with $L = CO$, clearly as a consequence of the availability from synthetic organometallic chemists of a large range of metal carbonyl clusters; few other ligands have been investigated.

The use of mixed-metal clusters has received attention, and it has recently been demonstrated, using high resolution analytical electron microscopy, that under certain conditions it is possible to obtain very small bimetallic particles having the same bulk composition as that of the starting cluster [26]. However, in many cases attempts to produce alloy particles have been frustrated by the predominance of segregation [27-31]. This general approach may nevertheless provide a valuable route to the production of metal particles in intimate contact with a monolayer of a metal oxide, itself coated onto a high surface area oxide.

Very little work has been carried out using metal vapour techniques. There are therefore significant gaps between possible preparative routes to supported metal clusters and what has actually been investigated.

Table II. Preparation of supported metal atom clusters.

-
1. Impregnation of support with solutions of polynuclear organometallic complexes M_xL_y , followed by removal of L thermally, under vacuum, with H_2 , photochemically, etc.
 2. Chemical modification of support to allow chemical bond formation between organometallic and support, followed by decomposition.
 3. Use of mixed-metal organometallics to allow the possibility of preparing bimetallics or alloys of known composition.
 4. Metal vapour techniques.
-

3.2. Characterisation of Supported Metal Clusters

Some of the most relevant techniques which may be used for the characterisation of supported metal clusters are summarised in Table III.

Table III. Techniques for the characterisation of supported metal atom clusters.

Electron microscopy
EXAFS
X-ray photoelectron spectroscopy
IR and Raman spectroscopy
UV-visible spectroscopy
Mössbauer spectroscopy
NMR spectroscopy
Temperature programmed decomposition/reaction
Chemical reaction probes

It cannot be stressed too strongly that the use of a single technique in isolation is unlikely to lead to an unambiguous interpretation and is more likely to confuse an issue; a combination or battery of as many techniques as possible should be applied to a particular problem.

Vibrational spectroscopy (particularly infrared) has found wide application in the characterisation of supported metal carbonyl clusters. Such studies have been facilitated by the advent of high-sensitivity Fourier transform instrumentation. However, the information provided should be used with caution — the behaviour of carbonyl stretching vibrations need not necessarily correlate in any definite or specific manner with the presence or absence of metal-metal bonding in a supported organometallic carbonyl species.

EXAFS is a technique which has come into its own within the last five years [32-34] and has provided conclusive evidence which can be interpreted in terms of retention of the clustered state in active ruthenium catalysts derived from $\text{Ru}_3(\text{CO})_{12}$, $\text{H}_4\text{Ru}_4(\text{CO})_{12}$ and in active osmium catalysts derived from $\text{Os}_3(\text{CO})_{12}$, $\text{H}_4\text{Os}_4(\text{CO})_{12}$, $\text{Os}_6(\text{CO})_{18}$, supported on silica, alumina, and titania in our joint work with Hull University (Fig. 2) [35]. A particular advantage of EXAFS is that it is a technique which, in prospect, can be used in situ to study working catalysts.

An under-utilised method of characterisation which should be emphasised is the use of chemical probes. Reactions such as $\text{H}_2\text{-D}_2$ exchange, alkene isomerisation, and alkene hydrogenation can be used as sensitive chemical probes of the intimate environment of metal atoms. Such reactions have been shown to provide information concerning site congestion and selectivity and in determining whether the extent of molecular crowding at active sites influences catalytic activity [36]. Again such chemical probes are effectively in situ methods of examining the working catalyst and can provide indirect information relevant to the characterisation of supported metal carbonyl clusters and small metal particles. They may, to some extent, counteract the inadequacies of the physical techniques.

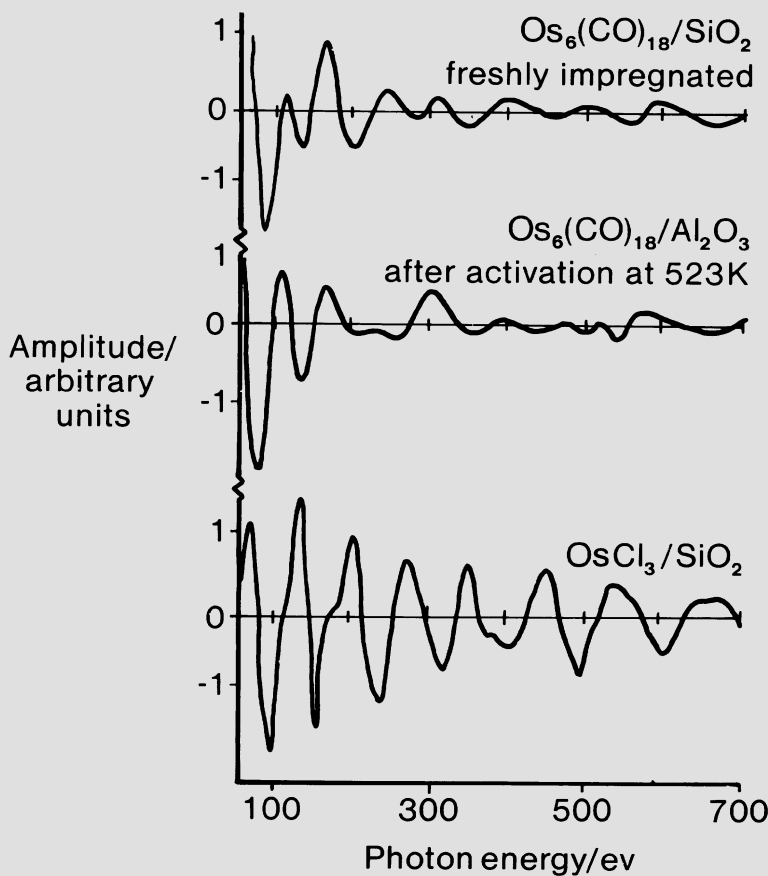


Figure 2. EXAFS spectra of supported osmium catalysts [35].

3.3. Catalysis by Supported Metal Clusters

The subject of particle size effects in heterogeneous catalysis, in particular the dependence or otherwise of catalytic activity and selectivity on metal particle size in the range 1-10 nm, is of interest to both industrial and academic circles. General trends that have emerged suggest that transformations such as those involving the reactions of unsaturated hydrocarbons, e.g., catalytic hydrogenation and isomerisation, are independent of metal particle size, i.e., are

structure insensitive. In contrast, the energetically more demanding reactions, such as those that involve the activation of C-H and C-C bonds in saturated hydrocarbons and the hydrogenation of carbon monoxide and of nitrogen, are structure sensitive. In the context of catalysis by metals derived from clusters, therefore, the area in which significant effects on catalytic activity and/or selectivity are most likely to be seen is that of the structure-sensitive reactions.

We have reviewed the literature in the area up to the end of 1980 [15,16]. Other reviews have also covered different aspects of the behaviour of catalysts derived from supported metal clusters [1,3,5-7,9-11,37,38], with particular emphasis on the hydrogenation of carbon monoxide. Table IV shows some representative examples of subsequent work in which at least some characterisation has been carried out to identify the major species present on the support. It is not, of course, implied that the species listed are necessarily responsible for the observed catalytic activity. It is apparent from Table IV that catalysts derived from supported metal clusters can show activity for a wide range of chemical transformations. From a careful analysis of the results contained in these references it is also clear that such materials can display catalytic activities and selectivities which are significantly different from those exhibited by their conventionally prepared counterparts (although examples of accurate comparisons are surprisingly sparse). For example, the supported iron catalyst obtained from $\text{Fe}_3(\text{CO})_{12}/\text{Al}_2\text{O}_3$ can give good selectivity to propene in the hydrogenation of carbon monoxide, behaviour which contrasts markedly with the Schulz-Flory product distribution observed with conventional Fischer-Tropsch catalysts [45]. This work also highlights one of the problem areas, namely, that such interesting selectivity differences are only relatively short-lived. Fig. 3 shows the product distribution at different times on stream; after 48 h, "conventional" Schulz-Flory behaviour is observed. During this period the catalyst is believed to have transformed from very small metal aggregates of particle size < 2 nm to large iron particles of ca. 20-50 nm. This seems to be a general problem, and in most cases the supported cluster compounds are stable only at relatively low temperatures (<423 K). Thus with only few exceptions the initial activities/selectivities are not maintained for prolonged periods unless very mild reaction conditions (particularly low temperatures) are used, under which the observed catalytic activities are rather low. Among the exceptions are the cluster-derived ruthenium and osmium catalysts which have been used for alkane hydrogenolysis reactions. Here long catalyst lifetimes have been observed [40] and, in the case of osmium [41], turnover numbers of up to two orders of magnitude higher than those displayed by conventionally prepared osmium catalysts have been measured (Table V), thus providing a positive answer to the second question posed in the introduction. The reason for this enhanced activity is not immediately clear, but may be due to a change in reaction mechanism when ruthenium and osmium clusters are used as catalyst precursors. Because the cluster-derived catalysts may have limited numbers of sites, it may be difficult for ethane to dissociate fully (that is for C_2H_6 to be converted to $\text{C}-\text{C} + 6\text{H}$), as is believed to

Table IV. Catalysis by supported clusters.

Catalyst precursor	Reaction	Temp/K	Major surface species identified	Ref.
[Pt ₃ (CO) ₆] _n ²⁻ /Al ₂ O ₃	Alkane isomerisation/hydrogenolysis	525	Pt crystallites (1.0-2.0 nm)	39
Ru ₃ (CO) ₁₂ /SiO ₂	Hydrogenolysis of alkanes and aromatics	473-523	Ru crystallites (1.5-2.0 nm)	40
Os ₃ (CO) ₁₂ /SiO ₂	Ethane hydrogenolysis Ethene, CO and CO ₂ hydrogenation	395-665	[Os(CO) _x C _y] _n /SiO ₂	41
Os ₃ (CO) ₁₂ /SiO ₂	Ethene hydrogenation	343-373	Hos ₃ (CO) ₁₀ O-Si	42
H ₂ RuOs ₃ (CO) ₁₂ /Al ₂ O ₃	Alkene isomerisation/hydrogenation	330	[H ₃ RuOs ₃ (CO) ₁₂] ⁻ Al ⁺	43
H ₄ Re ₄ (CO) ₁₂ /SiO ₂	Propene metathesis	423	Re ₄ (CO) ₁₂ (OH) ₄	44
Fe ₃ (CO) ₁₂ /Al ₂ O ₃	CO/H ₂ → alkenes/alkanes	543	[HFe ₃ (CO) ₁₁] ⁻ Al ⁺ initially	45
Ru ₃ (CO) ₁₂ /MgO	CO/H ₂ → methanol/hydrocarbons	<500	[Ru ₆ C(CO) ₁₆] ²⁻ + Ru crystallites	46
H ₂ Os(CO) ₄ /MgO	CO/H ₂ → C ₁ -C ₄ hydrocarbons	548	[H ₃ Os ₄ (CO) ₁₂] ⁻ + [Os ₁₀ C(CO) ₂₄] ²⁻	47

be the situation which obtains on surfaces of conventional catalysts; ethane may therefore retain most of its hydrogen prior to C-C bond rupture.

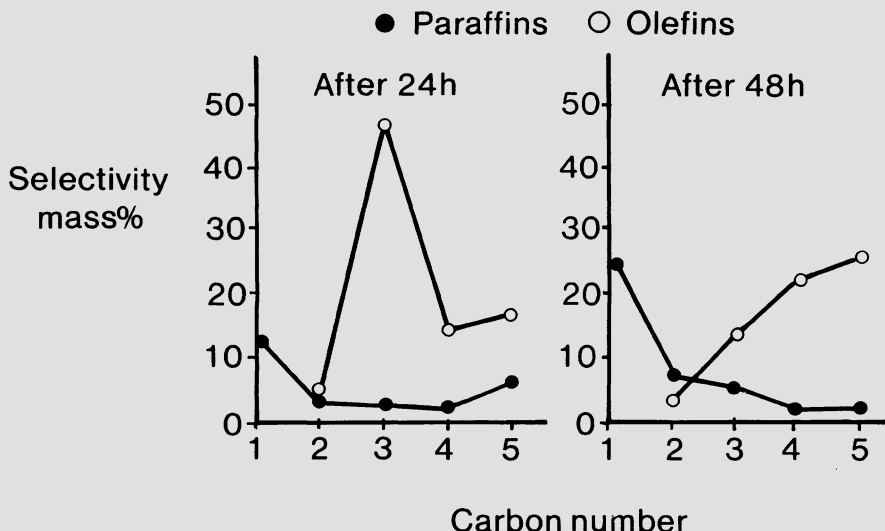


Figure 3. Selectivities observed in Fischer-Tropsch synthesis at 543 K with $\text{Fe}_3(\text{CO})_{12}/\text{Al}_2\text{O}_3$ as catalyst precursor [45].

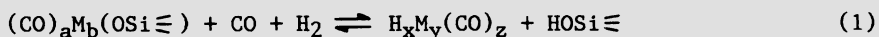
Table V. Ethane hydrogenolysis: apparent activation energies and turnover numbers giving a comparison between Os cluster-derived materials and metallic Os/SiO₂.

Catalyst precursor	$E_a/\text{kJ mol}^{-1}$	Temp/ K	$N_{500\text{K}}/\text{molecules site}^{-1}\text{ s}^{-1}$
$\text{Os}_3(\text{CO})_{12}/\text{SiO}_2$	32	425-500	6.8×10^{-2}
$\text{Os}_3(\text{CO})_{12}/\text{Al}_2\text{O}_3$	52	540-665	
$\text{Os}_3(\text{CO})_{12}/\text{TiO}_2$	81	400-475	
$\text{H}_2\text{Os}_{10}\text{C}(\text{CO})_{24}/\text{SiO}_2$	36	350-425	
$\text{H}_2\text{Os}_{10}\text{C}(\text{CO})_{24}/\text{Al}_2\text{O}_3$	51	570-625	
$\text{H}_2\text{Os}_{10}\text{C}(\text{CO})_{24}/\text{TiO}_2$	46	475-540	
Metallic Os/SiO ₂	114	475-595	1.5×10^{-4}

Less dramatic effects are observed in respect of the behaviour of these catalysts towards the hydrogenation of alkenes and of carbon monoxide. The hydrogenation of ethene in the presence of the osmium cluster-derived catalysts requires a significantly higher temperature than hydrogenation in the presence of a conventional metal catalyst; the activation energies are also higher, as summarised in Table VI. Positive orders of reaction in ethene for the cluster-derived catalysts compared with zero order for conventional catalysts suggest that ethene adsorption on the cluster-derived catalysts is weak. Hence higher temperatures are required to obtain measurable rates from low steady-state concentrations of adsorbed ethene. In the case of this reaction, therefore, the behaviour of the cluster-derived catalyst is similar to that of a carbon monoxide-poisoned conventional osmium catalyst. This analogy may also account for the unusual stability of these catalysts on exposure to air [48].

Carbon monoxide hydrogenation in the presence of the cluster-derived catalysts is, for the most part, similar to carbon monoxide hydrogenation in the presence of conventional catalysts; the activation energies are comparable and the principal products (methane and carbon dioxide) are the same. However, the cluster-derived catalysts are generally significantly less active than their conventional counterparts, although some (notably the silica-supported material) have comparable activity (Table VI). Since the carbonyl ligands are retained throughout the hydrogenation reaction, these results may suggest that there is a significant proportion of inactive carbon monoxide present on the surface of a conventional catalyst during hydrogenation.

The reactions of silica-supported osmium clusters have been studied at elevated pressures of carbon monoxide and hydrogen by in situ infrared spectroscopy to test their stability under more forcing conditions [49]. The catalytically active species are found to sinter to polycrystalline metallic osmium at 523 K in 10 atm of carbon monoxide or of hydrogen but, under 10 atm of a 1:1 (CO + H₂) mixture they are converted quantitatively at 473 K to Os₃(CO)₁₂, and at 523 K to H₄Os₄(CO)₁₂. The reversible interconversion of molecular cluster compounds and active anchored states has thus been demonstrated. The situation is summarised in Fig. 4. These observations clearly demonstrate the serious limitations of these materials as catalysts for the hydrogenation of carbon monoxide under the typical conditions of industrial processing. The displacement of the equilibrium in Eq. 1 to the right under relatively modest CO + H₂ pressures shows (i) the driving force in favour of the formation of free hydridometal carbonyl and/or metal carbonyl species and (ii) the relative ease with which the cluster-support interaction may be severed, notwithstanding the fact that the Os-O bond is very strong.



These facts, coupled with the well-established facile interconversions in solution of metal carbonyl clusters of second-row transition metals such as Rh [50], make it unlikely that the present generation of metal

Table VI. A comparison of activation energies and rates for conventional and cluster-derived catalysts.

Catalyst precursor	Reaction		
	C ₂ H ₄ + H ₂ → C ₂ H ₆	CO + 3 H ₂ → CH ₄ + H ₂ O	log ₁₀ r ₃₉₀ ^b
E _a ^a	E _a ^a	E _a ^a	log ₁₀ r ₆₀₅ ^b
H ₂ Os ₃ (CO) ₁₀ /SiO ₂	42(378-406 K)	0.25	114(485-561 K)
Os ₃ (CO) ₁₂ /Al ₂ O ₃	50(390-500 K)	-1.65	95(540-645 K)
Os ₃ (CO) ₁₂ /TiO ₂	44(355-390 K)	-0.15	93(485-570 K)
Os ₆ (CO) ₁₈ /SiO ₂	41(385-425 K)	-0.09	73(590-665 K)
Os ₆ (CO) ₁₈ /TiO ₂	45(325-425 K)	-0.54	80(465-605 K)
H ₂ Os ₁₀ C(CO) ₂₄ /Al ₂ O ₃	53(520-590 K)	-2.25	122(520-590 K)
Os/Al ₂ O ₃	35(290-320 K)		119(500-560 K)

^a E_a in kJ/mol

^b Rates, r, in μmol/g of catalyst.

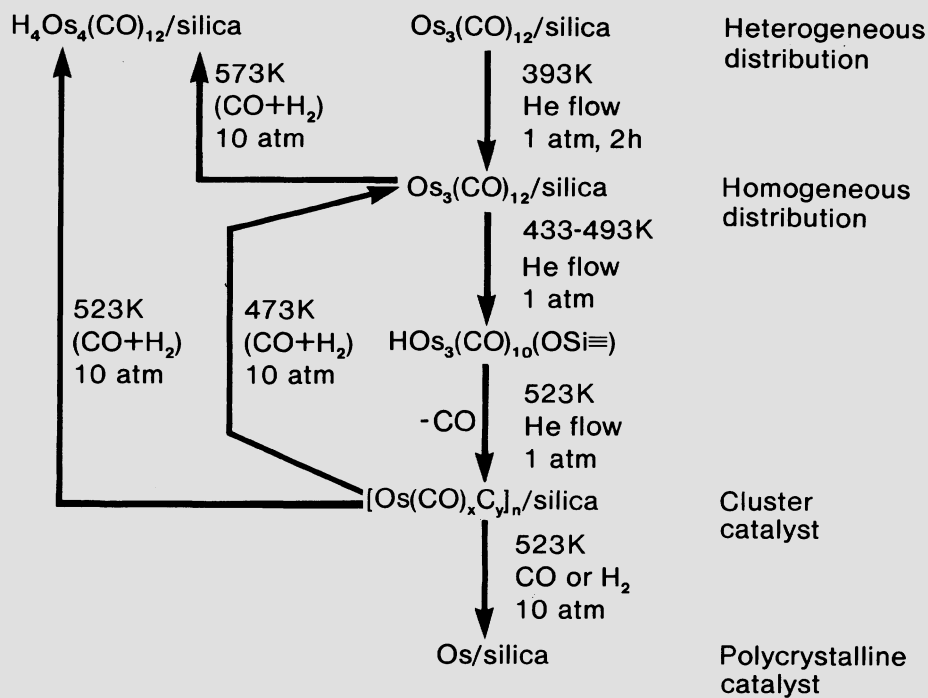


Figure 4. Transformations observed between supported molecular cluster and active catalyst for $\text{Os}_3(\text{CO})_{12}/\text{SiO}_2$ in the presence of carbon monoxide and hydrogen.

cluster catalysts on neutral supports will find industrial application in reactions involving carbon monoxide and hydrogen.

However, contrasting results have been reported for osmium clusters on a strongly basic support, magnesia. Molecular anionic clusters such as $[\text{H}_3\text{Os}_4(\text{CO})_{12}]^-$ are formed under CO hydrogenation conditions, and the strong surface acid-base interactions can at least minimise the loss of metal carbonyls from the support under reaction conditions [47].

In many respects the situation parallels closely that which obtains following the many unsuccessful attempts to develop heterogeneous versions of homogeneous catalysts for hydroformylation [51] and related reactions. In most of these cases the catalysis is

accompanied by slow leaching of metal from the support either into solution or into the vapour phase.

The situation with respect to reactions not involving carbon monoxide and hydrogen is somewhat different. Particularly in the case of alkane hydrogenolysis, supported cluster-derived catalysts behave reproducibly, can display catalytic activities which are considerably superior to those exhibited by their conventional counterparts, and are stable over extended periods. However, the structures of these catalysts are not well known, and they are not considered to be molecular analogues.

Other catalytic reactions on metals derived from clusters which have received attention are the structure-insensitive reactions such as the hydrogenation and isomerisation of alkenes. These reactions can clearly provide useful chemical probes, as discussed in Section 3.2, when careful comparisons with conventionally prepared catalysts are made, but they are unlikely to be find practical application. Discrepancies between the results obtained in different laboratories have clearly demonstrated that details such as support pretreatment (state of hydroxylation, etc.), method of loading the cluster compound on to the support (solution impregnation, sublimation, etc.), and subsequent method of catalyst activation (heating in hydrogen vs. vacuum/helium, etc.) can be very important in determining the state of aggregation/fragmentation of the metal species and hence the resultant catalytic behaviour. In particular, the influence of the support on the catalytic properties of the cluster-derived materials is receiving considerable attention. The acid-base chemistry and surface hydroxyl group concentration of the support have been shown to lead to pronounced effects on cluster-derived materials. Recent advances in surface organometallic chemistry are providing a basis for rationalising such observations.

4. FUTURE PROSPECTS FOR METAL CLUSTER-DERIVED CATALYSIS

The limitations and shortcomings of investigations of catalysis by metals derived from molecular metal clusters, up to the present time, have been highlighted in this paper. Extension of the present approaches to include the use of hetero-polymetallic cluster precursors may lead to catalysts of enhanced stability, although not, as already pointed out, with the metals necessarily in the alloy form, or even in intimate contact. The incorporation of potential catalyst promoters, e.g., alkali metals, into the cluster precursors may lead to catalysts of enhanced activity and longer term stability [52]. More comparative data with conventionally prepared catalysts are certainly required.

Few studies have been carried out with catalysts obtained from reactions of the metal clusters M_xL_y in which L is not CO. The reason for this is that metal carbonyl clusters are the most readily available starting materials. There are surprisingly few examples of the production of metal clusters from the metal atoms themselves. Future directions in this area are therefore most likely to involve new (or at least different) synthetic approaches. Recent developments which merit

consideration in this context are, first, the application of advances in metal vapour chemistry to the production of heterogeneous catalysts (including colloidal metals and slurry phases) and, second the synthesis of metal clusters in the gas phase by the laser evaporation of metals into pulsed supersonic nozzles.

4.1. Metal Vapour Chemistry

This area of chemistry is a development into the macroscale of matrix isolation spectroscopy as practiced in the 1960's on the microscale [53]. Recent research with a catalytic emphasis owes its origin largely to the work of Klabunde [54] and Ozin [55]. In the former approach, rather ill-defined materials may be obtained by the co-condensation of resistively heated metals with the vapours of organic ligands at 77 K followed by slow warm-up and contacting with a support material. Refinement of the experimental techniques has allowed the possibility of preparing the organometallic derivatives in a cleaner, more controlled manner from metal atom-solution reactions at \sim 173 K rather than co-condensation at 77 K. Such product solutions may be subsequently impregnated anaerobically onto a support (SiO_2 , Al_2O_3 , zeolite, etc.) at low temperatures, followed by slow warm-up for catalytic characterisation and evaluation.

Although the majority of metal vapour synthesis work has led to the generation of mononuclear species, e.g., $\text{M}(\text{arene})_2$, it is now established with certainty that dinuclear [56] and trinuclear clusters [57] can be obtained as products of the evaporation of the heavier metals. Thus, with careful attention to experimental conditions, e.g., evaporation rates, metal:ligand ratios, etc., the controlled preparation of aggregated metal species may be facilitated.

In general the macroscale technique has been limited to the use of condensable gases (particularly hydrocarbons) as ligands, but with the advent of the latest cryopumping systems of higher cooling capacity the use of non-condensable gases such as carbon monoxide, nitrogen, and methane is now possible [58]. The use of nitrogen in particular offers an attractive route to the direct (essentially single step) preparation of supported metals in this manner, viz :



4.2. Generation of Clusters in the Gas Phase

A second potential approach towards the production of supported clusters from metal atoms is cluster growth in the gas phase, followed by quenching and interaction with a support material. This is rather further removed from any immediate application than the metal vapour route described above.

Gas dynamic approaches for growing microclusters in the gas phase, with the production of metal smokes, have been known for some time, but in general this method has been limited to relatively large particles of mean diameters greater than 2-5 nm. This technique has recently been extended by Andres and co-workers [59] with the development of a multiple expansion cluster source which has enabled the generation of copper clusters with mean sizes claimed to be controllable from 0.2 to 2.5 nm.

A more recent innovation is the work of Smalley and Kaldor *et al.* [60,61], in which laser vaporisation of bulk metal substrates within a pulsed supersonic helium expansion has been used to generate intense beams of naked metal clusters, which are detected by laser photoionisation and time-of-flight mass spectrometry. The technique is capable of routinely generating clusters of up to 15-20 atoms of even the most refractory of metals, including molybdenum and tungsten, thus facilitating the primary aim of the work, namely, spectroscopic studies of metal clusters in the gas phase. Typical cluster size distributions are illustrated in Fig. 5. It is worth emphasising that detection of the clusters is by mass spectrometry and that none have yet been isolated on the macroscale. This work is still in its infancy, and many exciting extensions of the technique are possible. For example, the chemisorption of hydrogen on to niobium and cobalt clusters has been reported to show very significant dependences on cluster size [62]. In addition, free iron clusters have been shown to react readily with oxygen and hydrogen sulphide, but they are inert towards methane [63]. However, how much these effects are consequences of the configuration of the equipment is difficult to estimate at this stage. Looking further ahead, the production of these metal cluster beams on the macroscale, followed by de-ionisation and focussing onto a target support material may allow the generation of heterogeneous catalysts by this route.

5. CONCLUSIONS

5.1. Homogeneous Catalysts

There is, in a few cases, strong circumstantial evidence for the mediation of homogeneously catalysed reactions by molecular metal cluster compounds. However, no totally new catalytic activities or selectivities have arisen as a consequence of the use of molecular metal clusters as catalyst precursors. The unequivocal demonstration of cluster catalysis is still a worthwhile intellectual objective, but, at the present stage of our knowledge, is unlikely to be of practical significance.

5.2. Heterogeneous Catalysts

There is now ample evidence to support the premise that heterogeneous catalysts derived from metal carbonyl clusters can display fundamentally different behaviour from that observed with conventionally prepared

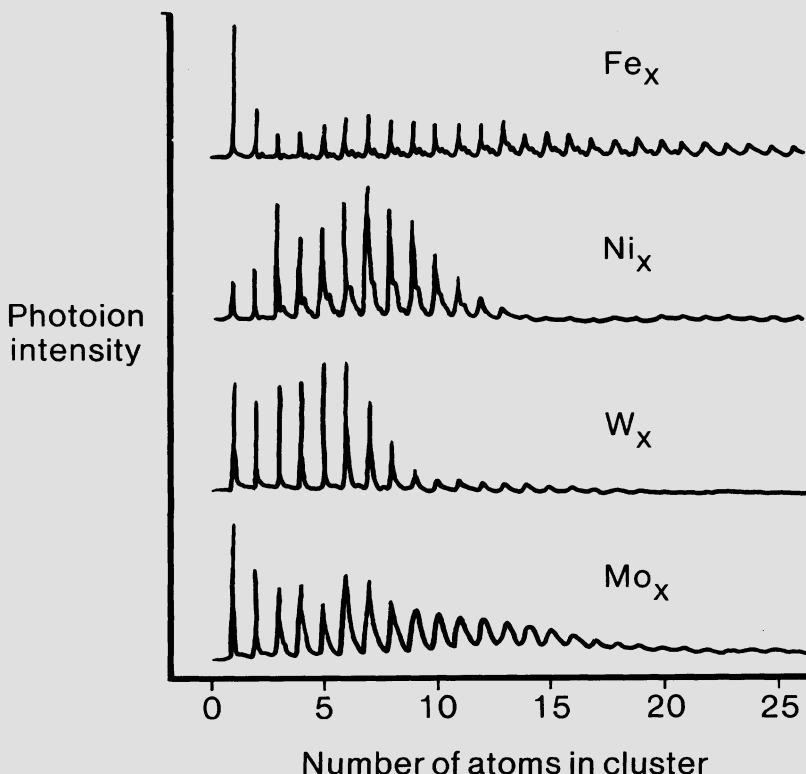


Figure 5. Time-of-flight mass spectra illustrating cluster size distributions obtained from metal beams [60,61].

catalysts. These catalysts may be applicable practically in the area of hydrocarbon transformations, particularly selective hydrogenolysis reactions. They display reproducible behaviour, and catalyst design, for optimisation of performance in particular reactions, is in principle possible by variation of starting cluster nuclearity and composition of the metal framework and the ligand environment, including the support. Recent advances in surface organometallic chemistry are helping to provide a basis for interpretation and rationalisation. A common weakness of catalysts derived from metal carbonyl clusters, particularly in reactions involving carbon monoxide and hydrogen, is their instability at high temperatures; bulk metallic aggregates often form. No totally new properties associated with structurally unique metal clusters have yet been realised. Other preparative techniques, e.g., metal vapour deposition or pulsed laser generation of metal clusters may enable the realisation of such goals.

6. REFERENCES

1. J.M. Basset, B. Besson, A. Choplin, F. Hugues, M. Leconte, D. Rojas, A.K. Smith, A. Theolier, Y. Chauvin, D. Commereuc, R. Psaro, R. Ugo, and G.M. Zanderighi, Fundamental Res. Homogeneous Catal. **4**, 19 (1984).
2. J. Huang and J. Huang, Huaxue Tongbau **64**, 35 (1984); Chem. Abstr. **101**, 43993 (1984).
3. B.C. Gates, Heterogeneous Catalysis, Proc. Symp. Ind.-Univ. Coop. Chem. Program., 1 (1984).
4. E.L. Muettterties, Proc. Electrochemical Soc. **84**, 343 (1984).
5. J. Zwart and R. Snel, J. Mol. Catal. **30**, 305 (1985).
6. L. Guczi, Adv. Catal., [Proc. 7th Natl. Symp. Catal.], 613 (1985).
7. S.D. Jackson and P.B. Wells, Platinum Metals Rev. **30**, 14 (1986).
8. A. Brenner, in Metal Clusters, (Ed. M. Moskovits), pp. 249-281, Wiley-Interscience, New York (1986).
9. B.C. Gates, in Metal Clusters, (Ed. M. Moskovits), pp. 283-310, Wiley-Interscience, New-York (1986).
10. M. Ichikawa, in Tailored Metal Catalysts, (Ed. Y. Iwasawa), pp. 183-263, Reidel, Dordrecht (1986).
11. Metal Clusters in Catalysis, (Eds. B.C. Gates, L. Guczi, and H. Knözinger), Elsevier, Amsterdam (1986).
12. J.J. Rooney, J. Mol. Catal. **31**, 147 (1985).
13. E.L. Muettterties, and M.J. Krause, Angew. Chem., Int. Ed. Engl. **22**, 135 (1983).
14. E.L. Muettterties, Catal. Rev.-Sci. Eng. **23**, 69 (1981).
15. R. Whyman, in Transition Metal Clusters, (Ed. B.F.G. Johnson), pp. 545-606, Wiley, London (1980).
16. S.D. Jackson, P.B. Wells, R. Whyman, and P. Worthington, Catalysis, Vol. 4, Specialist Periodical Report, pp. 75-99, Royal Society of Chemistry, London (1981).
17. R.M. Laine, J. Mol. Catal. **14**, 137 (1982).
18. C.U. Pittman, R.H. Ryan, W.D. Wilson, G. Wilemon, and M. Absi-Halabi, Preprints, Am. Chem. Soc., Div. Pet. Chem. **25**, 714 (1980).
19. M.G. Richmond, M. Absi-Halabi, and C.U. Pittman, J. Mol. Catal. **22**, 367 (1984).
20. C.U. Pittman, M.G. Richmond, M. Absi-Halabi, H. Beurich, F. Richter, and H. Vahrenkamp, Angew. Chem., Int. Ed. Engl. **21**, 786 (1982).
21. Y. Doi, S. Tamura, and K. Koshizuka, Inorg. Chim. Acta **65**, L63 (1982); J. Mol. Catal. **19**, 213 (1983).
22. D.C. Bailey and S.H. Langer, Chem. Rev. **81**, 109 (1981).
23. J. Evans, Chem. Soc. Rev. **10**, 159 (1981).
24. E. Mantovani, N. Palladino, and A. Zanobi, J. Mol. Catal. **3**, 285 (1978).
25. L.F. Nazar, G.A. Ozin, F. Hugues, J. Godber, and D. Rancourt, J. Mol. Catal. **21**, 313 (1983).
26. A. Choplin, L. Huang, A. Théolier, P. Gallezot, J.M. Basset, U. Siriwardane, S.G. Shore, and R. Mathieu, J. Am. Chem. Soc. **108**, 4224 (1986).

27. J.R. Shapley, S.J. Hardwick, D.S. Foose, and G.D. Stucky, Preprints, Am. Chem. Soc., Div. Pet. Chem. 25, 780 (1980).
28. L. Guczi, Z. Schay, K. Lázár, A. Vizi, and L. Marko, Surf. Sci. 106, 516 (1981).
29. A. Choplin, M. Leconte, J.M. Basset, S.G. Shore, and W.L. Hsu, J. Mol. Catal. 21, 389 (1983).
30. Y. Iwasawa and M. Yamada, J. Chem. Soc., Chem. Commun., 675 (1985).
31. J.R. Budge, B.F. Lücke, B.C. Gates, and J. Toran, J. Catal. 91, 272 (1985).
32. N. Binsted, S.L. Cook, J. Evans, and G.N. Greaves, Springer Proc. Phys. 2, 226 (1984).
33. M. Ichikawa, T. Fukushima, T. Yokoyama, N. Kosugi, and H. Kuroda, J. Phys. Chem. 90, 1222 (1986).
34. J. Evans, Chem. Brit. 22, 813 (1986).
35. D.J. Hunt, S.D. Jackson, R.B. Moyes, P.B. Wells, P.B. Worthington, and R. Whyman, J. Mol. Catal. 20, 289 (1983).
36. D. McMunn, R.B. Moyes, and P.B. Wells, J. Catal. 52, 472 (1978).
37. M. Ichikawa, CHEMTECH 12, 674 (1982).
38. R. Pierantozzi, Chem. Ind. (Dekker) 22, 115 (1985).
39. F. Garin, O. Zahraa, C. Crouzet, J.L. Schmitt, and G. Maire, Surf. Sci. 106, 466 (1981).
40. A.F. Simpson and R. Whyman, J. Organomet. Chem. 213, 157 (1981).
41. S.D. Jackson, R.B. Moyes, P.B. Wells, and R. Whyman, J. Catal. 86, 342 (1984).
42. J.M. Basset, B. Besson, A. Choplin, and A. Theolier, Philos. Trans. R. Soc. London, A 308, 115 (1982).
43. J.R. Budge, J.P. Scott, and B.C. Gates, J. Chem. Soc., Chem. Commun., 342 (1983).
44. P.S. Kirlin and B.C. Gates, J. Chem. Soc., Chem. Commun., 277 (1985).
45. D. Commereuc, Y. Chauvin, F. Hugues, J.M. Basset, and D. Olivier, J. Chem. Soc., Chem. Commun., 154 (1980); F. Hugues, P. Bussiere, J.M. Basset, D. Commereuc, Y. Chauvin, L. Bonneviot, and D. Olivier, Paper A28, 7th Internat. Congr. Catal., Tokyo (1980).
46. R. Pierantozzi, E.G. Valagene, A.F. Nordquist, and P.N. Dyer, J. Mol. Catal. 21, 189 (1983).
47. H.H. Lamb and B.C. Gates, J. Am. Chem. Soc. 108, 81 (1986).
48. D.J. Hunt, S.D. Jackson, R.B. Moyes, A.F. Simpson, P.B. Wells, and R. Whyman, J. Chem. Soc., Chem. Commun., 85 (1982).
49. B.S. Nicholls, S.D. Jackson, R.B. Moyes, A.F. Simpson, P.B. Wells, and R. Whyman, J. Catal., in press.
50. P. Chini, G. Longoni, and V.G. Albano, Adv. Organomet. Chem. 14, 285 (1976); P. Chini, J. Organomet. Chem. 200, 37 (1980).
51. D. Valentine and A. Madonik, Preprints, Am. Chem. Soc., Div. Pet. Chem. 27, 608 (1982).
52. G.B. McVicker and M.A. Vannice, U.S. Patent 4,192,777 (1980).
53. G.A. Ozin, M.P. Andrews, L.F. Nazar, H.X. Huber, and C.G. Francis, Coord. Chem. Rev. 48, 203 (1983).
54. K.J. Klabunde and Y. Tanaka, J. Mol. Catal. 21, 57 (1983).
55. G.A. Ozin, CHEMTECH 15, 488 (1985).

56. M.L.H. Green, D. O'Hare, and J.M. Wallis, J. Chem. Soc., Chem. Commun., 233 (1984); J.A. Bandy, F.G.N. Cloke, M.L.H. Green, D. O'Hare, and K. Prout, J. Chem. Soc., Chem. Commun., 240 (1984).
57. M.L.H. Green and D. O'Hare, J. Chem. Soc., Chem. Commun., 355 (1985).
58. J. Godber, H.X. Huber, and G.A. Ozin, Inorg. Chem. **25**, 2909 (1986).
59. R.S. Bowles, J.J. Kolstad, J.M. Calo, and R.P. Andres, Surf. Sci. **106**, 117 (1981).
60. J.B. Hopkins, P.R.R. Langridge-Smith, M.D. Morse, and R.E. Smalley, J. Chem. Phys. **78**, 1627 (1983).
61. R.L. Whetton, D.M. Cox, D.J. Trevor, and A. Kaldor, Surf. Sci. **156**, 8 (1985).
62. M.E. Geusic, M.D. Morse, and R.E. Smalley, J. Chem. Phys. **82**, 590 (1985).
63. R.L. Whetten, D.M. Cox, D.J. Trevor, and A. Kaldor, J. Phys. Chem. **89**, 566 (1985).

SOLUBLE AND SUPPORTED METAL CATALYSTS FOR HYDROCARBON OXIDATION IN LIQUID AND VAPOR PHASE

James E. Lyons
Sun Company
Marcus Hook, PA 19061
USA

ABSTRACT. Because organic oxygenates are such a large and industrially important class of compounds, there is intense interest in their production by selective catalytic oxidation of hydrocarbons. Numerous commercial catalytic liquid- and vapor-phase processes are currently in operation, however efficient processes for many desirable oxidative transformations have not yet been developed, and some existing routes are poorly understood. This report is a summary of emerging catalytic routes (1) from alkenes to epoxides, diols, α,β -unsaturated acids and esters; (2) from aromatics to phenols, aromatic acids, and oxidative cleavage products; and (3) from alkanes to alcohols, carbonyl compounds, and oxidative coupling products. Much of this chemistry occurs in the liquid phase; suggestions are made for surface catalysis of some of these reactions. Significant progress in understanding the nature of surface oxidation reactions and in achieving new process advances in surface-catalyzed oxidation might be made by applying principles of inorganic, organic, and organometallic solution chemistry.

1. INTRODUCTION

The majority of the high-volume organic chemical monomers produced industrially from hydrocarbon raw materials contain only the elements of carbon, hydrogen, and oxygen [1]. Many of these monomers are manufactured by direct reaction of a hydrocarbon substrate with molecular oxygen [2]. Although they are often difficult to initiate, hydrocarbon oxidations can be hard to stop short of the most thermodynamically stable products: carbon dioxide and water. In addition, a given hydrocarbon may possess several potential sites for attack by oxygen. Thus, kinetic control of both the position and the depth of hydrocarbon oxidation is a formidable technical challenge.

For this reason, a wide variety of metal catalysts with the ability to activate oxygen, hydrocarbons, or both have been devised for the purpose of catalyzing selective oxidations of the major classes of hydrocarbons: alkenes, aromatics, and alkanes. Although numerous

advances have been made in both the homogeneous and heterogeneous catalytic oxidation of hydrocarbons, progress in many areas is still needed. This report is a summary of some of the more important catalytic oxidations that are practiced industrially. We will ask what transformations one might wish to carry out that are currently beyond the scope of efficient catalytic processing, and we will survey some recent developments in newly emerging areas of oxidation chemistry which may ultimately lead to superior catalytic processes. As we consider both homogeneous and heterogeneous catalytic reactions, we will suggest ways in which surface organometallic chemistry and the molecular approach to surface catalysis could benefit the field of catalytic oxidation.

2. INDUSTRIAL CATALYSIS OF HYDROCARBON OXIDATION

2.1. Alkenes

Valuable products are produced from the oxidation of both ethylene and propylene (Figs. 1 and 2). Ethylene is epoxidized with oxygen in the vapor phase over a silver catalyst, and propylene is epoxidized with an alkyl hydroperoxide in the liquid phase using a molybdenum catalyst system. Vinylic oxidation products or their stable isomers, including acetaldehyde, acetone, and vinyl acetate, have been manufactured by a series of related catalytic reactions. These reactions occur either in solutions of palladium complexes or on the surfaces of supported palladium catalysts. Bismuth molybdate is an effective catalyst for allylic oxidations of propylene, which are of paramount importance to the chemical industry. Propylene is oxidized in the vapor phase to give acrolein for acrylic acid manufacture or, in the presence of ammonia, to give acrylonitrile. Second- and third-generation catalysts, including antimony-uranium oxides, have been developed for acrylonitrile production.

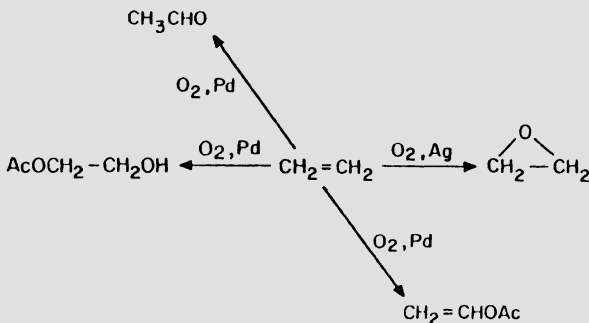


Figure 1. Catalytic oxidations of ethylene.

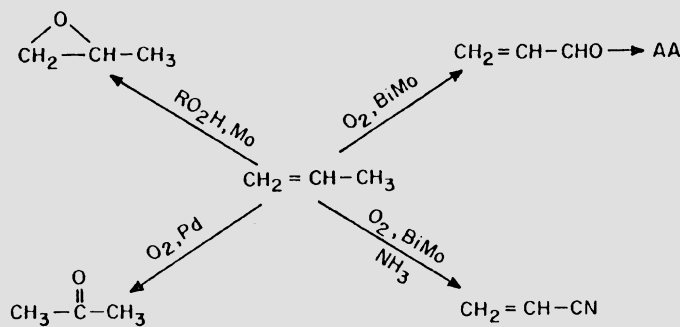


Figure 2. Catalytic oxidations of propylene.

2.2. Aromatics

Important industrial products are manufactured by direct oxidation of aromatic rings as well as by the selective oxidation of alkyl side chains on aromatic hydrocarbons (Figs. 3 and 4).

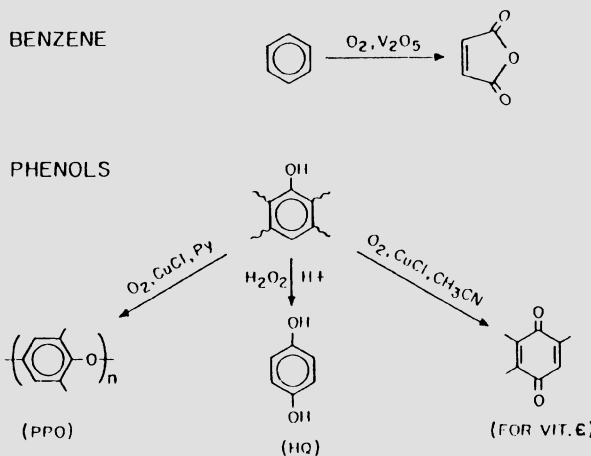


Figure 3. Catalytic oxidations of aromatic rings.

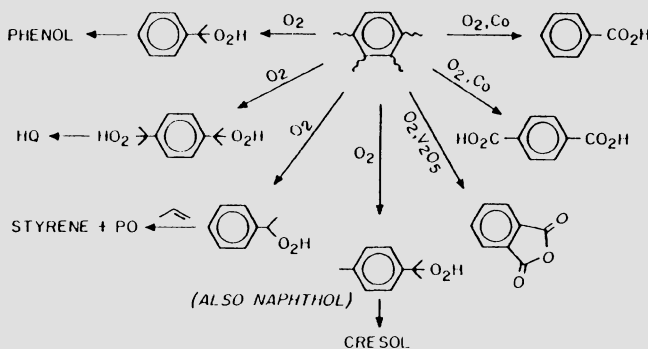


Figure 4. Catalytic oxidations of side chains on aromatic rings.

For many years the pathway of choice for industrial production of maleic anhydride was the vapor-phase oxidation of benzene over V_2O_5 . Phenols are oxidized in the liquid phase to give polyphenylene oxide or quinones in the presence of copper catalysts. Methyl groups are oxidized to the corresponding carboxylic acid functions by homogeneous cobalt catalysts in the liquid phase, and α -xylene is converted in the vapor phase to phthalic anhydride over V_2O_5 -containing catalysts. Isopropyl groups are readily autoxidized in the absence of a metal catalyst to give hydroperoxides, which undergo rearrangement to phenols in the presence of an acid catalyst.

2.3. Alkanes

Fewer oxidations of alkanes are practiced commercially than oxidations of the more reactive alkenes and aromatics (Fig. 5). Since methane is so resistant to controlled oxidation, very high temperatures are required to produce such products as synthesis gas or acetylene. Butane is readily oxidized to acetic acid in the presence of first-row transition metals in the liquid phase, but commercial processes using this approach are fraught with many by-products. Vapor-phase oxidation of butane over iron-promoted vanadyl pyrophosphate $[(VO)_2P_2O_7]$ is a more recently developed alternative to the older route to maleic anhydride via oxidative cleavage of benzene. Catalytic liquid-phase oxidation of cyclohexane gives nylon precursors. Autoxidation of isobutane in the absence of metal catalysts produces *tert*-butylhydroperoxide, a valuable reagent used for commercial oxidation of propylene to produce propylene oxide and co-product *tert*-butyl alcohol.

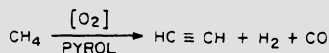
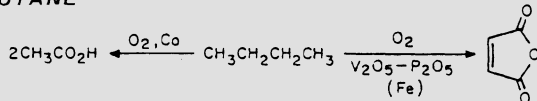
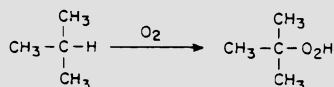
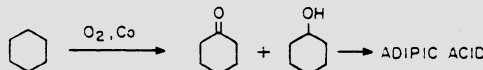
METHANE**BUTANE****ISOBUTANE****CYCLOHEXANE**

Figure 5. Commercial oxidations of alkanes.

3. NEW APPROACHES

3.1. Alkene Oxidations

A list of some new catalytic alkene transformations that one might like to be able to achieve using molecular oxygen would certainly include the reactions shown in Fig. 6. The direct air-epoxidation or "glycolation" of alkenes, their selective allylic oxidation, and their oxidative carbonylation over active and selective catalysts would all be of immense synthetic and industrial utility.

3.1.1. Direct Alkene Epoxidation. The epoxidation of alkenes by hydroperoxides is practiced industrially using both homogeneous and heterogeneous catalysts. The mechanism of this reaction (Fig. 7) has been thoroughly investigated. The utility of olefin epoxidation for the production of specialty products as well as commodity chemicals is now being exploited. The elegant stereoselective and regioselective epoxidations of allylic alcohols to give optically active products is an example of the synthetic versatility of this reaction [4].

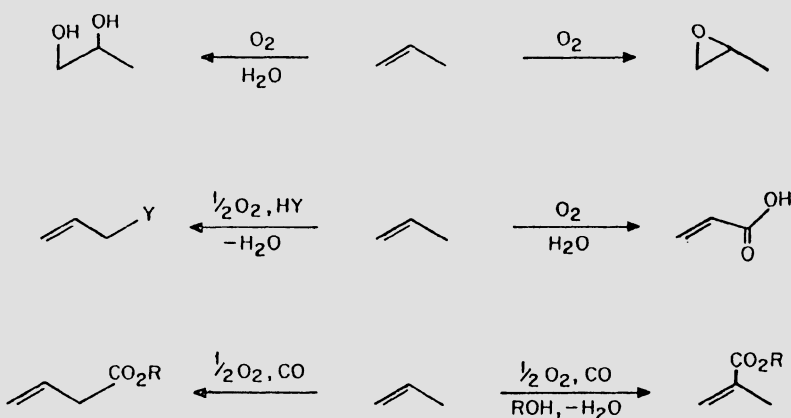


Figure 6. Alkene oxidations requiring new or improved catalysts.

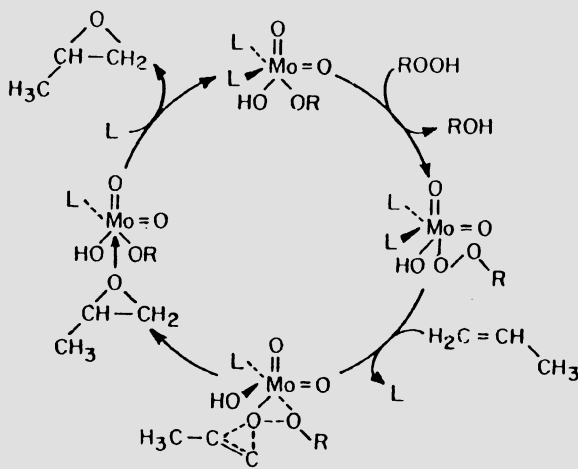


Figure 7. Alkene epoxidation catalyzed by Mo(VI).

Early work [5,6] showed that stereoselective direct air-oxidation of alkenes to epoxyalcohols was possible in the presence of vanadium complexes (Fig. 8). Reaction proceeded via autoxidation of the alkene to an allylic hydroperoxide and its decomposition to an allylic alcohol. This initial reaction could be accelerated by a first-row

group VIII metal complex. The allylic alcohol then became strongly coordinated to the vanadium center and was epoxidized by the newly forming allylic hydroperoxide. This produced an epoxy alcohol and left an allylic alcohol behind in the coordination sphere of the vanadium [7]. In this way, epoxy alcohols were formed regioselectively from substituted alkenes using mixtures of group VIII metal complexes and vanadium complexes as the catalyst. Understanding the molecular role of the metals in this homogeneous catalytic reaction made it possible to design a heterogeneous analogue which had the advantage of positioning a cobalt center close to a vanadium site on a molecular sieve support. This dual-metal exchanged zeolite catalyzed stereoselective oxidation of cyclohexene to cis-1,2-epoxycyclohexene-1-ol [8].

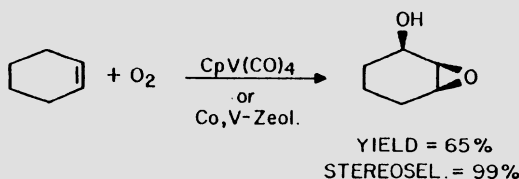
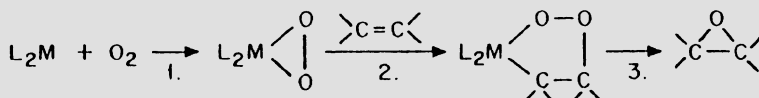


Figure 8. Stereoselective oxidation of cyclohexene to cis-1,2-epoxycyclohexane-1-ol.

Epoxy alcohol formation is a special case of direct oxidation of alkenes with molecular oxygen. A more general and more broadly applicable case would be the direct air oxidation of an alkene to an epoxide. Intensive efforts to achieve this in many laboratories over a 20-year period have yet to lead to a major synthetic route or an industrial process. Early work showed that a route involving reaction of a metal complex with O_2 to form a peroxy species which epoxidized an alkene via a peroxidic metallacycle was possible [9] (Fig. 9). It was found, however, that the low-valent group VIII metals which bound oxygen directly gave peroxides which did not readily epoxidize alkenes, and the group IVB-VIB metals which formed high-valent metal peroxy



$\text{M} = \text{Pt, Pd, Ni (1., 2.) ; Mo (2., 3.)}$

Figure 9. Oxygen activation and alkene epoxidation.

complexes capable of epoxidizing alkenes were not easily generated from molecular oxygen. Rhodium(I) appeared to be a partial exception [10-12], and direct O₂-oxidation of an alkene occurred catalytically through metal peroxy and metallacyclic peroxide. The reaction product, however, was a methyl ketone, not an epoxide.

An imaginative approach to this problem involved the use of a nitro group in a metal complex to carry the oxygen to the alkene. A metal nitrosyl was then formed which could be converted back to a nitro group with molecular oxygen [13,14]. Catalytic reactions were conducted in this manner, and metallacyclic intermediates were implicated. A tetraphenylporphyrinatocobalt nitro complex worked cooperatively with a transition metal halide to give catalytic alkene oxidations (Fig. 10). If the transition metal halide was palladium(II), which promotes β -hydrogen elimination, methyl ketones were formed, whereas when the transition metal halide was Ti(III), which does not promote β -elimination, epoxides were formed instead. Although this chemistry was not developed to the synthetically or commercially practical stage, it is tempting to speculate on the molecular design of a surface analogue where the dual metal cooperativity might be enhanced by proximity, as was the case in epoxy alcohol formation.

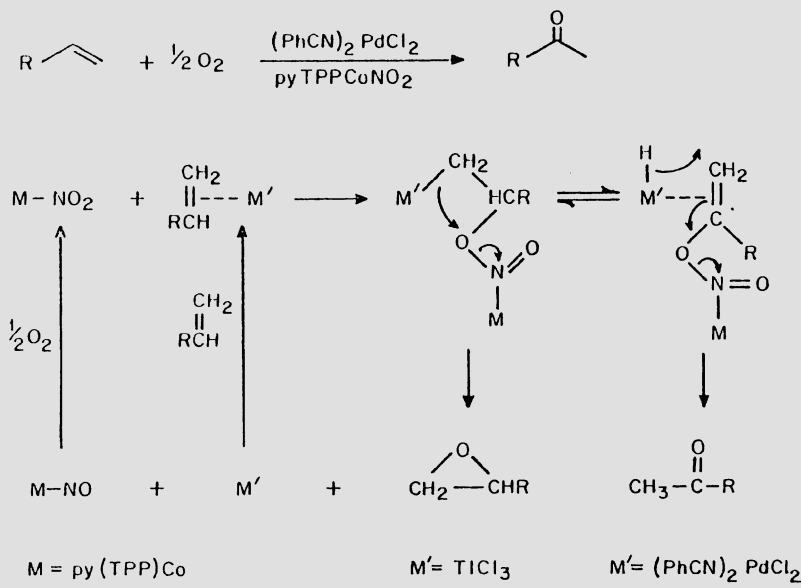


Figure 10. Catalytic oxygenation of alkenes to ketones or epoxides.

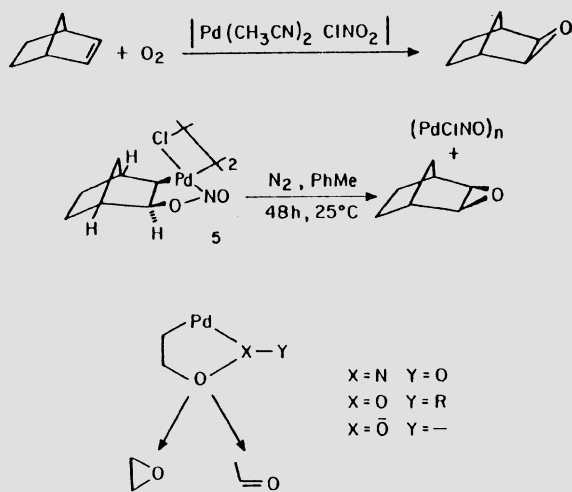
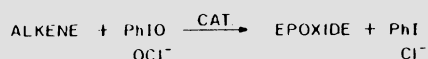


Figure 11. Alkene epoxidations catalyzed by palladium nitro complexes.

● DIRECT EPOXIDATION



CAT = MTPP_X, M = Mn, Fe, Cr

● WITH O₂

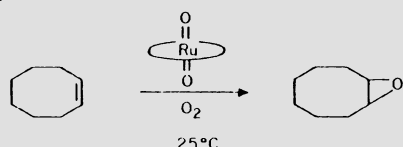


Figure 12. Oxometalloporphyrin catalysts for alkene epoxidation.

It is worthy of note that palladium nitro complexes alone are capable of catalyzing direct oxidation of alkenes through metallacyclic peroxide intermediates and that the structure of the alkene (ease of R-H elimination) determines whether epoxides or methyl ketones are produced (Fig. 11). A variety of palladium-catalyzed alkene oxidations appear to proceed via metallacyclic intermediates.

Metalloporphyrin complexes have been shown to catalyze epoxidation of alkenes (Fig. 12), and in this case metal oxo intermediates have been implicated [19-21]. In most cases strong oxidants are required; however, it has recently been reported that a ruthenium *trans*-dioxo complex catalyses direct epoxidation of an alkene with molecular oxygen as the oxidant [22]. It is believed that porphyrinato metal complex-catalyzed epoxidations are related to alkene epoxidations catalyzed by cytochrome P-450 or other active enzymatic systems. It has recently been shown that creating site-isolation by anchoring (tetraphenylporphinato)manganese(III) acetate to a rigid polymer support considerably enhances the rate of epoxidation of cyclohexene by sodium hypochlorite [23].

3.1.2. Direct Glycol Formation. It has long been known that mixtures of thallium and copper halides catalyze the direct oxidation of ethylene to ethylene glycol in water [24]. More recent work has shown that mixtures of copper and osmium oxyhalides also catalyze direct glycol formation through metallacyclic osmate esters (Fig. 13) [25].

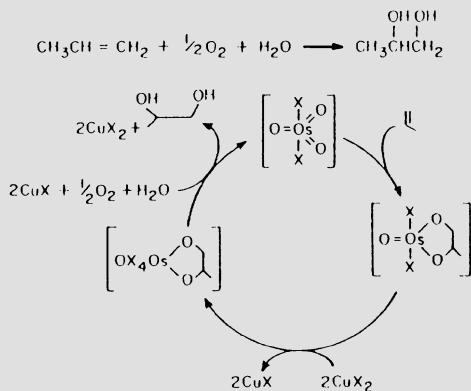


Figure 13. Propylene glycol from reaction of propylene with oxygen catalyzed by $\text{OsO}_4/\text{CuCl}_2$.

Although development of these chemistries has been limited, there could be significant utility for a direct air-oxidation of ethylene to ethylene glycol under mild conditions to supplant the currently

practiced two-step route *via* ethylene oxide as an intermediate. Whenever dual metal cooperativity is required, as it is in both of these systems, it is of interest to consider molecular design of a surface catalyst to accomplish similar chemistry.

3.1.3. Allylic Oxidation. The Wacker reaction and related palladium-catalyzed oxidations which proceed *via* nucleophilic attack on coordinated alkene have been widely practiced in industry to produce acetaldehyde, acetone, and vinyl acetate. An alternative pathway is available to alkenes in the coordination sphere of palladium(II) complexes, which could lead to another important family of oxidation products. Insertion into the allylic C-H bond of 1-alkenes gives π -allyl complexes which, on attack by external nucleophiles, would produce a family of allylic oxidation products including α,β -unsaturated alcohols, carbonyl compounds, and carboxylic acids. Electron-withdrawing anionic ligands such as trifluoroacetate enhance the ability of the palladium center to insert into C-H bonds in this manner [26] (Fig. 14). Catalytic conversion of propylene to allyl acetate has been achieved in high selectivity in the presence of catalytic quantities of palladium(II) trifluoroacetate [27].

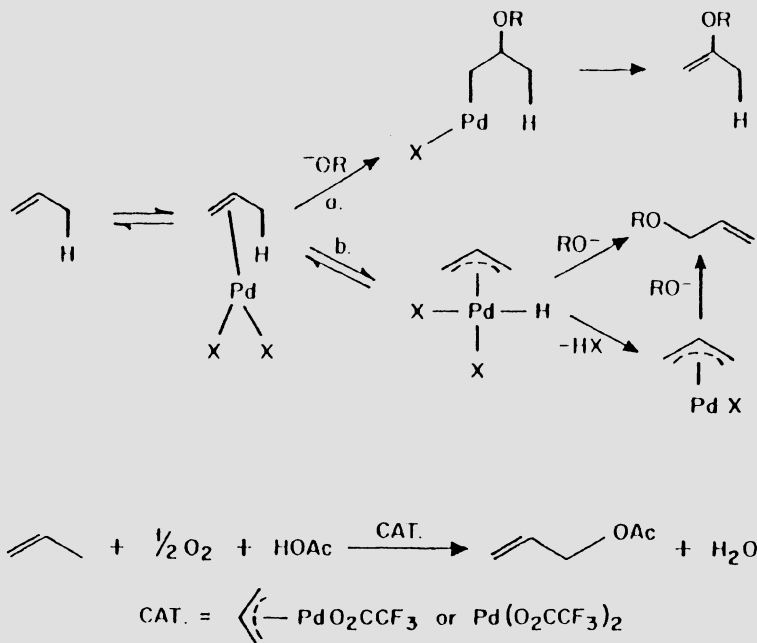


Figure 14. Palladium-catalyzed allylic oxidation of an alkene.

Another route to catalytically active π -allyl intermediates proceeds via oxidative addition to a coordinatively unsaturated palladium(0) center (Fig. 15). This usually requires a good leaving group such as acetate in the allylic position [28]. A cationic π -allyl complex has been isolated and shown to be a reaction intermediate. When the leaving group is H, as it is in 1-alkene, the reaction is also disfavored thermodynamically unless the hydrogen which would be produced is oxidatively converted to water.

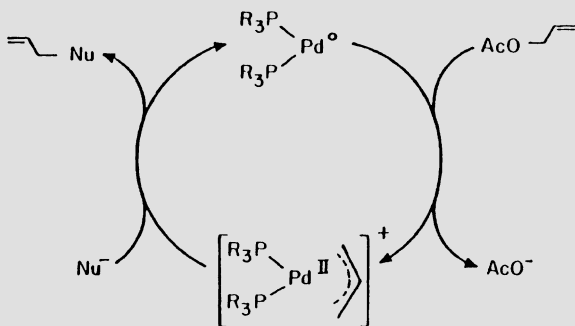


Figure 15. A π -allyl intermediate in an allylic substitution reaction.

Heterogeneous palladium catalysts are known to activate the C-H bond of 1-alkenes and, hence, it became of interest whether an efficient catalytic alkene oxidation could be accomplished in a manner analogous to that shown in Fig. 15 in the presence of a supported palladium(0) center (Fig. 16). It has been found that such a reaction proceeds smoothly when $HY = HOAc$ over Pd/SiO_2 in the vapor phase [29] and over Pd/C in the liquid phase [30] to form allyl acetate nearly quantitatively from propylene. When the alkene is either cis- or trans-2-butene, a mixture of linear and branched allylic acetates is formed together with small amounts of vinylic acetates (Fig. 17). This result was disappointing since selective production of linear allylic acetates in this way could have provided a low-cost route to the 1,4-diacetate, a butanediol intermediate [30]. π -Allyl complexes formed from butadiene can be regioselectively acetoxylated using palladium complexes in the liquid phase to give 1,4-diacetates exclusively [31]. This result encourages one to speculate that by proper control of surface geometry one might be able to selectively prepare 1,4-butene diacetates from butenes by acetoxylation.

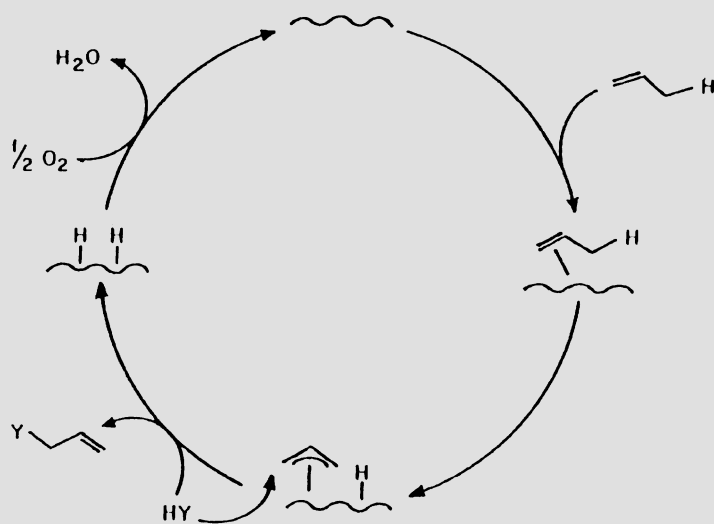


Figure 16. An alkene oxidation mechanism involving oxidative addition of propylene to a Pd surface.

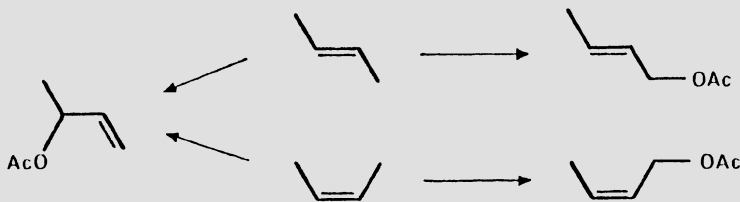


Figure 17. Allylic acetoxylation of 2-butenes.

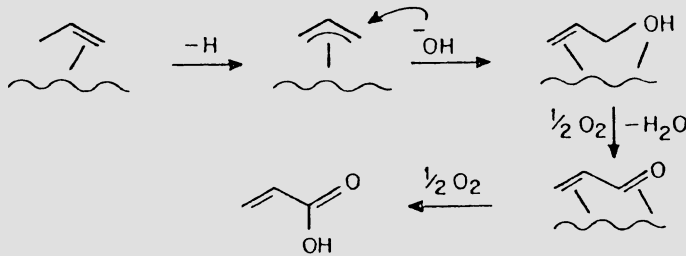


Figure 18. Proposed pathway from propylene to acrylic acid over a palladium catalyst.

When HY in Fig. 15 is HOH, acrylic acid is formed in high yields during mild liquid-phase oxidation over Pd/C [30,32-35]. Presumably, allyl alcohol is the initial product, which is rapidly oxidized further on the surface of the catalyst (Fig. 18). In a similar manner, isobutylene is oxidized to methacrylic acid and methacrolein, while 2-butene is oxidized to crotonic acid and crotonaldehyde.

3.1.4. Oxidative Carbonylation. The oxidative carbonylation reaction is one of the most versatile synthetic catalytic oxidation reactions [36-40]. It is catalyzed in solution by $\text{Pd}^{\text{II}}/\text{Cu}^{\text{II}}$ mixtures (as in Wacker chemistry) or it can be run over heterogeneous palladium catalysts such as $\text{Pd}/\text{V}_2\text{O}_5$ [41] which contain strong O_2 -regenerable oxidants to keep palladium in the catalytically active oxidation state. Fig. 19 shows the breadth of reaction possibilities using alcohol as a nucleophile to give alkyl carbonate, oxalate, acrylate, succinate, crotonate, methacrylate, cinnamate, or adipate, depending on the alkene charged and reaction conditions. Nitrogen-containing nucleophiles are now being used to produce isocyanates or carbamates. Although the only current commercial application of this reaction is in the copper-

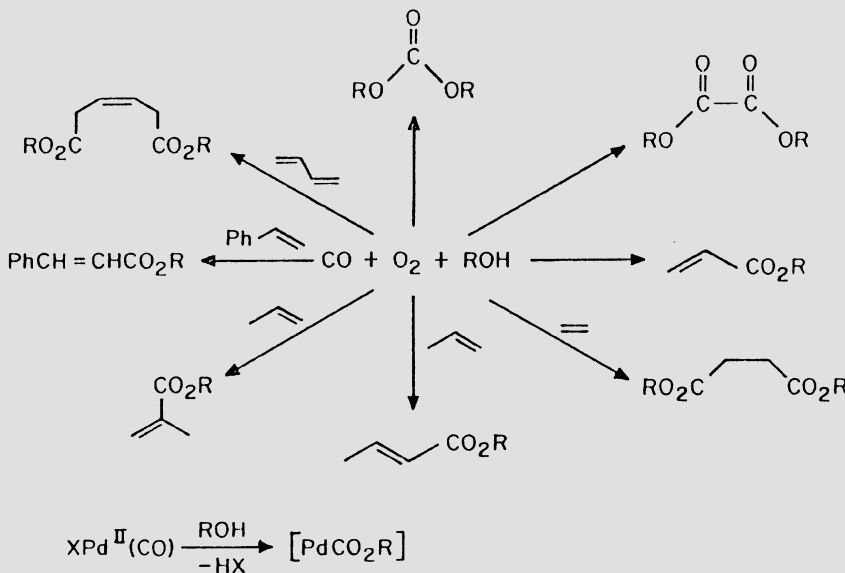


Figure 19. Oxidative carbonylation reactions catalyzed by palladium salts in solution.

catalyzed conversion of CO, O₂, and alcohols to carbonates, a bright future seems to be in store for this chemistry.

The oxidation state of the catalytically active site is of primary importance, both in alkene oxidation and oxidative carbonylation using either homogeneous or heterogeneous catalysts. The oxidation of an alkene to a vinylic oxidation product using Wacker chemistry requires properly tuned Pd(II) centers. An oxidant strong enough to create these centers is required in order to prevent formation of Pd(0), which is effective for producing vinylic oxidation products. The same considerations seem to hold for the oxidative carbonylation reactions, and therefore Pd(II)/Cu(II) couples are effective in solution and Pd/V₂O₅ couples are reactive heterogeneous catalysts in vapor-phase operation. Thus in both vinylic oxidations and in oxidative carbonylations the palladium catalyst should be maintained in the Pd(II) oxidation state.

On the other hand, strongly electron-withdrawing groups in the coordination sphere of the palladium increase its electrophilicity and its ability to oxidatively add allylic C-H bonds. In this reaction Pd(II) is oxidized to Pd(IV), and allylic rather than vinylic oxidation products may predominate. Palladium(II) trifluoroacetate is therefore an excellent solution-phase catalyst for allylic oxidation, and in this case palladium must be maintained in a higher oxidation state for efficient catalysis ($Pd^{+2} \rightleftharpoons Pd^{+4}$). This suggests that strong oxidants that are regenerable with O₂ might be preferable co-catalysts for this reaction.

Another means of catalyzing allylic oxidations of 1-alkenes is to create π -allyls by oxidative addition to low-oxidation-state metal centers. As we have seen, this is particularly effective for heterogeneous allylic oxidation of alkenes. It is important that strong oxidants be avoided in these systems since formation of Pd(II) will lead to vinylic rather than allylic oxidations. For example, the addition of permanganate to the Pd/C-catalyzed oxidation of propylene to acrylic acid in water (Fig. 18) changes the product abruptly from acrylic acid to acetone. Thus, much can be learned regarding molecular design of selective heterogeneous palladium oxidation catalysts from consideration of solution organometallic chemistry which directly applies to surface catalytic species.

3.2. Aromatic Oxidations

Among those aromatic oxidations which cannot yet be done efficiently in a catalytic manner are the direct hydroxylation of an aromatic ring using molecular oxygen and the oxidative carbonylation of an aromatic to aryl carboxylic acid. A reaction which has been given considerable attention in recent years, the oxidative cleavage of an aromatic ring, could also be useful if developed further. Partial oxidation of methyl aromatics to benzyl alcohols and benzaldehydes as well as oxidative cleavage of phenyl methyl bonds to give phenolic derivatives could also have utility.

3.2.1. Aromatic Hydroxylation. Direct hydroxylation of benzene to phenol using molecular oxygen is a difficult reaction for which no efficient catalyst has been developed. A unique hydroxylation reaction has been reported recently in which a vanadium peroxy complex is capable of attacking an aromatic ring to form a phenolic product (Fig. 20) [41]. Interestingly, ring attack occurs preferentially, rather than side chain oxidation. The radical nature of the attacking species is somewhat reminiscent of Fenton chemistry [42], but the product profile is entirely different. If developed into a catalytic process, such a mild, selective aromatic hydroxylation reaction could have great synthetic utility.

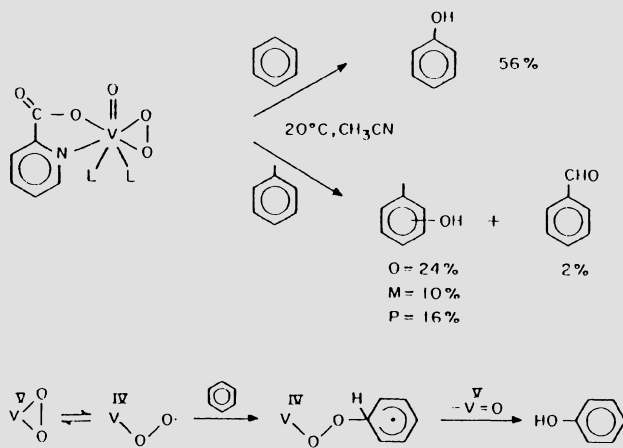
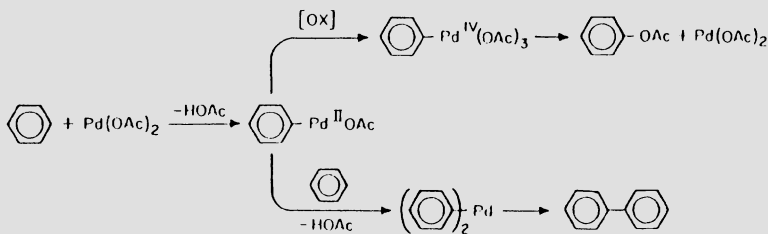


Figure 20. Oxidation of aromatics by a vanadium peroxy complex.

Acetoxylation of benzene to phenyl acetate can be accomplished using either homogeneous or heterogeneous palladium catalysts in the liquid phase (Fig. 21) [43-46]. Again high-oxidation-state Pd(IV) intermediates have been implicated, which may arise by oxidation of Pd(II) aryls. Strong oxidants such as permanganate, dichromate, or peroxydisulfate can be used under mild conditions. Molecular oxygen is effective only under forcing conditions [30,47]. Palladium acetate or Pd/SiO₂ has been used to produce acetoxylation products in the liquid phase. It would seem that Pd/V₂O₅ might provide a more strongly oxidizing surface for reactions with O₂ at high temperature than Pd/SiO₂.

● WITH STRONG OXIDANTS



Stock; Henry; Eberson

● WITH O₂

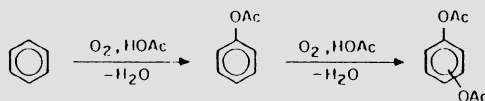
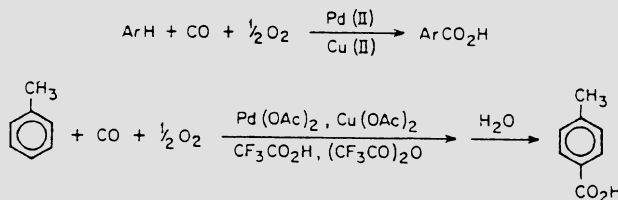


Figure 21. The roles of Pd(II) and Pd(IV) in acetoxylation of aromatic rings.

3.2.2. Oxidative Carbonylation of Aromatics. The oxidative carbonylation of aromatic rings (Fig. 22), is much more difficult to achieve than oxidative carbonylation of alkenes. Earlier work was done under forcing conditions of temperature and pressure; however, Pd(II)/Cu(II)



CONDITIONS: 45°C, 100 psig

YIELD: 6744 % (Pd), 312 % (Pd + Cu)

ISOMER DISTRIBUTION: o - 25 %

m - 9 %

p - 66 %

Figure 22. Oxidative carbonylation of aromatics catalyzed by palladium complexes in solutions.

couples work to some extent under mild conditions [2]. It seems that high pressures of CO inhibit coordination of the arene by saturating the coordination sphere of the metal. Much more work must be done to provide an efficient catalyst for this reaction. The promise of direct production of aromatic carboxylic acids from inexpensive starting materials may stimulate more work in this area.

3.2.3. Phenol Oxidations. Much work has been done on the copper-catalyzed oxidation of phenols in the liquid phase (Fig. 23). Depending on the nature of the starting phenol and on the copper catalyst, a wide array of products is possible *via* selective oxidative transformations. Selective production of polyphenylene oxides [48,49], quinones [50], coupling products [51], and oxidative cleavage products [52] have all been accomplished. Polyphenylene oxides are produced industrially on a large scale by copper-catalyzed oxidation of 2,6-di-substituted phenols. Copper(I)-catalyzed oxidation of 2,3,6-trimethylphenol to the corresponding *para*-quinone is carried out during the commercial production of vitamin E [53]. Chemistry of the latter type has been suggested for the commercial production of hydroquinone and antioxidants having the *para*-quinone structure.

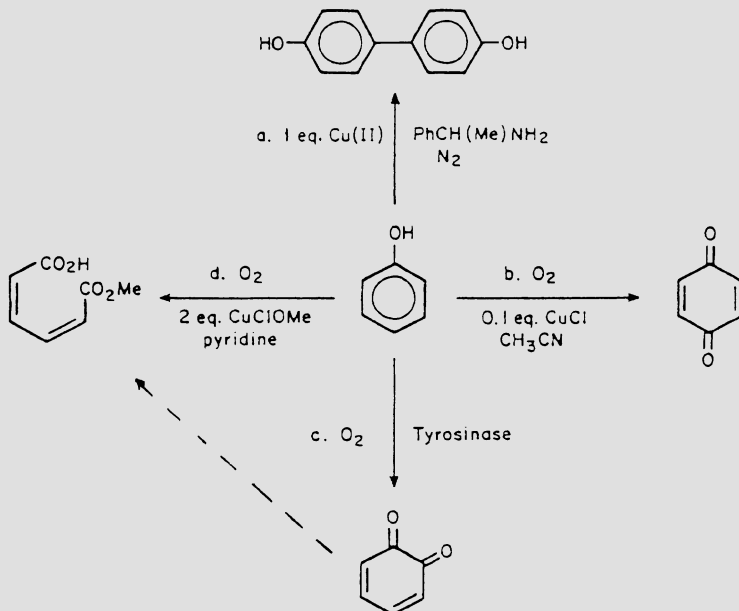


Figure 23. Some copper-mediated aromatic oxidations.

One can rationalize much of this chemistry on the basis of bound radical species, and evidence for such species has recently been found [54]. A very different mechanism has been suggested for the selective formation of quinones catalyzed by copper in a binucleating macrocycle which mimics tyrosinase (Fig. 24) [55]. Quinones may be intermediates in oxidative cleavage reactions of phenols. One can speculate about whether a supported analogue of a dicopper complex having binucleating macrocyclic ligands could be used to advantage in either quinone synthesis or in oxidative cleavage reactions.

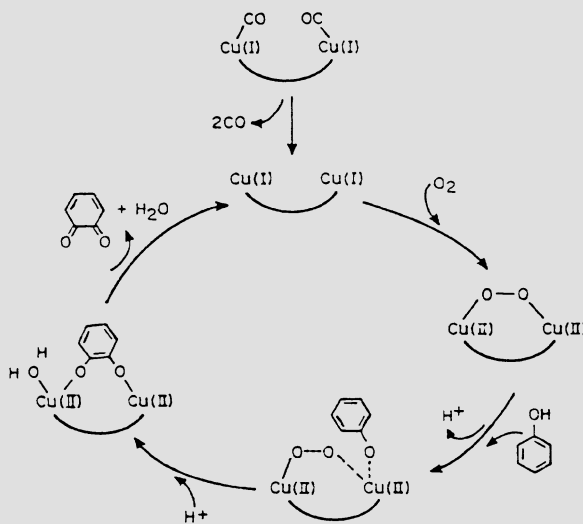


Figure 24. Proposed mechanism for the oxidation of phenol to *o*-benzoquinone catalyzed by a dicopper complex in a binucleating macrocycle.

3.2.4. Methyl Aromatic Oxidations. Activation of the C-H bond of methyl aromatics has long been known to occur in the presence of strong oxidants such as Co(III) (Fig. 25) [56]. It is interesting to consider the possible effect of an oxide surface containing high-oxidation-state cobalt on proton removal. Facile C-H bond cleavages might indeed occur *via* this type of molecular surface catalysis. In any case, benzylperoxy radicals are the ultimate product, and they can be encouraged to undergo a number of different selective oxidation reactions, depending on conditions and reaction medium (Fig. 26) [1].

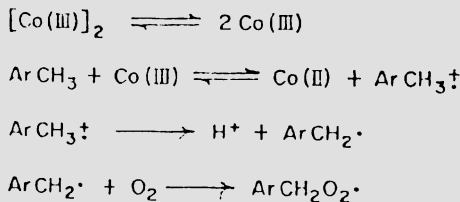


Figure 25. Cobalt(III) in benzylic oxidations.

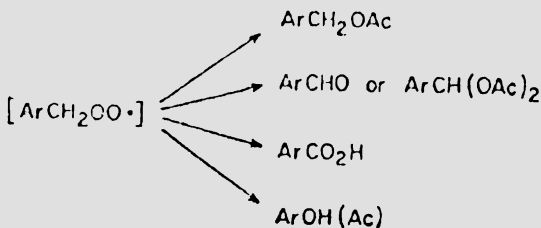


Figure 26. Possible selective transformations of benzylperoxy radicals to stable oxidation products in acetic acid.

A particularly intriguing reaction involving benzyl radicals is the oxidative cleavage of methyl aromatics in the presence of strong oxidizing acids to give a phenolics and formaldehyde in equimolar amounts (Figs. 27 and 28) [57-59]. Improvements in selectivity and rate are needed, but catalytic technology based on this chemistry could have broad application if adequately developed.

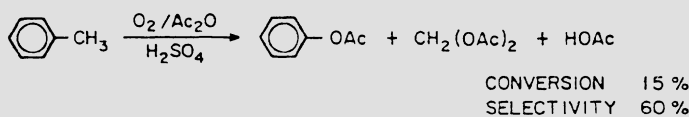
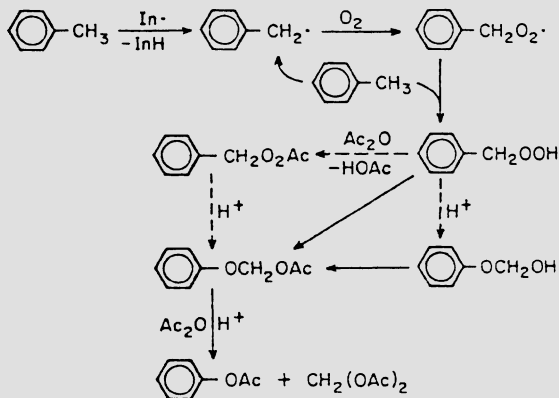
PROPOSED PATHWAY

Figure 27. Radical-initiated oxidation of toluene to phenyl acetate in acetic acid solution of a strong acid.

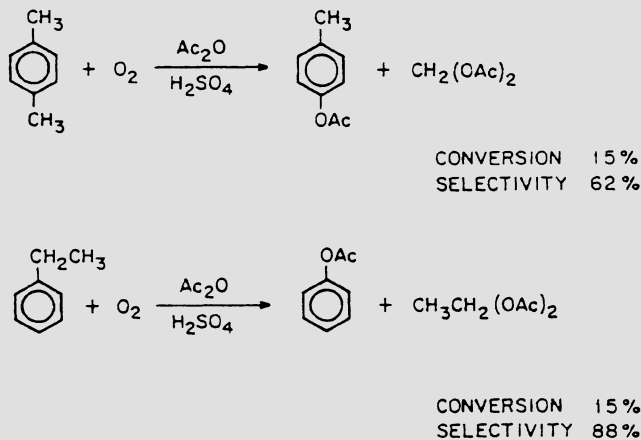


Figure 28. Oxidative cleavage of methyl aromatics in acetic acid solutions containing sulfuric acid.

Finally, it is interesting to note that advances in molecular catalysis of aromatic oxidation are making inroads into areas once considered strictly the domain of enzymatic catalysis (Fig. 29). Direct ring hydroxylation, oxidative cleavage, alkyl group hydroxylation, and *ortho*-quinone formation now have precedent in homogeneous catalysis. Molecular design of surface catalysts having proton and electron mobility and specific spatial characteristics may one day rival the enzymes in selectivity and rate.

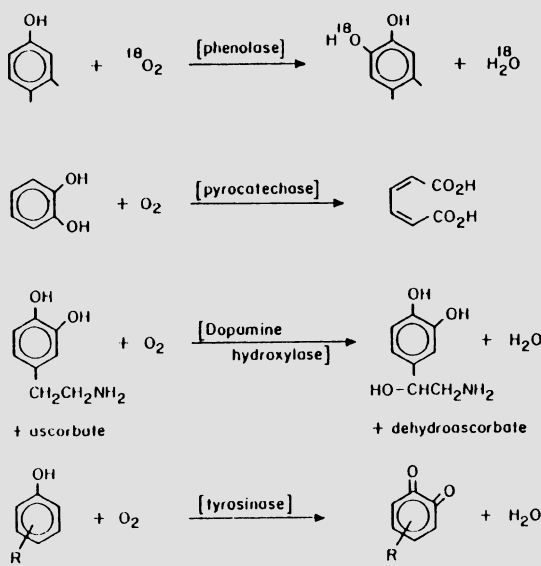


Figure 29. Enzymatic oxidation of aromatic compounds.

3.3. Alkane Oxidations

The most difficult group of hydrocarbons to oxidize and one which until recently has resisted attempts at selective mild catalytic activation is the alkanes. Among those transformations currently desired (Fig. 30) are direct conversion of methane to methanol, formaldehyde, or higher hydrocarbons; direct hydroxylation of light alkanes; and smooth selective oxidative dehydrogenation of alkanes.

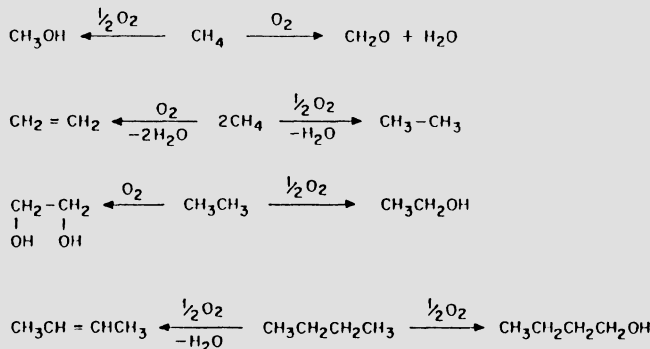


Figure 30. Some alkane oxidations for which selective catalysts are desired.

First-row transition metal salts and complexes have long been known to promote alkane oxidations, but their role is mainly to increase reaction rates by generating initiating radicals [1]. Cobalt(III) complexes are reported to interact differently with alkanes (Fig. 31) [60]. In order to explain high reactivity and abnormal selectivity, an electron transfer mechanism has been suggested which is similar to that proposed for activation of alkyl aromatics (Fig. 25). In contrast to some other C-H activation schemes, such a pathway is quite thermodynamically favorable, provided that the proton released from the cation radical is suitably solvated by the reaction medium. Specific surface solvation of protons released in such a pathway could further enhance the effectiveness of this chemistry. Molecular design of heterogeneous catalysts having high-oxidation-state metals on oxidic supports might prove to be highly useful here.

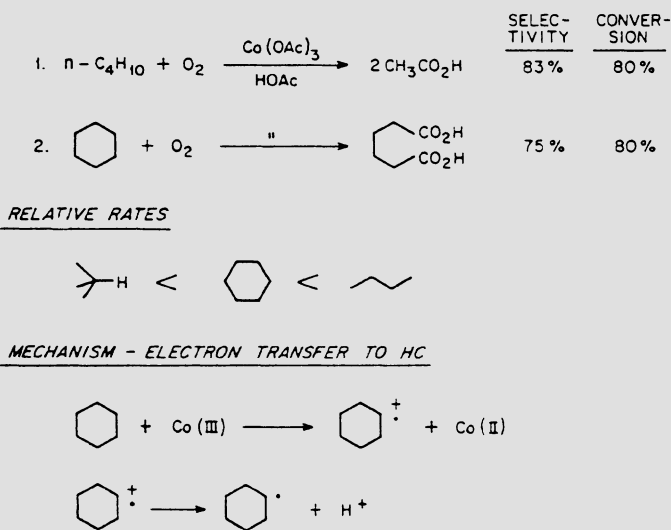


Figure 31. Cobalt(III) in alkane oxidations.

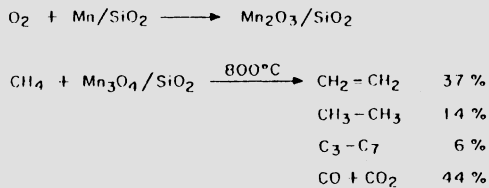
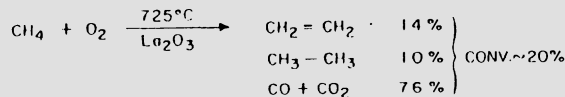
STEP-WISE OVER REDUCIBLE METAL OXIDES**CATALYTIC OVER La_2O_3** VIA METHYL RADICALS

Figure 32. Oxidative coupling of methane over supported metal catalysts.

An interesting approach to the oxidative coupling of methane to higher hydrocarbons is shown in Fig. 32. High-temperature one- or two-step oxidations of methane over reducible metal oxides produce methyl radicals which condense to C_2^+ hydrocarbons in the gas phase [61-65]. Recent work has demonstrated selectivities to C_2 and higher hydrocarbons of greater than 70% from methane at conversions of nearly 20% [66-69]. Reports of both moderate- and low-temperature oxidation of methane to methanol have appeared in the patent literature [70-74].

A recent case of unusual alkane oxidation chemistry has been reported (Fig. 33), in which metal carbene complexes have been implicated [75]. In a case in which primary, secondary and tertiary C-H bonds are available, neither tertiary C-H bonds (favored by radical abstraction) nor primary C-H bonds are attacked; instead secondary C-H bonds react.

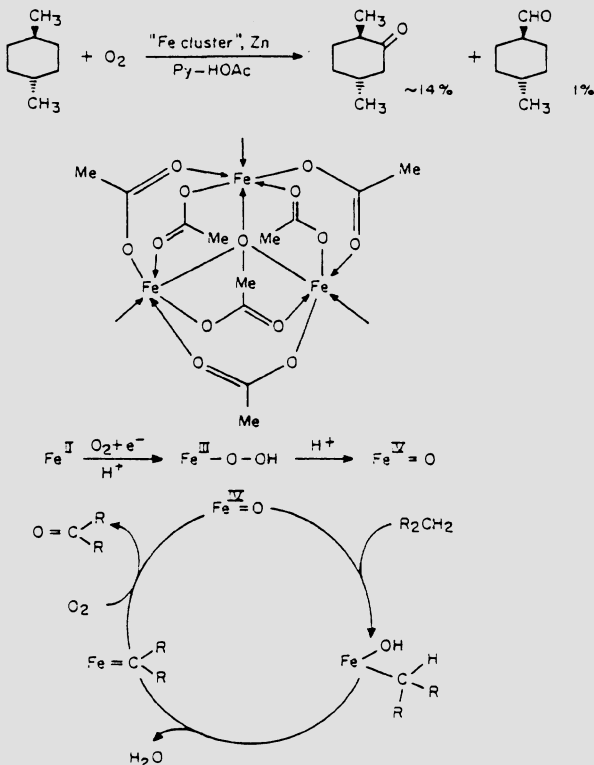
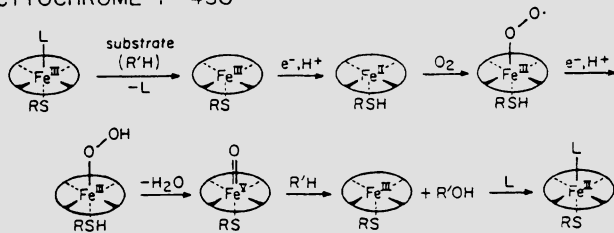


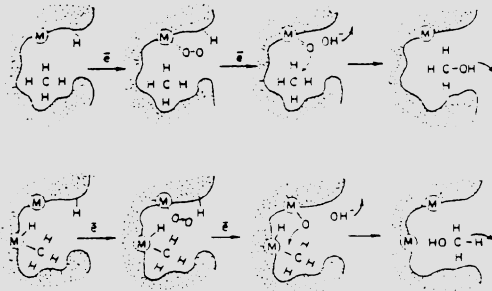
Figure 33. A tri-iron complex catalyzes selective alkane oxidations.

Among the most rapid and selective alkane activation catalysts are the biological systems such as cytochrome P-450 and methane monooxygenase (Fig. 34). Although incompletely understood, these catalysts are thought to have metal centers capable of binding and cleaving dioxygen. Active metal oxo complexes are believed to be capable of hydroxylating C-H bonds in a selective manner [76]. Biomimetic systems are under intensive investigation in attempts to better understand and apply this chemistry. Even if one were to generate active metal oxo complexes from dioxygen in a biomimetic system, it would likely be difficult to devise a selective catalytic process because the same metal center could be able to form superoxo, peroxy, bridged peroxy, and other active oxygen species (Fig. 35). Indeed these could be necessary intermediates in the formation of metal oxo complexes. This may be an area in which surface catalysts prepared using carefully designed molecular species with proximate dual metal centers and electron-regenerable co-reductants might someday be the truly selective biomimetic catalysts.

CYTOCHROME P-450



METHANE MONOOXYGENASE



A HYPOTHETIC MECHANISM OF ENZYMATIC METHANE OXIDATION
 A - METHANE BINDING IN HYDROPHOBIC POCKET;
 B - METAL ION TAKING PART IN METHANE BINDING

Figure 34. Alkane oxidations by biological systems.

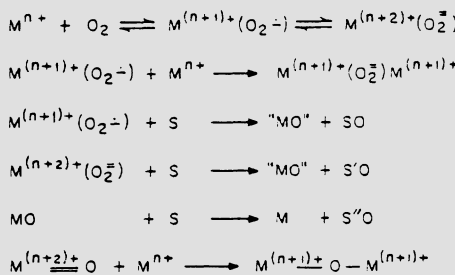


Figure 35. Some common reaction intermediates in metal-catalyzed oxidations.

4. SUMMARY

Selective oxidation catalysts are often multifunctional systems requiring elaborate cooperative effects between active centers. Some are bimetallic, or even multimetallic. Some catalysts have complex ligand systems. Others contain acidic or basic promoters. Electron transfer and proton mobility are desirable characteristics. Oxidation catalysts must facilitate numerous molecular transformations in a highly organized manner in order to accomplish the extensive bond-breaking, bond-making, electron transfer, and tautomerization reactions that occur during hydrocarbon oxidations. We have seen that activity and selectivity can depend on the geometrical arrangement of catalyst components.

Nowhere is cooperativity between sites on a catalyst more necessary than in catalytic oxidation. No diatomic molecule is as diverse in its reactions or as difficult to control as dioxygen — yet as productive of important products. Molecular design of multifunctional surfaces provides an opportunity to create an environment for control of the reactions of molecular oxygen with hydrocarbons.

Of course, selective heterogeneous oxidation catalysts will also possess many practical advantages. Active surfaces could avoid corrosion problems that plague some homogeneous catalyzed oxidations. In addition, continuous oxidation over a surface provides the opportunity to readily remove product as formed before it further oxidizes to an undesirable product. A major problem in homogeneous catalytic oxidation is that of oxidizability of ligand systems. Supports which are resistant to oxidation have an obvious advantage here.

Thus, for both theoretical and practical reasons, the molecular design of active surface catalysts holds the promise of creating a family of new oxidation catalysts which are superior both to currently used homogeneous liquid-phase catalysts and to empirically derived heterogeneous systems with selectivities that could be improved. The power of this approach will ultimately be realized in the creation of selective oxidation catalysts which perform oxidations that are beyond the scope of current catalyst systems.

5. REFERENCES

1. J.E. Lyons, Applied Industrial Catalysis, vol. 3, Academic Press, New York (1984).
2. J.E. Lyons, Hydrocarbon Process., November, 107 (1980).
3. R.Sheldon, Aspects of Homogeneous Catalysis, vol. 4, Reidel, Dordrecht (1981).
4. K.B. Sharpless, Chemistry in Britain, January, 38 (1986).
5. K. Allison, P. Johnson, G. Forster, and M. Sparke, Ind. Eng. Chem., Prod. Res. Dev. 5, 166 (1966).
6. J.E. Lyons and J.O. Turner, Tetrahedron Lett., 2378 (1974).
7. J.E. Lyons, Adv. Chem. Ser. 132, 64 (1974).
8. J.E. Lyons, U.S. Patent 4,021,369 (1977).
9. H. Mimoun, Rev. Inst. Français du Pétrole 33, 259 (1978).
10. C. Dudley, G. Read, and P. Walker, J. Chem. Soc., Dalton Trans., 1926 (1974).
- 11a. D. Holland and D. Milner, J. Chem. Soc., Dalton Trans., 2440 (1975).
- 11b. H. Mimoun, M. Mercedes Perez Macherand, and I. Seree de Roch, J. Am. Chem. Soc. 100, 5437 (1978).
12. J.D. Solar, F. Mares, and S.E. Diamond, Catal. Rev. - Sci. Eng. 27, 1 (1985).
13. M. Andrews and K. Kelley, J. Am. Chem. Soc. 103, 2894 (1981).
14. B. DePoorter and B. Meunier, J. Chem. Soc., Perkin Trans. 2, 1735 (1985).
15. D. Mansuy, J. LeClaire, M. Fontecave, and P. Donsette, Tetrahedron 40, 2847 (1984).
16. J.T. Groves and T.E. Nemo, J. Am. Chem. Soc. 105, 5786 (1983).
17. C.J. Chang and F. Ebenia, J. Chem. Soc., Chem. Commun., 778 (1981).
18. C.L. Hill, J.A. Smegal, and T.J. Henley, J. Org. Chem. 48, 3277 (1983).
19. I. Tabushi and N. Koga, Tetrahedron Lett., 3681 (1979).
20. B. Meunier, E. Guillet, M.-E. DeCarvalho, and R. Poilblanc, J. Am. Chem. Soc. 106, 6668 (1984).
21. M.W. Ne and T.C. Bruice, J. Am. Chem. Soc. 104, 6123 (1982).
22. J.T. Groves and R. Quinn, J. Am. Chem. Soc. 107, 5790 (1985).
23. A.W. Van der Made, J.W.H. Smeets, R.J.M. Nolte, and W.F. Drenth, J. Chem. Soc., Chem. Commun., 1204 (1983).
24. J. Kollar, Belgian Patent 766,001 (1971).

25. R.G. Austin, R.C. Michaelson, and R.S. Myers, Chem. Ind. **22**, 269 (1985).
26. B.M. Trost and P.J. Metzner, J. Am. Chem. Soc. **102**, 3572 (1980).
27. L. Laussin, J.-P. Laloz, and H. Mimoun, French Patent 2,450,802 (1980).
28. P.R. Auburn, P.B. Mackenzie, and B. Bosnich, J. Am. Chem. Soc. **107**, 2033 (1985).
29. W. Swodenk and G. Scharfe, U.S. Patent 3,925,452 (1975).
30. J.E. Lyons, G. Suld, and C.-Y. Hsu, in Homogeneous and Heterogeneous Catalysis, (Eds. Yu. Yermakov and V. Likholobov), p. 117, VNU Science Press, Utrecht (1986).
31. J.-E. Backvall, J.-E. Nystrom, and R.-E. Nordberg, J. Am. Chem. Soc. **107**, 3676 (1985).
32. T. Seiyama, N. Yamazoe, J. Hojo, and M. Hayakawa, J. Catal. **24**, 173 (1972).
33. K. Fujimoto and T. Kunugi, J. Jpn. Petrol. Inst. **17**, 739 (1974).
34. R. David and S. Estienne, U.S. Patent 3,624,147 (1971).
35. J.A. Hinnenkamp, U.S. Patent 4,435,598 (1984).
36. D.M. Fenton and K.L. Olivier, CHEMTECH, **22** (1972).
37. R. Ugo, in Catalysis in C₁ Chemistry, (Ed. W. Keim), p. 156, Reidel, Dordrecht (1983).
38. R.A. Sheldon, in Chemicals from Synthesis Gas, p. 140, Reidel, Dordrecht (1983).
39. D.M. Fenton, K.L. Olivier, and G. Riale, Am. Chem. Soc. Div. Petr. Chem. Preprints **14**, C77 (1969).
40. D.M. Fenton and P.J. Steinwand, J. Org. Chem. **37**, 2034 (1972).
41. H. Mimoun, L. Saussine, E. Daire, M. Postel, J. Fischer, and R. Weiss, J. Am. Chem. Soc. **105**, 3101 (1983).
42. C. Walling, Acc. Chem. Res. **8**, 125 (1975).
43. P.M. Henry, J. Org. Chem. **36**, 1886 (1971).
44. L. Eberson and L. Gomez-Gonzales, Acta Chem. Scand. **27**, 1162 (1973); **27**, 1249 (1973); **27**, 1253 (1973).
45. L. Eberson and L. Jonsson, Acta Chem. Scand. **28**, 597 (1974); **28**, 771 (1974); **30**, 361 (1976).
46. L.M. Stock, K. Tse, L.J. Vorvick, and S.A. Walstrom, J. Org. Chem. **46**, 1759 (1981).
47. V.H.-J. Arpe and L. Hornig, Erdöl und Kohle **23**, 79 (1970).
48. A.S. Hay, Adv. Polym. Sci. **4**, 497 (1967).
49. A.S. Hay, J. Polym. Sci. **58**, 581 (1962).
50. J.E. Lyons and C.-Y. Hsu, in Biological and Inorganic Copper Chemistry, vol. II, p. 57, Adenine Press, New York (1985).
51. G. Davies and M. El-Sayed, Inorg. Chem. **22**, 1257 (1982).
52. M.M. Rogic, M.D. Swerdluff, and T.R. Deemin, in Copper Coordination Chemistry: Biochemical and Inorganic Perspectives, (Eds. K.P. Karlin and J. Zubietta), p. 259, Adenine Press, New York (1983).
53. W. Brenner, U.S. Patent 3,796,732 (1974).
54. J.S. Thompson, in Biological and Inorganic Copper Chemistry, vol. II, p. 1, Adenine Press, New York (1985).

55. J.E. Bulkowski and W.E. Summers (III), in Copper Coordination Chemistry: Biochemical and Inorganic Perspectives, (Eds. K.P. Karlin and J. Zubieta), p. 1, Adenine Press, New York (1983).
56. Reviewed in R. Sheldon and J. Kochi, Adv. Catal. 25, 274 (1976).
57. A. Bashkirov, V. Kugel, I. Vygodskaya, F. Novak, and E. Sokolvar, Neftekhimiya 19, 107 (1979).
58. J.E. Lyons, G. Suld, R.W. Shinn, and C.-Y. Hsu, Ind. Eng. Chem., Prod. Res. Dev. 19, 468 (1980).
59. J.E. Lyons, G. Suld, R.W. Shinn, and C.-Y. Hsu, in Catalysis of Organic Reactions, (Ed. W. Moser), p. 111, Dekker, New York (1981).
60. A. Onophenko and J. Shultz, J. Org. Chem. 38, 999 (1973); 38, 3729 (1973).
61. K. Otsuka, Q. Liu, and A. Morikawa, J. Chem. Soc., Chem. Commun., 586 (1986).
62. C.-H. Lin, K.D. Campbell, J.-X. Wang, and J.H. Lunsford, J. Phys. Chem. 90, 534 (1986).
63. G.E. Keller and M.M. Bhasin, J. Catal. 73, 9 (1982).
64. V.W. Hensen and M. Baerns, Chem.-Ztg. 107, 223 (1983).
65. C.A. Jones, J.J. Leonard, and J.A. Sofranko, U.S. Patents 4,443,644 to 4,443,649; 4,443,984 (1984).
66. J.B. Kimble and J.H. Koltz, Energy Progress 6, 226 (1986).
67. J.A. Sofranko, J.J. Leonard, and C.A. Jones, J. Catal. 103, 302 (1987).
68. C.A. Jones, J.J. Leonard, and J.A. Sofranko, J. Catal. 103, 311 (1987).
69. C.A. Jones, J.J. Leonard, and J.A. Sofranko, Energy and Fuels 1, 12 (1987).
70. D.A. Dowden and G.T. Walker, UK Patent 1,244,001 (1971).
71. H.J.F. Stroud, UK Patent 1,398,385 (1975).
72. R.-S. Lin, M. Iwamoto, and J.H. Lunsford, J. Chem. Soc., Chem. Commun., 78 (1982).
73. M.M. Kahn and G.A. Somorjai, J. Catal. 91, 263 (1985).
74. P. Pritchai and K. Klier, Chem. Rev.-Sci. Eng. 28, 13 (1986).
75. D.H.R. Barton, J. Boivin, N. Anbalik, and K.M. Schwartzentruber, Tetrahedron Lett., 4219 (1984).
76. J.T. Groves and T.E. Nemo, J. Am. Chem. Soc. 105, 6243 (1983).

REACTIONS OF ORGANOMETALLIC COMPOUNDS WITH SURFACES OF SUPPORTED AND UNSUPPORTED METALS

Yuri A. Ryndin and Yuri I. Yermakov
Institute of Catalysis
Novosibirsk 630090
USSR

ABSTRACT. Interactions of organometallic compounds with metal surfaces can be used to produce metal films and coatings as well as to modify the properties of metal catalysts for hydrocarbon conversion. The literature is reviewed, and results are evaluated characterizing the interaction of metal carbonyl clusters with surfaces of supported metals under mild conditions. The reactions lead to the preparation of highly dispersed bimetallic particles, which have homogeneous compositions and nonadditive properties in CO hydrogenation and hydrocarbon conversion.

1. INTRODUCTION

The interaction of organometallic compounds with surfaces of metal oxide supports is widely used to obtain supported catalysts containing surface metal ions in various coordinations and ultradispersed sulphide or metallic particles [1]. In recent years, an increasing interest has been shown in application of the interaction of organometallic compounds with surfaces of supported metals for obtaining bimetallic catalysts.

There are many opportunities for purposeful variation of the activity and selectivity of supported metal catalysts provided by the use of modifying elements which produce, with the active metal, alloy particles (or "bimetallic clusters" according to Sinfelt [2]). When these catalysts are prepared by conventional impregnation or adsorption methods, the formation of bimetallic particles occurs in the step of high-temperature reduction and is accompanied by production of bimetallic particles of different composition, accompanied by sintering [2]. These disadvantages can be overcome, in part, by anchoring bielemental compounds with a metal-promoter bond to the support surface [3]. However, in this case variations of the metal-promoter ratio are limited, and there may be oxidation of the promoter by hydroxyl groups of the support.

In this connection, new methods of preparation of bimetallic catalysts via interaction of organometallic compounds of the promoter

with the surface of a supported metal seem to be of special interest. Methods of modification of Pt/Al₂O₃ catalysts by treating them with alkyl compounds of group IVA metals [4-7] or with metal carbonyl clusters [8-10] are available. However, these methods do not exclude the possibility of segregation of elements, even in the step of supporting the metal, because the organometallic compounds react both with platinum and Al₂O₃ surfaces.

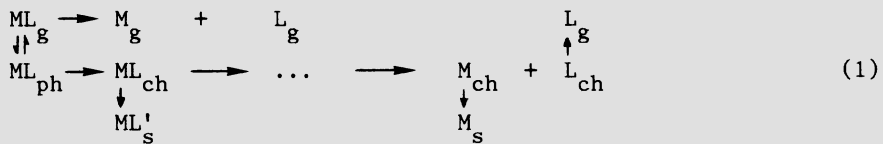
An alternative method of preparation of bimetallic catalysts [11-14] is based on the direct interaction of metal carbonyl clusters with surfaces of supported metals under mild conditions. In this work, a comparison is made of various methods of preparation of mixed metallic particles by interaction of organometallic compounds with metal surfaces.

2. INTERACTION OF ORGANOMETALLIC COMPOUNDS WITH UNSUPPORTED METALS

In the last 20 years, organometallic compounds have found wide application for production of metal films having useful protective or electrical properties [15-17]. This process involves thermal decomposition of the organometallic compound on the metal surface and, therefore, can serve as example of the interaction between such compounds and metal surfaces. Substantial experience accumulated in this area may be helpful in the development of metal catalysts. In this instance, we would like to mention a great contribution made to the area of interest by representatives of Gorkii [16] and Moscow [17] schools.

The process of precipitation of metal films consists of the following steps: evaporation of the organometallic compound, its transport to the heated surface, adsorption and dissociation on the metal surface, and completion of the metal lattice. The growth rate of a metal film is typically up to 10⁴ atomic layers per second.

The mechanism of the interaction of the organometallic compound with the surface of a growing metal film is as follows [16]:



where ML is the metal complex and ML' is the decomposition side product; g refers to the gas phase, ph to physical adsorption, ch to chemisorption, and s to the solid state.

Reactions in the adsorbed layer involve the steps of physical adsorption and chemisorption and a multistep process of thermal dissociation (represented by the dotted line). By selecting conditions of the process, it is possible to minimize the formation of side products ML', such as carbides and nitrides; some steps of thermal decomposition can be catalyzed by adatoms M_{ch} or by metal films M_s.

The dissociation of organometallic compounds occurs via a homolytic rupture of M-L bonds, giving metal atoms and ligand molecules. Ligands with an odd number of electrons and with substituents X ($X = H$, halogen, or alkyl) in the β -position can split off, producing olefin and MX. This reaction leads to contamination of the growing metal film.

Metal carbonyls are most convenient to use as starting compounds for obtaining clean metal films. Work in this area is reviewed in a recent monograph [17].

A film grows as a result of metal carbonyl adsorption on a low-index plane of the metal, followed by thermal dissociation of the carbonyl, diffusion of the resulting adatom into the atomic step of the growing metal crystal, and addition to the crystal (Fig. 1).

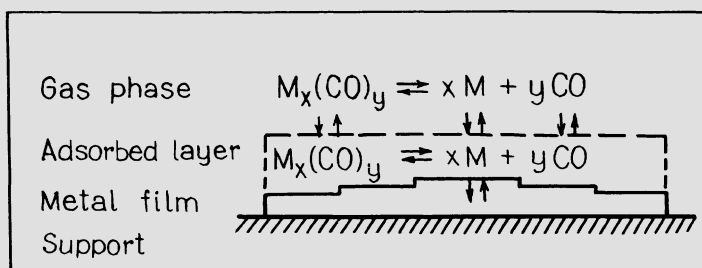


Figure 1. Scheme of the growth of a metallic film at thermal decomposition of carbonyls (adapted from V.G. Syrkin [17]).

Molecular dissociation of the carbonyl can be complicated by the secondary process of metal reaction with CO, giving carbides and oxides that contaminate the film; for this reason, thermal decomposition of the carbonyl is carried out at a minimal temperature.

Thus, from a brief consideration of this vast area, we may conclude that metal carbonyls are most appropriate precursors for modifying supported metals and that they should be supported on metal surfaces at minimal temperatures in order to avoid formation of side products.

The interaction of organometallic compounds with monocrystal surfaces seems to be an interesting field of research, which can be performed using modern physical methods such as LEED and Auger spectroscopy. Such an approach would make possible elucidation of the first step and, possibly, of the mechanism of the reaction of interest. However, we are unaware of any work in this direction.

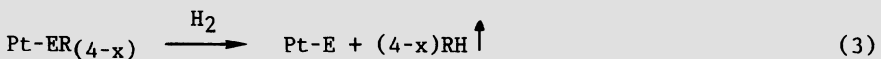
3. INTERACTION OF ORGANOMETALLIC COMPOUNDS WITH SUPPORTED METALS

High reactivities of organometallic compounds with surfaces of metal oxide supports [1,18] makes their reaction specifically with the metal

surface very difficult to bring about. Therefore, there is little work reported in this area. A proposed [4-7] method of supporting alkyls of group IVA metals (ER_4) on the surface of Pt/Al_2O_3 is based on the reaction



To exclude the interaction of ER_4 with -OH groups of Al_2O_3 , reaction (2) was carried out under controlled conditions using diluted solutions of metal alkyl compounds. The occurrence of reaction (2) is confirmed by chemical analysis of the RH evolved. Further decomposition of the complexes formed by hydrogen at 100-400°C leads to alloy particles:



Reaction (2) was also used to obtain $(Pb+Ni)/Al_2O_3$ catalysts that show a high selectivity in acrylonitrile hydrogenation [5,6], and $(Rh+Sn)/Al_2O_3$ catalysts [7a].

The $(Sn+Pt)/Al_2O_3$ catalysts have revealed some peculiar features in the conversion of n-hexane at 500°C as compared to Pt/Al_2O_3 : (a) a decrease in activity with increasing Sn/Pt ratio, and (b) an increase in selectivity with respect to benzene [7]. These peculiarities were accounted for by ligand and electronic effects of tin, which forms alloys with platinum.

Recently, Antos has suggested a novel method of modifying Pt/Al_2O_3 catalysts for reforming and dehydrogenation of hydrocarbons [8-10]. The method consists of impregnation of a prereduced Pt/Al_2O_3 with an anhydrous solution of $Re_2(CO)_{10}$ [8], $Rh_6(CO)_{16}$ [9], or $Ru_3(CO)_{12}$ [10] in an inert atmosphere and drying and pyrolysis of the supported metal carbonyl at 100-300°C in hydrogen. Modification of the known reforming catalysts by rhenium enhances the yield of C_5+ hydrocarbons [8].

On the basis of the results [11-14], it can be assumed that upon modification, metal carbonyl clusters can react both with the surface of Al_2O_3 [19] and with the surface of platinum; however, the mechanism of this latter interaction is not known yet.

4. STUDY OF THE INTERACTION OF METAL CARBONYL CLUSTERS WITH SURFACES OF SUPPORTED METALS

4.1. Peculiarities of the Catalyst Preparation Method

A Pd/SiO_2 catalyst, prepared by the decomposition of anchored allyl complexes and containing palladium particles 10-15 Å in size [1,18], as well as a Cu/SiO_2 catalyst, containing copper particles less than 30 Å in size (Table I), were used as carriers.

The interaction of metal carbonyls with surfaces of palladium and copper was carried out by two methods:

(1) Adsorption of carbonyls of ruthenium, rhodium, or cobalt from a pentane solution onto the surface of supported palladium (or copper) at 25°C. Under these conditions, no adsorption of supported carbonyls on SiO_2 was observed [11]. After an excess unreacted carbonyl had been washed off with pentane, the catalyst was dried under vacuum at 25°C and reduced with hydrogen at 200-500°C.

(2) Treatment of reduced Pd/SiO_2 and Cu/SiO_2 with vapours of chromium, manganese, or iron carbonyls at 50-100°C under vacuum. Unreacted carbonyls were removed by evacuation. Then the catalyst was reduced with hydrogen at 500°C.

All procedures of catalyst preparation and transfer into the reactor or into the spectrometer cell were performed under vacuum.

Table I. Bimetallic catalysts obtained by interaction of metal carbonyl compounds with the surfaces of supported metals

Metal carbonyl	Supports	
precursor	Pd/SiO_2 $d_{\text{Pd}} = 10-15 \text{ \AA}$	Cu/SiO_2 $d_{\text{Cu}} < 30 \text{ \AA}$
$\text{Cr}(\text{CO})_6$	II	-
$\text{Mn}_2(\text{CO})_{10}$	II	-
$\text{Fe}(\text{CO})_5$	II	II
$\text{Co}_2(\text{CO})_8$	I	I
$\text{Ru}_3(\text{CO})_{12}$	I	II
$\text{Rh}_2(\text{CO})_4\text{Cl}_2$	I	-
$\text{Rh}_4(\text{CO})_{12}$	I	I
$\text{Rh}_6(\text{CO})_{16}$	II	-

I: adsorption of metal carbonyl from pentane at 25°C;

II: treatment with metal carbonyl vapour under vacuum at 50-100°C.

4.2. Interaction of $\text{Ru}_3(\text{CO})_{12}$ with Pd/SiO_2

4.2.1. Infrared spectroscopy. After adsorption of $\text{Ru}_3(\text{CO})_{12}$ on Pd/SiO_2 , washing with pentane, and drying at 25°C, the spectrum of the sample exhibits absorption bands at 2003, 2070, and 2133 cm^{-1} [11], which are essentially different from the spectrum of the ruthenium cluster [20]. This result indicates that the initial ruthenium carbonyl cluster undergoes substantial changes caused by its chemical interaction with the surface of Pd/SiO_2 . Note for comparison that the spectrum of $\text{Ru}_3(\text{CO})_{12}$, supported on SiO_2 by sublimation under vacuum, is characterized by a set of frequencies typical of the initial cluster, which indicates the absence of the chemical interaction of $\text{Ru}_3(\text{CO})_{12}$ with the surface of silica under these conditions [19].

The adsorption of the ruthenium complex on the surface of Pd is confirmed by the fact that the saturating concentration of the supported $\text{Ru}_3(\text{CO})_{12}$ comprises one ruthenium atom per 3-5 palladium surface atoms (Table II). In addition, the absence of absorption bands from CO adsorbed on palladium is due to the blockage of its surface by the adsorbed ruthenium complex.

Table II. Maximum amount of adsorbed $\text{Ru}_3(\text{CO})_{12}$ on the surface of palladium upon treatment of Pd/SiO_2 catalysts reduced at 300°C with an excess $\text{Ru}_3(\text{CO})_{12}$ in pentane solution at 25°C .

Initial Pd/SiO_2 catalyst	Amount of adsorbed $\text{Ru}_3(\text{CO})_{12}$, %	Dispersion of palladium ^a , Pd_S/Pd_t	Ru/Pd_S^b
0.9% Pd/SiO_2	0.14	0.83	0.20
4.0% Pd/SiO_2	0.73	0.58	0.33
7.6% Pd/SiO_2	0.62	0.48	0.18

^a Calculated from the results of hydrogen titration on the basis of the assumption that the stoichiometry of HT is 3; expressed as fraction of surface palladium atoms.

^b Ratio of the number of chemisorbed ruthenium atoms to the number of surface palladium atoms.

Sample evacuation at 150°C decreases the intensity of absorption bands at 2003 and 2070 cm^{-1} and slightly increases that at 2133 cm^{-1} ; subsequent CO adsorption at 25°C restores the initial spectrum [11]. However, a different behaviour of the intensities of these absorption bands seems to indicate that they belong to at least two surface compounds: a complex adsorbed on Pd and a complex oxidized by hydroxyl groups of SiO_2 , located nearby palladium particles. Absorption bands at 2133 and 2070 cm^{-1} may be assigned to a partially oxidized ruthenium cluster [19].

4.2.2. EXAFS data [12]. Figs. 2 and 3 illustrate radial distributions of atoms (RDA), obtained by studying fine structure of the extended K-edge of the X-ray absorption of ruthenium, together with their probable assignment with corrections for a phase shift.

The RDA curve of $\text{Ru}_3(\text{CO})_{12}$ (Fig. 2, curve ①) has a set of interatomic distances which correspond well to the known structure of this cluster [20]. The nearest environment of Ru has carbon atoms of the carbonyl group at a distance of 1.90 \AA and Ru atoms at a distance of 2.82 \AA , and the ruthenium-oxygen distance of the carbonyl group (3.02 \AA) may contribute to the last coordination maximum. The subsequent coordination peaks can be assigned to the ruthenium-carbon (3.58 \AA) and ruthenium-oxygen (4.08 \AA) distances of carbonyl groups bound to the neighbouring ruthenium atoms.

The RDA curve for (Ru+Pd)/SiO₂ after Ru₃(CO)₁₂ adsorption (Fig. 2, curve ②) shows two distinct groups of peaks. The first group corresponds to the structure of the initial cluster. However, the structure of the adsorbed Ru₃(CO)₁₂ is perturbed, i.e., at constant Ru-Ru distances, the Ru-CO distance is increased, and CO groups are probably partly removed [12]. The second group of peaks is close in its position to the Ru-O distance in bulk oxides and seems to result from the oxidation of the cluster by the support -OH groups located near palladium particles [12].

Infrared and EXAFS data suggest that the products of Ru₃(CO)₁₂ interaction with palladium are Ru₃(CO)_x fragments coordinated on the surface of palladium as well as the oxidation products of the ruthenium cluster located around the perimeter of palladium particles.

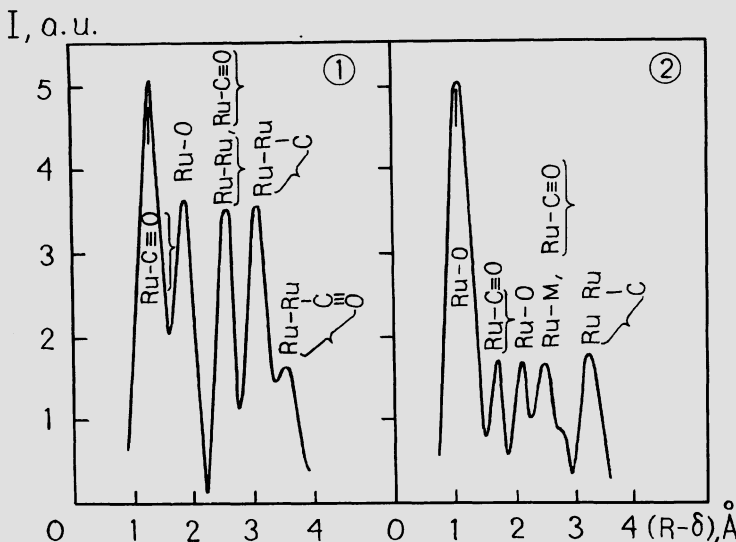


Figure 2. RDA curves for ①, Ru₃(CO)₁₂ and ②, (0.73% Ru + 4.0% Pd)/SiO₂ after adsorption of Ru₃(CO)₁₂ from pentane and drying at 25°C. — indicates observed distances.

4.3. Formation of Ru-Pd Particles

According to transmission electron microscopy (TEM) data [13], supporting of Ru₃(CO)₁₂ on Pd/SiO₂ and subsequent reduction leads to a 2-3 Å increase in the size of metallic particles, the size distribution remaining quite narrow.

The RDA of a Ru-Pd catalyst reduced at 200°C is shown in Fig. 3. It has coordination maxima at $(R - \delta_i) = 2.42$ and 3.60 \AA , which may be assigned to the metal-metal distance and correspond well to the distance of the first and to second coordination spheres of a

body-centered cubic lattice of bulk ruthenium and of a face-centered cubic lattice of bulk palladium.

An infrared spectrum of CO adsorbed on a ruthenium-palladium catalyst has a set of adsorption frequencies different in their position from the bands typical of pure ruthenium and palladium [11]. This fact indicates the absence of pure ruthenium and palladium particles, i.e., the formation of alloyed particles.

A comparison of TEM data indicating a narrow size distribution with the data of Table II at an approximate constancy of the Ru/Pd ratio gives evidence that this ratio is nearly the same in all species and is equal to the overall catalyst composition [11-14].

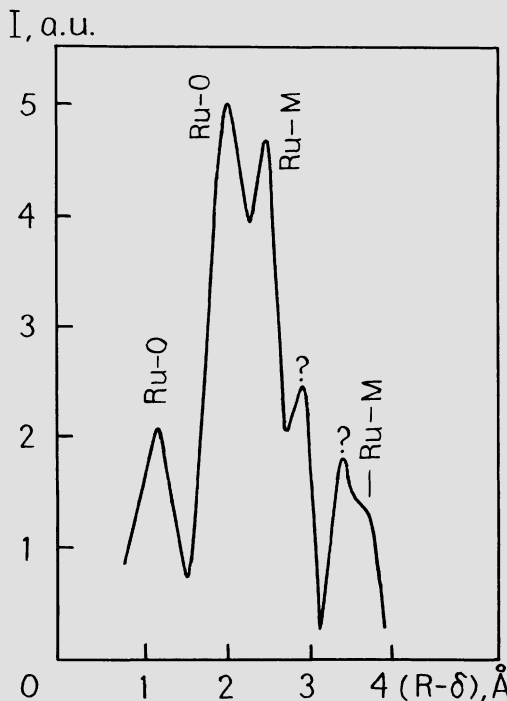


Figure 3. RDA curves for $(0.73\% \text{ Ru} + 4.0\% \text{ Pd})/\text{SiO}_2$ catalyst reduced at 300°C .

4.4. Catalytic Properties of $(\text{Ru+Pd})/\text{SiO}_2$

4.4.1. Ethane hydrogenolysis. The dependence of the activity of Ru-Pd catalysts and of the activation energy on their composition is plotted in Fig. 4. The activity of ruthenium at 200°C is seven orders of magnitude higher than that of palladium, which is consistent with literature data [2]. With increasing content of ruthenium, the activity

of the bimetallic catalysts increases, approaching the activity of pure ruthenium, whereas the activation energy falls to the value typical of Ru/SiO₂.

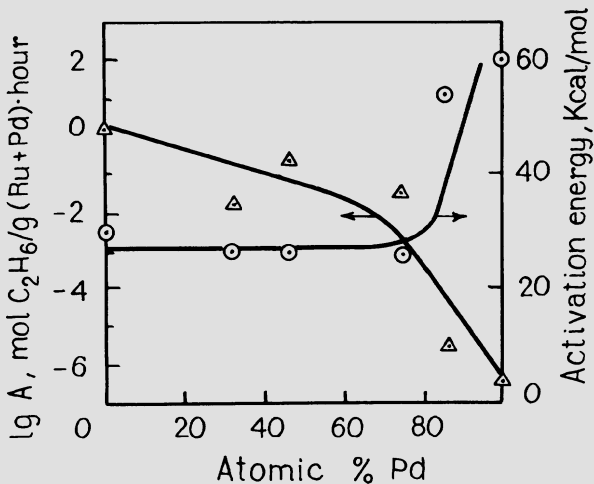


Figure 4. Activity and activation energy for ethane hydrogenolysis of Ru-Pd catalysts. T_r = 200°C, P_{C₂H₆} = 50 Torr, P_{H₂} = 150 Torr.

4.4.2. CO hydrogenation. The main products of CO hydrogenation on Ru/SiO₂ are normal paraffins and olefins, whose yield falls exponentially with increasing molecular weight. The selectivity with respect to methanol does not exceed 10%. As was shown previously [21], the formation of methanol with a selectivity higher than 90% is typical of Pd/SiO₂.

Fig. 5 shows the dependence of the CO hydrogenation activity of Ru-Pd catalysts on their composition. The addition of ruthenium to the Pd/SiO₂ catalyst decreases the methanol formation rate by 1-2 orders of magnitude. The activity of (Ru+Pd)/SiO₂ catalysts for the CH₃OH synthesis is significantly lower than that calculated on the assumption of additive properties of monometallic samples.

A similar dependence of the activity of bimetallic catalysts on their composition is observed in the synthesis of hydrocarbons; with increasing content of palladium, the activity drops by 1-2 orders of magnitude. Supporting of iron, cobalt, ruthenium, or rhodium carbonyls on Cu/SiO₂ also suppressed the activity of these metals for synthesis of hydrocarbons from CO and H₂ by 1-2 orders of magnitude.

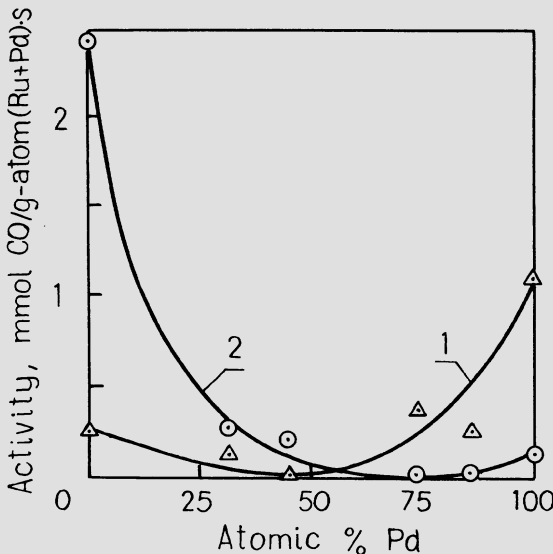


Figure 5. Activity for CO hydrogenation of Ru-Pd catalysts. $T_r = 250^\circ\text{C}$, $P = 10 \text{ atm.}$, $\text{CO: H}_2 = 1:2$.
Curve 1, activity for synthesis of CH_3OH ; curve 2, activity for synthesis of $\text{C}_1\text{-C}_6$ hydrocarbons.

4.4.3. Possible reasons for nonadditive properties of (Ru+Pd)/ SiO_2 catalysts. According to the ideas developed by Ponec and Sachtlar [22,23] in the theory of bimetallic catalysts containing alloy species, the analysis of catalytic properties should take into account, first, the effect of dilution of surface metal atoms by those of less active metals, which leads eventually to a decrease in concentration of multiple active centers for the reaction. In a number of cases, it is also necessary to consider the ligand effect, that is, the presence of the second metal in the nearest environment of a given atom, which may affect its electronic, chemisorptive, and, consequently, catalytic properties. For bimetallic particles of more than 10 \AA in size, the surface composition can differ from that of the bulk. In view of these ideas, we now consider the properties of Ru-Pd catalysts.

A sharp fall in activity of bimetallic catalysts for ethane hydrogenolysis with increasing palladium content seems to be due to dilution of ruthenium atoms by less-active palladium atoms. As the palladium content grows, the surface concentration of multiple active centers for ethane hydrogenolysis (consisting of several ruthenium atoms) decreases. But the nature of these centers appears to be unchanged, since the activation energy for the reaction remains constant.

According to isotopic and infrared data [14], the formation of hydrocarbons from CO and H₂ on ruthenium occurs via the dissociative adsorption of CO. The dissociation seems to proceed on multiple active centers, the number of atoms (n) of which can be estimated on the basis of the assumption of homogeneous composition and equal surface and bulk compositions of bimetallic particles from the formula [22,23]

$$A = A_0(1 - x)^n, \quad (4)$$

where A₀ is the activity of a pure metal and A is its activity after the addition of a less active metal with mole fraction x. The treatment of data in Fig. 5 (curve 2) by this formula gives the value n = 4. Consequently, in accord with this value, the smallest active center required for the dissociative chemisorption of CO consists of four ruthenium atoms.

As is known [25], on palladium, a molecular adsorption of CO is predominant, which determines its high selectivity with respect to methanol. The decrease in palladium activity towards methanol synthesis can hardly be explained by the effect of ruthenium dilution, since molecular adsorption of CO and its hydrogenation to CH₃OH can, most probably, proceed on smaller centers than are required for dissociative adsorption of CO. This phenomenon may be accounted for by the ligand effect, that is, by the change of electronic properties of a palladium atom due to the presence of ruthenium atoms in its first coordination sphere.

4.5. Effect of Nuclearity of a Supported Cluster on Catalytic Activity

Of special theoretical interest in catalysis by metals is the question of the smallest number of atoms in the active center for a given reaction. For example, for ruthenium, the smallest number of atoms in the active center for CO dissociation is equal to 4. The proposed method for obtaining bimetallic catalysts opens up additional possibilities for experimental study of this problem by changing nuclearity of a cluster supported on a metal carrier.

As the most convenient reaction for this study we may take benzene hydrogenation, which occurs at low temperatures. In this reaction, the catalytic activity of rhodium is two orders of magnitude higher than that of palladium (Table III). It seems, therefore, of interest to compare the properties of (Rh+Pd)/SiO₂ catalysts. It can be expected that at low reduction temperatures (100°C) a metallic framework of an adsorbed rhodium cluster may be preserved, as in the case of Ru₃(CO)₁₂ on palladium (Fig. 2, curve ②).

After supporting rhodium clusters on Pd/SiO₂, the activity for benzene hydrogenation per surface palladium atom (Pd_S) increased. The effect depends upon nuclearity of the supported cluster. Since palladium is far less active than rhodium, the activity observed can reasonably be attributed to Rh_S. Even in this case, the activity of rhodium is one order of magnitude lower than that of Rh/SiO₂. Such a decrease in activity of rhodium can be due either to a poisoning effect of ligands or to a size effect. If we assume that at 100°C ligands are

removed completely, a Rh_n ($n \leq 6$) fragment attached to a relatively inert palladium support should be one order of magnitude less active than a rhodium particle 40 Å in size. This conclusion is quite surprising, because, as is known, benzene hydrogenation is a structure insensitive reaction. Besides, this result indicates that large particles of metallic rhodium are absent in $(\text{Rh}+\text{Pd})/\text{SiO}_2$ catalysts.

Table III. Catalytic properties of $(\text{Rh}+\text{Pd})/\text{SiO}_2$ catalysts, obtained using rhodium clusters of different nuclearity and reduced with H_2 at 100°C, for benzene hydrogenation.

$T_r = 90^\circ\text{C}$, $P_{\text{C}_6\text{H}_6} = 50$ Torr, $P_{\text{H}_2} = 300$ Torr.

Catalyst composition, wt.%	Initial rhodium cluster	$A \cdot 10^2$ molec. C_6H_6 atom Pd _s	$A \cdot 10^2$ molec. C_6H_6 atom Rh _s
1.8% Pda	-	0.53	-
0.4% Rh + 1.8% Pd	$\text{Rh}_2(\text{CO})_4\text{Cl}_2$	0.81	2.6
0.3% Rh + 1.8% Pd	$\text{Rh}_4(\text{CO})_{12}$	2.10	9.0
0.4% Rh + 1.8% Pd	$\text{Rh}_6(\text{CO})_{16}$	0.78	2.5
0.8% Rh ^a	-	-	109

^a Reduced at 300°C.

4.6. Effect of the Nature of the Second Element on the Properties of $(\text{M} + \text{Pd})/\text{SiO}_2$.

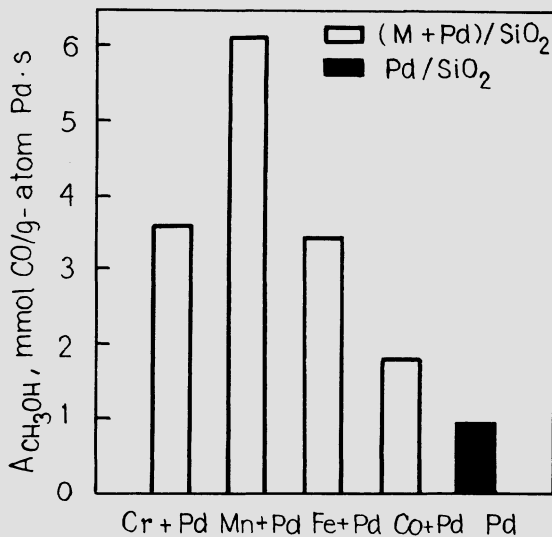
For a systematic study of the ligand effect on the properties of supported palladium, we have synthesized a series of catalysts $(\text{M} + \text{Pd})/\text{SiO}_2$ (M is a metal of the first transition period) using the proposed method. As has been mentioned previously, one can expect the formation of highly dispersed and compositionally homogeneous bimetallic particles in these catalysts.

Table IV illustrates nonadditive catalytic properties of the $(\text{Co} + \text{Pd})/\text{SiO}_2$ system. As distinct from palladium, CO hydrogenation on Co/SiO_2 gives predominantly hydrocarbons. The addition of cobalt has little effect on the activity of palladium and its selectivity for methanol, but leads to formation of ethanol in appreciable amounts. The action of palladium on the properties of cobalt for CO hydrogenation and ethane hydrogenolysis is similar to its action on ruthenium, i.e., the activity of cobalt in these reactions fall by one order of magnitude.

The addition of chromium, manganese, or iron enhances the activity of Pd for methanol formation from CO and H_2 by a factor of 4-6, the selectivity remaining almost unchanged (Fig. 6).

Table IV. Catalytic properties of (Co + Pd)/SiO₂.

Catalyst composition, wt.%	Activity in CO hydrogenation at 250°C and P = 10 atm, mmol CO/g atom (Pd+Co)/s			Ethane hydrogenolysis at 300°C	
	CH ₃ OH	$\sum_{n=1}^6 C_n$	C ₂ H ₅ OH	A, $\frac{\text{mol C}_2\text{H}_6}{\text{g(Pd + Co)} \cdot \text{h}}$	E, kcal/mol
1.8%Pd	0.97	0.05	0.0	0.063	60
0.4%Co + 1.8%Pd	1.30	0.18	0.08	0.073	45
1.0%Co	0.17	2.3	0.0	0.90	32

Figure 6. Influence of the nature of M on the activity of (M + Pd)/SiO₂ catalysts in the synthesis of methanol at 250°C.

The increase in activity of (M + Pd)/SiO₂ catalysts for the formation of methanol in the order of additives Co < Fe < Mn is in agreement with the decrease of filling the 3d-level of the second element in this order. The change of electronic properties of palladium upon alloying with a promoter may cause the change of its catalytic properties. It is necessary in this case to take into account the

possibility of enrichment of the surface of bimetallic particles with manganese having a smaller heat of sublimation than palladium. Moreover, the heat of CO adsorption is the greatest on manganese. The presence of mixed Pd-Mn ensembles, which can activate both CO and H₂, may be a reason for the high activity of this catalyst for methanol synthesis.

5. CONCLUSIONS

The literature and our data give evidence for interesting possibilities of interaction of organometallic compounds with the surfaces of supported metals for obtaining bimetallic catalysts. The use of this novel reaction of metal carbonyl clusters with metal surfaces allows the second metal to be selectively supported on the surface of a metal particle under mild conditions. The bimetallic catalysts obtained have some advantages over conventional catalysts:

- (1) Homogeneous composition of mixed particles. The composition of each bimetallic particle approximately corresponds to the overall catalyst composition.
- (2) High dispersion of mixed particles less than 10-15 Å in size. Since in these particles almost all the atoms are on the surface, in view of the results stated above the surface composition of all bimetallic particles is approximately the same and corresponds to the overall catalyst composition.

These features of bimetallic catalysts, obtained by the proposed method, provide the possibility for studying the peculiarities of the catalytic action of bimetallic particles under conditions excluding segregation and sintering of metals, as well as heterogeneity of composition of mixed particles and differences of their surface composition from the bulk composition.

6. ACKNOWLEDGMENTS

The authors are grateful to their colleagues L.V. Gorodova and Yu.N. Nogin for synthesis and study of the catalysts; A.A. Davydov for infrared experiments, D.I. Kochubey and M.A. Kozlov for providing EXAFS measurements, and V.I. Zaikovskii for TEM analysis.

7. REFERENCES

1. Yu.I. Yermakov, B.N. Kuznetsov, and V.A. Zakharov, Catalysis by Supported Complexes. Studies in Surface Science and Catalysis, v. 8, Elsevier (1981).
2. J.H. Sinfelt, Adv. Catal. 23, 91 (1973).
3. V.I. Zaikovskii, V.I. Kovalchuk, Yu.A. Ryndin, L.M. Plyasova, B.N. Kuznetsov, and Yu.I. Yermakov, React. Kinet. Catal. Lett. 14, 99 (1980). V.L. Kuznetsov, A.F. Danilyuk, I.S. Kolosova, and Yu.I. Yermakov, React. Kinet. Catal. Lett. 21, 249 (1982).

4. J. Margitfalvi, M. Hegedus, S. Gobolos, E. Kern-Talas, P. Szedlacsek, S. Szabo, and F. Nagy, Proc. 8th Intern. Congr. Catal. 4, 903 (1984).
5. J. Margitfalvi, E. Kern-Talas, S. Gobolos, and M. Hegedus, The 9th North American Meeting of the Catalysis Society, P-24, Houston (1985).
6. J. Margitfalvi, E. Kern-Talas, and S. Gobolos, The 12th International Conference on Organometallic Chemistry, p. 518, Vienna (1985).
7. J. Margitfalvi, M. Hegedus, P. Szedlacsek, and F. Nagy, Appl. Catal. 15, 69 (1985).
- 7a. Ch. Travers, J.P. Bournonville, and G. Martino, Proc. 8th Intern. Congr. Catal. 4, 891, (1984).
8. G.J. Antos, U.S. Patents 4,159,939; 4,175,031; 4,183,805; 4,197,188; 4,206,040; 4,206,041; 4,212,769; 4,193,863; 4,231,897; 4,290,921; 4,292,207; 4,298,504; 4,353,815.
9. G.J. Antos, U.S. Patent 4,174,298.
10. G.J. Antos, U.S. Patents 4,175,056; 4,210,561; 4,358,399.
11. Yu.A. Ryndin, L.V. Gorodova, O.V. Tyunina, A.A. Davydov, and Yu.I. Yermakov, React. Kinet. Catal. Lett. 26, 79 (1984).
12. D.I. Kochubey, M.A. Kozlov, L.V. Gorodova, Yu.A. Ryndin, and Yu.I. Yermakov, React. Kinet. Catal. Lett. 26, 91 (1984).
13. Yu.A. Ryndin, L.V. Gorodova, V.I. Zaikovskii, and Yu.I. Yermakov, React. Kinet. Catal. Lett. 26, 103 (1984).
14. Yu.A. Ryndin, L.V. Gorodova, D.I. Kochubey, M.A. Kozlov, and A.A. Davydov, The 1st Italian-Soviet Seminar on Catalysis, p. 165, Messina (1984).
15. Vapor Deposition, (Eds. C.F. Powell, J.H. Oxley, and J.M. Blocher, Jr.) John Wiley and Sons, Inc. (1968).
16. Deposition of Films and Coatings by Decomposition of Organometallic Compounds, (Ed. G.A. Rasuvaev), Nauka, Moscow (1981).
17. V.G. Syrkin, Gas-Phase Metallization through Carbonyls, Metalurgiya, Moscow (1985).
18. Yu.I. Yermakov, Catal. Rev.-Sci. Eng. 12, 92 (1976).
19. V.L. Kuznetsov, A.T. Bell, and Yu.I. Yermakov, J. Catal. 65, 374 (1980).
20. M.I. Bruce and F.G.A. Stone, Angew. Chem., Int. Ed. Engl. 7, 427 (1968).
21. Yu.A. Ryndin, R.F. Hicks, A.T. Bell, and Yu.I. Yermakov, J. Catal. 70, 287 (1981).
22. V. Ponec, Catal. Rev.-Sci. Eng. 11, 41 (1975).
23. W.M.H. Sachtle and R.A. Van Santen, Adv. Catal. 26, 69 (1977).
24. Y. Kobori, H. Yamasaki, Sh. Naito, T. Onishi, and K. Tamari, J. Chem. Soc., Faraday Trans. 1 78, 1474 (1982).
25. G. Broden, T.N. Rhodin, and G. Brucner, Surf. Sci. 59, 593 (1976).

LOW-NUCLEARITY METAL CLUSTERS: STRUCTURE AND REACTIVITY

Pierre Gallezot

Institut de Recherches sur la Catalyse, C.N.R.S.
Conventionné à l'Université Claude Bernard Lyon I
2, avenue Albert Einstein
69626 Villeurbanne Cedex
France

ABSTRACT. Recent studies of supported and unsupported naked metal clusters of low-nuclearity are examined with the aim of comparing their structure and reactivity to those of molecular clusters. It is shown that naked clusters can be prepared with a nuclearity comparable to that of molecular clusters. Moreover, their structure is flexible in response to adsorbates which act as the ligands in coordination compounds. Transformations of molecular clusters into naked clusters and vice versa are examined. The reactivities of unsupported clusters (cluster beams) and of low-nuclearity bimetallic clusters involving two complementary active sites are also discussed.

1. INTRODUCTION

The comparison between molecular metal clusters and small metal particles is usually difficult. First, their nuclearities are incommensurate. Metal particles containing several hundred atoms can hardly be compared to molecular species containing at most a few tens of atoms. Second, the precise arrangement of metal atoms and ligands in molecular clusters is known from crystal structure analysis, whereas the structure of the metal skeleton and the position of the surface ligands in metal aggregates are for the most part unknown. This is why the latter are often viewed as small, rigid pieces of bulk metal, although molecular clusters exhibit a variety of atom packings. Third, it is common to compare the surface chemistry of metal particles with that of single crystal surfaces rather than to apply the concepts of organometallic chemistry.

This paper is a report of recent experimental observations concerning the structure and properties of naked metal clusters which ease the comparison with molecular clusters. The same nuclearity range will be considered: naked clusters M_m , with $m < 60$, will be compared to molecular clusters M_mL_n , with $m < 55$. The transformations of molecular clusters into naked clusters and vice versa, with or without changes in nuclearity and/or composition, will be discussed. Recent studies

showing that the structures of naked clusters are flexible in response to adsorbed species will be reported. Finally, the reactivities of supported and unsupported clusters will be discussed in relation to their nuclearity and composition.

2. NUCLEARITY OF NAKED CLUSTERS

2.1. Unsupported Clusters

Rapid progress has been made in the preceding five years in the production and characterization of metal cluster beams. Details of the technology of production and analysis can be found in review articles [1-3]. Pulsed beams of metal clusters are obtained by expanding and condensing in a high-pressure helium stream metal vapors produced by pulsed laser vaporization. Reactant molecules can be introduced into the gas phase along the pathway of metal cluster beams. The nuclearity of the clusters and the products of the reaction between clusters and added molecules can be identified by mass spectroscopy.

For most metals, mass spectra show a wide nuclearity distribution without "magic number" peaks. Therefore, naked clusters with a complete closed-shell structure (regular polyhedra) do not have any particular stability, in contrast to molecular clusters. This distinction arises because the latter have highly symmetrical ligand envelopes favoring closed shell structures, whereas naked clusters may have a random nuclearity because there is no symmetry requirement for the addition of metal atoms.

2.2. Supported Clusters

Functional groups of support materials may act as ligands stabilizing metal clusters and maintaining a low nuclearity. Thus it has been shown [4] that 1-nm Pt or Ir clusters can be obtained with a high selectivity at the edges of graphite basal planes, provided that functional groups acting as anchoring sites are present. Fig. 1 gives a TEM view showing 1-nm Pt clusters decorating the steps of a pre-functionalized graphite flake.

The best way to control the nuclearity of metal clusters is to trap them in the calibrated pores of zeolites. The production of clusters engaged in zeolites has been described in a recent review [5]. Metal loading is carried out either by ion exchange and reduction or by adsorption and decomposition of organometallic complexes. If these treatments are performed under proper conditions, the clusters can be obtained at precise locations in the zeolite micropores, which impose an upper limit on the cluster size. Thus in faujasite-type zeolites, the supercages can accommodate up to 60 metal atoms.

The nuclearity of platinum clusters in Y-type zeolite has been studied by comparing the distribution of interatomic distances obtained experimentally with the Radial Electron Distribution (RED) technique [6,7] and various distributions calculated from model clusters with an f.c.c. structure. Fig. 2 shows that the experimental distribution



Figure 1. TEM view of a graphite flake (high surface area LONZA graphite) showing 1-1.5 nm Pt clusters along the steps of basal planes [4].

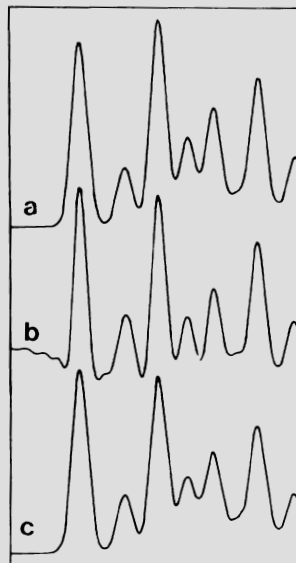


Figure 2. Distribution of interatomic distances in platinum clusters encaged in Y-zeolites. Curve a, distribution calculated for a 40-atom truncated f.c.c. tetrahedron (see Fig. 3). Curve b, experimental distribution obtained with the RED technique from X-ray scattering data. Curve c, calculated distribution for a mixture of 40-atom truncated tetrahedra and of six-atom octahedra.

(curve b) is very similar to that calculated from a 40-atom truncated tetrahedron (curve a). A schematic model is given in Fig. 3.

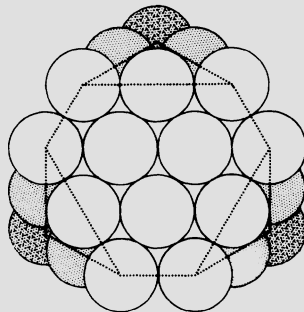


Figure 3. Pictorial representation of a f.c.c. 40-atom truncated tetrahedron.

Interestingly, this model cluster has the same symmetry as the cage; therefore the oxygen anion polyhedron forming the cage walls acts almost as the ligand shell in molecular clusters, controlling the nuclearity and the morphology of the metal skeleton. Accordingly Pt clusters in the zeolite mordenite, which has parallel cylindrical pores, appear as oriented cylinders on TEM micrographs [8].

It is noteworthy that in Fig. 2, although there is a good fit between curves a and b, the first peak corresponding to the nearest neighbors in platinum metal is higher in the experimental distribution. This means that a number of interatomic vectors contributing mainly to the first peak are not accounted for by the model. Therefore, these interatomic vectors are due to very small clusters with $m < 6$. Indeed a distribution (curve c) calculated with a mixture of 40-atom tetrahedra and six-atom octahedra gives a better fit to the experimental distribution. It can be concluded that the dimensions of zeolite cages control the upper limit of the nuclearity range, but low nuclearity clusters can be accommodated without morphology and nuclearity constraints.

2.3. Transformations of Molecular Clusters into Naked Clusters

Many attempts have been made to peel off the ligands of molecular clusters in the hope of preparing naked clusters retaining the initial nuclearity. From the large body of results reported in the literature, it is evident that most of the attempts have led to increases in nuclearity. However, in many cases the proper tools to characterize low-nuclearity naked clusters in liquids or on solid supports have been lacking; hence, only the larger species have been detected.

High-resolution TEM is one of the best tool to pinpoint isolated clusters larger than trimers, provided that the support is thin enough or the clusters are located on the support edges. Indeed a few TEM

studies provide convincing evidence for the preparation of stripped clusters retaining the nuclearity of the molecular precursor. Thus, osmium clusters formed from $\text{Os}_3(\text{CO})_{12}$ were shown dangling at the edge of alumina [9]. Very good pictures of rhodium clusters formed from $\text{Rh}_6(\text{CO})_{16}$ supported on non-porous alumina were reported by Iijima and Ichikawa [10]. Fig. 4 gives a TEM view of a catalyst prepared by decomposition of $\text{Ir}_4(\text{CO})_{12}$ on alumina [11]. The arrowed black dots correspond to iridium clusters with a nuclearity smaller than ten. The nuclearity could be determined by quantitative measurement of the scattered electrons. This type of measurement could be performed in a dedicated, scanning transmission electron microscope equipped with a field-emission gun (FEG-STEM). Indeed single heavy atoms on thin support have been detected, and nuclearities of clusters have been measured with a FEG-STEM [12].

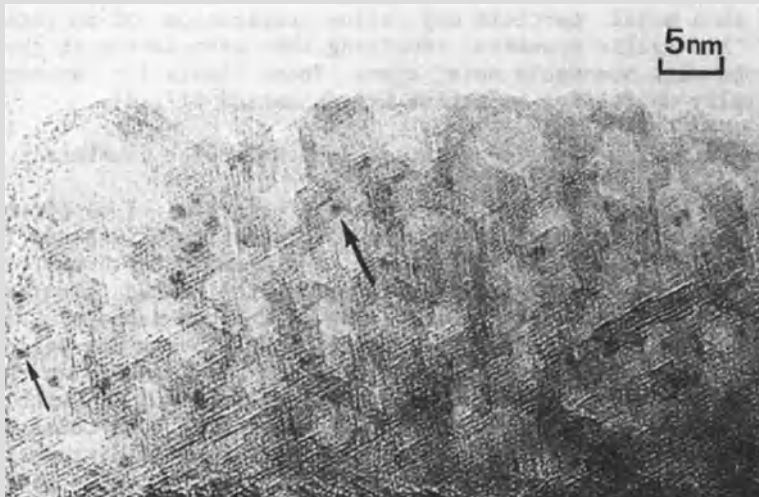


Figure 4. TEM views taken with a JEOL 200 C microscope of decomposed $\text{Ir}_4(\text{CO})_{12}$ clusters on alumina platelets.

The preparation of bimetallic particles which would retain the composition of an heteronuclear molecular cluster precursor is another interesting challenge. There have been many such attempts, which in some cases led to interesting catalytic materials. However, the precise characterizations of the nuclearity and composition of the individual particles are often lacking. Recently Fe-Os, Fe-Ru, and Fe-Co particles supported on magnesium oxide have been prepared with the same metal composition as their precursors [$\text{H}_2\text{FeOs}_3(\text{CO})_{13}$, $\text{H}_2\text{FeRu}_3(\text{CO})_{13}$, and $\text{HFeCo}_3(\text{CO})_{12}$, respectively] [13]. The measurement of the composition was done by high resolution spatial EDX analysis (1 nm^2 analysis window) in a FEG-STEM. Although the nuclearity of the final particles

was higher than that of the precursors, the preexistence of metal-metal bonds in the heteronuclear molecular cluster favors the formation of naked clusters without change of composition. It was suggested that the particles grow by addition of the clusters stripped of their ligands.

Another precise way to build bimetallic clusters is to adsorb and decompose an organometallic complex on naked metal clusters. This technique has been used to prepare Pt-Mo clusters supported in zeolites [14]. One-nm Pt clusters were first obtained by the usual ion-exchange and reduction process, and then $\text{Mo}(\text{CO})_6$ vapors were adsorbed and decomposed under reducing atmospheres. The Mo atoms freed by the thermal decomposition are deposited on top of the Pt atoms according to the rules of f.c.c. packing. They progressively inhibited chemisorption on the Pt atoms underneath. The catalysts thus produced have been characterized by techniques including TEM, H_2 and CO chemisorption, and temperature-programmed desorption [14,15] as well as EXAFS and radial distribution using anomalous X-ray scattering data [16]. This technique of preparation based on the decomposition of organometallic complexes adsorbed on a metal particle may allow preparation of an interesting class of bimetallic clusters involving the association of group VIII metal atoms with non-noble metal atoms. These bimetallic systems could be especially useful for selective hydrogenation [17,18].

2.4. Transformation of Naked Clusters into Molecular Clusters

There is no example of the direct transformation of supported naked clusters into molecular clusters by a mere addition of ligands followed by a restructuring. However, there are examples of transformations occurring via monomeric species, whereby the naked cluster first disintegrates into mononuclear complexes which then migrate, agglomerate, and form molecular clusters. The two-step process may well operate under isothermal conditions. This mechanism of conversion has been observed by Bergeret *et al.* [19]. Upon reaction of CO with 1-nm Rh clusters engaged in Y zeolite at room temperature, the total disintegration of the metal occurred, as evidenced by the disappearance of Rh-Rh distances in the radial electron distribution (RED) and by the appearance of $\text{Rh}^{\text{I}}(\text{CO})_2$ species detected by infrared (IR) spectroscopy. After addition of a mixture of CO and H_2O , a slow process took place whereby the monomeric species were converted into $\text{Rh}_6(\text{CO})_{16}$, characterized by RED and by IR spectroscopy. Previously, Bassett *et al.* [20] had reported that $\text{Rh}_6(\text{CO})_{16}$ can be synthesized from $\text{Rh}^{\text{I}}(\text{CO})_2$ on alumina. Since these latter species were formed from $\text{Rh}_6(\text{CO})_{16}$ oxidation by the protons of the support, a catalytic cycle for the water gas shift reaction was thus demonstrated.

$\text{Ir}_6(\text{CO})_{16}$ can also be formed under mild conditions from iridium cations in zeolite [21]. Thus Fig. 5 gives the RED of a $\text{Ir}^{\text{III}}\text{Y}$ zeolite before (curve a) and after (curve b) treatment by $\text{CO} + \text{H}_2\text{O}$ mixtures at 440 K. The distribution shown in curve b is in good agreement with that calculated for isolated $\text{Ir}_6(\text{CO})_{16}$ clusters from known crystal data. The mechanisms of these *in-situ* syntheses either from naked metal clusters or from cations are not yet established, but the transport and redox processes involved are probably favored in the zeolite matrix. However

high-nuclearity $[Ru_6C(CO)_{16}]^{2-}$ and $[Os_{10}C(CO)_{24}]^{2-}$ clusters were also synthesized directly from Ru and Os halide salts on MgO [22].

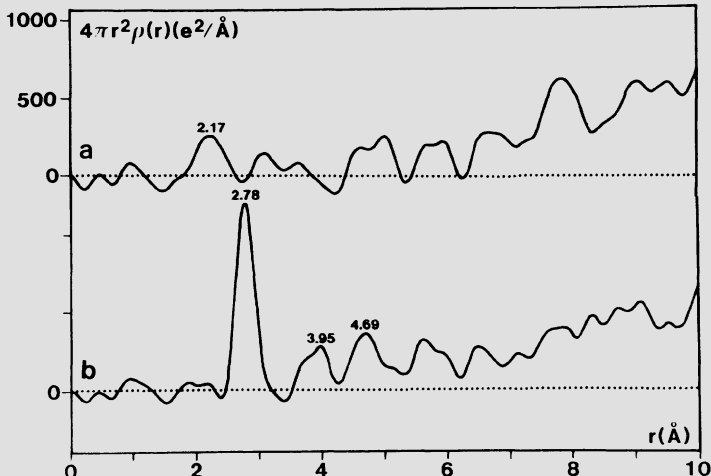


Figure 5. Radial electron distribution. Curve a: distribution characterizing Ir^{III}Y zeolite (no Ir-Ir distances can be observed). Curve b: distribution obtained after treatment of the sample with a CO+H₂ mixture (the large peak at 2.78 Å corresponds to Ir₆(CO)₁₆ clusters).

3. STRUCTURAL FLEXIBILITY OF NAKED METAL CLUSTERS

Molecular clusters exhibit a wide variety of atomic arrangements depending on the binding energy and symmetry of the ligand shell. Furthermore, for a given metal skeleton, the distances between metal atoms depend upon the local ligand coordination, and therefore a broad range of distances between nearest neighbours is observed. In contrast, naked metal clusters are often viewed as rigid isolated pieces of bulk metal wherein each atom is at a fixed position relative to its neighbours. Characterizations of the structure of naked or adsorbate-covered clusters are now available from EXAFS and RED techniques, which can be used to probe the local structure in any material [6]. The RED technique has been applied successfully to study the structure of metal clusters encaged in Y-zeolite, which can be prepared with a narrow range of nuclearities [5].

Structure analogies between metal aggregates covered with various adsorbates and molecular clusters have been discussed recently [23]. The structure of a metal cluster containing 20-40 atoms is flexible. The adsorbates acting as surface ligands displace the metal atoms from the ideal equilibrium positions that they would occupy in a perfect

f.c.c. packing. The displacement disorder increases as a function of the binding energy and of the coverage.

The structure of the metal skeleton can also be modified by the support acting as a multidentate ligand. Changes in particle morphology, e.g., from spheres to rafts wetting the support, are now well documented, even for comparatively large particles [24]. Moreover, when the nuclearity is small, epitaxial interactions with support atoms can induce contraction or expansion of the metal lattice. Thus the lattice of 1-1.5-nm Pd particles is expanded by 2 to 4% because of strong epitaxial interactions with MgO [25]. It has been shown [26] by electron nanodiffraction in a STEM that the f.c.c. structure of 1-2-nm Pt particles on graphite is distorted, the smaller the particles, the larger the distortion. Thus in 2-nm Pt particles, the angle between (111) and (100) planes is 57° instead of the theoretical value of 54°74' in regular f.c.c. Because of the interaction with the carbon atoms of the basal plane, these angles tend to take on values close to 60°, the angle between the atom rows in the graphite basal plane. The distortion is even more marked on 1-nm Pt particles. On the other hand, no distortion is observed for Pt particles supported on amorphous charcoal because Pt and C atoms can no longer be in registry. A demonstration of how the metal and support atoms are bonded together is yet to be made. In the case of graphite, one can expect that the bonding is essentially similar to metal-arene bonds with electron transfer of the π -electrons to the d-orbitals of the metal.

The structural flexibility of naked metal clusters is quite comparable to that of molecular clusters. One can wonder whether the mobility of the surface ligands and even of the metal atoms can be compared to those observed on molecular clusters. Unfortunately, only a few experiments have been done characterizing the dynamics of metal clusters and their adsorbates. The lack of data is explained by the difficulty of applying NMR, which has been so useful for probing the dynamics of atoms in molecular clusters; NMR cannot be applied as easily to metal clusters which do not have uniform nuclearity and ligand coverage.

4. REACTIVITY OF NAKED METAL CLUSTERS

The most interesting new results characterizing the reactivity of naked clusters have been obtained with unsupported clusters by mixing pulsed cluster beams with pulsed flows of various reactant molecules and analyzing the products by photoionization mass spectroscopy (see section 2.1.). As far as supported clusters are concerned, we will focus our attention on a new class of low-nuclearity bimetallic clusters formed by the decomposition of organometallic complexes.

4.1. Unsupported Clusters

Kaldor et al. [3] have reported a wealth of data characterizing the reactivity of Fe and Pt clusters. They have shown that the reaction of Fe_x with hydrogen is nuclearity dependent [27]. A striking correlation

was found between the ionization potential (IP) and the hydrogen chemisorption: the lower the IP, the higher the reactivity. This can be explained by the enhanced ability of clusters with a higher Fermi level (lower IP) to give electron density to the antibonding σ^* orbital of the hydrogen molecule and thus to promote dissociative adsorption of hydrogen. This scheme is in agreement with the Saillard and Hoffmann [28] description of H₂ activation on metals, according to which the critical factor in surface activation of hydrogen is an initial electron transfer from the metal to the hydrogen molecule; in contrast, for H₂ activation by an organometallic complex, the initial step is an electron transfer from the H₂ molecule to the metal atom.

The reactivity of Pt clusters with several hydrocarbons has been investigated by Trevor *et al.* [29]. Whatever their nuclearities, Pt clusters form adducts with benzene. A variable number of C₆H₆ molecules can be added; thus, for the dimer Pt₂, the most abundant adduct is Pt₂(C₆H₆)₂. Furthermore, clusters larger than trimers may dehydrogenate benzene, the extent of dehydrogenation depending upon the nuclearity and the number of adducts. Reactions of saturated hydrocarbons with Pt clusters are even more interesting in view of the comparison which can be made with reactions on metal surfaces. Thus, the spectra obtained after reaction of Pt clusters with cyclohexane are similar to those observed for benzene adducts, suggesting that cyclohexane is dehydrogenated into benzene even on a single Pt atom. Saturated molecules like n-hexane and 2,3-dimethylbutane are dehydrogenated on dimers and larger clusters, the extent of dehydrogenation being nuclearity dependent. Although the C/H ratios of the products are typical of those in aromatic molecules, the dehydrocyclisation reaction does not occur because the linear and branched molecules give similar products.

To sum up, unsupported clusters containing a few atoms are highly reactive. They tend to become coordinatively saturated by activating C-H bonds, but there is no evidence for C-C bond breaking, in agreement with the theory according to which large ensembles of metal atoms are needed. However the comparison between the reactivity of a cluster beam and that of a metal surface should be made with caution since the temperature and pressure at which the cluster beams react are not well known.

4.2. Supported Clusters

The reactivity of supported metal particles as a function of their size has been much debated in the literature of heterogeneous catalysis. However, to know with accuracy how many atoms are required for a particular reaction, we must await further experiments with cluster beams such as those described in the previous section. Indeed supported metal catalysts are not well suited to provide answers to this question, since even the most homogeneous of them still exhibit a large range of nuclearities, and their reactivity can be modified by the support. In the meantime, it is now widely accepted that one or two atoms are required to activate H-H, C-H, or O-H bonds, whereas the activation of C-C and N-N bonds requires a larger ensemble of atoms.

The question of the dependency of reaction rates on the number of atoms present in a particle has prompted many studies of the catalytic properties of alloys. The aim was to determine how and why the catalytic activity of a given metal is affected by dilution with atoms of another metal that is inactive for the reaction considered. Although this question is of interest, it has been addressed so much that other types of bimetallic catalysts have been somewhat neglected, except by people working at the interface of homogeneous and heterogeneous catalysis. Thus Yermakov pioneered the preparation of low nuclearity bimetallic clusters using organometallic compounds to bring together the two elements [30,31]. One of his last achievements was the assembling of Pd and Co carbonyl complexes anchored on the same site of a phosphinated silica [32]. This catalyst is much more active in propene hydroformylation than homonuclear Pd or Co complexes. The synergy was interpreted as evidence of the formation on the contiguous Pd and Co atoms of highly reactive Pd-H and Co-C bonds. This suggestion was substantiated by a calculation of the enthalpies of the different steps of the hydroformylation reaction proceeding on Pd-Pd, Co-Co, and Pd-Co contiguous sites. In addition, close proximity of the Pd and Co sites is required so that the hydride ligand from Pd can be transferred to the acyl ligand coordinated to Co.

In the Pd-Co catalyst, the synergy is due to the specific and complementary roles of Pd and Co sites for the activation of the reactant molecules. This type of dual-site mechanism had been invoked previously by Gallezot *et al.* [15,33,34] to account for the catalytic properties of Pt-Mo clusters in hydrogenolysis and CO + H₂ reactions. The synergy was attributed to a preferential dissociative adsorption of hydrocarbon or CO on the Mo atoms and of hydrogen on the Pt atoms. Since the two elements are associated in the same cluster (see section 2.3.), the Pt component provides the dissociated hydrogen required to hydrogenate hydrocarbon fragments adsorbed on the Mo component.

These bimetallic systems can be considered as a new class of bimetallic catalysts, the properties of which cannot be interpreted by geometric (ensemble) or electronic (ligand) effects. Synergetic effects reported for other bimetallic catalysts which, like Pt-Mo, incorporate in the same cluster the noble metal atoms and easily oxidized metal atoms, could probably be interpreted by similar dual-site mechanisms.

5. CONCLUSIONS

During the last few years, new experimental results have shown that the structure and chemistry of molecular clusters and of naked clusters are more closely related than it was thought before:

- (1) The "nuclearity gap" has been almost suppressed. Indeed naked clusters with a nuclearity smaller than 50-60 can be produced selectively either on a support (especially in zeolite cages) or in pulsed beams. Since, at the same time, up to 55-atom molecular clusters have been synthesized [35], there is an overlap of nuclearity.
- (2) The "structure gap" has lost most of its significance. Although the structure of naked clusters cannot be determined with the same preci-

sion as the crystal structure of molecular clusters, structural data obtained by RED do show that the metal skeleton of a naked cluster is not a rigid small piece of bulk metal. Adsorbates modify the interatomic distances and the lattice symmetry to the same extent as the ligand shell controls the geometry of molecular clusters. Structural flexibility is now a concept valid both for molecular and naked clusters. Investigations of the dynamics of structure flexibility are now required.

(3) Transformations of molecular clusters into naked clusters can be performed without changes (or with only minor changes) in nuclearity. Moreover, heteronuclear clusters can yield bimetallic naked clusters without changes in composition. These transformations can be evidenced only with highly sophisticated tools such as high-resolution analytical microscopy and EXAFS or RED. During these transformations, the preexistent metal-metal bonds seem to be preserved. In contrast, the reverse transformations of naked clusters into molecular clusters known so far proceed via monomeric intermediates, i.e., after an initial breakdown of the metal skeleton. However, direct synthesis of molecular clusters by addition of ligands to a naked metal skeleton could possibly be realized in the future in the products of the reaction of cluster beams with very reactive ligands like carbon monoxide.

(4) As the nuclearity of naked clusters goes down, it is more and more difficult to decide whether the active species grafted on surfaces are in the form of a coordination compound or of a metal cluster. This is especially true for hydroformylation catalysts such as those described by Yermakov *et al.* [32] and Ichikawa [36]. This distinction becomes meaningless as the nuclearities of metal clusters and coordination complexes become similar.

6. REFERENCES

1. R.L. Whetten, D.M. Cox, D.J. Trevor, and A. Kaldor, Surf. Sci. **156**, 8 (1985).
2. L. Wöste, in Contribution of Cluster Physics to Materials Science and Technology, (Eds. J. Davenas and P.M. Rabette), NATO ASI Series E, p. 1, M. Nijhoff Pub. Co., Boston (1986).
3. A. Kaldor, D.M. Cox, D.J. Trevor, and R.L. Whetten, in Catalyst Characterization Science, (Eds. M.L. Deviney and J.L. Gland), ACS Symp. Ser. 288, p. 111, Am. Chem. Soc., Washington (1985).
4. D. Richard and P. Gallezot, in Proc. 4th Internat. Congr. on the Preparation of Catalysts, Louvain 1986, Elsevier, Amsterdam (1987).
5. P. Gallezot, in Metal Clusters, (Ed. M. Moscovits), p. 219, John Wiley and Sons, New York (1986).
6. P. Gallezot, in Catalysis - Science and Technology, (Eds. J.R. Anderson and M. Boudart), vol. 5, p. 221, Springer Verlag, Berlin (1984).
7. G. Bergeret and P. Gallezot, in Proc. 8th Internat. Congr. Catal. Berlin 1984, vol. 5, p. 659, Verlag Chemie, Weinheim (1984).
8. P. Gallezot, unpublished results.

9. J. Schwank, L.F. Allard, M. Deeba, and B.C. Gates, J. Catal. **84**, 27 (1983).
10. S. Iijima and M. Ichikawa, J. Catal. **94**, 313 (1985).
11. A. Choplin, C. Leclercq, A. Theolier, and P. Gallezot, to be published.
12. M. Isaacson, D. Kopf, M. Ohtsuki, and M. Utlan, Ultramicroscopy **4**, 97 (1979).
13. A. Choplin, L. Huang, A. Theolier, P. Gallezot, J.M. Basset, U. Siriwardane, S.G. Shore, and R. Mathieu, J. Am. Chem. Soc. **108**, 4224 (1986).
14. T.M. Tri, J.P. Candy, P. Gallezot, J. Massardier, M. Primet, J.C. Vedrine, and B. Imelik, J. Catal. **79**, 396 (1983).
15. T.M. Tri, J. Massardier, P. Gallezot, and B. Imelik, J. Mol. Catal. **25**, 151 (1984).
16. M. Samant, G. Bergeret, G. Meitzner, P. Gallezot, and M. Boudart, J. Phys. Chem., submitted.
17. J.L. Margitfalvi, in Homogeneous and Heterogeneous Catalysis, (Eds. Yu. Yermakov and V. Likhobov), p. 945, VNU Science Press, Utrecht (1986).
18. O.A. Ferretti, L.C. Bettega de Pauli, J.P. Candy, G. Mabilon, and J.P. Bournonville, in Proc. 4th Internat. Congr. on the Preparation of Catalysts, Louvain 1986, Elsevier, Amsterdam (1987).
19. G. Bergeret, P. Gallezot, P. Gelin, F. Lefebvre, C. Naccache, Y. Ben Taarit, and B. Shannon, J. Catal. **104**, 279 (1987).
20. J.M. Basset, B. Besson, A. Choplin, and A. Theolier, Philos. Trans. R. Soc. London, A **308**, 115 (1982).
21. G. Bergeret, F. Lefebvre, and P. Gallezot, in New Developments in Zeolite Science and Technology, p. 803, Elsevier, Amsterdam (1986).
22. H.H. Lamb, T.R. Krause, and B.C. Gates, J. Chem Soc., Chem. Commun., 821 (1986).
23. P. Gallezot, in Homogeneous and Heterogeneous Catalysis, (Eds. Yu. Yermakov and V. Likhobov), p. 987, VNU Science Press, Utrecht (1986).
24. H. Poppa, Vacuum **34**, 1081 (1984).
25. K. Heinemann, F. Osaka, H. Poppa, and M. Avalos-Borjas, J. Catal. **83**, 61 (1983).
26. P. Gallezot, Ch. Leclercq, I. Mutin, Ch. Nicot, and D. Richard, J. Microsc. Spectrosc. Electron. **10**, 479 (1985).
27. R.L. Whetten, D.M. Cox, D.J. Trevor, and A. Kaldor, Phys. Rev. Lett. **54**, 1494 (1985).
28. J.Y. Saillard and R. Hoffmann, J. Am. Chem. Soc. **106**, 2006 (1984).
29. D.J. Trevor, R.L. Whetten, D.M. Cox, and A. Kaldor, J. Am. Chem. Soc. **107**, 518 (1985).
30. Yu.I. Yermakov, J. Mol. Catal. **21**, 35 (1983).
31. Yu.I. Yermakov, B.N. Kuznetsov, and V.A. Zakharov, Catalysis by Supported Complexes, Elsevier, Amsterdam (1981).

32. B.L. Moroz, O.N. Shumito, E.A. Paukshtis, V.A. Likhobolov, N.N. Bulgakov, E.N. Yurchenko, and Yu. I. Yermakov, in Homogeneous and Heterogeneous Catalysis, (Eds. Yu. Yermakov and V. Likhobolov), p. 1127, VNU Science Press, Utrecht (1986).
33. T.M. Tri, J. Massardier, P. Gallezot, and B. Imelik, J. Catal. **85**, 244 (1984).
34. F. Borg, P. Gallezot, J. Massardier, and V. Perrichon, C₁ Mol. Chem. **1**, 397 (1986).
35. G. Schmid, in Structure and Bonding **62**, p. 51, Springer Verlag, Berlin (1985).
36. M. Ichikawa, in Homogeneous and Heterogeneous Catalysis, (Eds. Yu. Yermakov and V. Likhobolov), p. 819, VNU Science Press, Utrecht (1986).

LARGE MOLECULAR METAL CARBONYL CLUSTERS: MODELS OF METAL PARTICLES

Giuliano Longoni, Alessandro Ceriotti, Mario Marchionna, and Giampietro Piro

Dipartimento di Chimica Inorganica e Metallorganica
e Centro del CNR per lo Studio della Sintesi e della
Struttura dei Composti dei Metalli di Transizione
Università' di Milano
via G. Venezian 21, 20133 Milano
Italy

ABSTRACT. The structures of large molecular metal carbonyl clusters often may be described as fragments of metal lattices stabilized by carbonyl ligands; these structures do not support the common belief that growth of metal aggregates occurs via icosahedral packing. Only a few examples of clusters possessing fivefold symmetry are known. It may be argued that ligands play a role in determining the cluster geometries. A similarity in magnetic behaviour of metal carbonyl clusters and metal crystallites is emerging, which seems to substantiate theoretical predictions of a transition from Pauli- to Curie-type behaviour on going from bulk to particulate metals. Interstitial carbide clusters also show bulk structural behaviour; however, the higher degree of freedom of molecular entities is often reflected in their unusual geometries, which may probably be related to those of carbidized metal particles. The reactions of carbide clusters, either with CO + H₂ or acids, give rise to stoichiometric formation of hydrocarbons; these reactions bear some formal resemblance to Fischer-Tropsch synthesis.

1. INTRODUCTION

Highly dispersed metals have always attracted a wide and multi-disciplinary interest because of their applications in catalysis as well as their fascinating electronic, structural, chemical, magnetic, electrical, and optical properties [1-5]. There is also active theoretical interest in these materials, which stems from the recognition of their belonging to the poorly understood regime of systems too big to be "atomic" and too small to be treated as "bulk matter".

Molecular metal carbonyl clusters (hereafter referred as clusters) are small (<15 Å) metal aggregates electronically saturated and stabilized by ligands and free charges [6], whereas small metal particles (hereafter referred as crystallites) are typically electronically unsaturated and stabilized either by more or less strong inter-

actions with a support (e.g., a metal oxide) or by trapping in the cavity of a zeolite or a more-or-less inert matrix [2,5]. Notwithstanding these differences [7], the possible analogies between the two have attracted attention and been the subject of several excellent reviews [8-11]. The view that a triangular array of metal atoms may already be sufficiently representative of a metal surface and, consequently, that bonding interactions, spectroscopic behaviour, and, to a certain extent, reactivity of cluster-bound molecules and atoms could provide a better understanding of the behaviour of corresponding moieties chemisorbed on a metal inspired the cluster-surface analogy [12-14].

It is not our purpose to review such a wide field; we focus on some more recent accomplishments in the field of large molecular metal carbonyl clusters pertaining to their structural, electronic, chemical, and magnetic behaviour, which have some relevance to the above analogies.

2. STRUCTURAL AND ELECTRONIC BEHAVIOUR OF LARGE MOLECULAR METAL CARBONYL CLUSTERS

The size and shape of small metal particles affect their electronic, chemisorptive and catalytic behaviour as well as their physical properties [1-5,15]. The detailed knowledge of these properties based on experimental results is still unsatisfactory. Theoretical approaches to this problem generally agree in concluding that the most favoured sequence of growth for a metal particle proceeds through the following: tetrahedron, trigonal bipyramidal, bicapped tetrahedron, pentagonal bipyramidal, icosahedron, etc. [2-4,8]. On further increasing the size of the metal particle, close-packed metal arrays might be expected to form, corresponding to their bulk properties, but these are commonly believed to be less stable than icosahedral packing on the basis of their inferior metal connectivity, because of the presence of (100) planes [3]. Bulk structural behaviour is thought to show up only for metal particles larger than 20-50 Å.

2.1. Large Molecular Metal Carbonyl Clusters and Metal Lattices

Both lower- ($N = 4-12$) and higher- ($N > 13$) nuclearity carbonyl clusters do not support the above view. In lower-nuclearity clusters, for instance, an octahedral arrangement of metal atoms is overwhelmingly favoured over a bicapped tetrahedral geometry, and there are no examples of clusters showing a pentagonal bipyramidal frame [6]. Furthermore, the great majority of large clusters show metal cores clearly related to fragments of typical metallic lattices. It may be probable that large clusters, being electronically saturated by the ligands and having the necessity of finding a compromise in the optimization of both M-CO and M-M interactions, could adopt metal arrangements different from those of bare metal crystallites.

Table I is a list of the large clusters containing at least one fully interstitial metal atom; these all adopt metal frames closely

related to fragments of metallic lattices. As shown in the table, in addition to the most common body centered cubic (bcc), face centered cubic (fcc) and hexagonal close packed (h) lattices, there is also an example of a less common complex close packing (ch), namely, that of $[Rh_{22}(CO)_{37}]^{4-}$ [27], adopting an ABAC sequence of layers.

Table I. Structural and electronic behaviour of large molecular metal clusters.

Cluster	Metal Lattice ^a	X ^b	Ref.
$[Rh_{13}(CO)_{24}H]^{4-}$	h	7	[16]
$[Rh_{13}(CO)_{24}H_2]^{3-}$	h	7	[17]
$[Rh_{13}(CO)_{24}H_3]^{2-}$	h	7	[18]
$[Rh_{12}Pt(CO)_{24}]^{4-}$	h	7	[19]
$[Rh_{11}Pt_2(CO)_{24}]^{3-}$	h	7	[19]
$[Rh_{14}(CO)_{26}]^{2-}$	bcc-cp	6	[20]
$[Rh_{14}(CO)_{25}]^{4-}$	bcc	6	[21,22]
$[Rh_{14}(CO)_{25}H]^{3-}$	bcc-cp	6	[23]
$[Rh_{13}Pt(CO)_{25}]^{3-}$	bcc-cp	6	[24]
$[Rh_{15}(CO)_{30}]^{3-}$	bcc	9	[25]
$[Rh_{15}(CO)_{27}]^{3-}$	bcc-cp	6	[21]
$[Rh_{17}(CO)_{30}]^{3-}$	h	6	[26]
$[Rh_{22}(CO)_{37}]^{4-}$	ch	6	[27]
$[Rh_{22}(CO)_{35}H_x]^{5-}$	bcc-cp		[28]
$[Rh_{22}(CO)_{35}H_x]^{4-}$	bcc-cp		[28]
$[Rh_{18}Pt_4(CO)_{35}]^{4-}$	bcc-cp	6	[29]
$Pd_{23}(CO)_{22}(PEt_3)_{10}$	fcc	9	[30]
$[Pt_{24}(CO)_{30}]^{2-}$	fcc	7	[31]
$[Pt_{26}(CO)_{32}H_x]^{2-}$	h	$7+x/2$	[31]
$[Pt_{38}(CO)_{44}H_x]^{2-}$	fcc	$7+x/2$	[31]
$[Ni_{38}Pt_6(CO)_{48}H]^{5-}$	fcc	7	[32]
$[Ni_{38}Pt_6(CO)_{48}H_2]^{4-}$	fcc	7	[32]

^a bcc = body centered cubic; fcc = face centered cubic;
h = hexagonal close packing; cp = close packing;
ch = complex close packing [33].

^b X = number of filled orbitals in excess to $6N$ [34].

It is worth noting that, although some bulk metals may present allotrophic forms, during crystallization each additional layer of metal atoms seems to know its own growth sequence, so that, for instance, a fcc metal never deviates from an ABC sequence in crystallization. In contrast, large clusters of a given metal may indifferently adopt one of the above metal packing lattices; thus, for instance, typical fcc bulk metals such as Rh and Pt indifferently adopt cluster frames derived from bcc, h, or ch lattices, as well as fcc close packing (Table I). Furthermore, several examples of mixed packing, which have been related to the phenomenon of surface reconstruction [10,11], are also known.

Bulk structural behaviour of intermetallic alloys can also be found in large bimetallic clusters. Thus, $[Fe_6Pd_6(CO)_{24}H]^{3-}$ [35] displays a metal frame which is related to a two-layer fragment of either a fcc or h superstructure such as are shown by the Cu₃Au and Ni₃Sn alloys, respectively [33]. In contrast, the $[Ni_{12-x}Pt_x(CO)_{21}H_{4-n}]^{n-}$ [36,37] for $x > 3$ suggests the disordered alloys which give rise to solid solutions.

Equilibrated bimetallic films and crystallites often have a surface composition substantially different from that of the bulk. In ultrahigh vacuum the metal with the lowest heat of atomization generally accumulates on the surface, whereas the bulk is richer in the metal with the highest heat of atomization [38,39].

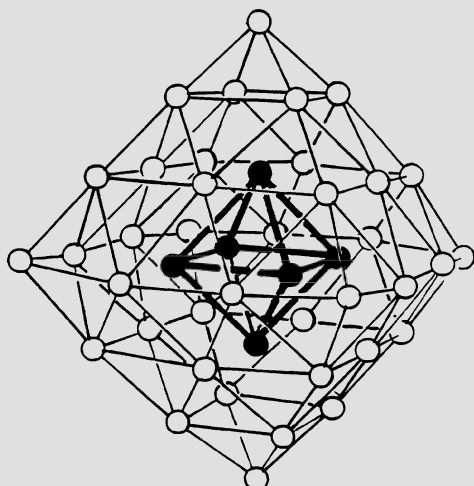


Figure 1. Schematic representation of the metal frame of $[Ni_{38}Pt_6(CO)_{48}H]^{5-}$ illustrating its "cherry" structure (platinum atoms are shown as blackened circles; inter-octahedral bonds are omitted for clarity).

The so-called "cherry" crystallites, in which a kernel of essentially one component is completely surrounded by a skin essentially composed by a second metal, have been proposed [40]. The structures of $[Rh_{12}Pt(CO)_{24}]^{4-}$ [19] and $[Ni_{38}Pt_6(CO)_{48}H]^{5-}$ [32] are nice molecular examples of the "cherry" model. As shown in Fig. 1, the structure of $[Ni_{38}Pt_6(CO)_{48}H]^{5-}$ consists of a Pt_6 octahedral kernel fully encapsulated in a Ni_{38} octahedron of frequency 3 [41]. In contrast to the previously cited $[Fe_6Pd_6(CO)_{24}H]^{3-}$, $[Ni_{38}Pt_6(CO)_{48}H]^{5-}$ conforms to the above trend of the bimetallic crystallites by accumulating the metal with the highest heat of atomization, namely, Pt, in the kernel. It seems likely that the energy gain associated with formation of Fe-CO interactions is at the origin of the opposite trend found in $[Fe_6Pd_6(CO)_{24}H]^{3-}$. Corresponding reversed distributions of metals are known to occur in bimetallic crystallites equilibrated under gas atmospheres, e.g., CO, H₂, or O₂, which are preferentially chemisorbed by only one of the two components [38,39].

As shown in Table I, large clusters related to close-packed lattices (fcc, h) generally present a number of filled cluster valence orbitals (CVO) equal to $6N + 7$, in agreement with the results of extended Hückel calculations performed on bare clusters [34]. The number of CVO in excess to $6N$ decreases to 6 in clusters related to bcc or mixed lattices.

2.2. Fivefold Symmetry in Large Molecular Metal Carbonyl Clusters

The occurrence of fivefold symmetry in vapor- or electro-deposited films, whiskers, and crystallites of several metals, e.g., Fe, Co, Ni, Cu, Pt, and Au, has been known for a long time [42,49]. An upsurge of interest in this phenomenon has recently been caused by the discovery of a metastable Mn-Al alloy [50], as well as by the suggested structure of the so called "footballene" C₆₀ cluster [51,52]. Several packing models with fivefold symmetry, which is supposed to challenge the rules of crystallography, have been put forward, e.g., multiple twinning of particles and pentagonal prismatic and icosahedral packings [48,53-56]. Some of these packing models are formally represented in large metal clusters. Table II is a summary of the large metal clusters showing either local or overall C₅ symmetry.

Both $[Rh_{15}(CO)_{28}C_2]^-$ [60] and $[Pt_{19}(CO)_{22}]^{4-}$ [61] adopt metal frames based on a bicapped pentagonal prism; the latter, which shows an idealized D_{5h} symmetry, is a nice experimental example of Bagley's packing model [53,54]. Thus, systematic capping of the square faces with extra Pt atoms could generate an infinite array of concentric pentagons with a unique fivefold rotation axis.

Icosahedral arrangement of atoms is common in borane chemistry [63], as well as in Au and Ag-Au clusters [64,65]. In contrast, this geometry, which may be related to Mackay's icosahedral packing model [55], was unusual in large metal clusters until this year. There are now four known clusters displaying this geometry, including the centered-icosahedra of $[Rh_{12}Sb(CO)_{27}]^3-$ [59] and $[Ni_{12}Sn(CO)_{22}]^{2-}$ [58], as well as the noncentered $[Ni_9(AsPh)_3(CO)_{15}]^{2-}$ and

$[\text{Ni}_{10}(\text{AsMe})_2(\text{CO})_{18}]^{2-}$ [57]. It is worth noting that the pentagonal antiprismatic arrangement in $[\text{Ni}_{12}\text{Sn}(\text{CO})_{22}]^{2-}$, versus the pentagonal prismatic arrangement in $[\text{Pt}_{19}(\text{CO})_{22}]^{4-}$, is reminiscent of the trigonal antiprismatic and trigonal prismatic features of the $[\text{Ni}_6(\text{CO})_{12}]^{2-}$ and $[\text{Pt}_6(\text{CO})_{12}]^{2-}$ clusters [66,67].

Table II. Large metal clusters having either local or overall fivefold symmetry.

Cluster	Geometry	Ref.
$[\text{Ni}_9(\text{AsPh})_3(\text{CO})_{15}]^{2-}$	icosahedron	[57]
$[\text{Ni}_{10}(\text{AsMe})_2(\text{CO})_{18}]^{2-}$	icosahedron	[57]
$[\text{Ni}_{12}\text{Sn}(\text{CO})_{22}]^{2-}$	icosahedron	[58]
$[\text{Rh}_{12}\text{Sb}(\text{CO})_{27}]^{3-}$	icosahedron	[59]
$[\text{Rh}_{15}(\text{CO})_{28}\text{C}_2]^-$	pentagonal prism	[60]
$[\text{Pt}_{19}(\text{CO})_{22}]^{4-}$	pentagonal prism	[61]
$[\text{HNi}_{34}(\text{CO})_{38}\text{C}_4]^{5-}$		[62]
$[\text{Ni}_{35}(\text{CO})_{39}\text{C}_4]^{6-}$		[62]

Cluster bonding theories [68-70] and experiments agree in indicating the same number of filled CVO for centered icosahedral, cubooctahedral and anticuboctahedral geometries. Why both $[\text{Rh}_{12}\text{Sb}(\text{CO})_{27}]^{3-}$ and $[\text{Ni}_{12}\text{Sn}(\text{CO})_{22}]^{2-}$ do not adopt geometries related to close packing, which would allow better lodging of the interstitial atom than does the icosahedral arrangement, is not straightforward. It seems probable that positive polarization of the interstitial atom and packing of the carbonyl groups around the metal core may play a determinant role. Thus, in $[\text{Ni}_{12}\text{Sn}(\text{CO})_{22}]^{2-}$, each Ni atom is three-connected to carbonyl groups, and these form an idealized polyhedron consisting of an interpenetrating tri-icosahedron.

It has been suggested that occurrence of fivefold symmetry in crystallites could be caused by occlusion of impurities of smaller atoms [42]. The structures of $[\text{HNi}_{34}(\text{CO})_{38}\text{C}_4]^{5-}$ (Fig. 2) and $[\text{Ni}_{35}(\text{CO})_{39}\text{C}_4]^{6-}$, which include pentagonal bipyramidal moieties in the metal frame, might mimic the nucleation process of fivefold symmetry.

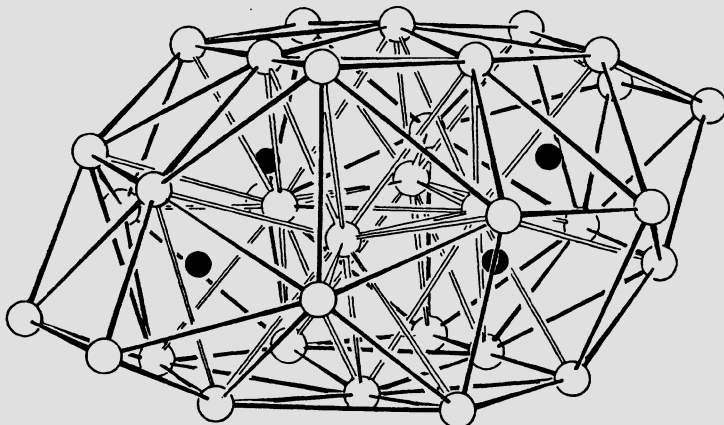


Figure 2. The metal frame of $[HNi_{34}(CO)_{38}C_4]^{5-}$ (carbide atoms are shown as blackened circles).

2.3. Large Metal Clusters containing Interstitial Carbide Atoms

The formal relationship between interstitial carbide molecular clusters and M-C binary phases with respect to coordination of the carbide atom and M-C bonding interactions has already been discussed in several reviews [10,11,71,72]. We confine ourselves to the latest results obtained in this field. The best example of bulk metal carbide structural behaviour in a large metal cluster is probably represented by the recently characterized $[HNi_{38}(CO)_{42}C_6]^{5-}$ penta-anion, which has been obtained by reaction of $[Ni_6(CO)_{12}]^{2-}$ with hexachloropropene [73]. The $Ni_{32}C_6$ inner core of this cluster is closely related to a fragment of the $Cr_{23}C_6$ binary phase [74].

The structure of the latter, as determined by neutron diffraction studies [74], exactly conforms to one of Andreini's space filling models [75,76], and, as schematically shown in two dimensions in Fig. 3A, derives from a three-dimensional alternation of Cr_{13} cuboctahedra and $Cr_{32}C_6$ truncated octahedra fused together along the square faces; the truncated tetrahedral holes generated by the above packing of polyhedra are occupied by unique Cr atoms. The structure of the truncated octahedral $Cr_{32}C_6$ moiety is emphasized in Fig. 3B, consisting of an inner empty cube of Cr atoms (generated by the central atoms of the eight hexagonal faces); each face of the cube is in staggered conformation with a square face of the outer truncated octahedron so to give rise to six square-antiprismatic holes which lodge the six carbide atoms. A completely identical $Ni_{32}C_6$ moiety, which also shows quite close molecular parameters, is contained in $[HNi_{38}(CO)_{42}C_6]^{5-}$.

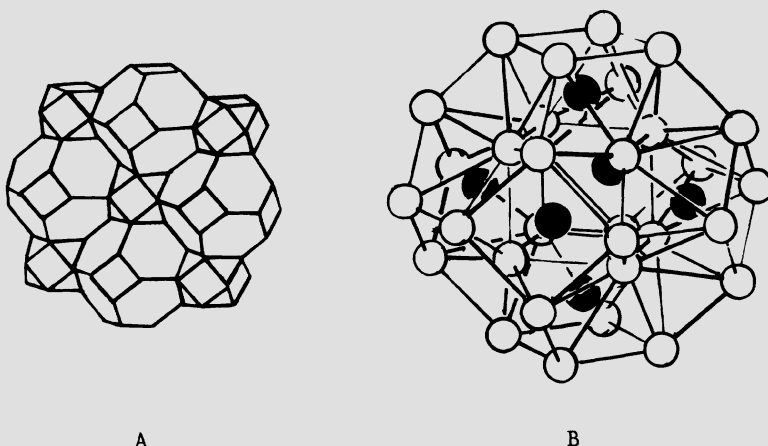


Figure 3. A, schematic representation of the structure of Cr_{23}C_6 ; B, perspective view of the truncated octahedral moiety, with carbide atoms shown as blackened circles.

Since the only well-characterized nickel carbide is the Ni_3C hexagonal phase lodging the carbon atoms in octahedral cavities [77], the above tight relationship seems to be suggestive of the possibility of a molecular approach to new M-C binary phases.

The metal frames of $[\text{HNi}_{34}(\text{CO})_{38}\text{C}_4]^{5-}$ (Fig. 2) and $[\text{Ni}_{35}(\text{CO})_{39}\text{C}_4]^{6-}$ allow one to envision the structural changes that may occur in small metal particles as a result of carbidization [78]. For instance, it is known that dissociative adsorption of CO and diffusion of carbon atoms in the metal lattice produce iron carbide phases, e.g., Fe_3C , Fe_5C_2 , and Fe_7C_3 , during Fischer-Tropsch synthesis [78]. The extremely complicated Ni_{34}C_4 framework, which consists of a Ni_{20} close-packed kernel enveloped by four trigonal prisms (lodging the carbide atoms), four pentagonal bipyramids, and poly-tetrahedral moieties, probably originates from the necessity to provide more suitable cavities for the carbide atoms than provided by a close-packed lattice. The preference of carbide atoms for cavities larger than octahedral in first-row transition metals is well documented both in large metal clusters (Table III) and in bulk metal carbides, probably stemming from the fact that octahedral lodging of carbon in metals with a radius of ca. 1.25 Å can be obtained only with a significant loosening of M-M interactions. Structural modifications such as those envisioned by $[\text{HNi}_{34}(\text{CO})_{38}\text{C}_4]^{5-}$ are likely to occur also in crystallites due to their shorter M-M interaction with respect to the bulk metal [79,80].

As shown in Table III, large metal clusters with $N > 10$ and containing the carbide atoms in cavities larger than octahedral constantly show $6N_M + 2N_C + 7$ filled CVO (N_C = number of carbide

atoms). The only exception is $[Ni_{16}(CO)_{23}C_2]^{4-}$, which has two extra CVO and contains two C_2 ($d_{C-C} = 1.38 \text{ \AA}$) fragments [81].

Table III. Selected Interstitial Poly-carbide Metal Clusters with $N > 10$.

Cluster	Carbon cage ^a	X^b	Ref.
$[Co_{11}(CO)_{22}C_2]^{3-}$	t.a.-t.p.	7	[82]
$Rh_{12}(CO)_{25}C_2$	t.a.-t.p.	7	[83]
$[Rh_{12}(CO)_{24}C_2]^{2-}$	t.p.	7	[84]
$[Rh_{12}(CO)_{23}C_2]^{3-}$	t.p.	7	[85]
$[Co_{13}(CO)_{24}C_2]^{4-}$	t.p.	7	[86]
$[Co_{13}(CO)_{24}C_2]^{3-}$	t.p.	7	[87]
$[Rh_{15}(CO)_{28}C_2]^{-}$	o.		[60]
$[Ni_{16}(CO)_{23}(C_2)_2]^{4-}$		9	[81]
$[HNi_{34}(CO)_{38}C_4]^{5-}$	t.p.	7	[62]
$[Ni_{35}(CO)_{39}C_4]^{6-}$	t.p.	7	[62]
$[HNi_{38}(CO)_{42}C_6]^{5-}$	s.a.	7	[73]

^a t.a. = tetragonal antiprism; t.p. = trigonal prism; o. = octahedron; s.a. = square antiprism;

^b $X =$ number of filled orbitals in excess to $6N_M + 2N_C$.

3. MAGNETIC BEHAVIOUR OF LARGE MOLECULAR METAL CARBONYL CLUSTERS

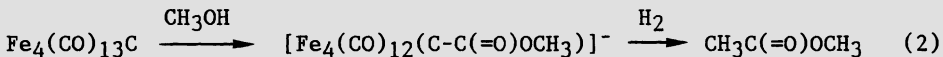
A transition from Pauli- to Curie-type magnetic behaviour has been predicted to occur on going from bulk to particulate metals as a result of the transition from a continuum to discrete electronic energy levels [88-91]. Properties of small particles of Ni and of Pt seem to confirm these theoretical predictions [92-94]. For instance, platinum crystallites having an average size of ca. 22 Å show a number of unpaired electrons per particle in the range 0.5-1 [94].

Molecular metal carbonyl clusters have been suggested to represent ideal models for experimental verification of this phenomenon, as they are models of metal particles of uniform size and known geometry and are available in high purity [95]. A systematic study of magnetic behaviour of osmium carbonyl clusters with $N = 3-10$ has shown temperature-independent magnetic behaviour down to 1.5 K for $Os_3(CO)_{12}$, $H_4Os_4(CO)_{12}$, $Os_7(CO)_{21}$, and $Os_{10}(CO)_{24}Cl_2$ [96]. The excess molecular susceptibility at 298 K increases with cluster size [96]. In contrast, $H_2Os_{10}(CO)_{24}C$ shows a temperature-dependent paramagnetism of the Curie

type at low temperature, which corresponds to a magnetic moment of 0.62 Bohr magnetons per cluster [95]. Analogous behaviour has been found for several platinum clusters with $N = 6-38$, as well as for Ni-Pt and Ni clusters [97,98].

4. CHEMICAL BEHAVIOUR OF INTERSTITIAL CARBIDES

The chemistry of carbide carbonyl clusters has undergone a rapid expansion in recent years also as result of the recognition that surface-bound carbides play an important role in catalytic CO hydrogenation to give hydrocarbons [99]. Tri-, tetra-, and penta-metal-coordinated carbon atoms, which bear strong analogies to surface-bound carbide atoms, are known for Fe, Ru, Os, and Co carbonyl clusters [71], and their fascinating chemical reactivity has attracted much interest because of the belief that in those cases the cluster-surface analogy could be extrapolated also to reactivity [14,71]. Two relevant examples of cluster-bound carbide reactivity are shown below [100,101]:



Reaction (1) may mimic the first step of the hydrogenation of surface-bound carbon atom to give methane, whereas reaction (2) may represent the synthesis of an organic molecule substantially from CO and H₂ [71].

The lack of reactivity of the carbon atom in interstitial carbide iron clusters, in comparison to the corresponding clusters with an exposed carbide atom, has been suggested to arise from the lack of a contribution of carbon atomic orbitals to the frontier cluster orbitals, rather than from trivial steric consideration [102]. The lack of reactivity, for instance with molecular hydrogen, is a common feature of most Ni and Co-Ni carbide clusters. However, reaction of most of the above clusters with hydrogen in the presence of CO or PPh₃ gives rise to hydrocarbons, e.g., CH₄, C₂H₄, and C₂H₆ under very mild conditions (25°C, 1 atm) [103,104]. As suggested by spectroscopic evidence and by the isolation of few intermediate derivatives, formation of hydrocarbons could be due to their progressive degradation to smaller clusters by elimination of mononuclear carbonyl species (e.g., reaction (3)) and, eventually, to progressive exposure of the carbide atoms. When starting from a mono-carbide, concomitant cluster recondensation steps, such as that exemplified by reaction (4) [81], could give dicarbide clusters and prelude to C₂ hydrocarbons (*vide infra*).

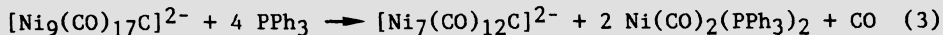
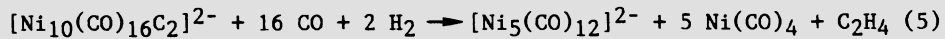


Table IV. Dicarbide clusters having short C-C interatomic separations.

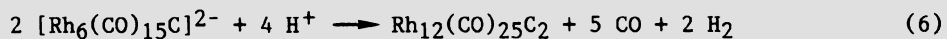
Cluster	$d_{C-C}/\text{\AA}$	Ref.
$\text{Co}_6(\text{CO})_{14}\text{C}_2\text{S}$	1.37	[105]
$[\text{Co}_{11}(\text{CO})_{22}\text{C}_2]^{3-}$	1.62	[82]
$\text{Rh}_{12}(\text{CO})_{25}\text{C}_2$	1.48	[83]
$[\text{Ni}_{10}(\text{CO})_{16}\text{C}_2]^{2-}$	1.40	[106]
$[\text{Co}_6\text{Ni}_2(\text{CO})_{16}\text{C}_2]^{2-}$	1.50	[107]
$[\text{Co}_3\text{Ni}_7(\text{CO})_{16}\text{C}_2]^{2-}$	1.49	[108]
$[\text{Co}_3\text{Ni}_7(\text{CO})_{15}\text{C}_2]^{3-}$	1.41	[104]
$[\text{Ni}_{16}(\text{CO})_{23}(\text{C}_2)_2]^{4-}$	1.38	[81]

Indeed several dicarbide clusters are now known and several show very short C-C interatomic separations (Table IV).

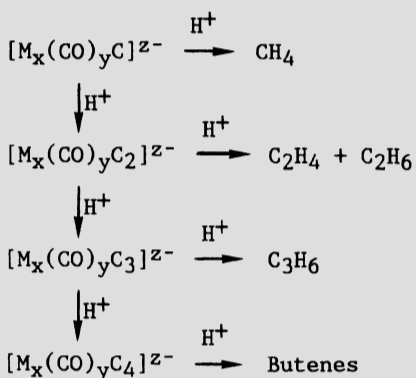
Furthermore, preformed dicarbide clusters on reaction with CO and H₂ can give almost pure ethylene, as shown, for example, below:



Hydrocarbons (C₁-C₄) have also been detected in the gas phase as the products of the reaction of Ni and Co-Ni carbide clusters with strong protonic acids. Isotopic tracer studies with $[\text{Ni}_9(\text{CO})_{17}^{13}\text{C}]^{2-}$ (95 % enrichment) and $[\text{Ni}_9(^{13}\text{CO})_{16}\text{C}]^{2-}$ (30-90 % enrichment) have indicated the carbide atom as the main source of the observed C₂-C₄ hydrocarbons [109], while the proton-induced reduction of carbon monoxide [110,111] seems to give only a minor contribution to the above. A possible mechanism, which is in keeping with the chemical behaviour of these carbide clusters and accounts for observation of higher hydrocarbons (C₂-C₄), is shown in Scheme I; this implies concomitant condensation reaction of a mono-carbide to poly-carbides induced by acids and metal-assisted conversion of carbon atoms, or moieties, with protons. Condensations of carbide to give dicarbide clusters induced by acids under controlled conditions have already been reported, as shown, for example, below [83]:



At this stage, however, it is not possible to rule out other mechanisms for both the above proton-induced formation of C₂-C₄ hydrocarbons and the previously described reaction of monocarbide clusters with CO and H₂ to give C₂ hydrocarbons. An as likely alternative could be the oligomerization of initially produced CH_x moieties [112].



SCHEME I

Anyhow, the proton-induced conversion of carbide atoms to give hydrocarbons, and their corresponding reaction with molecular hydrogen under mild conditions, are indicative of a close analogy in the reactivity of molecular and bulk carbides. Analogous chemical behaviour is indeed shown by bulk metal carbides [113]. The above stoichiometric reactions, in conjunction with the remarkable proton-induced reduction of CO discovered by Whitmire and Shriver [110], allow one to mimic Fischer-Tropsch products with clusters.

5. ACKNOWLEDGMENTS

We thank Prof. B.T. Heaton, Prof. M. Manassero, Dr. F. Demartin and Dr. N. Masciocchi for their contributions in providing some uncited results.

6. REFERENCES

1. J.R. Anderson, Structure of Metallic Catalysts, Academic Press, London and New York (1975).
2. S.C. Davis and K.J. Klabunde, Chem. Rev. 82, 153 (1982).
3. J.J. Burton, Catal. Rev. 9, 209 (1974).
4. J. Koutecky and P. Fantucci, Chem. Rev. 86, 539 (1986).
5. J.C. Phillips, Chem. Rev. 86, 619 (1986).
6. B.F.G. Johnson, Transition Metal Clusters, J. Wiley and Sons, New York (1980).
7. M. Moskovits, Acc. Chem. Res. 12, 229 (1979).
8. J.M. Basset and R. Ugo, Aspects of Homogeneous Catalysis, (Ed. R. Ugo), v. 3, p. 137, Reidel, Dordrecht and Boston (1977).

9. E.L. Muetterties and M.J. Krause, Angew. Chem., Int. Ed. Engl. **22**, 135 (1983).
10. P. Chini, Gazz. Chim. Ital. **109**, 225 (1979).
11. P. Chini, J. Organomet. Chem. **200**, 37 (1980).
12. E.L. Muetterties and J. Stein, Chem. Rev. **79**, 479 (1979).
13. R. Ugo and R. Psaro, J. Mol. Catal. **20**, 53 (1983).
14. R.D. Adams and I.T. Horvath, Prog. Inorg. Chem. **33**, 127 (1985).
15. R.C. Baetzold, Inorg. Chem. **20**, 118 (1981).
16. G. Ciani, A. Sironi, and S. Martinengo, J. Chem. Soc., Dalton Trans., 519 (1981).
17. V.G. Albano, G. Ciani, S. Martinengo, and A. Sironi, J. Chem. Soc., Dalton Trans., 978 (1979).
18. V.G. Albano, A. Ceriotti, P. Chini, G. Ciani, S. Martinengo, and W.M. Anker, J. Chem. Soc., Chem. Commun., 860 (1975).
19. A. Fumagalli, S. Martinengo, and G. Ciani, J. Chem. Soc., Chem. Commun., 1381 (1983).
20. S. Martinengo, G. Ciani, and A. Sironi, J. Chem. Soc., Chem. Commun., 1140 (1980).
21. S. Martinengo, G. Ciani, A. Sironi, and P. Chini, J. Am. Chem. Soc. **100**, 7097 (1978).
22. J.L. Vidal and R.C. Schoening, Inorg. Chem. **20**, 265 (1981).
23. G. Ciani, A. Sironi, and S. Martinengo, J. Organomet. Chem. **192**, C42 (1980).
24. A. Fumagalli, S. Martinengo, G. Ciani, and A. Sironi, XVI Cong. Naz. Chim. Inorg., Ferrara, 402 (1983).
25. J.L. Vidal, L.A. Kapicak, and J.M. Troup, J. Organomet. Chem. **215**, C11 (1981).
26. G. Ciani, A. Magni, A. Sironi, and S. Martinengo, J. Chem. Soc., Chem. Commun., 1280 (1981).
27. S. Martinengo, G. Ciani, and A. Sironi, J. Am. Chem. Soc. **102**, 7564 (1980).
28. J.L. Vidal, R.C. Schoening, and J.M. Troup, Inorg. Chem. **20**, 227 (1981).
29. A. Fumagalli, S. Martinengo, G. Ciani, N. Masciocchi, and A. Sironi, XVIII Cong. Naz. Chim. Inorg., Como, 148 (1985).
30. E.G. Mednikov, N.K. Eremenko, Yu.L. Slovokhotov, and Yu.T. Struchov, J. Organomet. Chem. **301**, C35 (1986).
31. A. Ceriotti, P. Chini, G. Longoni, D.M. Waschecheck, E.J. Wucherer, L.F. Dahl, M. Marchionna, and R.A. Montag, unpublished results.
32. A. Ceriotti, F. Demartin, G. Longoni, M. Manassero, M. Marchionna, G. Piva, and M. Sansoni, Angew. Chem., Int. Ed. Engl. **24**, 696 (1985).
33. A.F. Wells, Structural Inorganic Chemistry, IVth, Clarendon Press, Oxford (1975).
34. G. Ciani and A. Sironi, J. Organomet. Chem. **197**, 233 (1980).
35. G. Longoni, M. Manassero, and M. Sansoni, J. Am. Chem. Soc. **102**, 7973 (1980).
36. A. Ceriotti, F. Demartin, G. Longoni, M. Manassero, G. Piva, G. Piro, M. Sansoni, and B.T. Heaton, J. Organomet. Chem. **301**, C5 (1986).

37. A. Ceriotti, P. Ingallina, G. Longoni, M. Marchionna, F. Demartin, and M. Manassero, unpublished results.
38. J.H. Sinfelt, Acc. Chem. Res. 10, 15 (1977).
39. W.M.H. Sachtler and R.A. Van Santen, Adv. Catal. 26, 169 (1977).
40. W.M.H. Sachtler, Vide 164, 67 (1973).
41. B.K. Teo and N.J.A. Sloane, Inorg. Chem. 24, 4545 (1985).
42. A.J. Melmed and D.O. Hayward, J. Chem. Phys. 31, 545 (1959).
43. F. Ogburn, B. Paretzkin, and H.S. Peiser, Acta Crystallogr. 17, 774 (1964).
44. M.A. Gedwill, G.J. Alstetter, and C.M. Weyman, J. Appl. Phys. 35, 2266 (1964).
45. R.L. Schwoebel, J. Appl. Phys. 37, 2515 (1966).
46. R.W. De Blois, J. Appl. Phys. 36, 1647 (1965).
47. G.L. Downs and J.D. Braun, Science 154, 1443 (1966).
48. S. Ino, J. Phys. Soc. Japan 21, 346 (1966).
49. A. Renou and M. Gillet, Surf. Sci. 106, 27 (1981).
50. D. Schechtman, I. Blech, D. Gratias, and J.W. Cahn, Phys. Rev. Lett. 53, 1951 (1984).
51. H.W. Kroto, J.R. Heath, S.C. O'Brien, R.F. Curl, and R.E. Smally, Nature (London) 318, 162 (1985).
52. A.D.J. Haymet, J. Am. Chem. Soc. 108, 319 (1986).
53. B. Bagley, Nature (London) 225, 1040 (1970).
54. B. Bagley, Nature (London) 208, 674 (1965).
55. A.L. Mackay, Acta Crystallogr. 15, 916 (1962).
56. D. Levine and P.J. Steinhardt, Phys. Rev. Lett. 53, 2477 (1984).
57. D.F. Rieck, R.A. Montag, T.S. McKechnie, and L.F. Dahl, J. Am. Chem. Soc. 108, 1330 (1986).
58. A. Ceriotti, F. Demartin, P. Ingallina, M. Manassero, M. Marchionna, N. Masciocchi, and M. Sansoni, XIX Cong. Naz. Chim. Inorg., Cagliari, 189 (1986).
59. J.L. Vidal and J.M. Troup, J. Organomet. Chem. 213, 351 (1981).
60. V.G. Albano, M. Sansoni, P. Chini, S. Martinengo, and D. Strumolo, J. Chem. Soc., Dalton Trans., 459 (1978).
61. D.M. Waschecheck, E.J. Wucherer, L.F. Dahl, A. Ceriotti, G. Longoni, M. Manassero, M. Sansoni, and P. Chini, J. Am. Chem. Soc. 101, 6110 (1979).
62. A. Ceriotti, A. Fait, G. Longoni, G. Piro, L. Resconi, F. Demartin, M. Manassero, N. Masciocchi, and M. Sansoni, J. Am. Chem. Soc. 108, 5370 (1986).
63. E.L. Muettterties and W.H. Knoth, Polyhedral Boranes, M. Dekker, New York (1968).
64. C.E. Briant, B.R. Theobald, J.W. White, L.K. Bell, D.M.P. Mingos, and A.J. Welch, J. Chem. Soc., Chem. Commun., 201 (1981).
65. B.K. Teo and K. Keating, J. Am. Chem. Soc. 106, 2224 (1984).
66. J.C. Calabrese, L.F. Dahl, A. Cavalieri, P. Chini, G. Longoni, and S. Martinengo, J. Am. Chem. Soc. 96, 2616 (1974).
67. J.C. Calabrese, L.F. Dahl, P. Chini, G. Longoni, and S. Martinengo, J. Am. Chem. Soc. 96, 2614 (1974).
68. J.W. Lauher, J. Am. Chem. Soc. 100, 5305 (1978).
69. K. Wade, Adv. Inorg. Chem. Radiochem. 18, 1 (1976).
70. B.K. Teo, Inorg. Chem. 23, 1251 (1984).

71. J.S. Bradley, Adv. Organomet. Chem. 22, 1 (1983).
72. M. Tachikawa and E.L. Muettterties, Prog. Inorg. Chem. 28, 203 (1981).
73. A. Ceriotti, F. Demartin, A. Fait, G. Longoni, M. Manassero, N. Masciocchi, G. Piro, and M. Sansoni, XVIII Cong. Naz. Chim. Inorg., Como, 137 (1985); J. Am. Chem. Soc. 108, 8091 (1986).
74. A.L. Bowman, G.P. Arnold, E.K. Storms, and N.G. Nereson, Acta Crystallogr. B28, 3102 (1972).
75. A. Andreini, Mem. Soc. Ital. Sci. 14, 75 (1907).
76. A.F. Wells, Three-Dimensional Nets and Polyedra, J. Wiley and Sons, New York, 145-148 (1977).
77. S. Nakagura, J. Phys. Soc. Japan 12, 482 (1957).
78. E.M. Dry, Catalysis, Science and Technology, Springer-Verlag, Berlin, 1, 159 (1981).
79. G. Apai, J.F. Hamilton, J. Stohr, and A. Thompson, Phys. Rev. Lett. 43, 165 (1979).
80. B. Moraweck, G. Clugnet, and A.J. Renouprez, Surf. Sci. 81, L631 (1979).
81. A. Ceriotti, G. Longoni, G. Piro, L. Resconi, M. Manassero, N. Masciocchi, and M. Sansoni, J. Chem. Soc., Chem. Commun., 1402 (1985).
82. V.G. Albano, D. Braga, G. Ciani, and S. Martinengo, J. Organomet. Chem. 213, 293 (1981).
83. V.G. Albano, P. Chini, S. Martinengo, M. Sansoni, and D. Strumolo, J. Chem. Soc., Dalton Trans., 459 (1978).
84. V.G. Albano, D. Braga, P. Chini, D. Strumolo, and S. Martinengo, J. Chem. Soc., Dalton Trans., 249 (1983).
85. D. Strumolo, C. Seregni, S. Martinengo, V.G. Albano, and D. Braga, J. Organomet. Chem. 252, C93 (1983).
86. V.G. Albano, D. Braga, P. Chini, G. Ciani, and S. Martinengo, J. Chem. Soc., Dalton Trans., 645 (1982).
87. V.G. Albano, D. Braga, A. Fumagalli, and S. Martinengo, J. Chem. Soc., Dalton Trans., 1137 (1985).
88. H. Frohlich, Physica 4, 406 (1937).
89. R. Kubo, J. Phys. Soc. Japan 17, 975 (1962).
90. R. Denton, B. Muhschlegel, and D.J. Scalapino, Phys. Rev. B7, 3589 (1973).
91. R. Kubo, A. Kanabata, and S. Kobayashi, Am. Rev. Matem. Sci. 14, 49 (1984).
92. J.H. Sinfelt, Rev. Mod. Phys. 51, 569 (1979).
93. R.F. Marzke, Catal. Rev. 19, 43 (1979).
94. R.F. Marzke, W.S. Glaunsinger, and M. Bayard, Solid State Commun. 18, 1025 (1976).
95. R.E. Benfield, P.P. Edwards, and A.M. Stacy, J. Chem. Soc., Chem. Commun., 525 (1982).
96. D.C. Johnson, R.E. Benfield, P.P. Edwards, W.J.H. Nelson, and M.D. Vargas, Nature (London) 314, 231 (1985).
97. B.K. Teo, F.J. Di Salvo, J. Wasachek, G. Longoni, and A. Ceriotti, Inorg. Chem. 25, 2262 (1986).
98. B.J. Pronk, H.B. Brom, L.J. De Jongh, G. Longoni, and A. Ceriotti, Solid State Commun. 59, 349 (1986).

99. P. Biloen and W.M.H. Sachtler, Adv. Catal. 30, 165 (1981).
100. M. Tachikawa and E.L. Muettterties, J. Am. Chem. Soc. 102, 4541 (1980).
101. J.S. Bradley, G.B. Ansell, and E.W. Hill, J. Am. Chem. Soc. 101, 7417 (1979).
102. J.W. Kolis, F. Basolo, and D.F. Shriver, J. Am. Chem. Soc. 104, 5626 (1982).
103. A. Ceriotti, R. Della Pergola, G. Longoni, M. Manassero, and M. Sansoni, J. Chem. Soc., Dalton Trans., 1181 (1984).
104. G. Longoni, A. Ceriotti, R. Della Pergola, M. Manassero, M. Perego, G. Piro, and M. Sansoni, Philos. Trans. R. Soc. London, A 308, 47 (1982).
105. G. Gervasio, R. Rossetti, P.L. Stanghellini, and G. Bor, Inorg. Chem. 23, 2073 (1984).
106. A. Ceriotti, G. Longoni, M. Manassero, N. Masciocchi, L. Resconi, and M. Sansoni, J. Chem. Soc., Chem. Commun., 181 (1985).
107. A. Arrigoni, A. Ceriotti, R. Della Pergola, G. Longoni, M. Manassero, N. Masciocchi, and M. Sansoni, Angew. Chem., Int. Ed. Engl. 23, 322 (1984).
108. A. Arrigoni, A. Ceriotti, R. Della Pergola, G. Longoni, M. Manassero, and M. Sansoni, J. Organomet. Chem. 296, 243 (1985).
109. B.T. Heaton, G. Longoni, M. Marchionna, and G. Piro, unpublished work.
110. K.H. Whitmire and D.F. Shriver, J. Am. Chem. Soc. 102, 1956 (1980).
111. M.A. Drezdzon and D.F. Shriver, J. Mol. Catal. 21, 81 (1983).
112. R.C. Brady III and R. Pettit, J. Am. Chem. Soc. 102, 6181 (1980).
113. L.E. Toth, Transition Metal Carbides and Nitrides, Refractory Materials, v. 7, Academic Press, New York, London (1971).

MOLECULAR MODELS OF EARLY TRANSITION METAL OXIDES: POLYOXOANIONS AS ORGANIC FUNCTIONAL GROUPS

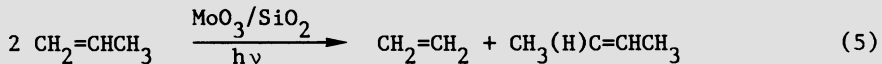
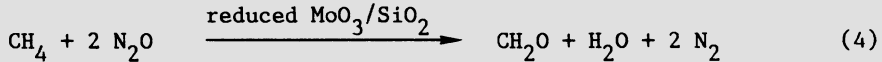
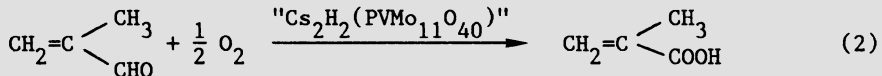
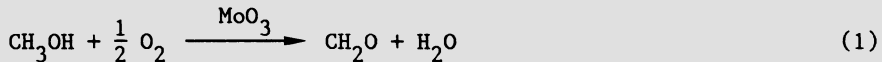
Victor W. Day
Crystalytics Company
Lincoln, Nebraska 68501
USA
Department of Chemistry
University of Nebraska
Lincoln, Nebraska 68588
USA

Walter G. Klemperer, Curtis Schwartz, Ren-Chain Wang
Department of Chemistry
University of Illinois
Urbana, Illinois 61801
USA

ABSTRACT. Early transition metal oxides are known to be effective heterogeneous catalysts or catalyst precursors for numerous organic transformations, including methanol oxidation to give formaldehyde, methacrolein oxidation to give methacrylic acid, propylene oxidation to give acrolein, methane oxidation to give formaldehyde, and propylene metathesis to give ethylene and butene. Due to the difficulty of characterizing surface-bound intermediates, efforts have been made to synthesize and study the reaction chemistry of analogous polyoxoanion derivatives containing organic subunits. Several polyoxomolybdate derivatives have been structurally characterized during the past decade that incorporate simple organic moieties believed to be surface intermediates in these heterogeneous systems, including $[(\text{HCO}_2)_2(\text{Mo}_8\text{O}_{26})]^{6-}$, $\text{CH}_2\text{Mo}_4\text{O}_{15}\text{H}^{3-}$, $\{[\text{CH}_3\text{C}(\text{CH}_2\text{O})_3]_2(\text{CH}_3\text{CH}_2\text{O})_2\text{Mo}_4\text{O}_8\}$, and $[(\text{CH}_3\text{O})_4(\text{Mo}_8\text{O}_{24})]^{4-}$. More recently, two polyoxoanion systems have been investigated that illustrate solution pathways for incorporating organic groups into polyoxoanions and effecting organic oxidations and dehydrations. In the first, the niobotungstic acid esters $\text{Nb}_2\text{W}_4\text{O}_{19}\text{R}^{3-}$, $\text{R} = \text{CH}_3, \text{CH}_3\text{CH}_2, (\text{CH}_3)_2\text{CH}, \text{and } (\text{CH}_3)_3\text{C}$, have been prepared by reacting the appropriate alcohol with either the niobotungstic acid $\text{Nb}_2\text{W}_4\text{O}_{19}\text{H}^{3-}$ or its anhydride $(\text{Nb}_2\text{W}_4\text{O}_{18})_{20}^{6-}$. In the second system, molybdophosphoric acid esters such as $(\text{P}_3\text{O}_9)\text{Mo}_3\text{O}_3\text{CH}_2\text{CH}_3^{2-}$ have been prepared from the appropriate alcohol and then degraded thermally or photochemically. The ethyl ester, for example, yields acetaldehyde plus ethanol thermally, and acetaldehyde, ethanol, plus ethylene photochemically.

1. MOLYBDENUM OXIDES IN HETEROGENEOUS CATALYSIS

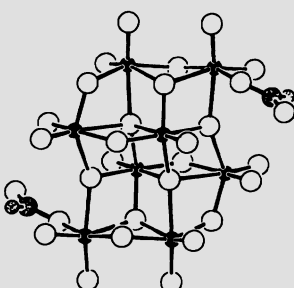
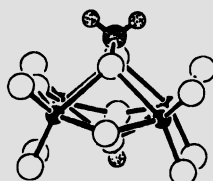
The remarkable variety of behavior displayed by early transition metal oxides toward organic molecules is clearly illustrated by the following selection of reactions catalyzed heterogeneously by molybdenum oxides:



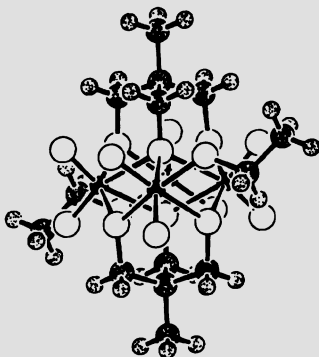
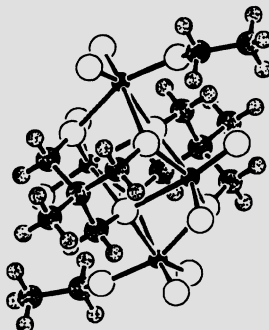
The "simple" partial oxidation of methanol to give formaldehyde can be achieved with great selectivity using molybdenum trioxide or ferric molybdate catalysts [1,2]. Aldehydes can also be partially oxidized to give carboxylic acids in a selective fashion using molybdates. A commercial process for conversion of methacrolein into methacrylic acid, eq. (2), utilizes a proprietary cesium phosphovanadomolybdate heteropolyanion catalyst [3]. Selective hydrocarbon oxidations of the type shown in eq. (3) are also industrially significant and can be performed using multicomponent bismuth molybdate-based catalysts [4]. For more drastic oxidations, reaction of N_2O with Mo^{V} centers in reduced MoO_3 on SiO_2 yields $\text{Mo}^{\text{VI}}\text{O}^-$ radical anions capable of oxidizing methane [eq. (4)] [5]. Finally, olefin metathesis catalysts can be prepared photochemically from propylene and MoO_3 on SiO_2 . The catalyst is believed to contain a molybdenum-bound methylene group obtained from reaction between the molybdenyl electronically excited state ($\text{Mo}^{\text{V}0^-}$)* and $\text{CH}_2=\text{CHCH}_3$ with liberation of CH_3CHO .

2. INCORPORATING CARBOXYL, CARBONYL, AND ALKOXY GROUPS INTO POLYMOLYBDATE STRUCTURES

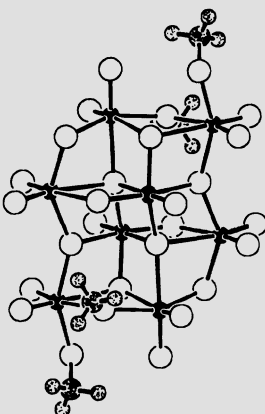
Since molybdenum oxide based heterogeneous catalysts are notoriously difficult to characterize on a molecular level, there has been considerable interest during the past decade in preparing polymolybdates containing simple organic subunits of the type involved in heterogeneous selective oxidations, namely, carboxyl, carbonyl, and alkoxy groups. The formate-containing species $[(\text{HCO}_2)_2(\text{Mo}_8\text{O}_{26})]^{6-}$ shown in 1 displays no surprising features from an organic point of view [7,8],

12

but the formaldehyde adduct $\text{CH}_2\text{Mo}_4\text{O}_{15}\text{H}^{3-}$, 2, is really an acetal derivative containing a CH_2O_2 subunit [9,10]. Several polymolybdates containing simple alkoxy groups have also been structurally characterized. One complex, $\{[\text{CH}_3\text{C}(\text{CH}_2\text{O})_3]_2(\text{CH}_3\text{CH}_2\text{O})_2\text{Mo}_4\text{O}_8\}$ (3), contains two ethoxy groups plus two tridentate chelating alkoxide ligands [11].

34

Structure 3, designed to illustrate the gross molecular features of this centrosymmetric species, has been reoriented in 4 to emphasize the local environment of the ethoxy groups. The structure of the second molybdenum polyoxoalkoxide of interest, $[(\text{CH}_3\text{O})_4\text{Mo}_8\text{O}_{24}]^{4-}$, is shown in 5 [12]. This structure contains two types of methoxy groups, one terminally bonded to a single molybdenum center and the other bridging between two molybdenum centers. For the sake of completeness, a third type of complex should be mentioned that contains a bridging alkoxide group, the $\text{PMo}_{12}\text{O}_{40}\text{R}^{2-}$ species, $\text{R} = \text{CH}_3$ and C_2H_5 [13].



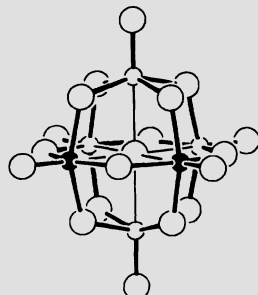
5

3. THE $\text{Nb}_2\text{W}_4\text{O}_{19}^{4-}$ ANION AND ITS SOLUTION CHEMISTRY

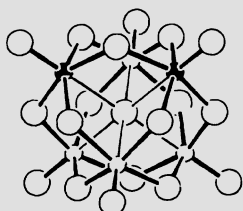
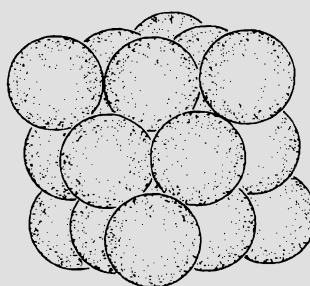
Although the polymolybdate compounds just surveyed serve as useful structural and spectroscopic models for surface-bound organic groups, they are not particularly well suited for modeling solid oxide oxidation chemistry. The $\{[\text{CH}_3(\text{CH}_2\text{O})_3]_2(\text{CH}_3\text{CH}_2\text{O})_2\text{Mo}_4\text{O}_8\}$ molecule contains complex organic chelating ligands in addition to the simple ethoxy groups of interest, and these complex ligands are likely to complicate studies designed to focus on ethoxy group oxidation.

The $[(\text{CH}_3\text{O})_4\text{Mo}_8\text{O}_{24}]^{4-}$ anion has been studied in the solid state as a sodium salt containing eight moles of methanol and shown to decompose with release of formaldehyde. Since thermal decomposition generates primarily dimethyl ether, however, there is some question whether organic decomposition products arise from free methanol or bound methoxide [12]. The $[\text{CH}_2\text{Mo}_4\text{O}_{15}\text{H}]^{3-}$ ion contains an acidic proton and degrades at relatively low temperatures by an acid/base, not redox, pathway [9].

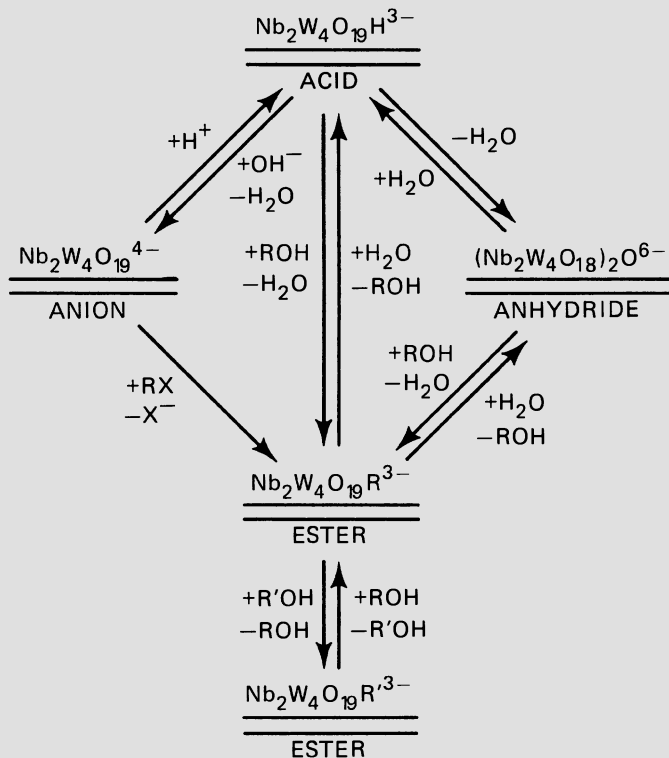
The $\text{Nb}_2\text{W}_4\text{O}_{19}^{4-}$ anion (see 6) was selected, for several reasons, for initial investigation of early transition metal polyoxoanion solution reactivity toward simple organic molecules. First, the $\text{Nb}_2\text{W}_4\text{O}_{19}^{4-}$ ion is known to have surface oxygens sufficiently reactive to bind organometallic units [14,15] and is therefore a good candidate for binding organic units. Second, water exchange studies have shown that the niobium-oxygen bonds in $\text{Nb}_2\text{W}_4\text{O}_{19}^{4-}$, like molybdenum-oxygen bonds in most polymolybdates, are far more labile than the tungsten-oxygen bonds [15]. The gross instability of the polymolybdate complexes discussed above might therefore be avoided in that the relatively inert $\text{Nb}_2\text{W}_4\text{O}_{19}^{4-}$ tungstate framework might prevent catastrophic structural

6

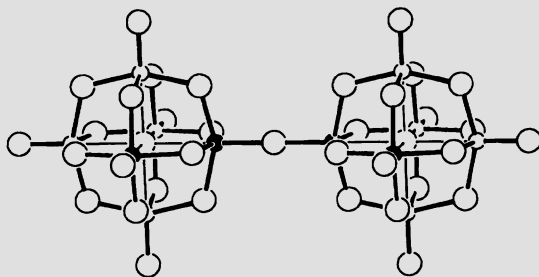
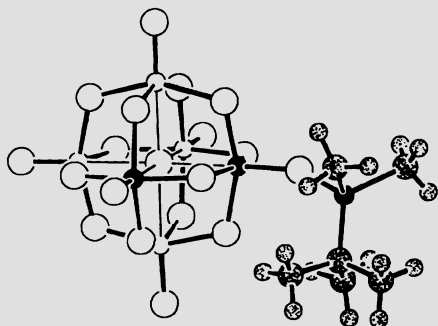
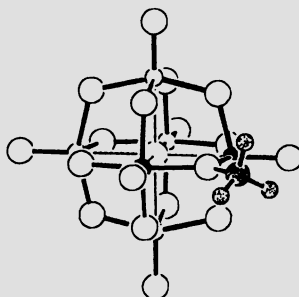
degradation as niobium-oxygen bonds are cleaved. Third, the $\text{Nb}_2\text{W}_4\text{O}_{19}^{4-}$ ion contains only d^0 Nb^{V} and W^{VI} metal centers and is a very poor oxidizing agent [16]. Attention can therefore be focussed on the binding of organic molecules without the added complication of redox chemistry. In contrast, studies of simple [17] and complex [12] d^0 organomolybdenum (VI) complexes (see 5) show varying degrees of instability with respect to internal redox reactions. Finally, the $\text{Nb}_2\text{W}_4\text{O}_{19}^{4-}$ ion has a rigid, close-packed structure, and its reactivity is therefore likely to be controlled in part by the same types of steric effects believed to influence solid oxide surface chemistry [18]. When the $\text{Nb}_2\text{W}_4\text{O}_{19}^{4-}$ structure is oriented as shown in 7, the structure is seen to contain three layers of close-packed oxygens arranged in a cubic close-packed fashion, with metal centers occupying octahedral interstices. Steric dimensions are readily apparent from the space-filling representation shown in 8.

78

Since the reaction of MoO_3 with alcohols to form surface-bound alkoxides has been studied in detail [18,19], initial investigations of the $\text{Nb}_2\text{W}_4\text{O}_{19}^{4-}$ ion have focused on the binding of alkoxy groups. The reactions outlined in Scheme I summarize the pathways available in solution to esters $\text{Nb}_2\text{W}_4\text{O}_{19}\text{R}$, $\text{R} = \text{CH}_3$, CH_3CH_2 , $(\text{CH}_3)_2\text{CH}$, and $(\text{CH}_3)_3\text{C}$,

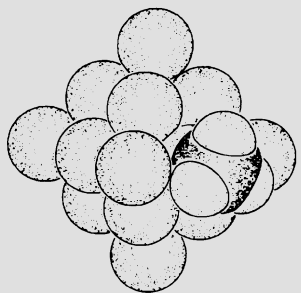
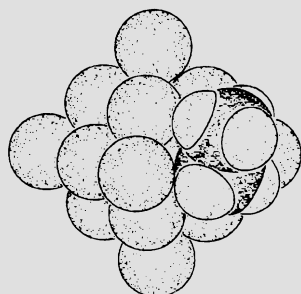
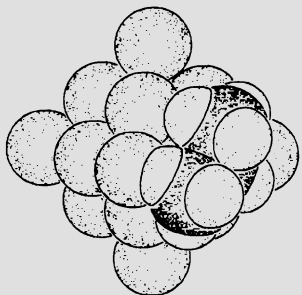
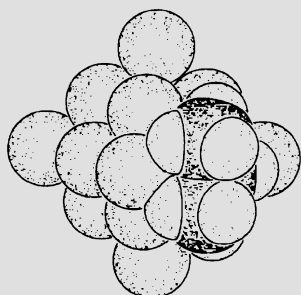


species that can be regarded as containing surface-bound alkoxide groups [20]. Attention will be focused here solely on the acid $\text{Nb}_2\text{W}_4\text{O}_{19}\text{H}^{3-}$, its anhydride $(\text{Nb}_2\text{W}_4\text{O}_{18})_2\text{O}^{6-}$, and the esters $\text{Nb}_2\text{W}_4\text{O}_{19}\text{R}^{3-}$. The acid, prepared in solution by protonation of $\text{Nb}_2\text{W}_4\text{O}_{19}^{4-}$, contains a proton bound predominantly to the bridging ONb_2 oxygen in $\text{Nb}_2\text{W}_4\text{O}_{19}^{4-}$ (see 6 and 7). In the absence of excess water in solution, this acid self-condenses to the anhydride $(\text{Nb}_2\text{W}_4\text{O}_{18})_2\text{O}^{6-}$, 9. Condensation of the acid with alcohols ROH , $\text{R} = (\text{CH}_3)_2\text{CH}$, $(\text{CH}_3)_3\text{C}$, and $[(\text{CH}_3)_3\text{C}](\text{CH}_3)_2\text{Si}$, yields esters in which the alkoxy (or siloxy) group occupies a terminal ONb oxygen site in $\text{Nb}_2\text{W}_4\text{O}_{19}^{4-}$ as shown in 10 for the silyl ester. Condensation with methanol or ethanol, however, yields esters in which the alkoxy group occupies the $\text{Nb}_2\text{W}_4\text{O}_{19}^{4-}$ ONb_2 bridging site, as shown in 11 for the methyl ester. The alkoxy group binding site observed upon esterification is seen to be determined by two factors. First, labeling studies show that esterification proceeds with retention of carbon-oxygen bonds and cleavage of metal-oxygen bonds. As a result, esterification occurs exclusively at the labile $\text{Nb}_2\text{W}_4\text{O}_{19}^{4-}$ oxygens bonded only to niobium, i.e., the ONb and ONb_2 oxygens.

91011

The steric bulk of the $\text{Nb}_2\text{W}_4\text{O}_{19}^{4-}$ ion also influences alkoxy group binding site preference. As is evident from the space-filling representation 12, a methoxy group can be accommodated at a bridging oxygen site without introducing any serious non-bonded repulsions. The same considerations hold true for the ethyl ester (see 13). Apparently, alkoxy groups prefer the bridging oxygen site in the absence of steric interference. Steric effects predominate, however, with bulkier alkoxy groups. The isopropoxy group, for example, cannot occupy a bridging oxygen site without introducing severe steric repulsions, regardless of what conformation is chosen (see 14 and 15), and therefore occupies a terminal ONb oxygen site.

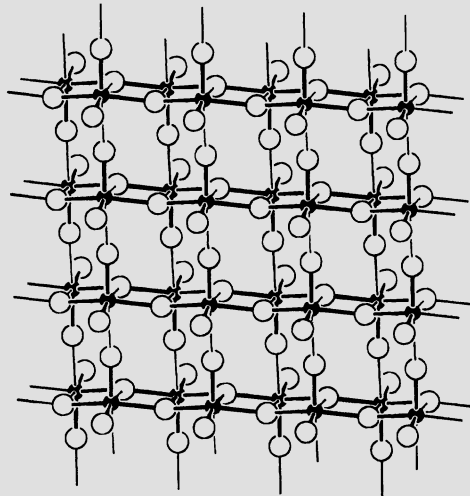
Note finally that the esters just described can also be prepared by alcoholysis of the anhydride $(\text{Nb}_2\text{W}_4\text{O}_{18})_2^{06-}$ (see Scheme I). If the solution chemistry of polyoxoanions is to be regarded as a model for solid oxide reactivity, the esterification reaction corresponds to

12131415

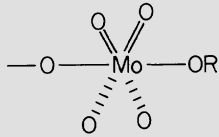
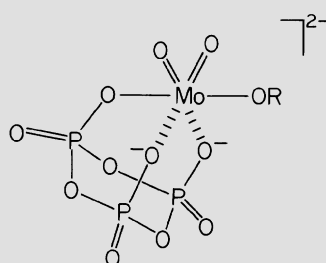
reaction of alcohols with oxide surface hydroxyls and the alcoholysis reaction corresponds to reaction of alcohols with dehydrated oxide surfaces.

4. ALCOHOL OXIDATION AND DEHYDRATION BY THE MOLYBDOPHOSPHATE ESTERS $P_3O_9MoO_3R^{2-}$

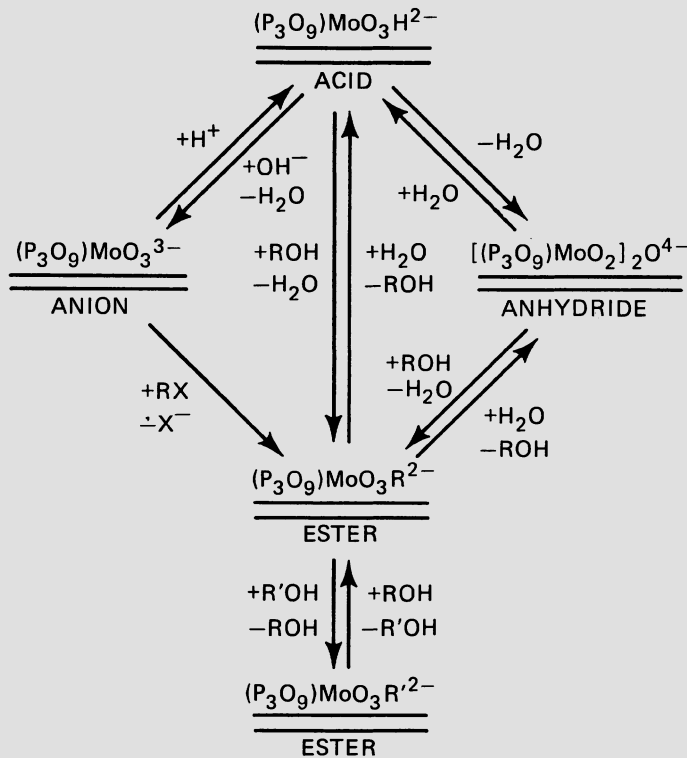
Having considered the incorporation of alcohols into polyoxoanion frameworks as alkoxide groups, we now turn to their transformation into aldehydes or ketones (oxidation) and alkenes (dehydration). As above, the selection of the polyoxoanion system to be studied was dictated in part by analogies with molybdenum trioxide chemistry. Molybdenum trioxide has a layer structure [21], and the structure of a single MoO_3 layer is shown in 16.

16

If strong molybdenum-oxygen bonds are distinguished from weak molybdenum-oxygen bonds by using thin lines when $d_{Mo-O} > 2.25 \text{ \AA}$ and thick lines when $d_{Mo-O} < 1.95 \text{ \AA}$, as in 16, the structure is seen to consist of weakly associated $(MoO_3)_n$ chains, where each molybdenum forms four strong intrachain Mo-O bonds and two weak interchain MoO⁻ bonds [21]. A reasonable extrapolation of this structure to surface-bound alkoxy groups is shown in 17, where the $(MoO_3)_n$ chain is terminated by a methoxy group and the terminal molybdenum is in the standard six-coordinate molybdate bonding mode involving two double bonds, two single bonds and two very weak bonds trans to the double bonds.

1718

This mode observed in MoO_3 as well a numerous polymolybdates [22], including the ethoxy and methoxy derivatives referred to above (see 4 and 5).

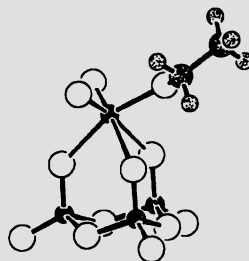
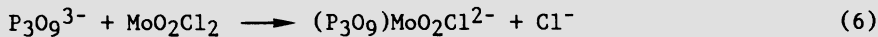


SCHEME II

On the basis of analogies with the MoO_3 structure just discussed, the hydrolytic inertness of phosphorous-oxygen bonds relative to molybdenum-oxygen bonds, and the enhanced stability associated with chelating ligands, the molybdophosphate structure of the type shown in 18 was targeted for study. The reaction scheme for $(\text{P}_3\text{O}_9)\text{MoO}_3\text{R}^{2-}$ shown in Scheme II can be envisioned by analogy with the established scheme for $\text{Nb}_2\text{W}_4\text{O}_{19}\text{R}^{3-}$ shown in Scheme I. To date, only a portion of this reaction scheme has been explored, and discussion here will focus exclusively on the synthesis, interconversion, and degradation of the alkyl esters $(\text{P}_3\text{O}_9)\text{MoO}_3\text{R}^{2-}$, chemistry that has been characterized in some detail [23].

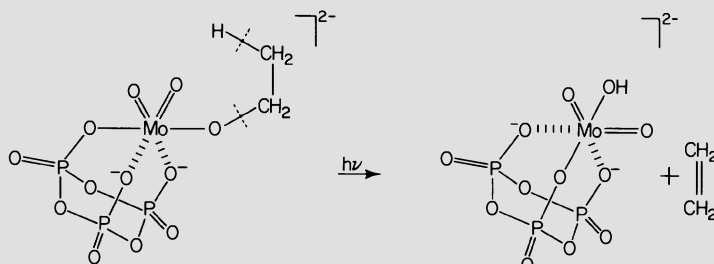
The methyl ester $(\text{P}_3\text{O}_9)\text{MoO}_3\text{CH}_3^{2-}$ can be prepared in good yield according to eq. (6) and (7). The corresponding ethyl, isopropyl, and trimethylsilyl esters are prepared by transesterification as shown in

eq. (8). The structure of the ethyl ester has been determined using single crystal X-ray diffraction techniques and is shown in 19.

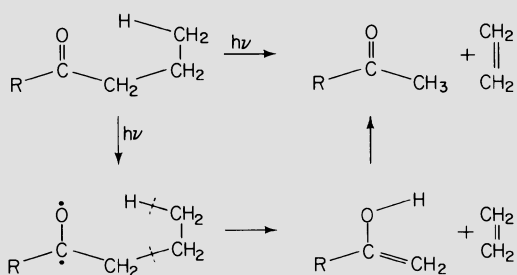


19

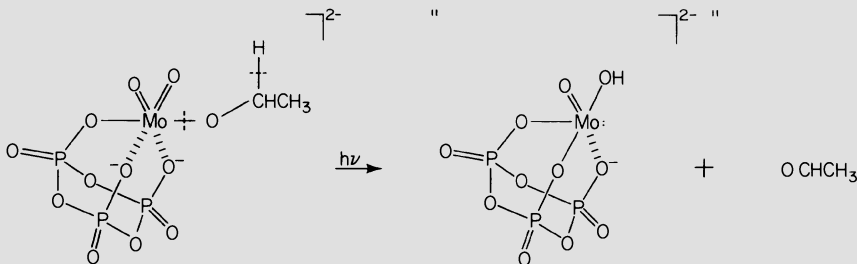
Both thermal and photochemical degradations of $(\text{P}_3\text{O}_9)\text{MoO}_3\text{CH}_2\text{CH}_3^{2-}$ have been examined in solution. Thermal decomposition in nitrobenzene at 180°C yields acetaldehyde and ethanol in approximately equal amounts. Photochemical decomposition in acetonitrile at ambient temperatures yields ethylene in addition to acetaldehyde and ethanol. Although mechanistic information concerning these transformations is not yet available, analogies between these reactions and related processes warrant brief discussion. First, the photochemical production of ethylene from $(\text{P}_3\text{O}_9)\text{MoO}_3\text{CH}_2\text{CH}_3^{2-}$ (Scheme III) can be viewed as a molybdenyl analogue of the well-documented carbonyl Norrish Type II intramolecular hydrogen abstraction reaction [24] (Scheme IV) proceeding by a six-membered ring transition state. Photochemical production of acetaldehyde might result either from a Type II process via a five-membered ring transition state (Scheme V) or from Mo-O₂H₅ cleavage, a molybdenyl analogue of the Norrish Type I carbonyl reaction [24]. We favor the former because of the close contact between an Mo-O



SCHEME III



SCHEME IV



SCHEME V

oxygen and CH_2 hydrogen observed in the crystalline ester (see 19). Thermal oxidation could proceed along a similar, heterolytic pathway.

5. CONCLUSIONS

Although there is a remarkable variety of behavior displayed by early transition metal solid oxides toward organic molecules, very little is understood concerning the molecular mechanisms of these processes. This situation stands in marked contrast to current mechanistic understanding of organic transformations occurring on metal surfaces. One reason for this disparity is the large body of solution chemical information regarding low-valent organometallic complexes and low-valent metal cluster compounds that serves as a guide for predicting and interpreting organic transformations on metal surfaces. A corresponding body of solution chemical data relevant to early transition metal solid oxide surface chemistry does not yet exist. Even though the solution chemistry of early transition metal polyoxoanions has been investigated extensively, the extreme structural complexity of organic early transition metal polyoxoanion derivatives has caused attention to be

focused largely on their inorganic rather than their organic features [22,25]. As indicated by the preliminary results cited above, however, organic derivatives of early transition metal polyoxoanions promise to offer a rich organic reaction chemistry, and the day may soon arrive when polyoxoanions are viewed as just another interesting and useful type of functional group for organic molecules.

6. ACKNOWLEDGMENTS

We acknowledge the National Science Foundation for support of the research reviewed above and are grateful to Dr. Egbert Keller from providing a copy of his SCHAKAL structural graphics program.

7. REFERENCES

1. C.J. Machiels, U. Chowdry, R.H. Staley, F. Ohuchi, and A.W. Sleight, in Catalytic Conversions of Synthesis Gas and Alcohols to Chemicals, (Ed. R.G. Herman), p. 413, Plenum Press, New York (1984).
2. C.J. Machiels and A.W. Sleight, Chem. Uses Molybdenum, Proc. Int. Conf., 4th, 411 (1982).
3. S. Nakamura and H. Ichihashi, in New Horizons in Catalysis. Proceedings of the 7th International Congress on Catalysis, Tokyo, 30 June-4 July, 1980, (Studies in Surface Science and Catalysis, 7b, Eds. T. Seiyama and K. Tanabe), p. 755, Elsevier, Amsterdam (1981).
4. R.K. Grasselli and J.D. Burrington, Adv. Catal. 30, 133 (1981).
5. H.-F. Liu, R.-S. Liu, K.Y. Liew, R.E. Johnson, and J.H. Lunsford, J. Am. Chem. Soc. 106, 4117 (1984).
6. M. Anpo, I. Tanahashi, and Y. Kubokawa, J. Chem. Soc., Faraday Trans. 1 78, 2121 (1982).
7. R.D. Adams, W.G. Klemperer, and R.-S. Liu, J. Chem. Soc., Chem. Commun., 256 (1979).
8. For a symmetrically bonded formate see: V.W. Day, M.R. Thompson, C.S. Day, W.G. Klemperer, and R.-S. Liu, J. Am. Chem. Soc. 102, 5971 (1980).
9. V.W. Day, M.F. Fredrich, W.G. Klemperer, and R.-S. Liu, J. Am. Chem. Soc. 101, 491 (1979).
10. For other molybdate-bound acetals, see reference 8.
11. A.J. Wilson, W.T. Robinson, and C.J. Wilkins, Acta Crystallogr., Sect. C 39, 54 (1983).
12. E.M. McCarron and R.L. Harlow, J. Am. Chem. Soc. 105, 6179 (1983); E.M. McCarron and A.W. Sleight, Polyhedron 5, 129 (1986).
13. W.H. Knoth and R.L. Harlow, J. Am. Chem. Soc. 103, 4265 (1981).
14. C.J. Besecker, V.W. Day, W.G. Klemperer, and M.R. Thompson, Inorg. Chem. 24, 44 (1985).
15. C.J. Besecker, V.W. Day, W.G. Klemperer, and M.R. Thompson, J. Am. Chem. Soc. 106, 4125 (1984).

16. M. Dabbabi, M. Boyer, J.P. Launay, and Y. Jeannin, J. Electroanal. Chem. 76, 153 (1977).
17. M.H. Chisholm, K. Folting, J.C. Huffman, and C.C. Kirkpatrick, Inorg. Chem. 23, 1021 (1984).
18. W.E. Farneth, R.H. Staley, and A.W. Sleight, J. Am. Chem. Soc. 108, 2327 (1986).
19. W.E. Farneth, F. Ohuchi, R.H. Staley, U. Chowdry, and A.W. Sleight, J. Phys. Chem. 89, 2493 (1985).
20. V.W. Day, W.G. Klemperer, and C. Schwartz, submitted for publication.
21. L. Kihlborg, Ark. Kemi 21, 357 (1963).
22. V.W. Day and W.G. Klemperer, Science 228, 533 (1985).
23. V.W. Day, W.G. Klemperer, and R.C. Wang, manuscript in preparation.
24. N.J. Turro, Modern Molecular Photochemistry, Chapters 10 and 1, Benjamin, Menlo Park, California (1978).
25. M.T. Pope, Heteropoly and Isopoly Oxymetalates, Chapter 7, Springer, New York (1983).

HOMOGENEOUS MODELS FOR MECHANISMS OF SURFACE REACTIONS: PROPENE AMMOXIDATION

Dominic M.T. Chan, William A. Nugent, William C. Fultz,
D. Christopher Roe, and Thomas H. Tulip
E.I. du Pont de Nemours & Co.
Central Research and Development Department
Experimental Station
Wilmington, DE 19898
USA

ABSTRACT. The proposed active sites on the surface of the catalyst for propene ammoxidation have been successfully modeled by structurally characterized pinacolato W(VI) tert-butyl imido complexes. These compounds exist as an equilibrating mixture of amine-bis(imido) and imido-bis(amido) complexes, the position of this equilibrium being dependent on the electronic nature of the glycolate ligand. Both of the C-N bond-forming reactions proposed in recent studies by Kartisek and Grasselli [*J. Catal.* 81, 489 (1983)] have been reproduced using discrete Group VI d⁰ organoimido complexes under mild conditions suitable for detailed mechanistic studies. These reactions are 1) oxidative trapping of radicals at molybdenum imido sites and 2) migration of the allyl group from oxygen to an imido nitrogen atom.

1. INTRODUCTION

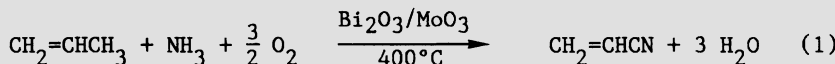
Transition metal catalysis plays a key role in the manufacture of commodity chemicals. The majority of these processes are heterogeneous transformations, which typically involve passing a gaseous mixture of the reactants over an immobilized catalyst bed at high temperature and sometimes high pressure. While these catalytic reactions have been employed for many years, little is known about the exact product formation mechanism in most processes. The major reason for this poor understanding is the difficulty in studying transient and reactive intermediates on the surface under reaction conditions. Although progress has been made in this area with the advent of advanced instrumentation, very much remains to be learned.

An alternative approach is to prepare homogeneous complexes to model the surface reactions. By judiciously selecting complexes and the experiments to perform with them, we hope to better understand and ultimately improve these heterogeneous reactions. In general, there are a number of objectives one hopes to achieve. First, by preparing stable and characterizable transition metal complexes with the functionalities

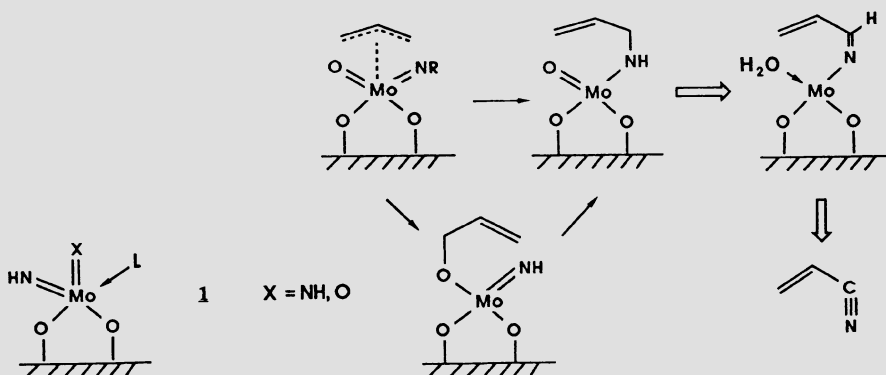
proposed to be present on the surface, we may examine the validity of hypotheses of the active site structure based on surface studies. Second, the structural information characterizing some of these synthetic species obtained via X-ray crystallography may provide insights into the structure of the species on the solid surface. Finally, we would like to use these synthetic complexes to duplicate the heterogeneous reaction in solution and thus facilitate mechanistic investigation. Obviously, in many cases we have to resort to stoichiometric reactions and/or reactions with model substrates. The mechanistic studies of propene ammonoxidation carried out at Du Pont illustrate these points [1,2].

1.1. Surface-catalyzed Propene Ammonoxidation

The ammonoxidation of propene is a major industrial process by which 8 billion pounds of acrylonitrile are produced annually. In this process, a mixture of propene, ammonia, and air is passed over a solid bismuth molybdate-containing catalyst:



Intense interest in the mechanism of this transformation [3] reflects its rather low yield (ca. 65%) when compared with other oxidation reactions (e.g., ca. 90% for oxidation of propene to give acrolein).



On the basis of studies on heterogeneous systems [3], the active sites on the catalyst surface were proposed [3d] to have structure 1 (scheme I). At various points in the catalytic cycle, the coordinated group L can be NH_3 , H_2O , or the elements of the allyl radical. The

rate-limiting step for acrylonitrile synthesis is the homolysis of allylic C-H bond of propene to produce a symmetrical allyl moiety [3] (presumably generated by the bismuth oxide as an adsorbed allyl radical) [4]. The critical C-N bond-forming step is much less well understood. On the basis of recent studies of heterogeneous systems by Grasselli *et al.* [5], two distinct pathways may be envisioned:

- 1) direct trapping of the allyl radical at molybdenum imido sites and
 - 2) initial trapping of the allyl radical at a molybdenum oxo group followed by an allyl migration from oxygen to an imido nitrogen atom.
- Neither of these reactions has direct precedent in homogeneous systems [6,7].

1.2. Research Objectives

There are a number of points we wished to address in our study:

1. Could we prepare discrete homogeneous analogues of the proposed surface intermediates? If so, would there be any unusual stereo-electronic features?
2. What is the reactivity of these types of imido complexes with respect to imido/oxo interconversions?
3. Could we observe C-N bond formation under laboratory conditions from radicals with these imido compounds?
4. Is it possible to observe an allylic O to N rearrangement with such complexes under mild conditions?

2. MODELING THE SURFACE-CATALYZED PROPENE AMMOXIDATION

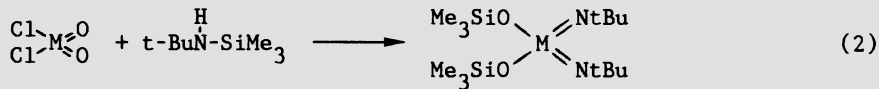
2.1. Preparation of Homogeneous Analogs of Surface Intermediates

Our first objective then was to prepare monomeric d^0 complexes of type A and B which may serve as models for the surface active sites.



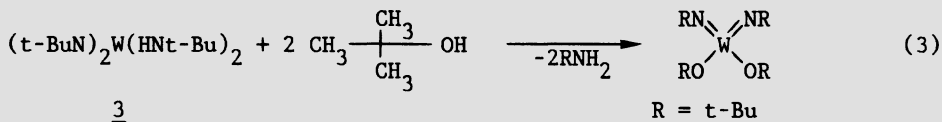
Type A complexes containing two imido and two alkoxy ligands were first prepared by Nugent [8]. For stability reasons, the t-butyl imido group was chosen as a model for the parent hydrido imido ($M=NH$) moiety throughout this study. The Cr(VI) and Mo(VI) complexes were obtained in

good yields by treating the corresponding metal dioxo dichloride with t-butyltrimethylsilyl amine under mild conditions:

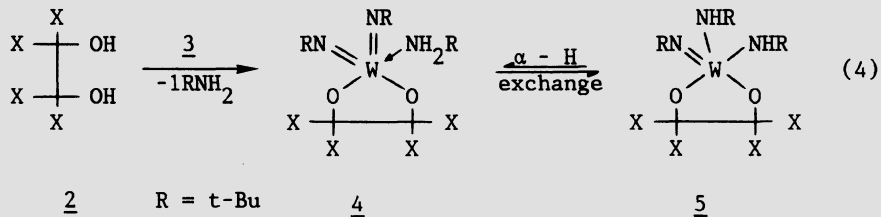


M = Cr, Mo

Although this approach failed with the W(VI) analogue, it does demonstrate the feasibility of converting an oxo ligand to an imido ligand. To prepare the tungsten species, we treated $(\text{t-BuN})_2\text{W}(\text{Hnt-Bu})_2$ (3) [9] with two equivalents of a hindered tertiary alcohol such as t-butyl alcohol to give $(\text{t-BuN})_2\text{W}(\text{Ot-Bu})_2$, with concomitant liberation of two equivalents of t-butyl amine:



These bis(imido) complexes are all quite stable and show no tendency to coordinate a fifth ligand, presumably due to steric crowding around the metal center. However, when one equivalent of a chelating diol is used instead, the reaction takes a different course resulting in the formation of type B complexes! Perfluoropinacol (2a) [10], pinacol (2b), and benzopinacol (2c) react readily at room temperature with an equimolar amount of $(\text{t-BuN})_2\text{W}(\text{Hnt-Bu})_2$ (3), as follows:



X	YIELD	RATIO	
a	CF ₃	92%	2.6
b	CH ₃	100%	1
c	Ph	96%	1
			1
			11
			20

In each case, ¹H and ¹³C solution NMR studies indicated the presence of two isomers [11]: the aminebis(imido) complex 4 and the imidobis(amido) complex 5. The ratio of 4/5 depends on the glycolate ligand. The more electron-withdrawing perfluoropinacolate (PFP) ligand favors structure

4, whereas the more electron-donating glycolates reverse this preference. ^1H NMR magnetization transfer studies confirm the solution equilibrium between 4a and 5a, presumably via α -hydrogen exchange processes [12]. However, in the solid state, the magic angle spinning ^{13}C NMR spectrum of each product indicates the presence of a single isomer: 4a in the PFP system and 5b and 5c in the pinacolato and benzopinacolato (BZP) complexes. Single-crystal X-ray diffraction studies confirm our structural assignment for aminebis(imido) 4a (Fig. 1) and bis(amido)imido 5c (Fig. 2). Both molecules adopted a distorted trigonal-bipyramidal geometry in which the chelating diol ligand occupies an axial and an equatorial site. The imido groups in both structures are almost linear, indicating significant π -bonding with the metal. Interestingly, in 4a the two imido ligands occupy equatorial sites, whereas in 5c the imido ligand is axial.

Thus we had successfully modeled the postulated surface active sites of the ammonoxidation by preparing the two types of complexes A and B. The functionality of the B type system agrees well with the proposed facile ligand exchange process on the surface. The fact that replacing two alkoxide groups in $(t\text{-BuN})_2\text{W}(\text{O}t\text{-Bu})_2$ by a chelating glycolate ligand clearly increases the tendency of the metal to coordinate a fifth ligand is pertinent to the recent demonstration that steric coordinative unsaturation of the molybdenum sites plays a key role in determining the course of propene oxidation [13].

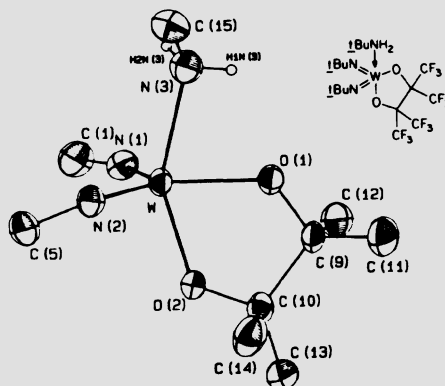


Figure 1. Perspective drawing of $(\text{PFP})\text{W}(\text{N}-t\text{-Bu})_2(\text{NH}_2\text{-}t\text{-Bu})$ (4a) with thermal ellipsoids at the 50% probability level. H atoms are represented by spheres of arbitrary radius. Fluorine atoms and methyl groups are omitted for clarity. Selected distances (\AA), W-N(1) = 1.741 (4), W-N(2) = 1.743(3), W-N(3) = 2.201(4), and angles, C(1)-N(1)-W = 166.6(3) $^\circ$, C(5)-N(2)-W = 164.0(3) $^\circ$, C(15)-N(3)-W = 127.4(3) $^\circ$.

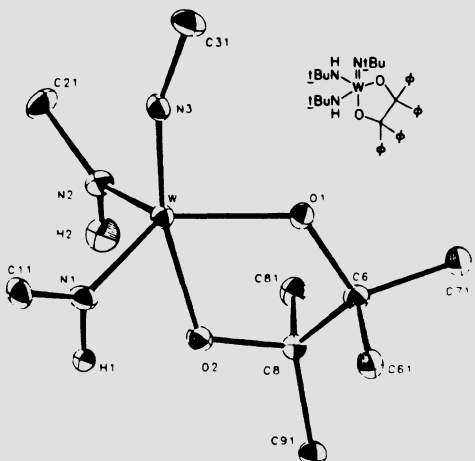
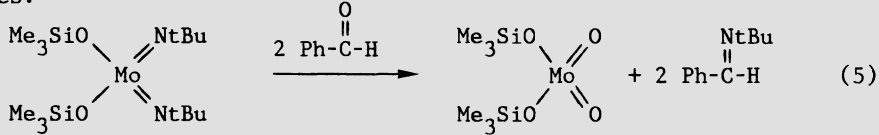


Figure 2. Perspective drawing of $(\text{BZP})\text{W}(\text{N}-\text{t-Bu})(\text{HN}-\text{t-Bu})_2$ (5c) with thermal ellipsoids at the 25% probability level. Methyl groups and part of the aromatic rings are omitted for clarity. Selected distances (\AA), $\text{W-N(1)} = 1.931(4)$, $\text{W-N(2)} = 1.924(5)$, $\text{W-N(3)} = 1.753(4)$, and angles, $\text{C}(11)-\text{N}(1)-\text{W} = 140.6(4)^\circ$, $\text{C}(21)-\text{N}(2)-\text{W} = 139.5(4)^\circ$, $\text{C}(31)-\text{N}(3)-\text{W} = 161.0(4)^\circ$.

The control of the equilibrium between 4 and 5 by the electronic nature of the glycolate ligands is relevant to the fundamental question of the influence of support acidity on the catalyst behavior in ammonoxidation.

2.2. Reactivities of the Homogeneous Analogues of Surface Intermediates

These d^0 imido complexes react readily with aldehydes such as benzaldehyde to give the t-butyl imine and the corresponding metal oxo complexes:



The transformation may involve a four-membered transition state with the exchange of a metal-nitrogen double bond for an energetically more favorable metal-oxo double bond as the driving force. We were also able to detect facile amine to imido ligand exchange by magnetization transfer studies:



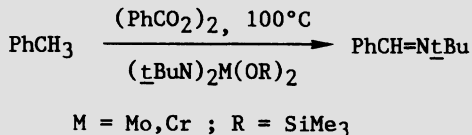
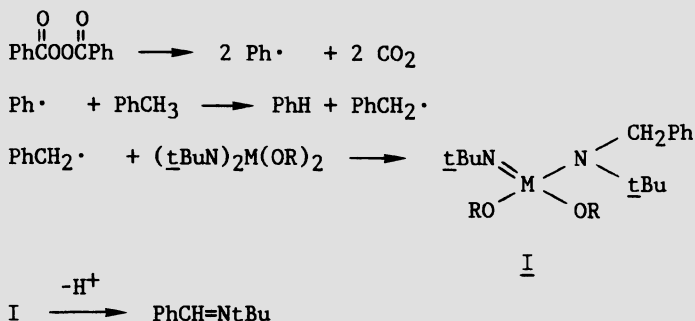
These observations again confirm the reactivity of these imido systems that we noted before. The properties of these model compounds imply that the imido catalytic surface is quite liable.

The successful preparation of structural analogues of 1 raised the hope that the chemistry of ammoxidation might also be reproduced in solution under mild laboratory conditions suitable for mechanistic studies. Thus we turned our attention to the critical C-N bond formation step to find out whether one can indeed produce ammoxidized product from a radical with a d⁰ imido metal center. For our studies, diimido complexes $(t\text{-BuN})_2\text{M}(\text{OSiMe}_3)_2$ ($\text{M} = \text{Cr}, \text{Mo}$) [8,9] were selected as models for the postulated active sites in ammoxidation. Benzyl rather than allyl radicals were chosen for study since the products of allyl radical oxidation are not expected to be stable under our reaction conditions and because benzyl and allyl exhibit similar behavior in oxidation reactions [14]. Indeed, when a solution of $(t\text{-BuN})_2\text{M}(\text{OSiMe}_3)_2$ in toluene was heated at 100°C in the presence of benzoyl peroxide as a radical initiator, benzylidene-t-butylamine was obtained in up to 52% yield (Table I). The remaining organic products were CO₂, bibenzyl, and the expected isomeric distribution of (ortho:meta:para = 63:21:16) of methylbiphenyls.

Table I. Products of peroxide-initiated reaction of imido complexes with toluene.

Imido Complex	PhCH = N <u>t</u> Bu	Products (mmol)	
		Phenyl Toluenes	Bibenzyl
$(t\text{-BuN})_2\text{Cr}(\text{OSiMe}_3)_2$	0.43	0.40	0.04
$(t\text{-BuN})\text{OCr}(\text{OSiMe}_3)_2$	0.52	0.40	none
$(t\text{-BuN})\text{V}(\text{OSiMe}_3)_3$	0.28	0.33	0.18
$(t\text{-BuN})_3\text{Re}(\text{OSiMe}_3)$	0.34	0.20	0.15
$(t\text{-BuN})_2\text{Mo}(\text{OSiMe}_3)_2$	0.06	0.22	0.05
$(t\text{-BuN})_2\text{W}(\text{OtBu})_2$	0.04	0.20	0.13
none	none	0.55	0.22

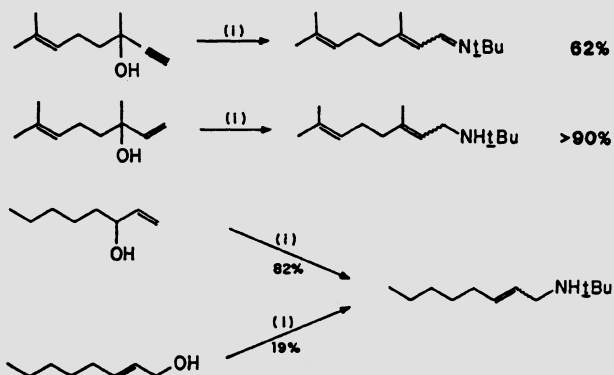
All runs contained 1 mmol imido complex, 1 mmol $(\text{PhCO}_2)_2$ in 10 ml PhCH₃ (100°C, 16 h).

TOLUENE AMMOXIDATION**Mechanism:**

We believe that initiator-derived phenyl radicals abstract benzylic hydrogen from toluene to produce benzyl radicals. The high yields of the imine suggest that benzyl radicals are efficiently trapped and oxidized by the imido complexes, presumably via the intermediacy of M(V) amido complexes. Apparently the amide ligand of this intermediate is further oxidized to the Schiff base, again consistent with the proposed chemistry on the heterogeneous catalyst surface [15].

Finally, we examined the novel O to N allylic transformation speculated to occur in the heterogeneous process. The bis(imido)bis(amido) tungsten complex $(\text{t-BuN})_2\text{W}(\text{Hnt-Bu})_2$ (3) was employed for model studies. Heating a 1:1 mixture of 3 with linalool (toluene, reflux) afforded, after hydrolysis, the rearranged (geranyl and neryl) amines in 90% (Table II). Similar results were obtained with other allylic alcohols. It is also noteworthy that allyl alcohol-1,1-d₂ afforded a mixture of 22% 1,1- and 78% 3,3-dideuterated allyl-t-butylamines. Interestingly, scrambling of isotopic label was also observed during heterogeneous ammoxidation of allyl-alcohol-1,1-d₂. This observation, along with the results for the isomeric octenols (Table II), suggests that the reaction does not proceed exclusively by a concerted electrocyclic rearrangement. A competing pathway, perhaps involving an allyl/metalated ion pair, must additionally be involved.

Table II. Amination with homogeneous imido complexes.



(i) 1 eq. $(\text{tBuN})_2\text{W}(\text{HNtBu})_2$, toluene, reflux, 24-72 h.

3. CONCLUSIONS

In conclusion, homogeneous analogues of active sites and of the two C-N bond forming processes proposed for the ammonoxidation of propene have been realized by our studies. While these observations constitute neither a necessary nor a sufficient condition for the mechanism of the surface process to be correct, they lend support to the proposals for the surface reaction and open the way to detailed mechanistic investigation of such elementary steps.

4. ACKNOWLEDGMENT

We thank Drs. Y.C. Lin and T.B. Marder for helpful discussion and Dr. R.D. Farlee for MAS C NMR studies. The technical assistance of J. Center and L. Lardear is gratefully acknowledged.

5. REFERENCES

1. D.M.T. Chan, W.C. Fultz, W.A. Nugent, D.C. Roe, and T.H. Tulip, J. Am. Chem. Soc. **107**, 251 (1985).
2. D.M.T. Chan and W.A. Nugent, Inorg. Chem. **24**, 1422 (1985).
3. For reviews on the mechanism of propene ammonoxidation see:
 - (a) G.W. Keulks, L.D. Krenzke, and T.M. Notermann, Adv. Catal. **27**, 183 (1978).
 - (b) J. Haber and A. Bielanski, Catal. Rev. Sci. Eng. **19**, 1 (1979).
 - (c) B.C. Gates, J.R. Katzer, and G.C.A. Schuit, Chemistry of Catalytic Processes, pp.325-389, McGraw-Hill, New York, (1979).
 - (d) J.D. Burrington, C.T. Kartisek, and R.K. Grasselli, J. Catal. **81**, 489 (1983).

4. W. Martir and J.H. Lunsford, J. Am. Chem. Soc. 103, 3728 (1981).
5. J.D. Burrington, C.T. Kartisek, and R.K. Grasselli, J. Catal. 87, 363 (1984).
6. However, oxidation of radicals with C-O bond formation to ligand oxygen atom is known:
J.K. Kochi, J. Org. Chem. 30, 1862 (1965).
F. Gaudemer and A. Gaudemer, Tetrahedron Lett. 21, 1445 (1980).
Rate constants for oxidation of alkyl radicals by permanganate are close to the diffusion-controlled limit:
S. Streenken and P. Neta, J. Am. Chem. Soc. 104, 1244 (1982).
7. An analogy can be made between O to N migration and the rearrangement of allylic and propargylic alcohols promoted by d⁰ vanadium and tungsten oxo complexes:
T. Hosogai, Y. Fujita, Y. Ninagawa, and T. Nishida, Chem. Lett. 357 (1982), and references cited therein.
See also: B.J. Kane, U.S. Patent 4,254,291 (1981).
8. W.A. Nugent, Inorg. Chem. 22, 965 (1983).
9. W.A. Nugent and R.L. Harlow, Inorg. Chem. 19, 1977 (1980).
10. (a) W.J. Middleton and R.V. Lindsey, J. Am. Chem. Soc. 86, 4948 (1964).
(b) G.W. Astrologen and J.C. Martin, J. Am. Chem. Soc. 98, 2895 (1976).
11. Spectroscopic assignments were based on other imido complexes ; see ref. 9 and W.A. Nugent, R.L. McKinney, R.V. Kasowski, and F.A. Van Catledge, Inorg. Chim. Acta 65, L91 (1982). The ratios of isomers 4 and 5 are determined by spectral integration of the ¹H NMR t-Bu signals.
12. Compare: S.M. Rocklage, R.R. Schrock, M.R. Churchill, and H.J. Wasserman, Organometallics 1, 1332 (1982).
13. Y. Iwasawa, T. Nakamura, K. Takamatsu, and S.J. Ogasawara, J. Chem. Soc., Faraday Trans. 1 76, 939 (1980).
See also: A.K. Rappe and W.A. Goddard III, J. Am. Chem. Soc. 104, 3827 (1982).
14. In fact, methylbenzenes, under ammoxidation conditions, are converted to the corresponding benzonitriles in high yield:
R.A. Sheldon and J.K. Kochi, in Metal-Catalyzed Oxidations of Organic Compounds, pp. 324-325, Academic Press, New York (1981).
15. The observation that the yield of the organic imine product never exceeded 50% based on metal suggests the possibility that the last step in the product formation is a bimolecular process requiring a second equivalent of metal oxidant.
16. J.D. Burrington, C.T. Kartisek, and R.K. Grasselli, J. Catal. 63, 235 (1980).

ORGANOMETALLIC OXIDES: FUTURE MODELS IN CATALYSIS? THE EXAMPLE OF TRIOXO(η^5 -PENTAMETHYLCYCLOPENTADIENYL)RHENIUM(VII)

Wolfgang A. Herrmann
Anorganisch-chemisches Institut
der Technischen Universität München
Lichtenbergstraße 4
D-8046 Garching
W.-Germany

ABSTRACT. Oxygen is present in most heterogeneous catalyst systems, either constituting the major component in oxidic supports or even on top of catalytically active surfaces. Since homogeneous catalysts generally convey higher product selectivities owing to well-defined structures and geometries of the respective organometallic compounds, there is a great demand of developing the chemistry of soluble organometallic oxides. The present review is concerned with general synthetic strategies, exemplified for the prototypal heptavalent rhenium compound trioxo(η^5 -pentamethylcyclopentadienyl)rhenium. It is shown that reductive deoxygenation of this title compound opens one important avenue to pentavalent rhenium compounds (e.g., (η^5 -C₅Me₅)ReOCl₂ and (η^5 -C₅Me₅)ReCl₄) that, in turn, are the starting points of further chemical transformations. A structural survey (X-Ray analyses) of various oxo containing organorhenium compounds of pseudo-tetrahedral geometry shows the π -bonded ring ligand to slip away from a central bonding mode, which effect is attributed to the strong trans influence of an oxo ligand.

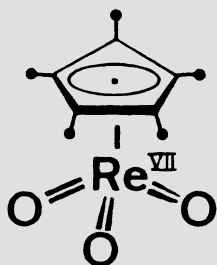
1. INTRODUCTION

One of the organometallic chemist's great challenges is the construction of compounds that may serve as models for either homogeneous or heterogeneous catalysts. Alkene metathesis provides an excellent and convincing example of how important organometallic model systems finally turn out to be for the better understanding of catalytic mechanisms, even though no safe conclusions for heterogeneous processes can be drawn from stoichiometric reactions carried out with soluble (homogeneous) species.

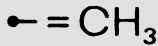
We have directed our interest towards some unprecedented organorhenium compounds that display the metal in high or intermediate oxidation states. The present chapter is an evaluation of the present state of this subject and a perspective on the exciting new field of "organometallic oxides".

2. HISTORICAL REMARKS

When the title compound, trioxo(η^5 -pentamethylcyclopentadienyl)-rhenium(VII) (1), was discovered in our laboratory by Serrano [1], there was much surprise about the existence and stability of this material. No one would have predicted that such a pleasant and versatile chemistry would be developed from this discovery. Some basic, synthetically useful reactions have been described in a number of publications [2-16], and the first comprehensive review has been published recently [17]. The goal of the present chapter is to summarize the key results obtained since this review was written (August, 1985). It is our intention to focus the eyes of our peers on a field that we believe may turn out to gain strongly in importance in both organometallic and inorganic chemistry. "Organometallic oxides" can be thought of for synthetic applications (e.g., construction of heterocycles involving metal oxide structural entities, stabilization of high-valent transition metals, etc.) and also for catalytic applications such as oxidation of unsaturated organic molecules (e.g., alkenes and alkynes) and alkene metathesis. Since it is always appropriate to first investigate the chemistry of a given key compound before beginning laborious catalytic studies, we have decided to provide as clear a picture as possible of the chemistry of the title compound and the chemical transformations of its derivatives.



1



Oxides and oxohalides of transition metals (vanadium, chromium, molybdenum, tungsten) stabilized by π -aromatic ligands such as the unique cyclopentadienyl ligand have been observed from time to time for more than 20 years. Thus, the Munich laboratory of E.O. Fischer reported on the synthesis of the vanadium compounds $(\eta^5\text{-C}_5\text{H}_5)\text{VOX}_2$ ($\text{X} = \text{Cl}, \text{Br}$) in 1958 [18], before Cousins and Green [19] synthesized related

molybdenum derivatives such as $(\eta^5\text{-C}_5\text{H}_5)\text{MoOCl}_2$ and $(\eta^5\text{-C}_5\text{H}_5)\text{MoO}_2\text{Cl}$. Further organometallic oxides exhibiting terminal oxo functionalities have been made since, but their number is still quite small:

$(\eta^5\text{-C}_5\text{H}_5)_2\text{Mo}_2\text{O}_4$ (cis) *	[19]
$(\eta^5\text{-C}_5\text{H}_5)_2\text{Mo}_2\text{O}_5$	[19]
$(\eta^5\text{-C}_5\text{H}_5)_2\text{W}_0$	[20]
$(\eta^5\text{-C}_5\text{Et}_5)_2\text{W}_0(\text{O}^t\text{But})$ *	[21]
$(\eta^5\text{-C}_5\text{Me}_5)_2\text{Cr}_2\text{O}_4$ (trans) *	[22]
$(\eta^5\text{-C}_5\text{Me}_5)_2\text{Mo}_2\text{O}_4$ (cis) *	[23-25]
$(\eta^5\text{-C}_5\text{Me}_5)_2\text{Mo}_2\text{O}_5$	[22]
$(\eta^5\text{-C}_5\text{Me}_5)_2\text{W}_2\text{O}_4$	[23, 24]
$(\eta^5\text{-C}_5\text{H}_4\text{CH}_3)_2\text{Mo}_0$ *	[20, 26]
$(\eta^5\text{-C}_5\text{H}_5)\text{WO}(\pi\text{-C}_2\text{H}_2)\text{R}$ [R = Me and C(=O)Me]	[27]
$(\eta^5\text{-C}_5\text{H}_5)\text{WOR}_3$ and $(\eta^5\text{-C}_5\text{H}_5)\text{WO}_2\text{R}$ *	[28]
[R = CH ₂ SiMe ₃]	[28]
$\{\eta^5\text{-(-CH}_2\text{C}_5\text{Et}_4)\}\text{WO}_2(\text{O}^t\text{C}_4\text{H}_9)]_2$	[29]
$\{\eta^5\text{-(-CH}_2\text{C}_5\text{Et}_4)\}\text{WOCl}_3)_2$	[29]

* The asterisk refers to compounds with structures confirmed by X-Ray crystallography.

Other organometallic oxorhenium complexes that have been reported in the literature are $\text{ReO}(\pi\text{-C}_2\text{H}_2)_2\text{I}$ [30], $\text{Re}(\text{CH}_3)_4\text{O}$ [31], $\text{Re}(\text{CH}_3)_3\text{O}_2$ [32], $\text{Re}(\text{CH}_3)\text{O}_3$ [33], $\text{Re}(\text{CH}_2\text{SiMe}_3)_4\text{O}$ [31], $\text{Re}_2(\text{CH}_2\text{SiMe}_3)_6\text{O}_3$ [31, 34], $\text{Re}_2(\text{CH}_3)_6\text{O}_3$ [34], and $\text{Re}(\text{O}^t\text{But})\text{O}_3$ [34]. The siloxy derivative $\text{Re}(\text{OSiMe}_3)\text{O}_3$ [35] may prove to be a starting material for new organometallic rhenium(VII) compounds. Wieghardt's recent compound $(\eta^3\text{-C}_6\text{N}_3\text{H}_{15})\text{ReO}_3^+\text{BF}_4^-$ [36] looks like a "more inorganic" congener of the title complex 1. High-nuclearity organometallic oxides are not considered here (for a review, see Ref. [37]); the remarkable compounds $(\eta^5\text{-C}_5\text{H}_5)_4\text{Cr}_4\text{O}_4$ [38], $(\eta^5\text{-C}_5\text{H}_5)_5\text{V}_5\text{O}_6$ [39], and $(\eta^5\text{-C}_5\text{H}_5)_6\text{Ti}_6\text{O}_6$ [40] represent highlights in this field.

3. SYNTHESIS OF TRIOXO(η^5 -PENTAMETHYLCYCLOPENTADIENYL)RHENIUM(VII)

Construction of metal oxide structures in inorganic coordination or organometallic compounds (monomeric or oligomeric species) follows treatment of appropriate precursors (e.g., metal oxides and halides) with various reagents such as elemental oxygen, hydrogen peroxide, nitrous and nitric oxide, trimethylamine oxide, nitrobenzene, t-butyl hydroperoxide, or the nickel complex [^tBu-NC]₂Ni($\eta^2\text{-O}_2$). Another possible strategy involves introduction of stabilizing organic ligands such as cyclopentadienyl (η^5) or benzene (η^6) into precursors such as transition metal oxides or halides. However, this method has not yet been very successful, probably because uncontrolled redox reactions occur at the high-valent metal (reduction) and at the organic ligand (oxidation) (e.g., reaction of ReO_3Cl with $\text{M}^+\text{C}_5\text{R}_5^-$) [15].

The title complex 1' is easily accessible by treatment of the low-valent carbonyl precursor species $(\eta^5\text{-C}_5\text{Me}_5)\text{Re}(\text{CO})_3$ with concentrated aqueous hydrogen peroxide in a boiling two-phase water/benzene system; yields as high as 80% can be reached, depending a little on the purity of the starting materials and the reaction conditions. Purification of 1' is commonly achieved by means of column chromatography on silica and subsequent recrystallization from n-hexane/methylene chloride solutions at temperatures below ambient. The closely related derivative trioxo($\eta^5\text{-ethyltetramethylcyclopentadienyl}$)rhenium(VII) (1') has just been synthesized in our group along the same lines.

The molecular geometry of 1' is depicted in Figs. 1, giving proof that we are indeed dealing with a mononuclear species containing short rhenium-oxygen bonds. The ReO interatomic distances of ca. 171 pm are

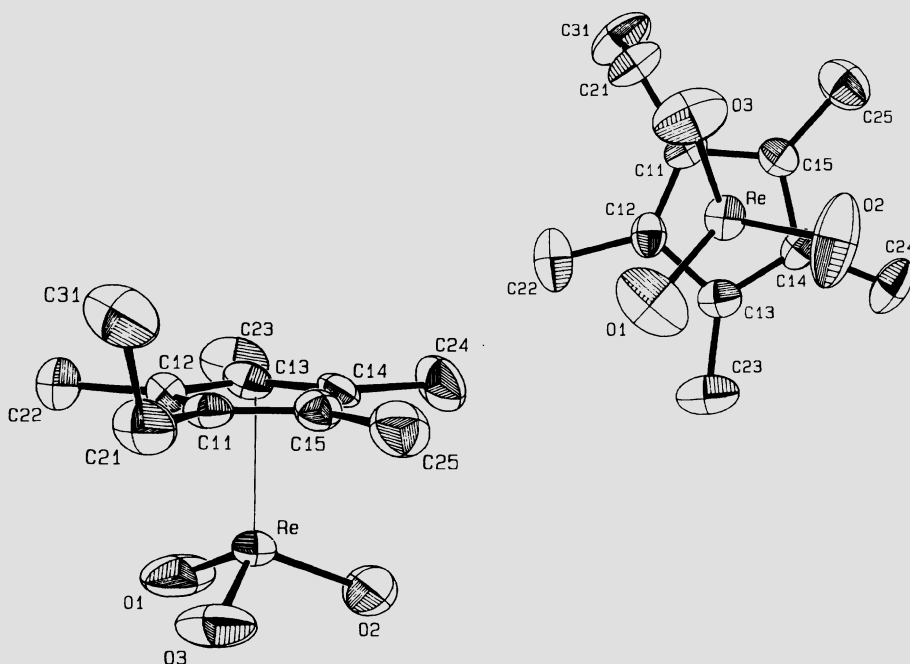


Figure 1. Molecular structure of the trioxorhenium(VII) compound $(\eta^5\text{-C}_5\text{Me}_4\text{Et})\text{ReO}_3$ (1') (ORTEP representation). At the right is a projection view down the five-membered π -ligand.
Selected bond lengths [pm] and angles [$^\circ$]: Re-O(1) 170.0(5); Re-O(2) 172.1(5); Re-O(3) 169.8(5); Re-C(11) 237.7(5); Re-C(12) 239.4(5); Re-C(13) 243.1(5); Re-C(14) 241.0(5); Re-C(15) 238.1(6); O(1),Re,O(2) 105.8(4); O(2),Re,O(3) 105.2(3); O(1),Re,O(3) 105.3(3).

consistent with ordinary double bonds. It thus appears that the three terminal oxo groups act as powerful π -donor ligands in this particular case, too. The overall geometry of the compound is best described as a slightly distorted trigonal pyramid if the five-membered π -ligand is considered to adopt the apex of this polyhedron.

The metal-to-carbon distances warrant a comment: they are all rather long as compared to the distances in structurally related compounds (Table I). Whether this rhenium-carbon bond lengthening in compounds of type 1 does result in any significant weakening of the bond towards an easier replacement of the cyclopentadienyl ligand remains an issue to be pursued in the future. Cycloaddition reactions at the ReO_3 fragment and reductions to lower-valent derivatives do not involve replacement of this π -ligand. The only cases in which we have observed at least partial elimination of this ligand are limited to the synthesis of the trinuclear ionic cluster compound $[(\eta^5\text{-C}_5\text{Me}_5)_3\text{Re}_3(\mu\text{-O})_6][\text{ReO}_4]_2$ containing two perrhenate counterions and the formation of the tetranuclear species $(\eta^5\text{-C}_5\text{Me}_5)_2\text{ReO}(\mu\text{-O})_2(\eta^5\text{-C}_5\text{Me}_5)\text{Re}(\text{OReO}_3)_2$ [5].

4. OXOHALIDE DERIVATIVES OF RHENIUM(V)

Most effective and useful is the reduction of the title compound 1 to the oxohalide complexes of composition $(\eta^5\text{-C}_5\text{Me}_5)\text{ReOX}_2$. Several synthetic routes have been worked out in our laboratory. The high thermodynamic stability of germanium dioxide has been exploited when we treated the title compound 1 with the dioxane adduct of germanium dichloride ($\text{GeCl}_2 \cdot \text{C}_4\text{H}_8\text{O}_2$) to make the dichloro rhenium(V) complex 3b in 75% yield (Scheme I). An indirect but nevertheless high-yield access to compounds 3a-d involves the isolable dinuclear intermediate 2 that is reportedly obtained *via* reductive deoxygenation of 1 with triphenylphosphane in the absence of oxygen. Compound 2 is quantitatively converted in fast reactions to the mononuclear difluoro-, dichloro-, and dibromo derivatives 3a-c when treated with aqueous hydrogen fluoride, chloride, and bromide, respectively, at room temperature. The diiodo compound 3d is best obtained by use of pyridinium hydroiodide ($\text{C}_5\text{H}_6\text{N}^+\text{I}^-$), starting from the same precursor 2 (Scheme I).

A further two-step synthetic procedure towards the oxohalide complexes of type 3 involves the intermediates 4 of composition $(\text{C}_5\text{Me}_5)\text{ReX}_4$. These latter compounds have been isolated for $\text{X} = \text{Cl}$ and Br (4b,c; Scheme I), but their exact nature has not yet been resolved since solutions appear to contain at least two species, suggesting the existence of both monomeric and dimeric units [42]. In any case, hydrolysis with stoichiometric amounts of water and pyridine (leading to formation of pyridinium chloride and bromide, respectively) at room temperature straightforwardly yields the desired mononuclear oxohalide derivatives 3b and 3c according to Scheme I. It is obvious that the tetrahalides of type 4 are subject to partial hydrolysis only (replacement of two halide ligands by one oxo ligand). Complete

Table I. Intramolecular distances between π -bonded cyclopentadienyl ligands and the metals attached to them [compounds containing (π -C₅R₅)Re groups].

Compound	M ^x	No. of Ligands ^a	d(M-C ₅ Me ₅) ^b [pm]	Ref.
A. C₅Me₅ Complexes				
(η^5 -C ₅ Me ₅) ₂ Re ₂ (CO) ₄ O	Re ^{II}	5 ^c	225-236	[2]
(η^5 -C ₅ Me ₅)Re(CO) ₂ [C ₂ (C ₆ H ₅) ₂ O ₂]	Re ^{III}	5	219(1) 223(1) 225(1) 219(1) 223(1)	[11] [11] [11] [10] [10]
(η^5 -C ₅ Me ₅)ReO[C ₂ (C ₆ H ₅) ₂ O ₂]	Re ^V	4	241(1) 244(1)	[10]
(η^5 -C ₅ Me ₅)ReO[C ₂ (C ₆ H ₅) ₂ O ₃]	Re ^V	4	239(2) 224(2) 226(1)	[10] [10]
(η^5 -C ₅ Me ₅)ReO[C ₂ O ₂ NC ₆ H ₅]	Re ^V	4	221(1) 224(1) 225(1) 219(3) 219(4)	[10] [10] [10] [5]
[(η^5 -C ₅ Me ₅) ₃ Re ₃ O ₆][ReO ₄] ₂	Re ^{V2/3} (cation)	5 (cation)	237(3) 229(4)	[5]
(η^5 -C ₅ Me ₅) ₂ Re ₂ O ₃ (OReO ₃) ₂	Re ^V	4/5	219-238	[5]
(η^5 -C ₅ Me ₄ Et)ReO ₃	Re ^{VI}	4	238-243	this work
(η^5 -C ₅ Me ₅)ReOC ₂ L ₂	Re ^V	4	247 247	[12]
(η^5 -C ₅ Me ₅)ReOI ₂	Re ^V	4	219 224 254	this work
			252 225	

Table I (continued)

$(\eta^5\text{-C}_5\text{Me}_5)_3\text{Re}_2\text{O}_3\text{Cl}_2$	Re V Re V	4 5	232-236 217 221 235 235	this work
$(\eta^5\text{-C}_5\text{Me}_5)\text{ReCl}_4(\text{PMe}_3)$	Re V	6	225 226 226	231 237 240
$(\eta^5\text{-C}_5\text{Me}_5)\text{ReO}(\text{CH}_3)_2$	Re V	4	214 223 223	247 250 250
$(\eta^5\text{-C}_5\text{Me}_5)\text{ReO}(\text{CH}_2\text{C}_6\text{H}_5)_2$	Re V	4	215 226 227	252 252 this work
$(\eta^5\text{-C}_5\text{Me}_5)\text{Re}[\text{O}_2\text{C}_6\text{C}_{14}]_2$ trans- $(\eta^5\text{-C}_5\text{Me}_5)\text{Re}(\text{CO})_2\text{Br}_2$	Re III Re III	5 5	(221-234) 225-236	[7] [49]
B. C₅H₅ Complexes				
$(\eta^5\text{-C}_5\text{H}_4\text{SiMe}_3)\text{Re}(\text{CO})_3$	Re I	4	230 (av.)	[50]
$(\eta^5\text{-C}_5\text{H}_4\text{COCH}_3)\text{Re}(\text{CO})_3$	Re I	4	228 (av.)	[51]
$(\eta^5\text{-C}_9\text{H}_7)\text{Re}(\text{CO})_3$	Re I	4	228(3) (av.)	[52]
$(\eta^5\text{-C}_5\text{H}_5)\text{Re}(\text{NO})(\text{CHO})[\text{P}(\text{C}_6\text{H}_5)_3]$	Re I	4	231(1) (av.)	[53]
$(\eta^5\text{-C}_5\text{H}_5)_2\text{Re}_2(\text{CO})_5$	Re I	5 ^c	224-234	[54]
trans- $(\eta^5\text{-C}_5\text{H}_5)_2\text{Re}(\text{CO})_2\text{H}(\text{CH}_2\text{C}_6\text{H}_5)$	Re III	5	229 (av.)	[55]

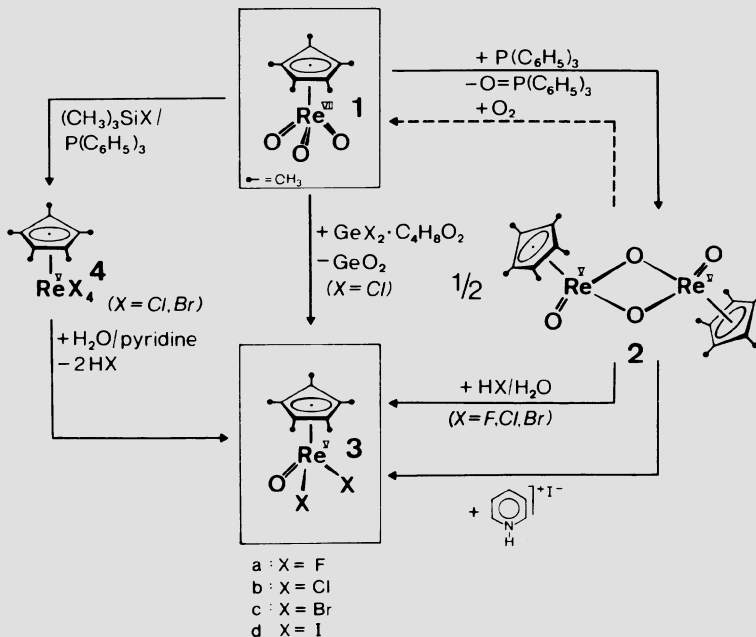
a The π -bonded C₅ ring ligands are assigned one position around the metal.

b Standard deviations refer to the least significant digit(s). If no entry is made, the standard deviation is less than 1 in the last given digit.

c Including Re-Re bond.

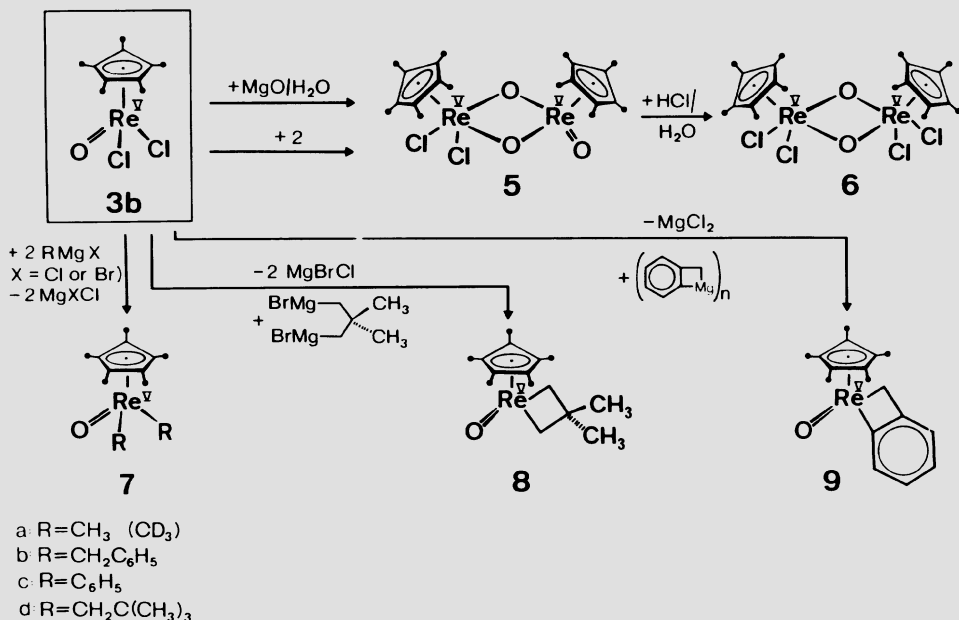
d Distorted pentamethylcyclpentadienyl ligand.

hydrolysis occurs, however, when these tetrahalides are treated with a large excess of water in an acetone solution, yielding the dimer $(\eta^5\text{-C}_5\text{Me}_5)_2\text{Re}_2\text{O}_4$ (2). The best and most convenient way of making compounds 4 is simultaneous treatment of the title compound 1 with chloro- and bromotrimethylsilane, respectively, and triphenylphosphane (Scheme I). Keeping in mind that action of the Lewis base triphenylphosphane upon 1 gives the reduced dimer 2 (Re^{V}), we see that this intermediate is likely to be formed in the synthesis of 4, too. This proposal has been confirmed by the observed clean transformation of 2 into 4 effected by the $(\text{CH}_3)_3\text{SiX}$ reagents. In other words, both the phosphane and the halosilanes are responsible for stepwise deoxygenation of the precursor compound 1. Compounds 4 are also formed from 1 in the absence of triphenylphosphane.



Further hydrolysis of the mononuclear oxohalides 3 may be achieved under basic conditions: treatment of the dichloro derivative 3b with magnesium oxide in the presence of water gives the unusual dimer 5 (Scheme II) [43]. The formation of this particular compound may be viewed as a result of condensation of unchanged $(\eta^5\text{-C}_5\text{Me}_5)\text{ReOCl}_2$ (3b) with its (hypothetical) hydroxy derivative $(\eta^5\text{-C}_5\text{Me}_5)\text{ReO(OH)}_2$. (The

methoxy derivative ($\eta^5\text{-C}_5\text{Me}_5$) $\text{ReO}(\text{OMe})_2$ of this latter species, however, proved to be stable under ordinary conditions [16]). It is interesting to note that 5 also results from combination of 3b with the highly reactive dimer 2 in the sense of a metathesis type reaction; it has in fact repeatedly been observed that the dimeric rhenium(V) compound 2 is a useful synthetic source for the ($\eta^5\text{-C}_5\text{Me}_5$) ReO_2 fragment. Compound 5 is a straightforward (quantitative) coupling product between these two species (Scheme II).



SCHEME II

The terminal oxo ligand remaining in compound 5 can be effectively replaced by two chloro ligands by means of hydrochloric acid, without any breakdown of the dinuclear Re_2O_2 core structure. An X-Ray crystallographic study carried out in our group by Eberhardt Herdtweck revealed the *cis* stereochemistry of this molecule (approximate C_s symmetry). The metal centers adopt a distorted tetragonal-pyramidal (Re1) and trigonal-pyramidal (Re2) coordination geometries (Fig. 2). Small distortion of the π -bonded ring ligand at Re(1) only is evident from Fig. 3.

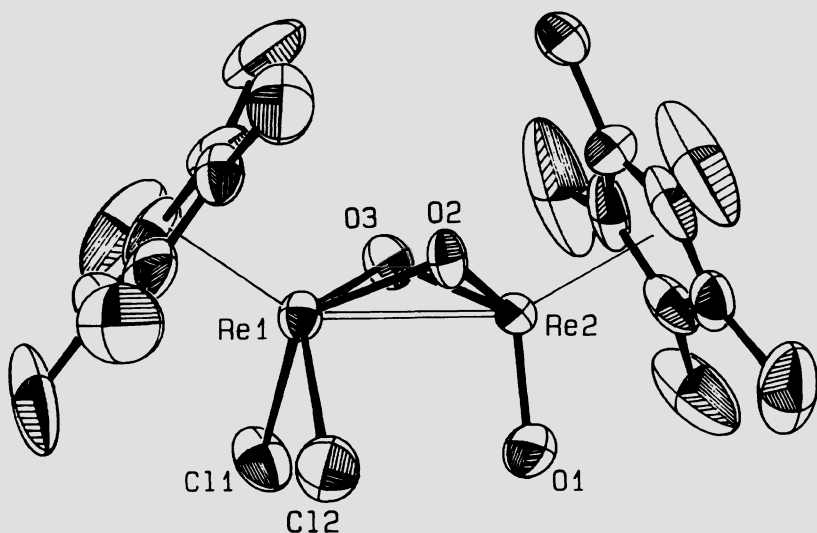


Figure 2. ORTEP drawing of the molecular structure of the dinuclear oxohalide complex $(\eta^5\text{-C}_5\text{Me}_5)_2\text{Re}_2\text{O}_3\text{Cl}_2$ (5).

Selected bond distances [pm] and angles [$^\circ$]: Re(1)-Re(2) 269.1(0); Re(1)-C1(1) 239.5(1); Re(1)-C1(2) 239.8(1); Re(2)-O(1) 168.1(3); Re(2)-O(2) 185.9(3); Re(2)-O(3) 186.5(3); Re(1)-O(2) 202.1(3); Re(1),O(2),Re(2) 87.7(1); Re(1),O(3),Re(2) 87.6(1).

Similar reductive deoxygenation reactions have been carried out with the ethyltetramethylcyclopentadienyl compound 1', as summarized in Scheme III. Once again, exhaustive deoxygenation occurs by means of the reagent combination $(\text{CH}_3)_3\text{SiX}/\text{P}(\text{C}_6\text{H}_5)_3$, yielding the tetrahalide derivatives 4'b ($\text{X} = \text{Cl}$) and 4'c ($\text{X} = \text{Br}$). Opposite to the observations made with the pentamethylcyclopentadienyl congeners 4b,c, these latter compounds are even more soluble in common organic solvents; for this simple reason, they promise a broader variety of chemical reactions. Hydrolysis with water and pyridine cleanly results in formation of the rhenium(V) oxohalides 3'b and 3'c, respectively. Further, the novel imido derivative $(\eta^5\text{-C}_5\text{Me}_4\text{Et})\text{ReCl}_2(\text{N}^t\text{Bu})$ (10'b) is obtained in virtually quantitative yield when 4'b is treated with excess *tert*-butylamine in a toluene solution. Since imido (NR) groups, like oxo ligands, are capable of stabilizing metal centers in high oxidation states by virtue of their pronounced π -donation, one can expect another field of extensive chemistry here [44]. Imido complexes of the present type may be synthesized not only with the above methodology ($\text{L}_x\text{MX}_2 + \text{H}_2\text{NR} \longrightarrow \text{L}_x\text{M=NR} + 2 \text{HX}$), but also by decarboxylative coupling of organometallic oxides with isocyanates ($\text{L}_x\text{M=O} + \text{OCNR} \longrightarrow \text{L}_x\text{M=NR} + \text{CO}_2$) [45].

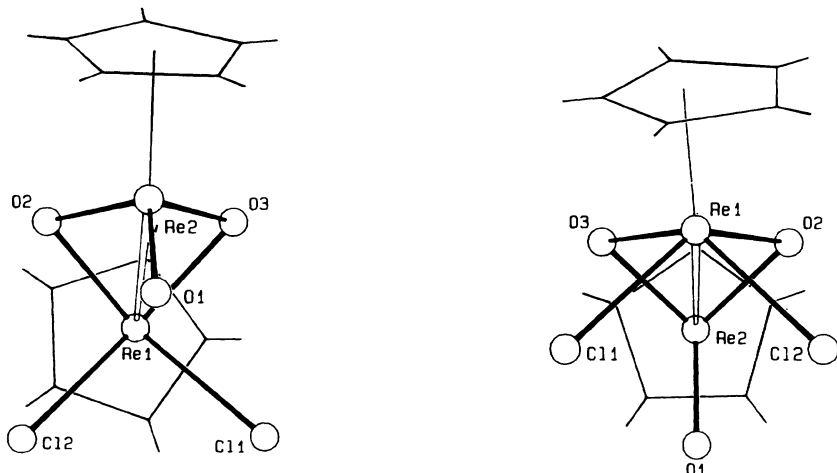
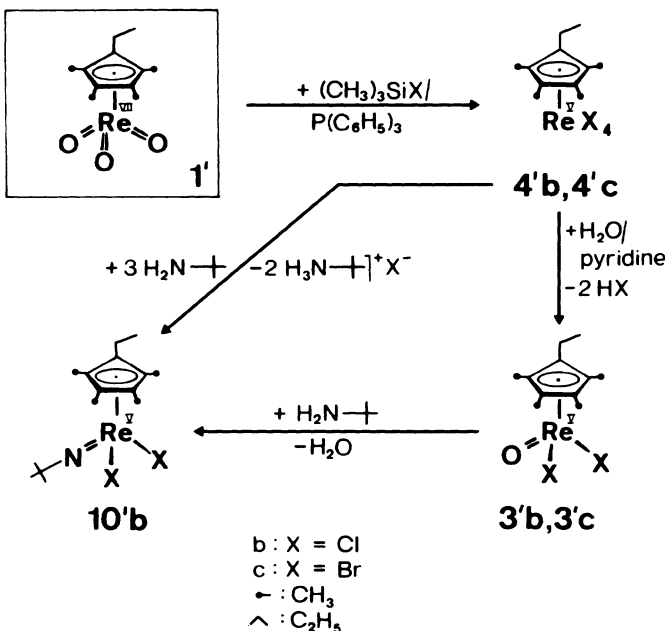


Figure 3. Schematic drawings of the molecular structure of compound 5:
 . Left: projection view onto the C_5Me_5 ring of the $(C_5Me_5)ReO_2Cl_2$ core.
 This picture shows out-of-centroid distortion at the π -bonding between
 the metal atom and the five-membered ring ligand.
 . Right: projection view onto the C_5Me_5 ring of the $(C_5Me_5)ReO_3$ core.



SCHEME III

5. OXOALKYL COMPOUNDS OF RHENIUM(V)

The oxohalide compounds of type 3 offered a unique possibility to further extend our work on oxoalkyl rhenium(V) compounds (Scheme II). While the parent dimethyl derivative 7a is accessible through reductive deoxygenation of the title compound 1 by means of trimethylaluminium or dimethylzinc [16], several homologues of this series, including the benzyl (7b), phenyl (7c), and neopentyl derivatives (7d) were synthesized in isolated yields around 70% using the Grignard approach [47]. The novel metallacycles 8 and 9 became accessible in a collaborative effort with the group of Bickelhaupt [46].

6. STRUCTURAL AND ELECTRONIC CONSIDERATIONS

Although we are dealing here with rather simple compounds, there are some intriguing structural aspects. In an extensive series of accurate X-ray structural determinations [48], Herdtweck has accumulated ample evidence for highly distorted π -coordination of the five-membered ring ligands in several key compounds under discussion. This effect has been documented in all $(\pi\text{-C}_5\text{Me}_5)\text{Re}$ complexes in which the metal atom exhibits an additional set of different ligands with distorted tetrahedral coordination, e.g., $(\text{C}_5\text{Me}_5)\text{Re}(\text{L}')_2$. One prominent example is the oxohalide compound $(\eta^5\text{-C}_5\text{Me}_5)\text{ReOCl}_2$ (3b) represented in Figs. 4 and 5. The view of Fig. 4 gives an excellent impression of how enormously the π -coordination of the pentamethylcyclopentadienyl ligand is distorted off the center of gravity. The two molecules present in the triclinic unit cell are arranged such that the out-of-centroid shift of the π -ligands is intermolecularly counterbalanced. If we disregard this peculiarity for a moment, then the basic structure of each molecule is described as a distorted trigonal pyramid, with two chlorine and one oxo ligand occupying the basal positions. The angle between the two chlorine ligands is much smaller ($85.4(1)^\circ$) than the $\text{Cl}(1/2),\text{Re},\text{O}$ angles ($105.3(2)^\circ$ and $106.2(2)^\circ$), with the sum of angles within the pyramidal ReOCl_2 entity amounting to 296.9° . This geometry is rather trivial but nevertheless entails distortion of π -coordination at the opposite ring ligand. It becomes clear from Fig. 5 that, in contrast to the architecture of the trioxo compound 1' (Fig. 1), the metal atom is no longer situated below the centroid of a regular pentagon but is rather shifted approximately parallel to the best plane of this ligand so that the carbon atoms C(15), C(11), and C(14) are much closer at the metal ($218.0(6)$, $229.5(5)$, and $229.5(6)$ pm, respectively) than the two remaining ring atoms C(12) and C(13) ($247.7(6)$ and $247.5(6)$ pm, respectively). Taking into account that the bond between the more distant carbon atoms C(12) and C(13) is significantly shorter ($139.3(8)$ pm) than the four other inter-ring distances (143.8 - 146.2 pm), a $\eta^3\text{-allyl}/\eta^2\text{-alkene}$ -type coordination of the pentamethylcyclopentadienyl ring must be concluded.

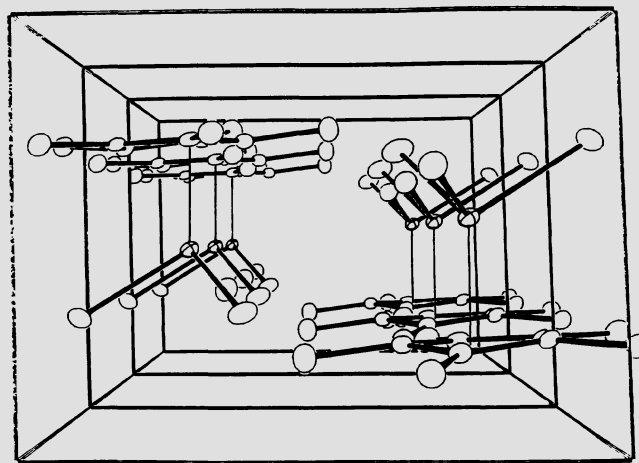


Figure 4. Perspective view of several unit cells of the rhenium(V) compound ($\eta^5\text{-C}_5\text{Me}_5$)ReOCl₂ (3b).

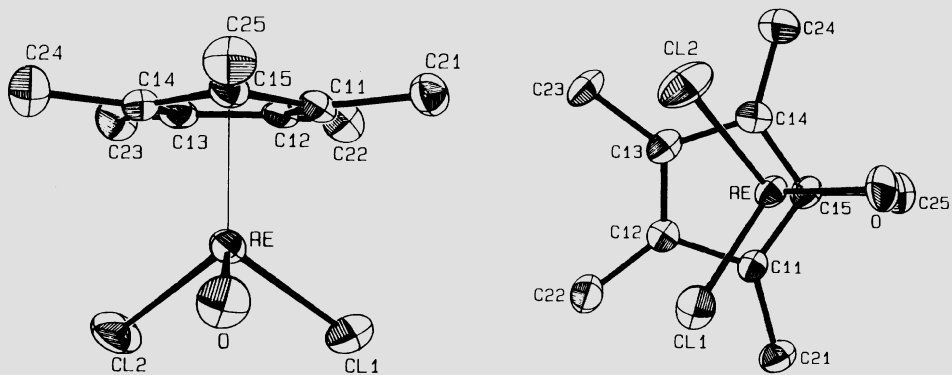


Figure 5. ORTEP drawing (left) of the molecular structure of compound 3b. Bond lengths [pm] and angles [°]: Re-O 170.0(4); C(12)-C(13) 139.3(8); Re-Cl(1) 234.8(2); C(13)-C(14) 145.4(9); Re-Cl(2) 234.5(2); C(14)-C(15) 144.5(8); Re-C(11) 222.5(5); C(15)-C(11) 143.8(8); Re-C(12) 247.7(6); Re-Cp* 195.5; Re-C(13) 247.5(6); Re-C(14) 222.5(6); Re-C(15) 218.0(6); Cl(1)-Re-Cl(2) 85.4(1); Cl(1)-Re-Cp* 123.0; Cl(1)-Re-O 105.3(2); Cl(2)-Re-Cp* 124.2; Cl(2)-Re-O 106.2(2); O-Re-Cp* 109.5. Right: ORTEP projection of the molecular structure down the orthonormal vector between the best plane of the C₅ ligand and the metal atom (thermal ellipsoids at 50% probability).

How does this acentric π -coordination arise? Structural comparison with related compounds listed in Table I provides some help in answering this question. It is to be noted that (1) the distances between rhenium and the attached pentamethylcyclopentadienyl ligand are generally somewhat shorter in low-valent compounds such as $(\eta^5\text{-C}_5\text{Me}_5)\text{Re}(\text{CO})_2\text{Br}_2$ and $(\eta^5\text{-C}_5\text{H}_4\text{SiMe}_3)\text{Re}(\text{CO})_3$ (Table I) [49-55], and that (2) substantial out-of-centroid coordination occurs only in rhenium compounds that display different ligands around the metal atom. Structural details of the low-valent reference compound tricarbonyl- $(\eta^5\text{-pentamethylcyclopentadienyl})\text{rhenium(I)}$ have not yet become available, but rhenium-carbon distances of roughly 230-235 pm seem to be a relatively good extrapolation from the data of closely related compounds (Table I). If we now compare with the recorded rhenium-carbon distances of the structurally analogous high-valent oxo derivative trioxo $(\eta^5\text{-ethyltetramethylcyclopentadienyl})\text{rhenium(VII)}$ (1'), then we encounter a significant bond lengthening in this latter case (Fig. 1, Table I). The rhenium-carbon distances of 238-243 pm are close to the set of longer distances in the unsymmetrical rhenium(V) derivatives $(\eta^5\text{-C}_5\text{Me}_5)\text{ReOR}_2$ ($\text{R} = \text{Cl}, \text{I}, \text{CH}_3, \text{CH}_2\text{C}_6\text{H}_5$), while the π -bonded organic ligand is rather symmetrically attached to the metal atom in the case of 1' (Fig. 1).

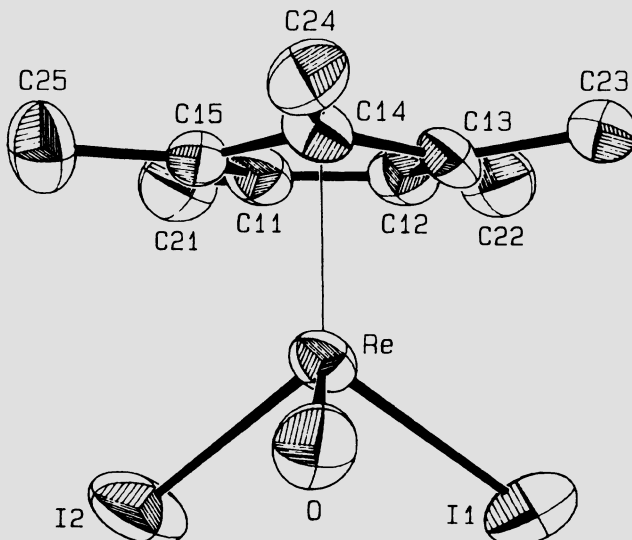


Figure 6. Structure of the diiodo derivative $(\eta^5\text{-C}_5\text{Me}_5)\text{ReOI}_2$ (3d). Selected bond lengths [pm] and angles [$^\circ$]: Re-O 168.7(3); Re-I(1) 268.1(0); Re-I(2) 267.6(0); Re-C(11) 253.5(4); Re-C(12) 251.7(4); Re-C(13) 223.7(4); Re-C(14) 218.6(4); Re-C(15) 225.4(4); I(1),Re,I(2) 88.8(0); I(1),Re,O 99.4(1); I(2),Re,O 101.7(4).

The conclusion to be drawn from these findings is quite obvious now: The oxo ligand, like nitrido ("naked" N) and carbyne (CR) groups, is a notorious π -donor ligand, and this property results in a strong trans influence, primarily labilizing the bonds on the opposite side of a given polyhedron. The selected compounds ($\eta^5\text{-C}_5\text{Me}_4\text{Et}$)ReO₃ (ReO₃ fragment) and ($\eta^5\text{-C}_5\text{Me}_5$)ReOC₂ (ReOC₂ fragment) demonstrate how dramatic this trans influence of terminal oxo ligands can be. Future studies are needed to show whether these architectural distortions of π -coordination within the class of compounds considered here do entail chemical consequences.

The picture does not basically change as we move to related compounds of composition (C₅Me₅)ReOR₂ [48]: thus, the diiodo derivative ($\eta^5\text{-C}_5\text{Me}_5$)ReOI₂ (3d) shown in Fig. 6 just adds to the conclusions drawn from the above-mentioned structures (Figs. 1, 4, and 5).

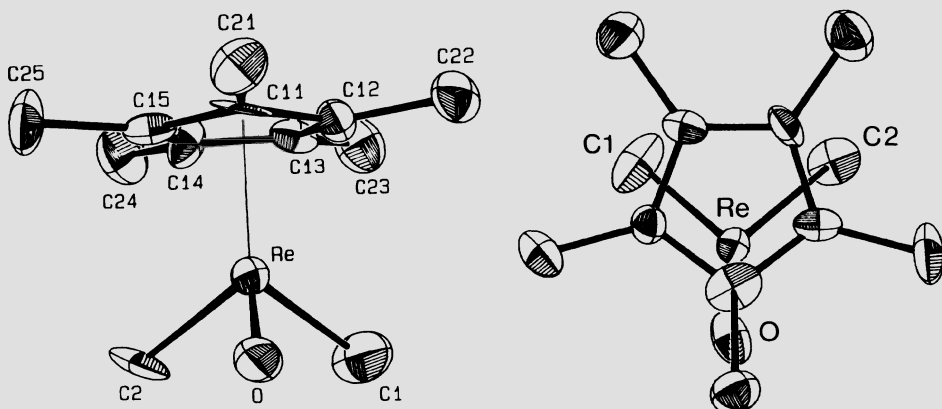


Figure 7. Left: Structure of the dimethyl derivative ($\eta^5\text{-C}_5\text{Me}_5$)ReO(CH₃)₂ (7a). Selected bond lengths [pm] and angles [$^\circ$]: Re-C(1) 212.9(12); Re-C(2) 216.1(10); Re-O 168.1(7); Re-C(11) 212.7(9); Re-C(12) 223.1(9); Re-C(13) 249.9(9); Re-C(14) 249.7(9); Re-C(15) 223.5(9); C(1),Re,C(2) 81.7(5); C(1),Re,O 97.0(4); C(2),Re,O 99.8(4); sum of angles within the ReOC₂ core: 278.5°. The C(13)-C(14) bond (137.3(13) pm) is shorter than the other four C-C bonds within the five-membered π -ligand (143-145 pm). **Right:** Projection of the molecular structure viewed down onto the best plane of the π -bonded pentamethylcyclopentadienyl ligand.

The differences in rhenium-carbon bond lengths are again around 30 pm (!), with the two longer ReC distances being trans to the Re=O group. Although the bulkier iodo ligands (compared with C1) may contribute slightly to this effect by steric (through space) repulsions, the dominating contribution is due to the electronic properties of the terminal oxo ligand. Otherwise, the Re-C(13) and Re-C(15) bonds (223.7(4) and 225.4(4) pm) should be about as long as the Re-C(11) and Re-C(12) bonds (253.5(4) and 251.7(4) pm, respectively). Figs. 6 and 8 should be compared with Figs. 1 (title compound) and 7 (oxodichloro complex 3b).

The same findings and interpretations apply to the dialkyl series ($\eta^5\text{C}_5\text{Me}_5$)ReOR₂ (R = CH₃, 7a; CH₂C₆H₅, 7b). Both compounds (Figs. 8 and 9) adopt the same overall geometry, with the distortion of the hydrocarbon π -ligand being even more pronounced than observed for the dichloro and diiodo derivatives 3b and 3d. The bond length difference is as high as 37 pm (compound 7b), and the five-membered ring ligand is no longer planar! Still, halogen vs. alkyl substituents at the rhenium atom do not appear to greatly influence the structural details in compounds of analogous composition.

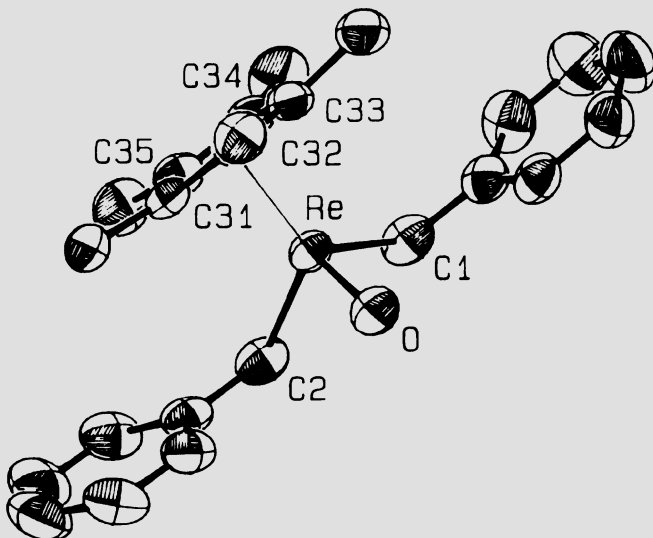


Figure 8. Structure of the dibenzyl derivative ($\eta^5\text{C}_5\text{Me}_5$)ReO(CH₂-C₆H₅)₂ (7b). Selected bond lengths [pm] and angles [$^\circ$]: Re-C(1) 217.5(3); Re-C(2) 216.3(3); Re-O 168.6(2); Re-C(31) 226.8(3); Re-C(32) 215.6(3); Re-C(33) 225.9(3); Re-C(34) 252.2(3); Re-C(35) 252.2(3); C(1),Re,C(2) 83.1(2); C(1),Re,O 98.6(1); C(2),Re,O 98.4(1); sum of angles within the ReOC₂ core: 280.1°. The C(34)-C(35) bond length (139.0(4) pm) is shorter than the other four C-C bonds within the five-membered π -ligand (143.4(4) - 144.7(4) pm).

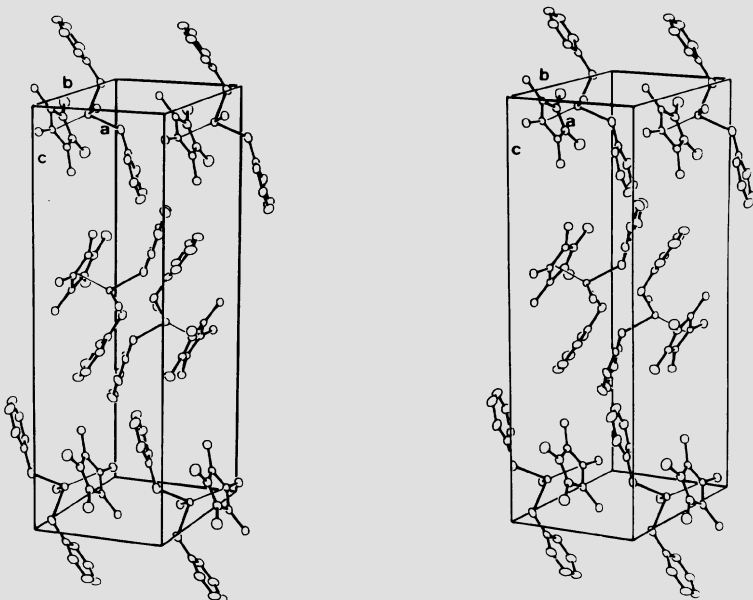


Figure 9. Stereoview of the unit cell of the dibenzyl rhenium(V) compound $(\eta^5\text{-C}_5\text{Me}_5)\text{ReO}(\text{CH}_2\text{C}_6\text{H}_5)_2$ (7b).

The comparative compilation of structural data presented in Table I suggests the following general conclusions:

- (1) There are two arbitrary sets of rhenium-to-carbon (C_5Me_5 ring ligand) bond distances, smaller or larger than ca. 235 pm.
- (2) The longer bonds are approximately trans to oxorhenium (ReO) groups. There is not too much of a difference, however, as to whether we are dealing with terminal or bridging oxo groups to cause this trans influence; in this respect, a comparison may be drawn between compounds of type $(\eta^5\text{-C}_5\text{Me}_5)\text{ReOX}_2$ on the one hand, and the dimer $(\eta^5\text{-C}_5\text{Me}_5)_2\text{Re}_2(\mu\text{-O})_2\text{OCl}_2$ (5) on the other.
- (3) The more strongly the trans influence comes to the fore, the shorter are the remaining rhenium-carbon distances. The latter ones may then even be much shorter (e.g., 214-223 pm in compound 7a; Fig. 7) than in low-valent compounds containing exclusively π -acceptor ligands such as carbon monoxide (e.g., 230 pm, average, in $(\eta^5\text{-C}_5\text{H}_4\text{SiMe}_3)\text{Re}(\text{CO})_3$, Table I).
- (4) The trans influence is not an additive one, because otherwise the rhenium-to-carbon bond lengthening in the congener of the title compound 1' ($d(\text{Re-C})$ 238-243 pm) should be even greater, approaching a value of ca. 250 pm (Table I).
- (5) The kind of distortion at the rhenium-cyclopentadienyl bonding depends from the coordination number. Thus, in compounds of type

$(\eta^5\text{-C}_5\text{Me}_5)\text{ReL}(\text{L}')_2$ (coordination number 4) the out-of-centroid distortion is directed toward one ring carbon atom (η^3 -allyl/ η^2 -alkene coordination; two short and three long Re-C bonds), whereas in compounds of type $(\eta^5\text{-C}_5\text{Me}_5)\text{ReL}_4$ (coordination number 5) two ring carbon atoms are closest to the metal (one short and four long Re-C bonds).

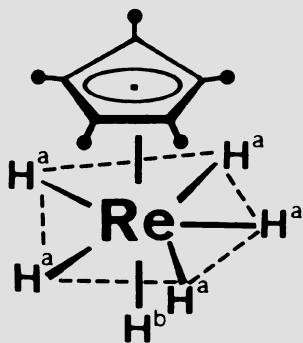
The terminal rhenium-oxygen bond lengths are in the range 168-172 pm in all compounds considered here. For comparison, the rhenium-oxygen bond lengths of some inorganic oxorhenium compounds are summarized below:

KReO ₄	172.3(4) pm	[56]
ReO ₃ Cl	170 pm	[57]
ReO ₃ (OSiMe ₃)	165 pm	[58]
Cs ₂ [ReO ₃ Cl ₃]	170(2) pm	[59]
(L ₃)ReO ₃ ⁺	175.6(5) pm	[60]
(L ₃ = <u>cyclo</u> -C ₆ H ₁₅ N ₃)		

7. PERSPECTIVES

We have stumbled into an ostensibly rich field of research which once again holds promise of furnishing strong links between inorganic (metal oxide) and organometallic chemistry [61]. High oxidation states of the participating transition metals are not at all the pivotal prerequisite for compounds that contain both organic ligands and oxo groups. Low and high oxidation numbers at the metals are attainable for π -aromatic functionalities as well as for oxo groups, and there is a plethora of possible ligand combinations between the extremes. It is good to know that a potent oxidizing agent such as rhenium(VII) "doesn't chew up the organic ligand" [62]. The title compound 1 convincingly amplifies on this statement.

Where are we heading? Further extension of our preparative work warrants high priority; the "relatives" of rhenium should be included: vanadium and niobium likewise are quite oxophilic and thus promise new "organometallic oxides", related ones and certainly surprising ones, too. First attempts in this direction have already been made in our research group. On the other hand, the synthetic future of rhenium compounds reviewed in this paper has just begun. Suffice to say that products like the amazing hexahydrido(η^5 -pentamethylcyclopentadienyl)-rhenium(VII), $(\eta^5\text{-C}_5\text{Me}_5)\text{ReH}_6$, synthesized from $(\eta^5\text{-C}_5\text{Me}_5)\text{ReCl}_4$ and LiAlH₄, presents another new key compound in high-valent organorhenium chemistry [63]. It will be of interest to see how various oxidation states of rhenium interconvert with each other, both electrochemically and on a preparative scale. Finally, the major opportunity is directed toward catalysis. Do alkylrhenium(V) compounds such as $(\eta^5\text{-C}_5\text{Me}_5)\text{ReO}(\text{CH}_3)_2$ produce species containing alkylidenerhenium(V) (Re=CH₂) fragments upon thermolysis, and can such units be generated by



other means? If yes, is alkene metathesis [64] feasible at such fragments? Note that rhenium, like molybdenum and tungsten, is known to constitute the most effective metal for alkene metathesis [64]!

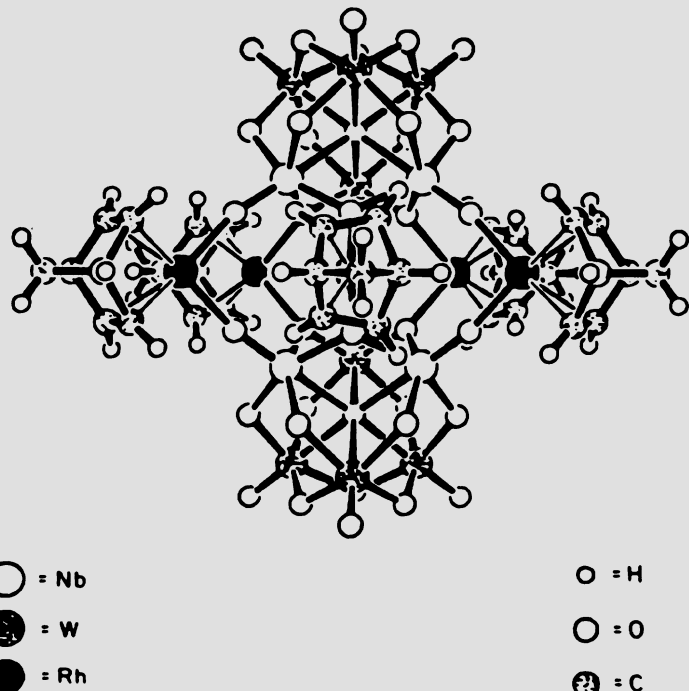


Figure 10. SCHAKAL drawing of the C_{2v} structure of Klemperer's "organo-metallic oxide goliath" $\{(\eta^5\text{-C}_7\text{H}_8)\text{Rh}\}_5(\text{cis-Nb}_2\text{W}_4\text{O}_{19})_2\}^{3-}$ [66].

Moreover, what is the fate of alkynes once coordinated to rhenium in high and intermediate oxidation states? Shall we find ourselves in a position of modelling organometallic oxides related to the mechanistically completely unclear SOHIO ammonoxidation process? A further possible utilization of oxorhenium and related compounds may be found in the functionalization of unsaturated organic compounds; reactivity patterns known from osmium tetroxide chemistry could arise here (e.g., glycols from alkenes) [65]. Considering the broad range of organometallic oxides landmarked by our "david" ($\eta^5\text{-C}_5\text{Me}_5$) ReO_3 and Klemperer's "goliath" $\{(\eta^5\text{-C}_7\text{H}_8)\text{Rh}\}_5(\text{cis-Nb}_2\text{W}_4\text{O}_{19})_2\}^{3-}$ [66], we expect a rich harvest in the years to come.

8. ACKNOWLEDGMENTS

I do not know what I should have done without the innovative, careful, and thoughtful experimental contributions of my coworkers Dr. Ricardo Serrano, Martina Flöel, Dr. Eberhardt Herdtweck, Dr. Ulrich Küsthardt, Jürgen Kulpe, Dr. Jun Okuda, and Dr. Erdmuthe Voss. The work summarized here would not have been possible without the active and continuous support by the Fonds der Chemischen Industrie, Hoechst Aktiengesellschaft, Degussa AG, Chemische Werke Hüls AG, the BASF Aktiengesellschaft, Procter & Gamble, and the German Bundesministerium für Forschung und Technologie. We express our gratitude for the financial help that we have been receiving from these companies and institutions. Miss Juliane Geisler is greatfully acknowledged for the preparation of the manuscript.

9. REFERENCES

1. W.A. Herrmann, R. Serrano, and H. Bock, Angew. Chem. **96**, 364 (1984); Angew. Chem., Int. Ed. Engl. **23**, 383 (1984).
Also see: Nachr. Chem. Techn. Labor. (Weinheim/Germany) **32** (3), S. 202 (1984).
2. W.A. Herrmann, R. Serrano, A. Schäfer, M.L. Ziegler, and E. Guggolz, J. Organomet. Chem. **272**, 55 (1984).
3. W.A. Herrmann, R. Serrano, U. Küsthardt, M.L. Ziegler, E. Guggolz, and Th. Zahn, Angew. Chem. **96**, 498 (1984); Angew. Chem., Int. Ed. Engl. **23**, 515 (1984).
4. W.A. Herrmann, R. Serrano, M.L. Ziegler, H. Pfisterer, and B. Nuber, Angew. Chem. **97**, 50 (1985); Angew. Chem., Int. Ed. Engl. **24**, 50 (1985).
5. W.A. Herrmann, R. Serrano, U. Küsthardt, E. Guggolz, B. Nuber, and M.L. Ziegler, J. Organomet. Chem. **287**, 329 (1985).
6. W.A. Herrmann, U. Küsthardt, M.L. Ziegler, and Th. Zahn, Angew. Chem. **97**, 857 (1985); Angew. Chem., Int. Ed. Engl. **24**, 860 (1985).
7. W.A. Herrmann, U. Küsthardt, and E. Herdtweck, J. Organomet. Chem. **294**, C33 (1985).
8. W.A. Herrmann, E. Voss, U. Küsthardt, and E. Herdtweck, J. Organomet. Chem. **294**, C37 (1985).

9. W.A. Herrmann, E. Voss, and M. Flöel, J. Organomet. Chem. **297**, C5 (1985).
10. U. Küsthhardt, W.A. Herrmann, M.L. Ziegler, Th. Zahn, and B. Nuber, J. Organomet. Chem. **311**, 163 (1986).
11. W.A. Herrmann, U. Küsthhardt, A. Schäfer, and E. Herdtweck, Angew. Chem. **98**, 818 (1986).
12. W.A. Herrmann, U. Küsthhardt, M. Flöel, J. Kulpe, E. Herdtweck, and E. Voss, J. Organomet. Chem. **314**, 151 (1986).
13. W.A. Herrmann, T. Cuenca, and U. Küsthhardt, J. Organomet. Chem. **309**, C15 (1986).
14. E. Voss, Ph.D. Thesis, Technische Universität München (1986).
15. U. Küsthhardt, Ph.D. Thesis, Technische Universität München (1986).
16. This compound was also reported by another research group:
A.H. Klahn-Oliva and D. Sutton, Organometallics **3**, 1313 (1984).
17. W.A. Herrmann, J. Organomet. Chem. **300**, 111 (1986).
- 18a. E.O. Fischer and S. Vigoureux, Chem. Ber. **91**, 1342 (1958).
- 18b. E.O. Fischer, S. Vigoureux, and P. Kuzel, Chem. Ber. **93**, 701 (1960).
19. M. Cousins and M.L.H. Green, J. Chem. Soc. A, 1567 (1964). - Structure of $(\eta^5\text{-C}_5\text{H}_5)_2\text{Mo}_2\text{O}_4$: Ref. [22]. Related compounds: R.H. Crabtree and G.G. Hlatky, Polyhedron **4**, 521 (1985).
20. M.L.H. Green, A.H.L. Lynch, and M.G. Swanwick, J. Chem. Soc., Dalton Trans., 1445 (1972).
21. R.R. Schrock, S.F. Pedersen, M.R. Churchill, and J.W. Ziller, Organometallics **3**, 1574 (1984).
22. M. Herberhold, W. Kremnitz, A. Razavi, U. Schöllhorn, and U. Thewalt, Angew. Chem. **97**, 603 (1985); Angew. Chem., Int. Ed. Engl. **24**, 601 (1985).
23. W.A. Herrmann, G. Ihl, and D. Mandon, unpublished results, cf. W.A. Herrmann, in Ref. [17].
24. G. Ihl, Ph.D. Thesis, Technische Universität München (1986).
25. Structure of $(\eta^5\text{-C}_5\text{Me}_5)_2\text{Mo}_2\text{O}_4$: H. Arzoumanian, A. Baldy, M. Pierrot, and J.-F. Petrignani, J. Organomet. Chem. **294**, 327 (1985).
26. N.D. Silavwe, M.Y. Chiang, and D.R. Tyler, Inorg. Chem. **24**, 4219 (1985).
27. H.G. Alt and H.I. Hayen, Angew. Chem. **97**, 506 (1985); Angew. Chem., Int. Ed. Engl. **24**, 497 (1985).
28. P. Legzdins, S.J. Rettig, and L. Sanchez, Organometallics **4**, 1479 (1985).
29. S.A. MacLaughlin, R.C. Murray, J.C. Dewan, and R.R. Schrock, Organometallics **4**, 796 (1985).
- 30a. J.M. Mayer and T.H. Tulip, J. Am. Chem. Soc. **106**, 3878 (1984).
- 30b. J.M. Mayer, D.L. Thorn, and T.H. Tulip, J. Am. Chem. Soc. **107**, 7454 (1985).
- 31a. J.F. Gibson, K. Mertis, and G. Wilkinson, J. Chem. Soc., Dalton Trans., 1093 (1975).
- 31b. K. Mertis, D.H. Williamson, and G. Wilkinson, J. Chem. Soc., Dalton Trans., 607 (1975).
32. J.F. Gibson, G.M. Lack, K. Mertes, and G. Wilkinson, J. Chem. Soc., Dalton Trans., 1490 (1976).

33. I.R. Beattie and P.J. Jones, Inorg. Chem. **18**, 2318 (1979).
34. P. Stavropoulos, P.G. Edwards, T. Behling, G. Wilkinson, M. Mottevalli, and M.B. Hursthouse, J. Chem. Soc., Dalton Trans., 2167 (1985); P. Edwards and G. Wilkinson, ibid., 2695 (1984).
35. M. Schmidt and H. Schmidbaur, Inorg. Synth. **9**, 149 (1967).
36. K. Wieghardt, C. Pomp, B. Nuber, and J. Weiss, Inorg. Chem. **25**, 1659 (1986).
37. Cf. Ref. [24], p. 52 ff.
- 38a Synthesis: E.O. Fischer, K. Ulm, and H.P. Fritz, Chem. Ber. **93**, 2167 (1960).
- 38b. Structure: F. Bottomley, D.E. Paez, and P.S. White, J. Am. Chem. Soc. **103**, 5581 (1981); ibid. **104**, 5651 (1982).
- 39a. F. Bottomley and P. White, J. Chem. Soc., Chem. Commun., 28 (1981).
- 39b. F. Bottomley, D. Paez, and P. White, J. Am. Chem. Soc. **107**, 7226 (1985).
40. J. Huffman, J. Stone, W. Krusell, and K.G. Caulton, J. Am. Chem. Soc. **99**, 5829 (1977).
41. V.N. Latyaeva, V.V. Pereshein, and A.N. Lineva, Tr. Khim. Khim. Teknol., 32 (1974).
42. W.A. Herrmann and J. Okuda, submitted for publication in Angew. Chem. (1986).
43. J. Kulpe, Diploma Thesis, Universität Frankfurt/Main (1986).
44. Cf. B.L. Haymore, E.A. Maatta, and R.A.D. Wentworth, J. Am. Chem. Soc. **101**, 2063 (1979), and Refs. quoted therein.
45. M.L.H. Green and K.J. Moynihan, Polyhedron **5**, 921 (1986).
46. H.J.R. de Boer, B.J. van de Heisteeg, M. Flöel, W.A. Herrmann, O.S. Akkerman, and F. Bickelhaupt, Angew. Chem. **99**, 88 (1987).
47. M. Flöel and W.A. Herrmann, unpublished results (1986).
48. W.A. Herrmann and E. Herdtweck, unpublished results (1985/86).
49. F.W.B. Einstein, A.H. Klahm-Oliva, D. Sutton, and K.G. Tyers, Organometallics **5**, 53 (1986).
50. W. Harrison and J. Trotter, J. Chem. Soc., Dalton Trans., 678 (1972).
51. T.L. Khotsyanova, S.I. Kuznetsov, E.V. Bryukhova, and Y.V. Makarov, J. Organomet. Chem. **88**, 351 (1975).
52. K.K. Joshi, R.H.B. Mais, F. Nyman, P.G. Owston, and A.M. Wood, J. Chem. Soc. (London) A, 318 (1968).
53. W.-K. Wong, W. Tam, C.E. Strouse, and J.A. Gladysz, J. Chem. Soc., Chem. Commun., 530 (1979).
54. A.S. Foust, J. Hoyano, and W.A.G. Graham, J. Organomet. Chem. **32**, C65 (1971).
55. E.O. Fischer and A. Frank, Chem. Ber. **111**, 3740 (1978).
56. C.J. Lock and G. Turner, Acta Crystallogr. (Copenhagen) **B31**, 1764 (1975); B. Krebs and K.D. Hasse, Acta Crystallogr. (Copenhagen) **B32**, 1334 (1976).
57. J.F. Lotspeich, A. Jaran, and A. Englebrecht, J. Chem. Phys. **31**, 633 (1959).
58. G.M. Sheldrick and W.S. Sheldrick, J. Chem. Soc. (London) A, 2160, (1969).
59. T. Lis, Acta Crystallogr. (Copenhagen) **B39**, 961 (1983).

60. K. Wieghardt, C. Pomp, B. Nuber, and J. Weiss, Inorg. Chem. **25**, 1659 (1986).
61. Recent review: W.A. Herrmann, Angew. Chem., Int. Ed. Engl. **25**, 56 (1986).
62. R. Dagani, Chem. Eng. News **62** (30), 28 (1984).
63. W.A. Herrmann and J. Okuda, unpublished results (1986).
64. Review: R.H. Grubbs, in Comprehensive Organometallic Chemistry (Eds. G. Wilkinson, F.G.A. Stone, and E.W. Abel), v. 8, chapter 54, p. 499, Pergamon Press, Oxford (1982).
65. Cf. C.C. Hinckley and P.A. Kibala, Polyhedron **5**, 1119 (1986).
66. C.J. Besecker, W.G. Klemperer, and V.W. Day, J. Am. Chem. Soc. **104**, 6158 (1982). Novel oxo clusters: F. Bottomley, L. Sutin, and P.S. White, J. Chem. Soc., Chem. Commun., 597 (1985); also see: M.J. Bunker, A. deCian, and M.L.H. Green, J. Chem. Soc., Chem. Commun., 59 (1977); J. Organomet. Chem. **131**, C40 (1977); J. Chem. Soc., Dalton Trans., 847 and 353 (1981); J. Organomet. Chem. **208**, 299 (1981).

ZEOLITE SYNTHESIS: AN OVERVIEW

Richard M. Barrer
Chemistry Department
Imperial College of Science and Technology
South Kensington, London SW7 2AY
U.K.

ABSTRACT. An account is given of zeolite synthesis, emphasizing the following aspects: the ranges in Si/Al ratios found for individual zeolites, and for the zeolite family as a whole; the mineralising role of water and OH⁻ ion and the effect of pH upon crystallisation kinetics; the guest-host relationship as a major factor in synthesis of all kinds of porous crystal; templates; the analysis of crystallisation kinetics in terms of linear growth rates and rates of nucleation; and Ostwald's law of successive transformations in zeolite chemistry. A phenomenological treatment of nucleation is also given.

1. INTRODUCTION

Zeolites are water-bearing tectosilicates, porous on the scale of molecules. As tectosilicates, they are 3-dimensional, 4-connected nets of tetrahedral units, T₄O, where T is usually Al or Si. The water content may be large, up to 50 % of the volume of the crystals, but the zeolites feel dry to touch. The water is readily distilled out of the crystals and can as readily be re-imbibed. The intracrystalline porosity takes the form of diverse 1-, 2-, or 3-dimensional networks of channels, or of cavities linked by shared windows.

This account is concerned with factors governing the synthesis of zeolites. It is an area of notable richness in chemical discovery, although as yet only a fraction of the framework topologies which can be made as models has been made in the laboratory.

2. HISTORICAL PERSPECTIVE

Zeolites have a long history, beginning with the discovery of stilbite in 1756 by Cronstedt [1]. In Table I are the names of naturally occurring zeolites in order of their discovery or their first naming, together with the IUPAC 3-letter designation of the framework topology. Some are variants only of a particular framework topology; for example, stilbite, stellerite, and barrerite all have the topology STI. In the

table there are 25 different kinds of framework topology, and there are several (cowlesite, partheite, goosecreekite, and perliallite) for which structural information is not yet adequate. Isotypes of the majority of these zeolites have been synthesized, in some instances by several different chemical pathways.

Table I. Dates of discovery or naming of natural zeolites.^a

Zeolite	Date	Zeolite	Date
Stilbite (STI)	1756	Gonnardite (THO)	1896
Natrolite (NAT)	1758	Wellsite (PHI)	1897
Chabazite (CHA)	1772	Dachiardite (DAC)	1905
Harmotome (PHI)	1775	Stellerite (STI)	1909
Analcime (ANA)	1784	Ferrierite (FER)	1918
Laumontite (LAU)	1785	Viseite (ANA)	1942
Thomsonite (THO)	1801	Yugawaralite (YUG)	1952
Scolecite (NAT)	1801	Wairakite (ANA)	1955
Heulandite (HEU)	1801	Bikitaite (BIK)	1957
Gmelinite (GME)	1807	Paulingite (PAU)	1960
Mesolite (NAT)	1813	Garronite (GIS)	1962
Gismondine (GIS)	1816	Tetranatrolite (NAT)	1969
Brewsterite (BRE)	1822	Mazzite (MAZ)	1972
Epistilbite (EPI)	1823	Barrerite (STI)	1974
Phillipsite (PHI)	1824	Cowlesite (-)	1975
Levynite (LEV)	1825	Merlinoite (MER)	1976
Herschelite (CHA)	1825	Svetlozarite (DAC)	1976
Edingtonite (EDI)	1825	Amicite (GIS)	1979
Faujasite (FAU)	1842	Partheite (-)	1979
Mordenite (MOR)	1864	Paranatrolite (NAT)	1980
Clinoptilolite (HEU)	1890	Goosecreekite (-)	1980
Offretite (OFF)	1890	Gobbinsite (GIS)	1982
Erionite (ERI)	1890	Willhendersonite (CHA)	1984
Kehoeite (ANA)	1893	Perliallite (-)	1984

^a The three letters in brackets denote the kind of framework topology as recommended by IUPAC [2].

Table II gives 18 examples of synthetic zeolites having topologies not yet found in nature, with the 3-letter IUPAC topological designations where these have been assigned. The table also indicates apparent isotypes prepared in different laboratories. Many other syntheses have been reported, some of which may represent novel structures [43]. Between them, Tables I and II contain 43 different topologies, but hundreds of other 4-connected tectosilicate nets are possible and present a challenge to chemical ingenuity, and potential industrial reward.

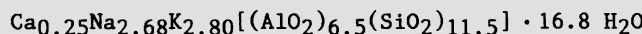
Table II. Examples of synthetic zeolites without known natural counterparts.

Designation	Actual or Possible Isotypes ^b	Notation for Framework Topology
Linde A [3]	N-Q [20], α [21], ZK-4 [22], ZK-21 [23], ZK-22 [23]	LTA
Linde L [4]	Ba-G, L [24]	LTL
Linde N [5]	Z-2 [25], (Na,TMA)-V [26], Na-V [27]	LTN
TMA-E [6]		EAB
Li-A(BW) [7]		ABW
Species P [8]	ZK-5 [28]	KFI
Beta [9]		-
Rho [10]		RHO
Losod [11]		LOS
ZSM-2 [12]		-
ZSM-3 [13]		-
ZSM-5 [14]	Silicalite I [29]	MFI
ZSM-11 [15]	Silicalite II [30]	MEL
ZSM-12 ^a [16]	TEA-silicalite [31], CZH-5 [32], Nu-13 [33]	-
ZSM-22 ^a [17]	Theta-1 [34], Nu-10 [35], ISI-1 [36], KZ-2 [37]	-
ZSM-23 ^a [18]	ISI-4 [38], KZ-1 [37]	-
ZSM-39 ^a [19]	Dodecasil-3C [39]	-
ZSM-48 ^a [19]	EU-2 [40], ZBM-30 [41], EU-11 [42]	-

^a Structures known but letter notations for framework topology not yet allocated.

^b By "isotypes" is here meant "structures having the same framework topologies".

Zeolite synthesis occurs in aqueous alkaline media, often at temperatures above 100°C. The first claim to have made a named zeolite, levynite, was that of St. Claire Deville in 1862 [44]. Solutions of Na- and K-silicates were heated in sealed glass tubes to 170°C, and tabular, hexagonal crystals were formed which had the composition



Reviews by Niggli and Morey [45] and Morey and Ingerson [46] have summarized and discussed hydrothermal chemistry from 1845 to 1937.

By the early 1940's, the ability of zeolites to act as quantitative molecular sieves in mixture separation had been abundantly established [47,48,49]. Initially three and later five categories of molecular sieve were described. Also in the early 1940's, systematic exploration of zeolite syntheses began in the author's laboratory and continued for nearly forty years. Early syntheses included analcime, edingtonite-type zeolites, mordenite, and Species P [8] with the

framework topology KFI of the zeolite ZK-5 [28] made later and by a different route. Species P was the first synthetic zeolite to be made which has no natural counterpart. Late in the 1940's, the interest of scientists at Linde Air Products was aroused, with zeolite A, faujasites X and Y, and zeolite L as early successes [4]. Zeolite synthesis remains an open field for discovery of novel structures.

3. LOW- AND HIGH-SILICA ZEOLITES AND POROSILS

The zeolite family as a whole shows a remarkable range in values of the ratio Si/Al. An arbitrary division into categories is given in Table III [52]. Category 2 includes nearly all the naturally occurring zeolites of Table I, many of which are Al-rich with $1 < \text{Si/Al} \leq 2$. Category 4 involves only synthetic zeolites without natural counterparts.

Table III. Si/Al ratios in 3-dimensional 4-connected nets (aluminate, aluminosilicate, silica).

Category:

1	2	3	4	5
---	---	---	---	---

Si/Al ratio:

$0 \leq \text{Si/Al} < 1$	$1 \leq \text{Si/Al} < 5$	$\text{Si/Al} > 5$	$\text{Si/Al} > 12$	$\text{Si/Al} = \infty$
---------------------------	---------------------------	--------------------	---------------------	-------------------------

Examples:

Aluminate Sodalite; bicchulite.	Zeolites Felspathoids (non-porous and porous) Felspars (non-porous)	Zeolites (ferrierite; svetlozarite)	Zeolites	Crystalline silicas (porous and non-porous)
---------------------------------------	--	---	----------	--

Individual zeolites may show considerable ranges in Si/Al ratios, as a result of isomorphous replacements such as



Compositional ranges reported for particular zeolites are illustrated in Table IV. One of the most remarkable examples of isomorphous replacement for a given framework topology is found with sodalite. The framework exists as a pure Ca-aluminate ($\text{Si/Al} = 0$); as a normal sodalite at the Löwenstein limit ($\text{Si/Al} = 1$); as a silica-rich form,

$\text{N}(\text{CH}_3)_4$ -sodalite, with $\text{Si}/\text{Al} = 5$ [53]; and as a porous crystalline silica, silica-sodalite, with $\text{Si}/\text{Al} = \infty$ [54].

The only porous crystalline silica (porosil) found naturally is melanophlogite, but, including melanophlogite [55], a number of porosils have now been made (silicalites I and II, dodecasils 1H [55a] and 3C [39], silica-sodalite [54], nonasil [56], and deca-dodecasil 3R [57]). Category 5 of Table III thus includes various porosils with topologies not observed in nature. There seems no theoretical reason why, in numbers and structural diversity, porosils could not eventually compare with zeolites.

Table IV. Ranges in $\text{SiO}_2/\text{Al}_2\text{O}_3$ reported in some zeolites of categories 2 and 4 [58].

Category 2		Category 4	
Name	$\text{SiO}_2/\text{Al}_2\text{O}_3$	Name	$\text{SiO}_2/\text{Al}_2\text{O}_3$
Chabazite	2.16 - 7.8	Beta	30 - 75
Faujasite	2.2 - 6.8	ZSM-5	25 - 1000
Zeolite A	2.0 - 6.8	ZSM-11	78 - 1000
Zeolite L	2.08 - 7.0	ZSM-12	45 - 160
Paulingite	2.9	ZSM-23(EU-13)	55 - 217
Levynite	3.35 - 4.43	ZSM-48	870 - 1340
		Nu-1	40 - 120
		Fu-1	20 - 40
		Zeta-1	25 - 32
		Zeta-3	60 - 74
		KZ-1	108
		KZ-2(Nu-10)	25 - 492

4. THE GUEST-HOST INTERACTION

It has been mentioned earlier that zeolites require an alkaline, aqueous medium in order to form. The water and OH^- are mineralisers because:

- (i) Alkaline aqueous solutions dissolve the solid reactants, and so promote mixing. Dissolved species are then free to nucleate crystals or to add to the surfaces of growing crystals.
- (ii) The water acts as a space filler and stabiliser within the porous crystal. The water is a guest molecule within a continuous host structure.

Porous crystals in general will not form in the absence of a critical loading of such a stabilising guest molecule. This has a thermodynamic basis: the guest-host complex is a type of solid solution in which, by mixing, each component lowers the chemical potential of

the other. The chemical potential of the host component can by this means be reduced below the chemical potential of the empty host crystal, and often below those of non-porous alternative phases. There would be no exciting world of porous crystals to explore without the stabilising role of guest molecules in their synthesis.

This role was given a thermodynamic basis some time ago [59], and has subsequently been emphasised further [60,61]. For a two-component solution consisting of lattice-forming units of the host, and of guest molecules, the Gibbs-Duhem relation at constant temperature, T, and pressure, P, can be integrated to give the lowering of chemical potential, $\Delta\mu$, per mole of lattice-forming units of the host:

$$\Delta\mu = (\mu_H - \mu_H^0) = V_H P - \frac{M_H RT}{m_A} \int_0^{a_A} \frac{x_A}{a_A} da_A \quad (1)$$

where

μ_H = chemical potential per mole of lattice-forming units of the host, H, containing x_A g of guest A per g of host.

μ_H^0 = the corresponding chemical potential for the host free of guest molecules.

V_H = the partial molar volume per mole of lattice-forming units of the host.

a_A = the activity of the guest, A, at a loading x_A .

P = the total pressure.

The activity, a_A , may often be replaced by the equilibrium pressure, P_A , of the guest, so that the integral may be obtained by measuring the equilibrium sorption isotherm, plotting x_A/P_A against P_A , and finding the area under the curve. The total pressure P and P_A are often the same and the term $V_H P$ is normally negligible compared with the value of the integral. It follows from equation (1) that:

- (1) The more rectangular the isotherm, the greater the value of the integral and the greater the lowering, $\Delta\mu$, of the chemical potential of the host; and therefore the greater its stabilisation by the guest.
- (2) The aluminous zeolites carry the greatest framework charges and the largest numbers of charge-neutralising cations. This very high polarity means that water, a polar molecule, is very strongly sorbed to give rectangular isotherms. Therefore, according to (1), water is a space filler and stabiliser par excellence in synthesis of aluminous zeolites.
- (3) As the zeolites become progressively richer in silica, their framework charge, cation density, and polarity decrease, and with this their affinity for water. Relative to water, the sorption and stabilising role of organic molecules will become progressively more important. Water and alkalinity are still required to promote solution and mixing of reactants, but increasingly one finds a need to add organic guest molecules, B, to promote formation of silica-rich zeolites. These molecules are chosen to have solubility in water, due to one or more polar groups, and they often help

(through -NH_2 , >NH , or >N groups) to maintain high pH. The guest molecules must of course have the right shape and size to fit into the cavities and channels of the zeolite that is desired, and, apart from this requirement, their stabilising role is then determined by the rectangularity of their sorption isotherms. The lowering of chemical potential of the host lattice per mole of lattice-forming units for two guest molecules, A (H_2O) and B (organic species) is

$$\Delta\mu = V_m P - \frac{M_{\text{H}}RT}{m_A} \int_0^{P_A} \frac{x_A}{P_A} dp_A - \frac{M_{\text{H}}RT}{m_B} \int_0^{P_B} \frac{x_B}{P_B} dp_B \quad (2)$$

where activities have been replaced by partial pressure and where usually $P = (P_A + P_B)$. Since both water and the organic are sorbed competitively from the same aqueous solution it is their mixture isotherms which would be needed to evaluate the integrals.

The above treatment indicates that, apart from the spatial requirement of being able to fit into cavities or channels and that of giving as rectangular isotherms as possible, the stabilising effect is non-specific. This accounts for the large variety of guest molecules which have been shown to be effective aids in making silica-rich porous crystals. This diversity is illustrated in Table V for ZSM-5 and dodecasil-1H. Dodecasil-1H is a porous crystalline silica with 32 SiO_2 lattice-forming units per unit cell. It contains in each unit cell $3 \times$ pentagonal 12-hedra (5^12), $2 \times$ 12-hedra (4^35^63) and $1 \times$ 20-hedron (5^12^68). The two 12-hedra are spheroidal with free diameters each ~ 5.7 Å, and the 20-hedron approximates an ellipsoid of revolution with free dimensions ~ 7.7 and ~ 11.2 Å. As with ZSM-5 and dodecasil-1H, various guest molecules have been successfully used in growing silica-rich zeolites KZ-1, KZ-2, ZSM-39, and ferrierite isotypes; and also in growing melanophlogite (Kr , Xe , CO_2 , CH_4 , N_2O , or CH_3NH_2), dodecasil-3C, nonasil, and deca-dodecasil-3R. In all such syntheses, the host crystal as it grew incorporated the guest molecules. In some porosil crystals the guest molecules are locked in specific intracrystalline cavities and cannot be fully removed. For siliceous zeolites and porosils such as silicalites I and II, the guest molecules can usually be oxidised to CO_2 , H_2O , etc, and the crystals freed of organic zeolitic matter.

Table V. Guest molecule aids in syntheses of ZSM-5 and dodecasil-1H.

ZSM-5 [62]	Dodecasil-1H [63]
Tetrapropylammonium hydroxide	Piperidine
Tetraethylammonium hydroxide	2-Methylpyrrolidine
Tripropylamine	Hexamethyleneimine
Ethylenediamine	2-Methylpyridine
Ethanolamine	Cyclohexylamine
Propanolamine	4-Methylpiperidine
Methylquinuclidine	Piperazine
Ammonia + ethanol	1,2-Diaminocyclohexane
Ethanol	Quinuclidine
Glycerol	2-Propylpiperidine
n-Propylamine	1,2,2,6,6-Pentamethylpiperidine
Di-n-Propylamine	Bornylamine
Di-n-Butylamine	1-Aminoadamantane
1,5-Diaminopentane	
1,6-Diaminohexane	
Morpholine	
Pentaerythritol	
Dipropylenetriamine	
Dihexamethylenetriamine	
Diethylenetriamine	
1-Alkyl,4-aza,1-azoniabicyclo[2.2.2]octane, 4-oxide, halide	
Hexanediol	

5. TEMPLATES

Apart from their general function as fillers and stabilisers of the growing host lattices, organic and inorganic species may induce nucleation of particular zeolites which will not nucleate and grow in their absence. This can be a very specific function, in which guest molecules or ions, or hydrated inorganic cations appear to act as templates around which the crystal structure nucleates and grows [64]. In aqueous solution some anions and cations have a structure-breaking effect on water while others have a structure-making effect [65]. For example, $(\text{CH}_3)_4\text{N}^+$ and $(\text{Et})_4\text{N}^+$ are structure-making: they are believed to form around them small water "ice-bergs". Such influences may also extend to silicate and aluminate ions. For example, the water network of clathrate hydrate type I and the silica network of melanophlogite have the same topology and rather similar unit cell dimensions. This is true also of clathrate hydrate type II and dodecasil-3C (or its isotype, zeolite ZSM-39).

A fuller account of template action is given elsewhere [64]. Here, two examples of template action, respectively involving an organic moiety and inorganic moieties, will suffice. Thus Table VI [66] shows

the influence of $(\text{CH}_3)_4\text{N}^+$ (TMA^+) upon the kind of zeolite formed when the other cations present were Na^+ or K^+ . The results in the Table show that relatively small proportions of the organic ion cause mazzite to replace faujasite in a sodic system, and offretite to replace zeolite L in a potassic system. Under prescribed conditions, anions also appeared to play a template role when sodalite and cancrinite were made from kaolinite [67,68]. The conditions were 2 g of kaolinite with 200 ml of 4-M NaOH containing 10 g of the salt, reacted for 5 days at 80°C.

Table VI. Dependence of zeolite type on the presence or absence of TMA^+ . Mixtures with $\text{SiO}_2/\text{Al}_2\text{O}_3 = 16-20$; $\text{H}_2\text{O}/\text{SiO}_2 = 14-20$; $T = 100^\circ\text{C}$, static conditions [66].

Zeolite grown	OH^-/SiO_2	Na^+/SiO_2	$\text{TMA}^+/\text{SiO}_2$	K^+/SiO_2
Zeolite Y ^a	0.8	0.8	0	0
ZSM-4 ^b	0.8	0.8	0.04	0
Zeolite Q ^b	0.7	0.6	0.14	0
Zeolite L ^c	0.8	0	0	0.8
TMA-0 ^d	0.9	0.09	0.09	0.8
TMA-offretite	1.1	0.10	0.10	0.7

^a Faujasite type

^c No natural counterpart

^b Mazzite type

^d Offretite type

6. NUCLEATION

Several steps and areas of study which can be involved in making a zeolite have been given as follows:

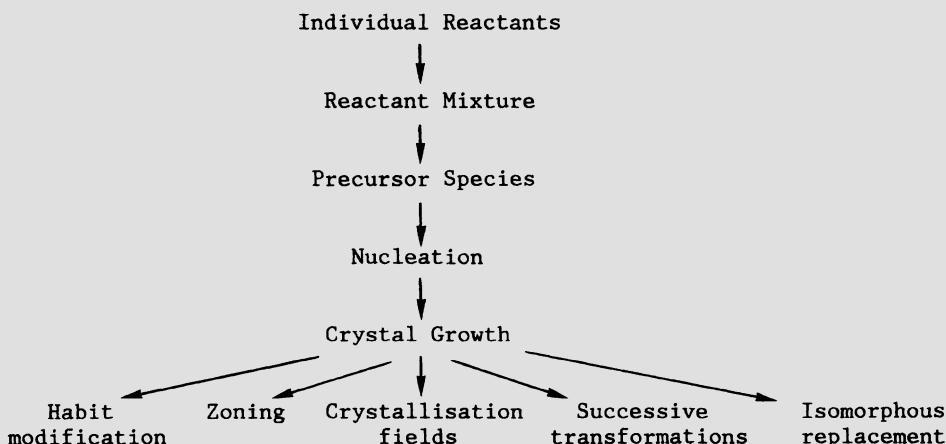


Table VII. Sodalite and cancrinite formation from kaolinite and alkaline salt solutions [67,68].

Sodalite with:	Cancrinite with:
NaOH aq only	Na ₂ SO ₄ added
NaCl added	Na ₂ SeO ₄ added
NaBr added	Na ₂ CrO ₄ ^c added
NaI added	Na ₂ MoO ₄ added
NaF ^a added	2 g Na ₂ FeO ₄ + Fe ^{III} + 12-M NaOH ^d
NaClO ₃ added	Na ₃ VO ₄ added
NaClO ₄ added	NaMnO ₄ added (large excess)
Na ₂ SO ₃ added	NaNO ₃
Na ₂ S ^b added	Cu(NH ₃) ₄ SO ₄ + excess NH ₃ added ^e
Na ₂ WO ₄ added	
Na ₃ PO ₄ added	
HCOONa added	
CH ₃ COONa added	
(COONa) ₂ added	

^a No evidence of intercalated NaF

^b Pale blue crystals

^c Pale yellow crystals

^d Pale brown crystals and another species

^e Pale blue crystals

In this section we consider nucleation in particular. The combination of nucleation and crystal growth leads to sigmoid curves of yield of crystals (as weight %) against time, as illustrated for mordenite in Fig. 1 [69]. The period during which no crystallisation can be detected is termed the induction time, although a strict measure of its duration is difficult to give. It is certainly not a period free of chemical happenings. There is next an interval during which the yield rate accelerates with time followed by one in which this rate decays asymptotically towards zero, as the chemical nutrients become exhausted.

During the induction period, and after, one may assume that, through chemical fluctuations, germ nuclei appear and disappear. Attention has earlier been drawn to the mobile equilibrium between various silicate anions in silicate solutions. The germ nuclei are composed of a small number, j , of lattice-forming units, but they are unstable because of positive free energy terms. One of these, Δg_0 , arises from the surface tension between the germ and the ambient medium. It is proportional in size to the surface area and hence to $j^{2/3}$. A second positive free energy term will arise if nucleation occurs in a restraining matrix, because of misfit. This strain free energy term, Δg_s , will be proportional to j . Thus, the free energy of formation of germ nucleus can be written as follows [10]:

$$\Delta g_j = \frac{j \Delta G}{N_A} + \Delta g_o + \Delta g_s \\ = -A_j + B_j^{2/3} + C_j \quad (3)$$

where ΔG is the negative free energy of formation of bulk zeolite containing Avogadro's number, N_A , of lattice-forming units and A , B , and C are positive coefficients. Initially the germ nuclei are not viable, i.e., the sum of two positive free energy terms is dominant.

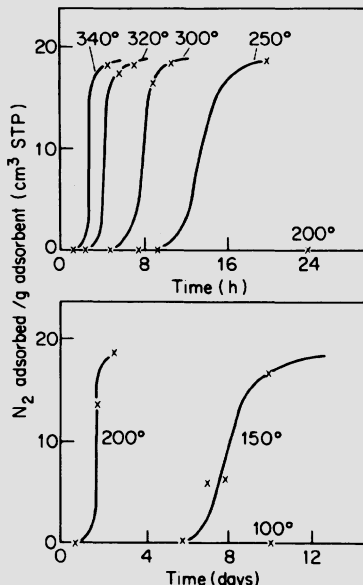


Figure 1. Characteristic sigmoid crystallisation curves illustrated for mordenite [69]. These show the strong effect of temperature upon nucleation and growth. Nitrogen sorption was used to estimate the yield of mordenite.

However, there is a turning point given by

$$d(\Delta g_j)/dj = 0 \quad (4)$$

so that the value of j at this point is given by

$$j = \frac{8}{27} \left[\frac{B}{A-C} \right]^3 \quad (5)$$

For values of j greater than this, addition of lattice-forming units occurs with a reduction in free energy and the nucleus has become viable, i.e., it will grow spontaneously into a crystal. The above behaviour is represented in Fig. 2 [70]. After a time interval, through chance buildup of nuclei to the critical size, one can expect a current of nuclei passing the saddlepoint. This current will grow to a maximum and will then decay towards zero as a greater and greater proportion of chemical nutrients is claimed by the growing crystals, with their much larger and constantly increasing total surface area, and also as the chemical nutrients become exhausted.

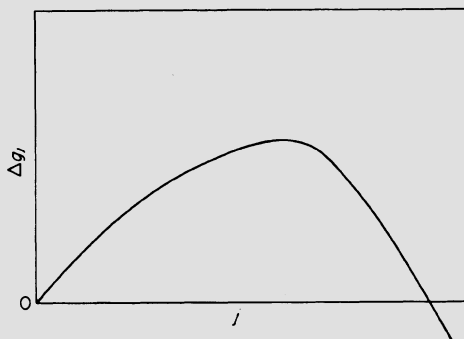


Figure 2. Formal representation of the free energy of formation, Δg_j , of a germ nucleus, composed of j structural units, as a function of j [70].

The above treatment does not tell us about events at the molecular level, but it is physically reasonable and has generality. Thus it applies equally to simpler systems such as nucleation and growth of salt crystals where the lattice-forming units are Na^+Cl^- pairs. However, whereas salt crystallisation leads only to one crystal structure, the complex nature of the magmas and solutions from which zeolites form can result in various chemical pathways, each leading to a different zeolite. There is not one but often a number of possible equations like equation (3), each involving a different kind of lattice-forming unit, and different coefficients A, B, and C. In zeolite synthesis we seek conditions under which the dominant current of germ nuclei across the saddlepoint of the relevant curve of Δg_j vs j is that of the zeolite we wish to synthesise.

7. CRYSTAL GROWTH

Analysis of sigmoid curves of yield (wt. % of crystals) against time, in which nucleation and growth are combined, would be assisted if the actual rates of deposition on growing crystals could be obtained. Several studies of this kind have been made.

Example 1. Kacirek and Lechert [71] analysed curves of percentage yield of faujasites (X and Y) against time when growth occurred largely on seeds. Seeds of Na-X of uniform size were used, and their linear growth rate was defined as

$$k = 0.5 \Delta l / \Delta t \quad (6)$$

where Δl is the increase in linear dimensions of a seed in time Δt . The chemical nutrients for growth were supplied from an aqueous hydrogel to which the seeds were added. It was assumed that

- (1) the linear growth rate was constant, irrespective of crystal size;
- (2) the yield (wt %) increased at a rate proportional to the total surface area of the crystals;
- (3) the compositions of gel and crystals were the same (not generally true); and
- (4) the number of crystals does not change with time (i.e., the effect of any fresh nuclei on the yield is minimal compared with the growth on the seed crystals).

With these assumptions, and starting with crystals of nearly the same size, idealised as spheres, all initially of radius r_0 , the equation for yield against time was

$$x = x_0 \left[1 + \frac{kt}{r_0} \right]^3 \quad (7)$$

where x_0 is the fraction of the total mass of gel and crystals which is seeds at time $t = 0$; and x is this fraction at time t . The term k is the linear growth rate of equation (4). This equation describes much of the course of the curves of yield against time, as shown in Fig. 3 [71]. Only as exhaustion of nutrients was approached were there deviations from the experimental curves. The linear growth rate constants, k , were evaluated from

$$k = \left[\left[\frac{x}{x_0} \right]^{1/3} - 1 \right] \frac{r_0}{t} \quad (8)$$

where x , x_0 , and r_0 are all measured quantities. They had large positive temperature coefficients indicative of the kinetic control of growth, not by diffusion in the aqueous medium, but by a chemical process as lattice-forming units combine with the growing surface of the crystals.

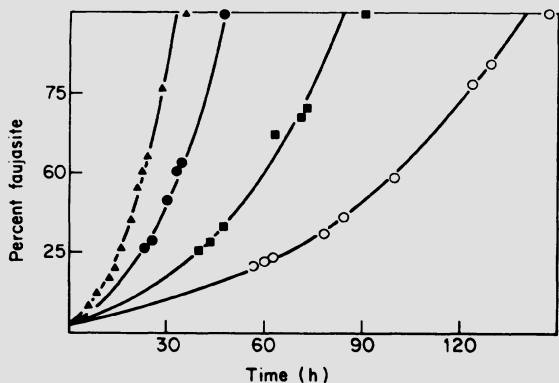


Figure 3. Crystallisation rates for faujasite growth from aqueous alkaline gel on seeds of faujasite (Na-X) for four different samples at 58, 68, 78, and 88°C. The full curves are calculated from equation (7) [71].

Example 2. Zdhanov and Samulevich [72] analysed curves of yield against time, without seeding, and starting from the aqueous gel. The analysis involved

- (1) measurement of the size distribution of the crystals in the final product; and
- (2) measurement of the linear dimensions of the largest crystals at each of a series of times. This involved stopping successively each of a series of identical synthesis runs.

The results of (2) confirmed (as assumed by Kacirek and Lechert [71]) that linear growth rates were indeed constant until near exhaustion of chemical nutrients, as seen in Fig. 4 [72]. Zdhanov and Samulevich, as a reasonable extension, assumed that all crystals grew at the same rate, whether the crystals were large or small, not only over the first parts of the curves of linear growth against t but also when linear growth rates were declining, near the end of any run. Therefore, for any crystal in the final product, knowing the growth rate, one could say at what time the germ of that crystal became a viable nucleus growing spontaneously. Thus, Fig. 5 [72] shows an experimental linear growth rate and a histogram of the final size distribution. A crystal of linear dimensions $4.5 \mu\text{m}$, for instance, formed from a nucleus which became viable after ~ 132 minutes, while one of dimension $16.5 \mu\text{m}$ was born after about 89 minutes, and so on.

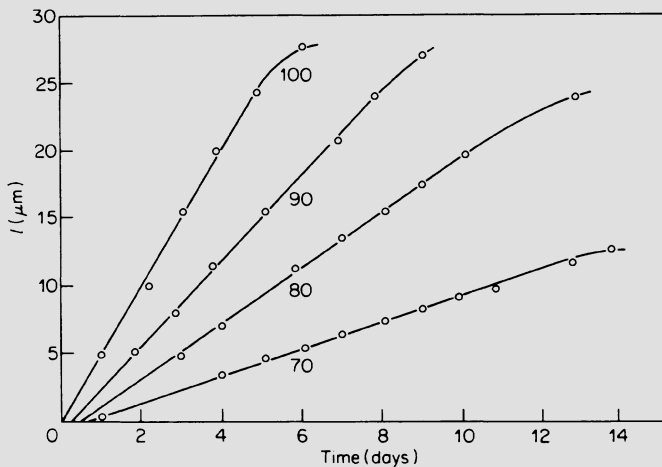


Figure 4. Growth in crystal size of the largest crystals in the faujasite zeolite Na-X [72]. The crystals were grown from gels at the temperatures ($^{\circ}\text{C}$) indicated by the figures on the graphs.

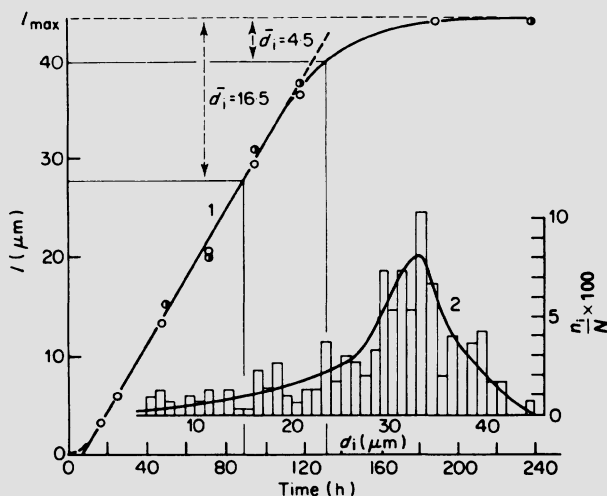


Figure 5. Curve 1 gives the linear growth rate of the largest crystals. Curve 2 is a histogram of the final crystal size distribution [72].

Finally, Fig. 6 [72] shows again the linear growth rate curve of the previous figure (curve 1); the nucleation rate (curve 2) derived from the final size distribution and linear growth rate; and the yield of faujasite against time derived from curves 1 and 2. This curve is sigmoid and was close to experimental points of yield against time.

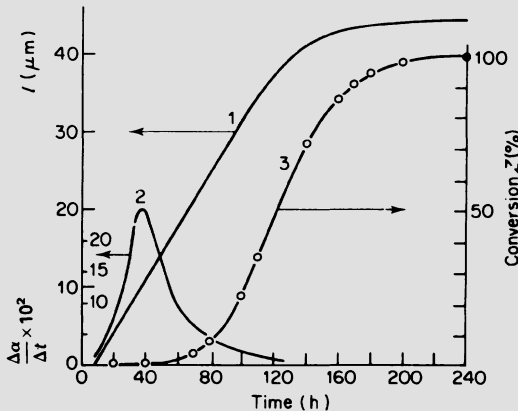


Figure 6. Curve 1 is curve 1 of Fig. 5. Curve 2 shows the change in nucleation rate with time, derived from curve 1 and the histogram of Fig. 5. Curve 3 gives the sigmoid graph of yield (wt %) against time derived from curves 1 and 2 [72].

The rate of nucleation peaks sharply and then declines towards zero as time increases. Most of the nucleation occurred before any significant mass of crystals had formed. Once crystals begin to grow, they compete with fresh nuclei for the chemical nutrients and, as predicted in Fig. 6, this competition largely suppresses formation of fresh nuclei in favour of crystal growth. According to this analysis, the more the nucleation rate curve overlaps the curve of yield against time, the wider should be the size distribution in the final yield of crystals. Conversely, the less this overlap, the more uniform the final crystal size should be.

Linear growth rate constants, k , have, as already mentioned, large temperature coefficients, as shown below for faujasite [72]:

T / °C	$k / \mu\text{m h}^{-1}$
70	0.0175
80	0.0375
90	0.0625
100	0.1071

Activation energies, E, for linear growth rates, based on the expression $k = k_0 \exp(-E/RT)$, appear to increase with the Si/Al ratio in the faujasites formed, as seen in the tabulation which follows [71]:

Si/Al	E/kcal mol ⁻¹
1.53	11.8
1.78	12.3
2.20	14.1
2.54	15.6

These energies of activation are too large for rate control by diffusion of chemical nutrients in the aqueous phase ($E \sim 5$ kcal mol⁻¹). They suggest control by condensation of structural units from solution onto the growing crystal surfaces, involving elimination of hydroxyl water between the structural unit and the surface. This process would be of two kinds:



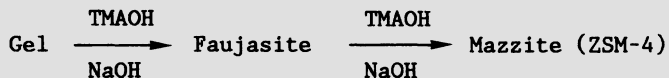
The more siliceous the zeolite, the greater the proportion of the second reaction, so that if E were larger for the second than for the first reaction, the rise in E with Si/Al ratio would be accounted for.

8. OSTWALD'S RULE OF SUCCESSIVE TRANSFORMATIONS

It is often the case that the first zeolite to appear is not stable when left for a longer time at the reaction temperature in contact with its mother liquor. The first-formed crystals slowly dissolve; a new type of zeolite nucleates and grows, thus consuming the first. Indeed this process may be repeated more than once, so that the second zeolite is consumed at a later time by yet another. Because the second zeolite usually has a different morphology and crystal size, rather than being a pseudomorph of the first, the transformation of the first into the second can reasonably be ascribed to a solution mechanism rather than to a solid-state rearrangement of the lattice of the first zeolite to give that of the second.

Thus it seems that the successive crystallisations, under given reaction conditions, proceed down a ladder of increasing stability, rung by rung. The zeolite which is least different in stability from the aqueous gel nucleates most readily, i.e., in the shortest time. This emphasises that kinetics rather than thermodynamics regulates nucleation. The theoretical kinetic explanation of this behaviour does not appear to have been given, but there are many instances of the

Ostwald rule in zeolite chemistry. One example is shown in Fig. 7 for the sequence:



To effect this sequence, the ratio TMA^+/Na^+ is adjusted as in Table VI. If the metastable crystals are isolated from the mother liquor once they have formed, they remain thereafter quite stable, which is further evidence of a solution mechanism for their transformation when in contact with the mother liquor. Many zeolites owe their preparation to this fact.

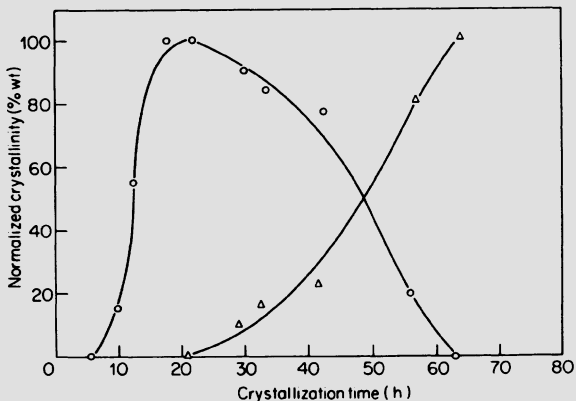


Figure 7. Yields of crystals against time at about 100°C. The ratio $\text{TMA}^+/(TMA^+ + \text{Na}^+)$ is such as ultimately to yield only mazzite (ZSM-4). Faujasite (o) appears first and then is progressively replaced by mazzite (Δ) [66].

9. SOME REACTION VARIABLES

Factors (other than such variables as temperature, composition, and pressure) which may determine the zeolite which crystallises include:

- (1) The nature of the reactants and their pretreatments.
- (2) Local composition variations in the aqueous magma.
- (3) Addition of special components (templates, trace impurities, dyestuffs).
- (4) The sequence in which components are added to the reaction mixture.
- (5) Low-temperature aging of the reaction mixture.
- (6) Excess alkalinity and pH.
- (7) Seeding.
- (8) Time.

Several of these factors have been considered earlier, such as the role of templates and the effect of time (sections 6, 7, and 8). Here we comment upon the factors (1) and (6) only. An account of the others is given elsewhere.

9.1. The Nature and History of Reactants

An illustration of the importance of the reactants and their pre-treatment is provided by the action of aqueous $\text{Ba}(\text{OH})_2 + \text{LiOH}$ upon kaolinite (oxide formula $\text{Al}_2\text{O}_3 \cdot \text{SiO}_2 \cdot 2 \text{H}_2\text{O}$) and upon metakaolinite (oxide formula $\text{Al}_2\text{O}_3 \cdot 2 \text{SiO}_2$). These materials, both with and without added silica, were sources of aluminium and silicon. The metakaolinite was obtained from the kaolinite by heating the kaolinite to 500-550°C. The reaction products given below were entirely different [73]:

From Metakaolinite	From Kaolinite
(Li, Ba) - ABW (zeolite)	(Ba, Li) - Q (like yugawaralite)
(Ba, Li) - edingtonite	(Ba, Li) - P* (non-zeolite, like cymrite)
(Ba, Li) - G, L (like zeolite LTL)	(Ba, Li) - T (a silicate)
(Ba, Li) - N (unidentified)	

Conversion of kaolinite to metakaolinite altered dramatically the dominant nucleation process under otherwise similar conditions of temperature, pressure, and overall composition.

9.2. Excess Alkalinity and pH

Within the crystallisation field of a given zeolite, increasing the alkalinity has a similar effect upon the kinetics of crystallisation as a rise in temperature. This is illustrated in Fig. 8 [69] for mordenite synthesis from gels at a series of increasing pH values. This figure is to be compared with Fig. 1 for the same zeolite at a series of increasing temperatures. Fig. 8 also shows that at pH 13.3 the mordenite first formed dissolves. Its successor is analcime.

The pH can also modify the Si/Al ratio in the zeolite. This can be seen in Fig. 9 [74] for chabazite- and edingtonite-type zeolites, K-G and K-F, respectively. The greater the concentration of KOH, the more nearly do the Si/Al ratios approach the Löwenstein limit of unity. If one keeps the concentration of the KOH constant but increases the volume of the solution, the smaller is the final yield of each of these two zeolites (Fig. 10) [74].

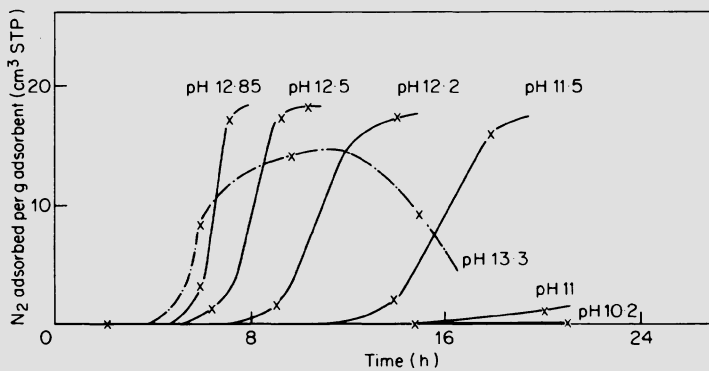


Figure 8. Influence of pH upon curves of yield against time for mordenite synthesis at 300°C [69].

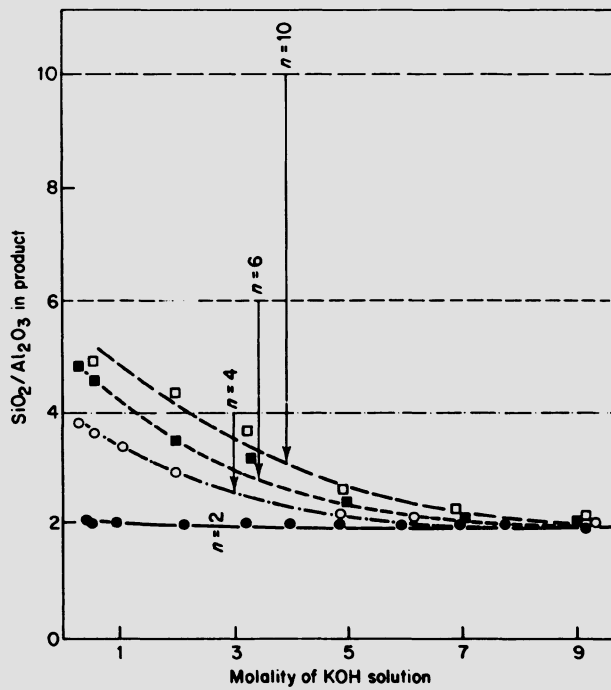


Figure 9. Effect of concentration of KOH solution upon the ratio SiO₂/Al₂O₃ in resultant zeolite crystals. The products are primarily chabazite-type K-G and edingtonite-type K-F [74].

The solution retains a larger amount of dissolved material, the greater the volume of solution at constant alkali concentration. This result suggests that zeolites exhibit a kind of solubility in their mother liquor. However, the ionic species in solution are not necessarily directly related to structural units of the zeolite framework. In silicate solutions, various silicate anions can co-exist in mobile equilibrium inter se. Aluminate solutions at high pH are simpler in that $\text{Al}(\text{OH})_4^-$ is the dominating species. In alumino-silicate solutions oxy-anions containing both Al and Si are possible [75].

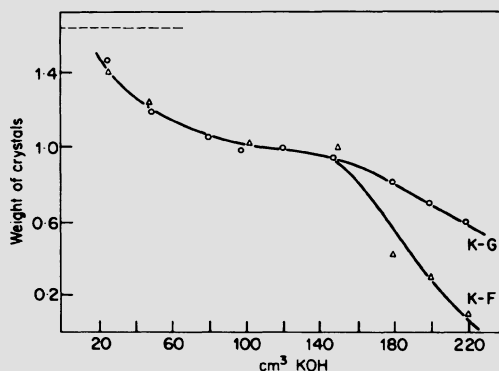


Figure 10. Effect of volume of KOH solution of constant concentration upon the yield of crystals from metakaolinite. \circ : 1-M KOH giving chabazite-type K-G; Δ : 6-M KOH giving edingtonite type K-F [74].

10. CONCLUDING REMARKS

For reasons of brevity, the important area of isomorphous substitution by direct crystal growth [76] has not been discussed, except for Al and Si. Framework substitutions of Al by Ga and Si by Ge can be extensive or complete; also, limited substitution of Al by Fe^{III} , B^{III} , Cr^{III} and the like has been claimed. Complete substitutions of the type



in crystalline forms of SiO_2 and of AlPO_4 having the same framework topologies are known [77]. Recently, by using organic molecules as templates and fillers, many porous AlPO_4 phases have been made, some of which, when the organic moiety is burnt out, can yield stable frameworks that are porous on the scale of molecules in the same way as zeolites. This subject is discussed by Rabo in the next chapter of this book. These AlPO_4 's, as they have been termed, are made from aluminium phosphate gels at considerably lower pH than zeolites [78].

Substitutions in AlPO's of the type



have recently been claimed [79] (the SAPO's); and also that of such metals, M, as Co^{II}, Zn^{II}, Mn^{II} and Mg^{II}, into the AlPO framework (the MAPO's) [80]. However, isomorphous substitution is too large an area to be dealt with here. The purpose of the present account has been to illustrate and discuss some of the features of aluminosilicate zeolite synthesis, and to give an idea of the scope and richness of this area of silicate science.

11. REFERENCES

1. A.F. Cronstedt, Akad. Handl. Stockholm 17, 120 (1756).
2. R.M. Barrer, Pure Appl. Chem. 51, 1091 (1979).
3. R.M. Milton, U.S. Patent 2,882,244 (1959).
4. D.W. Breck and N.A. Acara, U.S. Patent 3,216,789 (1965).
5. Union Carbide, U.S. Patent 3,414,602 (1968).
6. R. Aiello and R.M. Barrer, J. Chem. Soc. A, 1470 (1970).
7. R.M. Barrer and E.A.D. White, J. Chem. Soc., 1167 (1951).
8. R.M. Barrer, J. Chem. Soc., 127 (1948).
9. R. Wadlinger, G.T. Kerr, and E.J. Rosinski, U.S. Patent 3,308,069 (1967).
10. H.E. Robson, D.P. Shoemaker, R.A. Ogilvie, and P.C. Manor, Adv. Chem. Ser. 121, 106 (1973).
11. W. Sieber and W.M. Meier, Helv. Chim. Acta 57, 1533 (1974).
12. J. Ceric, U.S. Patent 3,411,874 (1968).
13. G. Kokotailo and J. Ceric, Adv. Chem. Ser. 101, 109 (1971).
14. M.K. Rubin, E.J. Rosinski, and C.J. Planck, U.S. Patent 4,151,189 (1979).
15. P.Chu, U.S. Patent 3,709,979 (1973).
16. E.J. Rosinski and M.K. Rubin, U.S. Patent 3,832,449 (1974).
17. D.H. Olson, E.W. Valyocsik, and R.B. Calvert, Eur. Patent A0102716 (1984).
18. C.J. Plank, E.J. Rosinski, and M.K. Rubin, U.S. Patent 4,076,842 (1978).
19. J.L. Schlenker, F.G. Dwyer, E.E. Jenkins, W.J. Rohrbaugh, G.T. Kokotailo, and W.M. Meier, Nature (London) 294, 340 (1981).
20. R.M. Barrer and P.J. Denny, J. Chem. Soc., 971 (1961).
21. G.T. Wadlinger, E.J. Rosinski, and C.J. Plank, U.S. Patent 3,375,205 (1968).
22. G.T. Kerr, Inorg. Chem. 5, 1537 (1966).
23. G.H. Kuhl, Inorg. Chem. 10, 2488 (1971).
24. R.M. Barrer and D.J. Marshall, J. Chem. Soc., 2296 (1964).
25. H.C. Duecker, A. Weiss, and C.R. Guerra, U.S. Patent 3,567,372 (1971).
26. R.M. Barrer and D.E Mainwaring, J. Chem. Soc., Dalton Trans., 2534 (1972).
27. C. Colella and R. Aiello, Annali di Chimica 61, 721 (1971).

28. G.T. Kerr, Science 140, 1412 (1963); Inorg. Chem. 5, 1539 (1966).
29. E.M. Flanigen, J.M. Bennett, R.W. Grose, J.P. Cohen, R.L. Patton, R.M. Kirchner and J.V. Smith, Nature (London) 271, 512 (1978).
30. D.M. Bibby, N.B. Milestone, and L.P. Aldridge, Nature (London) 280, 664 (1979).
31. R.W. Grose and E.M. Flanigen, U.S. Patent 4,104,294 (1978).
32. D.A. Hickson, U.K. Patent Appl. GB 2,079,735A (1981).
33. T.V. Whittam, Eur. Patent A0059059 (1982).
34. S.A.I. Barri, H. Phillip, and C.D. Telford, Eur. Patent A0057049 (1982).
35. P.J. Hogan, A. Stewart, and T.V. Whittam, Eur. Patent A0065400 (1982).
36. Idemitsu Kosan Co., Japan Pat. Appl. 154,037 (1982).
37. L.M. Parker and D.M. Bibby, Zeolites 3, 8 (1983).
38. K. Takatsu and N. Kawata, Eur. Patent A102497 (1984).
39. H. Gies, Z. Kristallogr. 167, 73 (1984).
40. J.L. Casci, B.M. Lowe, and T.V. Whittam, U.K. Patent Appl. 2,077,709A (1981).
41. L. Marosci, M. Schwartzmann, and J. Stabenow, Eur. Patent A0046504 (1982).
42. A. Araya and B.M. Lowe, J. Catal. 85, 134 (1984).
43. R.M. Barrer, Hydrothermal Chemistry of Zeolites, p. 212, Academic Press, London (1982).
44. H. de St. Claire Deville, C.R. Séances Acad. Sci. 54, 324 (1862).
45. P. Niggli and G.W. Morey, Z. Anorg Allg. Chem. 83, 369 (1913).
46. G.W. Morey and E. Ingerson, Econ. Geol. 32, 607 (1937).
47. R.M. Barrer, J. Soc. Chem. Ind. 64, 130 (1945).
48. R.M. Barrer and L. Belchetz, J. Soc. Chem. Ind. 64, 131 (1945).
49. R.M. Barrer, J. Soc. Chem. Ind. 64, 133 (1945).
50. R.M. Barrer, Brit. Chem. Eng. May Issue, p. 1 (1959).
51. D.W. Breck and E.M. Flanigen, in Molecular Sieves, (Soc. Chem. Ind.), p. 47 (1968).
52. Ref. 43, p. 262.
53. C. Baerlocker and W.M. Meier, Helv. Chim. Acta 52, 1853 (1969).
54. D.M. Bibby and M.R. Dale, Nature (London) 317, 157 (1985).
55. H. Gies, H. Gerke, and F. Liebau, Neues Jahrb. Mineral Monatsh. 3, 119 (1982).
- 55a. H. Gerke and H. Gies, Z. Kristallogr. 166, 11 (1984).
56. F. Liebau, personal communication.
57. H. Gies, Z. Kristallogr. 175, 93 (1986).
58. Ref. 43, p. 253.
59. R.M. Barrer, J. Phys. Chem. Solids 16, 84 (1960).
60. R.M. Barrer, Philos. Trans. R. Soc. London A311, 333 (1984).
61. R.M. Barrer, in Zeolites, Synthesis, Structure, Technology and Application, (Eds. B. Drzaj, S. Hocevar, and S. Pejovnik), p. 1, Elsevier (1985).
62. B.M. Lok, T.R. Cannan, and C.A. Messina, Zeolites 3, 282 (1983).
63. H. Gies, Nachr. Chem. Tech. Lab. 33, 387 (1985).
64. Ref. 43, pp. 157-170.
65. Y. Marcus, J. Chem. Soc., Faraday Trans. 1 82, 1 (1986).
66. L.D. Rollmann, Adv. Chem. Ser. 173, 387 (1979).

67. R.M. Barrer, J.F. Cole, and H. Sticher, J. Chem. Soc. A, 2475 (1968).
68. R.M. Barrer and J.F. Cole, J. Chem. Soc. A, 1516 (1970).
69. D. Dominé and J. Quobex, in Molecular Sieves, (Soc. Chem. Ind.), p. 78 (1968).
70. Ref. 43, pp. 133-137.
71. H. Kacirek and H. Lechert, J. Phys. Chem. 79, 1589 (1975); and 80, 1291 (1976).
72. S.P. Zdhanov and N.N. Samulevich, Proc. 5th Int. Conf. Zeolites (Ed. L.V.C. Rees), p. 75, Heyden (1980).
73. R.M. Barrer, R. Beaumont, and C. Colella, J. Chem. Soc., Dalton Trans., 934 (1974).
74. R.M. Barrer and D.E. Mainwaring, J. Chem. Soc., Dalton Trans., 1254 (1972).
75. Ref. 43, pp. 106-119.
76. Ref. 43, Chap. 6.
77. Ref. 43, p. 294.
78. S.T. Wilson, B.M. Lok, and E.M. Flanigen, U.S. Patent 4,310,400 (1982).
79. B.M. Lok, C.A. Messina, R.L. Patton, R.T. Gajek, T.R. Cannan, and E.M. Flanigen, J. Am. Chem. Soc. 106, 6092 (1984).
80. N.J. Tapp, N.B. Milestone, and L.J. Wright, J. Chem. Soc., Chem. Commun., 1801 (1985).

NEW DIRECTIONS IN MOLECULAR SIEVE SCIENCE AND TECHNOLOGY

Jule A. Rabo
Union Carbide Corporation
Old Saw Mill River Road
Tarrytown, New York 10591
USA

ABSTRACT. Progress in molecular sieve science and technology is reviewed in the fields of synthesis, catalyst characterization, and catalysis. In synthesis, the molecular sieve crystal types and compositions have been greatly expanded from zeolites and pure silica materials to aluminophosphate-based molecular sieves representing more than two dozen crystal structures and many more chemical compositions, with up to six framework metals chosen from 13 elements. These new molecular sieves represent a variety of chemical properties, and they display weak to medium-strong acid catalytic activity.

Advances in crystal characterization have been made in X-ray crystallography and in electron microscopy by the use of reiterative refinements using independently determined parameters. NMR-MAS has grown to be the most effective tool to describe the environment, and possibly the ordering, of framework cations. Far infrared spectroscopy has the potential to provide detailed information characterizing the chemical environment of extra-framework cations and small occluded metal clusters.

Catalysis with silicon-enriched Y zeolites and with aluminophosphate-based molecular sieves provides new technological opportunities in catalytic cracking and in shape-selective catalysis, including conversion of methanol to small alkenes, oligomerization of alkenes, and synthesis of p-xylene.

1. INTRODUCTION

Progress in zeolite science and technology has gained new momentum in recent years. Major advances have been achieved in the discovery of new molecular sieves, expanding the portfolio of known microporous crystals from zeolites and pure silica structures to new compositions. The characterization of microporous materials has greatly expanded, particularly by the application of solid-state NMR spectroscopy and by improved techniques in electron microscopy and crystallography. The large family of recently discovered new crystal structures and composi-

tions provides new opportunities in catalysis for new applications. Thirty five years after the discovery of synthetic zeolites Linde® A and Linde® X, there is no sign of maturity either in zeolite science or in zeolite technology. It seems that this field is capable of continuous expansion both in the materials science and in application to technology.

This review gives a brief account of recent progress in molecular sieve synthesis, characterization, and catalysis. The term molecular sieve, instead of zeolite, is used here with the intention to reflect the expansion of the materials base from metal aluminosilicate zeolites to microporous crystals of new compositions. Completeness is not the objective of this review. The intention is, rather, to point to principal areas of progress, using representative examples from the literature.

2. SYNTHESIS OF A NEW GENERATION OF MOLECULAR SIEVES

In this review the topic of synthesis covers both the primary synthesis work as well as important secondary chemical modifications of molecular sieve crystals. The first is the source of new crystal forms, pore structures, and new chemical compositions, while the latter leads to changes in composition and chemical or catalytic properties, without substantial changes in the crystal framework. In chemical modifications, preference is given to chemical substitution over the thermal or hydrothermal modifications often described in the earlier literature.

2.1. Synthesis of Aluminophosphate Type Molecular Sieves

Several families of new molecular sieves based on a novel aluminophosphate family have been recently described by Flanigen *et al.* [1]. These materials may consist of Al and P as the only tetrahedral framework atoms (T), or they may include additional T atoms chosen from 13 elements, with valence from one to five. These new compositions may contain up to six different T elements. The whole aluminophosphatebased molecular sieve family represents more than two dozen crystal structures and about 200 chemical compositions.

The aluminophosphate-based molecular sieves are synthesized by hydrothermal crystallization from reactive aluminophosphate gels containing all the framework elements and an organic template. The organic template plays a structure-directing role, and upon synthesis it is incorporated in the structural voids of the crystal.

The aluminophosphate-based materials are classified on the basis of composition and crystal structure. With the composition formula $(El_x, Al_y, P_z)O_2$, where El represents one or several additional T elements, a set of acronyms has been adopted; for example, the $(Al, P)O_2$ is AlPO₄, the $(Si_x, Al_y, P_z)O_2$ is SAPO, and more complex compositions are MeAPO, MeAPSO or ElAPO, ElAPSO, with Me or El representing additional T elements.

The major structures of the aluminophosphate ($AlPO_4$)-based molecular sieve family represent a large variety of crystal forms

Table I. Typical structures in AlPO₄-based molecular sieves [1].

Species	Structure type	Pore size/ nm	Saturation H ₂ O Pore Vol/cm ³ g ⁻¹
Large Pore			
5	Novel,determined	0.8	0.31
36	Novel	0.8	0.31
37	Faujasite	0.8	0.35
40	Novel	0.7	0.33
46	Novel,determined	0.7	0.28
Intermediate Pore			
11	Novel,determined	0.6	0.16
31	Novel	0.65	0.17
41	Novel	0.6	0.22
Small Pore			
14	Novel,determined	0.4	0.19
17	Erionite	0.43	0.28
18	Novel	0.43	0.35
26	Novel	0.43	0.23
33	Novel	0.4	0.23
34	Chabazite	0.43	0.3
35	Levynite	0.43	0.3
39	Novel	0.4	0.23
42	Linde Type A	0.43	0.3
43	Gismondine	0.43	0.3
44	Chabazite-like	0.43	0.34
47	Chabazite-like	0.43	0.3
Very Small Pore			
16	Novel	0.3	0.3
20	Sodalite	0.3	0.24
25	Novel	0.3	0.17
28	Novel	0.3	0.21

including 15 novel structures as well as several structures with topologies related to zeolite crystals (Table I). Each structure type is identified by a number. Thus, AlPO₄-5 or other AlPO₄-acronyms specifically identify the chemical compositions and the type of crystal structure. The numbers identifying the structure are arbitrarily chosen, and they do not relate to structures used for identifying zeolites (ZSM-5, etc) or minerals. In Table I the important crystal forms are arranged according to pore size, showing crystals with large, intermediate, small, and very small pores. It should be noted that these new molecular sieves display the whole pore size range represented by zeolites. Significantly, there are five large-pore materials with

pore sizes similar to those of large-pore zeolites Y or L, and three intermediate-pore materials with each representing a novel crystal form. Table I also gives information concerning the pore volumes of the various species. It also indicates the structure type, if known, and whether the crystal structure has been determined.

The binary aluminophosphate molecular sieve family AlPO₄ exhibits constant chemical composition with an Al to P ratio of unity. This fixed composition provides electrically neutral framework structures. Consequently, there are no extra framework cations or protic acidity. The binary aluminophosphates are mildly hydrophilic, in contrast to the strongly hydrophilic zeolites and hydrophobic silica molecular sieves. The AlPO₄ crystals generally have excellent thermal and hydrothermal stability, similar to that of stable zeolites.

The ternary SAPO molecular sieves represent an important family of aluminophosphate-based materials with a structural diversity exceeding that of the AlPO₄ materials. Here, in addition to structures also found with AlPO₄ materials, several new crystal types were synthesized with either large or intermediate pore sizes (Table II). If one considers the presence of silicon as a result of a T atom substitution into an aluminophosphate framework, then the silicon appears mainly to replace the phosphorus. Such a mechanism leads to a framework with a net negative electric charge on the (AlO₄) unit adjacent to the P-deficient (TO₄) site. The consequence of such a structural arrangement is the presence of exchangeable cations, which may include metal ions or H⁺. As a result of increased polarity provided by the net negative framework charge and the exchangeable cations, the SAPO materials display moderate to high hydrophilic character. In addition, in the protic form, all SAPO species display a wide spectrum of carboniogenic catalytic activity. The SAPO materials also show high thermal and hydrothermal stability, similar to that of the AlPO₄ crystals.

The other ternary and multicomponent materials may contain one or more species from a group of 13 elements, including several transition metals. With these materials the theoretical T atom "substitution mechanism" envisioned for the incorporation of new elements is different and more complex than that envisioned for the SAPO's. Here, bi- and trivalent metals seem to substitute for aluminum, giving rise to a net negative (Me²⁺) or neutral (Me³⁺) framework charge. Similar to those of SAPO's, these negatively charged frameworks also display ion-exchange properties. They can be prepared in protic form, displaying acid catalytic activity.

The thermal and hydrothermal stabilities of the MeAPO, MeAPSO, ElAPO, and ElAPSO families identified in Tables II and III are more diverse than those of the AlPO₄ and SAPO families. Here, the stability depends on both chemical composition and crystal form. Many species display stability similar to that of AlPO₄'s and SAPO's, while others show significantly reduced crystal retentions when exposed to high temperatures or severe hydrothermal conditions.

Table II. Selected structures and compositions in binary, ternary and quaternary systems [1]^a.

Structure type	AlPO ₄	SAPO	MeAPO	(Me elements)	MeAPSO	(Me elements)
Large pore						
5	X	X	X	(Co,Fe,Mg,Mn,Zn)	X	(Co,Fe,Mg,Mn,Zn)
36	-	-	X	(Co,Mg,Mn,Zn)	X	(Co,Mg,Mn,Zn)
37	-	X	-		-	
40	-	X	-		-	
46	-	-	-		X	(Co,Fe,Mg,Mn,Zn)
Intermediate pore						
11	X	X	X	(Co,Fe,Mg,Mn,Zn)	X	(Co,Fe,Mg,Mn,Zn)
31	X	X	-		X	(Co,Fe,Mg,Mn,Zn)
41	-	X	-		-	
Small pore						
14	X	-	X	(Mg,Zn)	-	
17	X	X	X	(Co,Fe,Mg)	X	(Co)
34	-	X	X	(Co,Fe,Mg,Mn,Zn)	X	(Co,Fe,Mg,Mn,Zn)
44	-	X	X	(Co,Mg,Mn,Zn)	X	(Co,Fe,Mg,Mn,Zn)
47	-	-	X	(Co,Mg,Mn,Zn)	X	(Co,Mg,Mn,Zn)
Very small pore						
20	X	X	X	(Mg)	X	(Co,Fe,Mg,Mn,Zn)

^a For elements Al, P, Si, Co, Fe, Mg, Mn and Zn. The X designation indicates compositions and structures observed in high purity which are well characterized.

The aluminophosphate species containing tetrahedral transition metal atoms (Co^{2+} , Mn^{2+} , $\text{Fe}^{3+,2+}$, Zn^{2+}) are of particular interest because of their potential accessibility to reactant molecules. Other compositions provide unusual examples of tetrahedral siting for Me^+ and Me^{2+} ions in an oxide lattice (Li, Mg, etc).

In addition to the large new families of aluminophosphate-based molecular sieves reported from Union Carbide's laboratories, recent reports by Bond *et al.* [2], Tapp *et al.* [3] and Pyke *et al.* [4] also describe aluminophosphate-type compositions containing aluminum, phosphorus, and additional elements. These molecular sieves represent ternary and occasionally quaternary aluminophosphate compositions with the -5 or the -11 type crystal structures identified in Table I, and they contain Zn [2], Co^{2+} [3], and Si, Ti, Zn, V, Fe, or Mg [4] as additional T elements. An interesting theoretical discussion of isomorphic metal substitution in molecular sieves has been published recently by Tielen *et al.* [5].

Table III. Selected ElAPO and ElAPSO structures and compositions [1].

Structure type	Compositional Systems	
	ElAPO, Elements	ElAPSO, Elements
Large Pore		
5	Be, Ga, Ge, Li, Ti	Be, Ga, Ti
36	Be, Ga	-
Intermediate Pore		
11	As, Be, Ti	As, Ge, Ti
41	-	B
Small Pore		
17	Ga, Ge	-
18	As, Ga, Ge, Ti	-
34	Be, Li	As, B, Be, Ga, Ge, Li, Ti
35	-	As, B, Ge, Ti
Very Small Pore		
20	Be, Ga, Ge, Li, Ti	Be, Ga

In addition to the disclosures in the scientific literature discussed above, the following United States patents describe aluminophosphate-based type molecular sieve compositions: 4,310,440; 4,473,663; 4,567,029; 4,554,143; 4,440,871; and 4,500,651.

2.2. Synthesis of Silica Sodalite in Nonaqueous Media

A new method for the synthesis of silica-rich or pure silica sodalite has been reported using nonaqueous synthesis media such as ethylene glycol or other suitable solvents [6]. The product tends to be silica-rich, and in the absence of aluminum it is pure silica with unit cell composition $\text{Si}_{12}\text{O}_{24} \times 2 \text{C}_2\text{H}_4(\text{OH})_2$. Interestingly, the silica sodalite occludes no sodium-containing molecules (NaOH) present in the synthesis system.

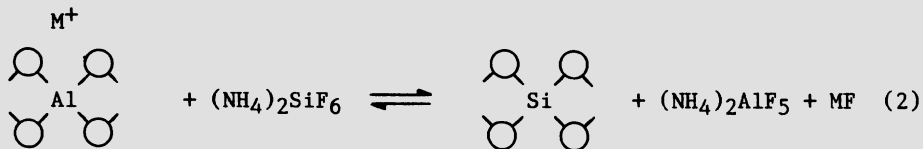
2.3. Nondestructive Post-synthesis Treatments

Important recent post-synthesis modifications of molecular sieves involve nondestructive changes in zeolite framework Si/Al ratios. Earlier it was reported by Beyer [7] that Y zeolite can be enriched in silicon by reaction with SiCl_4 vapor:



The treatment with SiCl_4 readily results in high Si/Al ratios, yielding products showing hydrophobic character. The silicon-enriched products display enhanced thermal stability, reflecting the higher stability of the Si-O versus the Al-O linkage.

More recently, a new method was described for the nondestructive silicon enrichment of zeolites. According to Skeels and Breck [8], the replacement of zeolite framework Al atoms by Si atoms can be achieved by the application of aqueous solutions of fluorosilicate reagents at mild reaction temperatures. A favored reaction scheme applied to Y zeolite is as follows:



The overall reaction seems to proceed through two consecutive steps. It is conceived that first framework Al atoms are removed from the Y zeolite by the hydrolysed fluorosilicate solution. Subsequently, Si atoms are inserted in a slower reaction step. Rapid dealumination without silicon insertion may cause crystal collapse while the silicon-enriched products become more stable relative to the starting Y zeolite.

By appropriate choice of reaction temperature, reagent application rate, and pH, it is possible to prepare Y zeolite products with $\text{SiO}_2:\text{Al}_2\text{O}_3$ ratios exceeding 3, such as 10 or 20 and greater values, with high chemical efficiency and without loss in crystallinity. In the silicon-enriched product, the remaining framework aluminum atoms maintain their tetrahedral coordination, as indicated by $\text{M}^+:\text{Al}$ ratios of near unity. A variety of chemical and crystallographic evidence demonstrates that the Si atoms are indeed inserted into framework sites vacated by Al atoms. For example, the material balance of the reaction system shows near-perfect stoichiometry between aluminum removed and inserted silicon. Crystallographic information and particularly the gradual changes in the lattice parameter a_0 observed with incremental reagent additions indicate good distribution of the inserted Si atoms throughout the Y zeolite crystal (Table IV).

Silicon enrichment of the Y zeolite results in major increase in thermal stability. At 60% replacement of the aluminum by silicon, changing the $\text{SiO}_2:\text{Al}_2\text{O}_3$ ratio from ~5 to 14.8, causes the DTA crystal collapse temperature to increase from 860 to 1128°C (Table V).

Consistent with the thermal stability results, the silicon-enriched Y zeolite derivatives display greatly enhanced hydrothermal stability, relative to reference low-soda Y zeolite. By comparison, following steam treatment, the low-soda NH_4Y (content of $\text{Na}_2\text{O} = 0.36\%$) retains only ~15% crystallinity, while the silicon-enriched product with $\text{SiO}_2:\text{Al}_2\text{O}_3$ of 11.7 retains ~90% crystallinity. Furthermore, the silicon-enriched product with 6.4 $\text{SiO}_2:\text{Al}_2\text{O}_3$ ratio already retains ~58% crystallinity [9].

Table IV. Chemical analyses of the starting zeolites and the products of the fluorosilicate reaction [8].

	Starting NH ₄ Y	LZ-210 (9.3)	LZ-210 (14.8)	Starting H ⁺ mordenite	LZ-211 (27.7)	NaY	Aluminum-depleted NaY
Na ₂ O, wt% ¹	1.88	1.04	0.61	0.21	0.10	12.4	7.2
Li ₂ O, wt% ¹	-	-	0.37	-	-	-	-
(NH ₄) ₂ O, wt% ¹	9.90	6.34	3.70	0	2.42	0	0
Al ₂ O ₃ , wt% ¹	22.68	14.28	9.74	10.80	5.53	22.2	14.0
SiO ₂ , wt% ¹	64.67	78.34	84.96	89.08	90.21	64.2	78.3
Fluoride, wt% ¹	0	0.05	0.15	0	0.01	0	0
SiO ₂ /Al ₂ O ₃	4.84	9.31	14.84	14.00	27.70	4.92	9.52
Na ⁺ /Al	0.14	0.12	0.10	0.03	0.03	0.92	0.85
Li ⁺ /Al	-	-	0.13	-	-	-	-
NH ₄ ⁺ /Al	0.85	0.87	0.75	-	0.86	0	0
Cation Equivalent M ⁺ /Al	0.99	0.99	0.98	0.03	0.89	0.98 ²	0.95 ³

¹ On an anhydrous basis

² Includes CaO/Al₂O₃ = 0.06

³ Includes CaO/Al₂O₃ = 0.10

The outstanding crystal stability of framework-silicon-enriched Y products obtained by aqueous fluorosilicate treatment has been most recently again demonstrated under very severe steaming conditions by Rabo *et al.* [9]. Accordingly, these materials at SiO₂/Al₂O₃ ratios greater than 6.5 display substantially superior hydrothermal stability relative to H-Y zeolite products of similar SiO₂/Al₂O₃ ratios obtained either by aluminum extraction (EDTA, acid treatment) or by steam stabilization.

In addition to the silicon enrichment of zeolites via post-synthesis chemistry, several recent reports by Anderson *et al.* [10], Chang *et al.* [11,12], and Dessau *et al.* [13] describe the aluminum enrichment of silica-rich or pure silica molecular sieves. Several authors independently described the treatment of silicalite or ZSM-5 by AlCl₃ vapor at about 400°C [10-13]. Following this treatment, the authors used different methods to remove excess AlCl₃, and in one case they used an ion-exchange technique following AlCl₃ treatment to remove aluminum incorporated as an exchangeable cation [11]. It is suggested that the AlCl₃ reacts with lattice defect sites such as hydroxyl nests, presumably existing in high-silica zeolites. The existence of lattice defects such as surface hydroxyls seems to be supported by the facile exchange of oxygen between zeolite and water, reported earlier [9a].

Table V. Physical properties of the starting zeolites and the products of the fluorosilicate reaction [8].

	Starting NH ₄ Y	LZ-210 (9.3)	LZ-210 (14.8)	Starting H ⁺ mordenite	LZ-211 (27.7)	NaY	Aluminum-depleted NaY
X-Ray Crystallinity, % I/I _S	100	106	93	100	106	100	68
Unit Cell, a ₀ , Å	24.67	24.49	24.39	NA	NA	24.689	24.652
Framework Infrared Asymmetric stretch, cm ⁻¹	1014	1044	1061	1076	1086	1019	1033
Symmetric stretch, cm ⁻¹	786	807	818	802	812	791	794
Crystal collapse temp by DTA, °C	860	1037	1128	-	-	980	980
Hydroxyl region infrared absolute absorbance, 3710 cm ⁻¹	0.000	0.040	0.158	0.266	0.310	0.000	0.330
O ₂ adsorption capacity, 90 K, 100 Torr, wt%	35.2	29.4	28.6	19.79	18.03	-	-
H ₂ O adsorption capacity, 298 K 46 Torr, wt%	32.1	29.8	28.8	16.17	13.55	-	-
Neopentane capacity, 298 K, 500 Torr, wt%	-	-	-	5.05	5.26	-	-

Convincing evidence for the incorporation of aluminum into tetrahedral lattice sites comes from ²⁷Al magic angle spinning (MAS) NMR, and from indirect evidence such as enhanced catalytic activity [12,13] and infrared spectroscopy. According to the best documented

^{27}Al MAS NMR work [10], following AlCl_3 treatment of silicalite, both tetrahedral and octahedral aluminum peaks are found, with about 1/3 of the aluminum in octahedral sites. The tetrahedral aluminum is presumed to occupy lattice sites, while the octahedral aluminum represents extra framework cation sites. In addition to the treatment with AlCl_3 , aqueous fluoroaluminates were also applied to enrich ZSM-5 in aluminum. Here, it is proposed that aluminum insertion is not limited to lattice defects. Thus, in this case the direct substitution of framework silicon by aluminum is suggested [11].

In addition to the application of highly reactive aluminum compounds (halides), the aluminum enrichment of ZSM-5 zeolite with "aquo species from Al_2O_3 " has been also reported [12]. This involves the hydrothermal treatment of ZSM-5 and active alumina mixtures. Presumably, the hydrous alumina species migrate into the zeolite, ultimately assuming sites as framework lattice T cations. The importance of the presence of a liquid water phase is emphasized, because no catalytic evidence for aluminum incorporation is observed by treatment in dry steam. Here again, the amount of tetrahedral aluminum is determined by ^{27}Al MAS NMR, indicating the presence of additional aluminum in the lattice following the treatment.

3. RECENT PROGRESS IN THE CHARACTERIZATION OF MOLECULAR SIEVES

The principal areas of progress in molecular sieve characterization are NMR spectroscopy, electron microscopy, X-ray crystallography, and far-infrared spectroscopy.

3.1. Nuclear Magnetic Resonance Spectroscopy

It is fortunate for zeolite science that in recent years this topic has attracted the attention of several leading NMR spectroscopists. The reason for the interest was the opportunity to apply solid-state NMR, using the MAS and a series of other sophisticated techniques, to characterize the adjacent T atom environment of framework T atoms in zeolites. This information was especially desirable because X-ray techniques do not readily distinguish Si from Al atoms, and because the interpretation of zeolite chemistry and catalysis rests upon the relationship and distribution of T atoms in the zeolite matrix. The most broadly applicable investigations deal with MAS NMR of ^{29}Si and ^{27}Al and with the characterization of hydrogen atoms of acidic sites. An independent area of NMR investigation is the use of xenon as a probe in the study of zeolites.

In the studies of zeolite T atoms by NMR spectroscopy, one goal was to check the validity of Löwenstein's rule, which forbids the existence of two or more Al atoms at adjacent T sites. This rule rests on the reasonable assumption that the net negative charge on tetrahedral alumina units would destabilize similar units at adjacent sites, and on the information that zeolite and silicate chemistry is fully consistent with this rule. The ^{29}Si and ^{27}Al MAS NMR spectroscopy has been applied to test and to verify this structural rule for Al. After

considerable investigation and debate, it has been shown by Bennett *et al.* [14] that recent MAS NMR evidence with zeolites is fully consistent with Löwenstein's rule. Thus, the existence of twin, adjacent tetrahedral alumina units is excluded from structural considerations.

Important and informative structural information for zeolites has been provided by ^{29}Si MAS NMR spectroscopy by Fyfe *et al.* [15,16], Klinowski [17,18], Thomas [19], and Blackwell *et al.* [14]. Here, with the ability to distinguish between Si sites with 0, 1, 2, 3, or 4 adjacent Al atoms, an opportunity developed to characterize the zeolite lattice, for example to do the following:

- (1) Distinguish between all five Si species with 0, 1, 2, 3, and 4 Al atoms at adjacent sites, (Fig. 1).
- (2) Distinguish between different structural sites for Si.
- (3) Calculate the Si/Al ratio of the zeolite crystal framework.

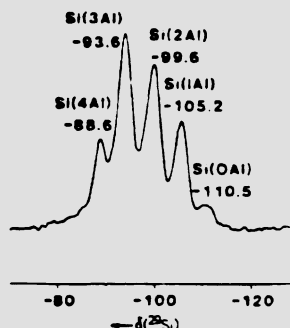


Figure 1. ^{29}Si -MAS-NMR spectrum at 79.8 MHz of zeolite ZK-4 showing five peaks, at the chemical shift values indicated, corresponding to the silicon environments shown in the figure [16].

In the case of Y zeolite with a single crystallographic T atom lattice site, the characterization of T atoms adjacent to Si allows the monitoring of important structural and chemical changes occurring in the zeolite framework. This method can be used to follow the framework dealumination process occurring in the steaming of H-Y zeolite. Here, while chemical analysis shows no change, the ^{29}Si MAS NMR spectra reveal the silicon enrichment, showing more Si with a higher number of Si atoms at adjacent sites (Fig. 2).

^{27}Al MAS NMR spectroscopy also contributed substantially to the elucidation of the siting of Al, both in as-synthesized zeolites and in steamed or chemically modified products. The most important aspect of

Al characterization is the quantitative determination of its tetrahedral vs. octahedral coordination (Fig. 3). Since pure alumina phases prefer octahedral Al coordination, it is expected that nonframework Al prefers octahedral sites. Thus, the determination of tetrahedral vs. octahedral Al provides information characterizing the Al in the zeolite framework and aiding in the determination of the framework Si/Al ratio. In addition, it reveals the formation of extra-framework alumina phases formed upon steaming or following other chemical treatment [15-19].

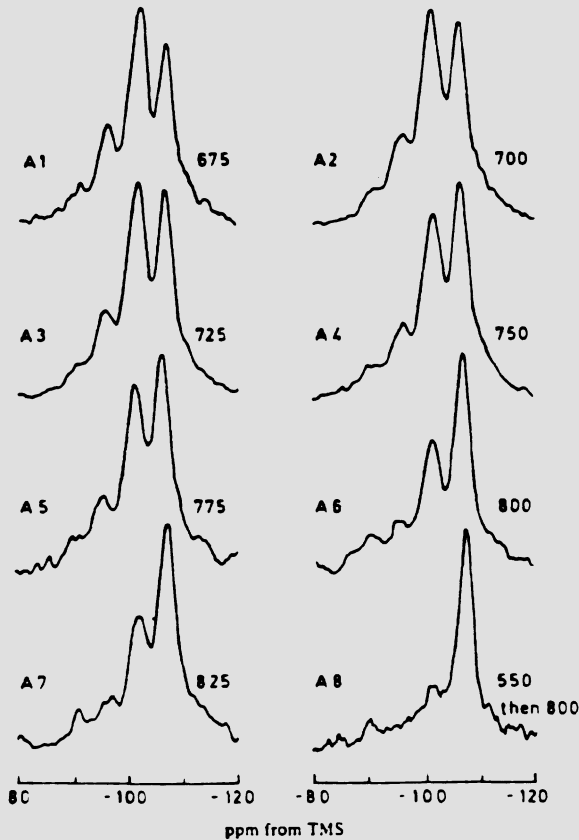


Figure 2. ^{29}Si MAS-NMR spectra of hydrothermally dealuminated samples [18]. The numbers next to the spectra refer to temperatures in $^{\circ}\text{C}$.

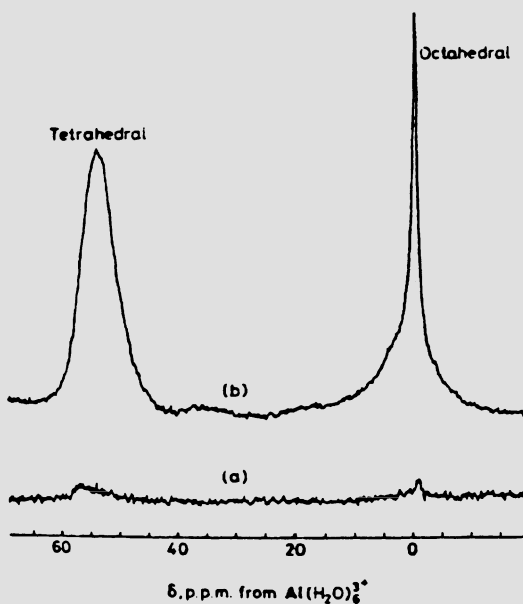


Figure 3. ^{27}Al MAS-NMR spectra at 104.22 MHz of the parent and the aluminated ZSM-5/silicalite, (500 scans with no line broadening).
 (a): Parent material with $\text{Si:Al} > 400$; (b): aluminated material with Si:Al ca. 50 [10].

Combined ^{29}Si and ^{27}Al MAS NMR spectroscopy yields quantitative characterization of as-synthesized zeolite crystals. However, in certain cases the quantitative interpretation on Al T atoms can become difficult because of line broadening, caused by interaction of the Al quadrupole moment with the adjacent electric field in the crystal. This problem can be further aggravated by nonsymmetrical electron distribution surrounding the Al atom. Attempts to quantify all Si and Al information further suffers when there are lattice defects such as OH groups attached to T atoms. While NMR techniques such as cross polarization identify hydroxylated species, the quantitative assessment of these species remains difficult. Thus, the presence of defect sites such as hydroxyl, frequently present in zeolites, renders difficult the quantitative characterization of the lattice of a practical zeolite catalyst.

A particularly important aspect of NMR studies relates to the characterization of hydrogen atoms of acidic groups attached to framework oxygen atoms. In a recent investigation directed to zeolite acidity, Pfeifer [20] reported an extensive experimental and theoretical characterization of Si, Al and H atoms, comparing silica-alumina gel, H-mordenite and H-Y zeolites. An interesting experimental aspect of the study is the application of a hydrogen free MAS sample holder

which can be sealed to render it applicable for proton MAS NMR studies. Important conclusions of this proton and ^{27}Al MAS NMR study are that upon dehydroxylation of H-Y there is no evidence for the formation of significant amounts of 3-coordinated Al and that the number of bridging OH groups and the number of 4-coordinated Al are equal, and that much less than half of the original 4-coordinated Al remains when dehydroxylation is complete. Surprisingly, the study of acidic groups shows similarity between the proton acidic species found in silica-alumina gel, H mordenite, and H-Y zeolite; they are all found at about 4-5 ppm. The similarity of the spectra of the acidic hydrogen species led the author to conclude that "the higher catalytic activity of H-Y zeolites and H-mordenites with respect to amorphous silica-aluminas is due to the higher amount of acidity (concentration of Brønsted sites) and not due to a special type of acidity" [20]. This conclusion is unexpected, and it is in opposition to the vast body of physical chemical and catalytic data published on this topic. The latter evidence supports the conclusion that protic acid sites in H-mordenite and H-Y zeolites are intrinsically stronger than similar sites in silica-alumina gel. Clearly, there is a need for further investigation to explain these unexpected proton NMR data.

An interesting new field is the NMR study of zeolites using adsorbed xenon as a probe, a method developed by Fraissard *et al.* [21-23]. The concept is to apply a nonreactive molecule that is particularly sensitive to its environment and to collisions with other chemical species to serve as a probe for determining properties of molecular-scale pores, such as those of molecular sieves. The probe chosen (^{29}Xe) must be detectable by NMR, since this technique is particularly suitable for the detection of electron perturbations in rapidly moving molecules.

In summary, the xenon NMR technique provides important new information characterizing the following:

- (1) The degree of short-range crystallinity in the zeolite lattice.
- (2) The existence of cavities and channels in the same sample; it is also possible to determine whether or not the channels are interconnected.
- (3) The approximate dimensions of pores in a zeolite of unknown structure.
- (4) The locations of strongly chemisorbed molecules, for example in the channels or in the side pockets of mordenite.
- (5) The relative strengths of the local electric fields in the cavities and channels.

With metal-loaded zeolites, this technique can be used to determine the quantitative distribution of molecules chemisorbed on the metal particles, the number of particles in the sample, and, consequently, the average number of atoms per metal particle. It can also be used to determine quantitatively the distribution of several gases simultaneously chemisorbed on these engaged particles and to determine the percentage of metal located inside or outside the zeolite crystallites.

With the emergence of molecular sieves of new compositions, such as the aluminophosphate family, the structural complexity of the molecular sieve lattice has been greatly increased. For the reasons discussed above, the various NMR techniques are expected to play a dominant role leading to the understanding of these materials [14], complementing X-ray and other techniques in the characterization of the atomic order in the molecular sieve lattices.

3.2. Electron Microscopy

Electron microscopy has been improved in resolution, as illustrated by Figs. 4 and 5. This improvement is mainly the result of combination of the microscopic data with crystallographic information and computer techniques, resulting in a highly refined method to visualize structural details of zeolites such as lattice defects, intergrowth, and the micropores themselves at near atomic level. The successful integration of information from several independent sources to attain iterative refinement is an important development in electron microscopy, and it also inspires the adoption of similar interacting techniques in other areas of crystal characterization. Excellent summaries of progress in this field have been recently published by Thomas [19], a major contributor to this field.

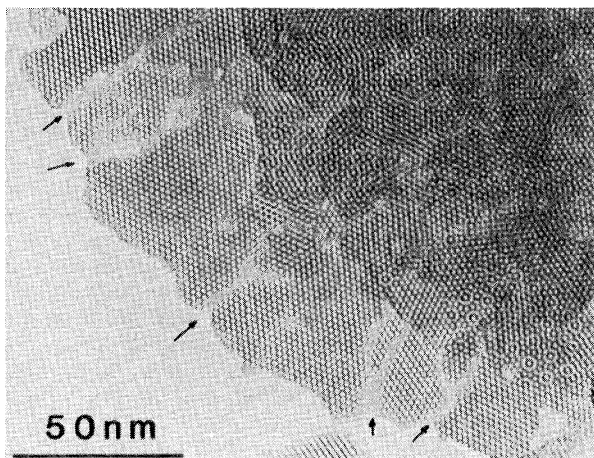


Figure 4. Typical electron micrograph showing 'estuarine' regions of noncrystallinity in a sample of zeolite L that had been partially dealuminated by hydrothermal treatments [19].

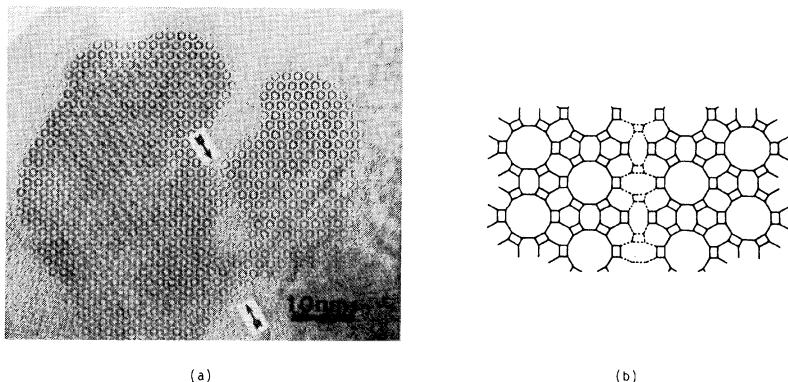


Figure 5. (a) Noncrystalline patches and locally defective (arrowed) regions in a specimen of synthetic mazzite. (b) A model of the structure at one type (dashed lines) of extended defect [19,19a].

3.3. Progress in Crystallography

Certain natural zeolites are found in crystal sizes well exceeding 100 μm in all dimensions, providing good opportunities to collect adequate X-ray diffraction information for accurate electron density maps and to allow the definition of the crystal lattice with a high degree of reliability. There are intrinsic problems in this crystallography with molecular sieve crystals, such as the large unit cell size, often combined with high symmetry (e.g., in Y zeolite) and with fractional occupation of certain crystallographic sites (cations). In addition, the presence of atoms at low coordination and/or low symmetry gives rise to high thermal vibrational amplitudes, all reducing the quality of the experimental data set. The problems cited above are further aggravated with crystals containing lattice defects such as those obtained upon steaming or other chemical treatments. For these reasons, the efficiency of the structure refinement programs applied for locating atomic positions is of great importance.

In order to improve structure refinement, a new program package was designed by Baerlocher *et al.* [24-26] for X-ray powder diffraction data, which is capable of refining structures with more than 100 structural parameters. First, a standard peak-shape function is determined from the observed profile. Then, in order to supplement the diffraction data, known interatomic distances and angles are applied as weighted constraints, and their expected range is imposed as boundary condition. This method enhances the least-squares convergence and substantially contributes to the refinement of complex structures. The

application of these "soft restrictions" on bond distances and angles in the structure refinement program facilitated locating extra framework atoms which would have been missed otherwise [24-26].

Interesting structural phenomena have been reported recently by Alberti regarding phase transitions in zeolites [27]. Some zeolites show heat-induced phases stable over a long periods. This stability is a consequence of the breaking of T-O-T bridges, causing topological changes in the framework. In some cases the framework of the heat-induced phase is topologically the same as that of a known mineral. Topological changes are explained on the basis of extra-framework cation movements, causing strain on the T-O-T bridges. The strain facilitates proton attack and the consequent breaking of these bonds. This process occurs only when water is present. The behavior of zeolites on heating may be categorized as follows:

- (1) Dehydration with rearrangement of extra-framework cations without considerable changes in the geometry of the framework and in the cell volume. Zeolite A, faujasite, natural chabazite, and mordenite provide examples of this thermal behavior.
- (2) Dehydration with considerable distortion of the framework and a decrease in the cell volume, followed by fast rehydration and reversion of the structure under ambient conditions. Natrolite has a thermal behavior of this type.
- (3) Dehydration with topological changes of the framework as a consequence of the breaking of T-O-T bridges. Examples of this behavior are provided by barrerite, stellerite, heulandite, and zeolite EAB.

These crystallographic studies are highly relevant to other aspects of zeolite chemistry, such as steam-induced transformations in the zeolite lattice.

3.4. Far-infrared Spectroscopy

Far-infrared spectroscopy, which has been extensively developed for zeolite characterization by Ozin and associates, is fast-becoming one of the most useful techniques for understanding structures of molecular sieves [28]. It is an ideal technique for probing the vibrations of the zeolite framework occurring between 250 and 400 cm⁻¹, as well as those of cations and occluded metal atoms or clusters with frequencies between 250 and 30 cm⁻¹. While the method is not new [29], recently it has been intensively pursued and extended. This technique can be used to identify zeolite cations and distinguish each cation in different crystallographic sites (Fig. 6). It has also been successfully applied to characterize silver clusters occluded in A zeolite. Interestingly, with silver clusters increasing in size from 2 to 10 atoms, the Ag-Ag frequency shows a continuous shift to a lower frequency. Far infrared spectroscopy can also be used to locate transition metal ions in zeolites. A recent comprehensive recent review of this field is available [28].

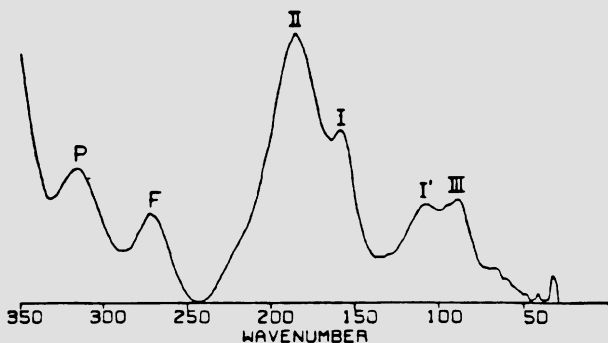


Figure 6. The far-IR absorbance spectrum of fully dehydrated Na₅₆Y. P denotes a pore opening mode and F an oxygen framework vibration [28, 28a].

4. RECENT ADVANCES IN MOLECULAR SIEVE CATALYSIS

Progress in molecular sieve catalyst technology is best reflected by the large variety of molecular sieve types and applications described in the literature. Rapid growth is also indicated by the commercial success of molecular sieve based catalysts. At present, in terms of sales values, about 40% of all heterogeneous catalysts applied in the industry contain molecular sieve as key component. The industrially relevant new applications use a variety of new-generation molecular sieves as well as new modifications of known zeolites.

4.1. Catalytic Cracking

In the cracking process, catalysts based on zeolite Y or its modified derivatives continue to dominate. Significant advances have been made recently to respond to market needs for higher gasoline octane number and greater catalyst stability, particularly for the treatment of residual feedstocks.

An important recent catalyst development is related to the nondestructive framework substitution of Si for Al in the Y zeolite, described above. Using this recently disclosed mild aqueous chemistry, silicon-enriched forms of the Y zeolite structure (called LZ-210) have been synthesized, greatly improving the thermal and hydrothermal stability of the Y crystal. Cracking catalysts prepared from these silicon-rich zeolites show substantially increased cracking activity retention, following severe steaming pretreatments. In addition,

finished catalysts using this zeolite show improved gasoline yield and higher coke selectivity. It has been reported that with these catalysts the production of high-octane gasoline can be achieved without the usually observed impairment in gasoline yield [9]. The high activity retention and high selectivity of these catalysts is interpreted by Long *et al.* [30] on the basis that these zeolites have less aluminum and more silicon atoms in the crystal at the start of catalyst preparation. Therefore, upon steaming and concurrent hydrolysis of framework aluminum atoms, these crystals develop fewer defect sites and fewer intracrystalline voids, formed from coalescent defect sites. Since defect sites contribute to the crystal decomposition rate, silicon-enriched crystals are expected to lose crystallinity at a lower rate than the aluminum-rich variety, which has higher defect site concentrations. The higher selectivity is explained on the basis that with the silica-rich crystals the amount of occluded amorphous silica-alumina debris formed upon steaming is reduced. With a higher fraction of selective zeolitic acid sites, and less occluded "debris acid" sites, recognized for low selectivity in cracking, higher gasoline and coke selectivity is expected, relative to H-Y zeolites [9,30].

Another interesting effort in catalytic cracking is the application of ZSM-5 zeolite as a catalyst additive to boost gasoline octane number [31-33]. Reportedly, even small amounts of ZSM-5 can readily increase the gasoline octane number by several units. However, the octane enhancement coincides with gasoline yield loss, with up to two percent yield loss for each octane unit gained. Such an application may be warranted if the ultimate refinery gasoline yield loss can be minimized by recycling the excess C₃-C₄ alkenes and the isobutane formed on ZSM-5, via alkylation process. Thus, an excess alkylation capacity is essential here for satisfactory process economy.

4.2. Aromatization of Hydrocarbons

The dehydrocyclization of n-hexane catalyzed by platinum-loaded alkali L zeolite reported by Bernard [34] became the subject of recent industrial development [35]. In contrast to the acidic commercial reforming catalyst, the new L zeolite catalyst reported by Hughes *et al.* [35] is nonacidic Pt-BaK-L zeolite. Presumably, the properties of platinum clusters by themselves account for all the catalytic activity. The catalyst is extremely sensitive to poisoning by sulfur, but with a thoroughly desulfurized feed, a one-year run has been successfully completed with refinery light naptha.

In the dehydrocyclization of alkanes, the nonacidic Pt-BaK-L catalyst shows a remarkable activity and selectivity advantage over the commercial, acidic reforming catalysts (Fig. 7 and Table VI). With n-hexane, the reaction rate advantage is eightfold. With higher carbon number alkanes, the rate advantage is less. However, even with n-nonane feed, a modest rate advantage is observed over the acidic catalysts. The aromatization selectivity of the L zeolite catalyst is very high (82-90%) and approximately constant for C₆-C₉ n-alkanes. In contrast, the selectivity of the acidic catalysts is lower, and it increases in the same carbon number range from 26 to 68 percent.

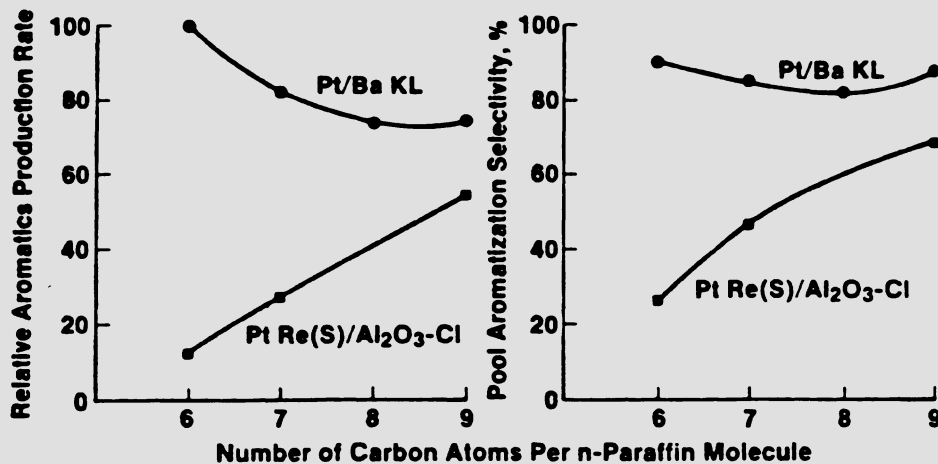


Figure 7. Effect of number of carbon atoms per molecule on rate and selectivity of aromatization of n-alkanes at 493°C and 18 LHSV [35].

Table VI. Conversion of n-octane in the presence of monofunctional and bifunctional platinum catalysts [35]^a.

	0.8Pt/BaKL-866	0.6Pt/Al ₂ O ₃ -Cl	Equilibrium
C ₈ aromatics (mols/100 mols of n-octane)	30	16	-
C ₈ -aromatics isomer distribution			
.ethylbenzene and o-xylene	88	63	32
.m- and p-xylene	12	37	68
Methylheptane isomer distribution			
.2-methylheptane	8	31	36
.3-methylheptane	34	47	48
.4-methylheptane	58	22	16

^a Reaction conditions: 460°C, 6 LHSV.

In the aromatization of alkylcyclopentanes, the Pt-BaK-L catalyst is nearly as active and selective as the acidic commercial catalysts. It is proposed that the efficiency of this catalyst in this reaction is related to the nonselective cyclic mechanism proposed by Gault and associates [36] which is also consistent with the nonequilibrium distribution of methylheptane isomers from the conversion of n-octane in the presence of the Pt-BaK-L catalyst (Table VI).

4.3. Catalysis by Silicoaluminophosphate Molecular Sieves

4.3.1. Conversion of Methanol to C₂-C₄ Alkenes. Highly selective conversion of methanol to light (C₂-C₄) alkenes catalyzed by the silicoaluminophosphate (SAPO) molecular sieves described above has been reported by Kaiser [37]. With the small pore SAPO-34 catalyst, the combined molar selectivities to light alkenes total up to 96% at ~100% methanol conversion, using practical reaction conditions [37]. Increasing reaction temperatures result in increased ethylene selectivity, with greater than 60% ethylene selectivity achieved at 450°C (Table VII). The rate of methane formation from methanol is very low under all reaction conditions. The SAPO-34 catalyst is readily regenerable via air activation, and it shows good durability upon extended use. The SAPO-34 converts not only methanol but also higher alcohols, aldehydes, methyl formate, and other oxygenates to mixtures of C₂-C₄

Table VII. Conversion of methanol to light alkenes catalyzed by SAPO-34 [37]^a.

Product	Reaction temperature/°C	
	375	450
Ethylene	43.0	61.1
Ethane	0.5	0.7
Propene	41.8	27.4
Propane	0.5	0.0
Butenes	10.8	5.4
C ₅	1.7	0.6
C ₆	0.0	0.0
Methane	1.3	4.8
 C ₂ -C ₄ Alkene efficiency		
	95.6	93.9
Run time, h	5.2	11.0

^a Reaction conditions:
 Feed: 70/30 H₂O/CH₃OH (weight)
 WHSV: ca. 2.8 h⁻¹
 CH₃OH Conversion: 100%

alkenes. The similarity of the alkene product composition obtained with these different feeds suggests the existence of similar product precursors in the reaction chain.

4.3.2. Reactions of Aromatics Catalyzed by Silicoaluminophosphate Molecular Sieves. The alkylation of toluene by methanol using silicoaluminophosphate molecular sieves has been described recently by Pellet et al. [38]. A variety of these molecular sieves with medium (~6 Å) and large pores (~8 Å) have been tested together with a ZSM-5 structure type zeolite LZ-105 used as a reference. The results show that the LZ-105 zeolite catalyst has higher activity than the SAPO catalysts. However, the near 100% alkylation selectivity of the medium-pore SAPO-11 and SAPO-31 versus the methyl group disproportionation reaction is maintained in a much larger temperature range relative to the LZ-105. Furthermore, the medium-pore SAPO catalysts and particularly the SAPO-11 show para selectivity, well exceeding the equilibrium concentration for this isomer in the product. Under similar conditions, the LZ-105 catalyst produces p-xylene only at equilibrium concentration.

The catalytic tests also show that the medium-pore SAPO's have much superior methylation selectivity relative to the large-pore SAPO-5 catalyst. This latter molecular sieve has very high methyl group disproportionation selectivity, the performance being similar to that of the LZ-105 catalyst at comparable temperature (Table VIII) [38].

The isomerization of xylenes catalyzed by SAPO-5 type crystals with compositions consisting of aluminum, phosphorus, and, in several cases, additional elements, including Ti, Mg, Zn and Fe has been described [4]. The data show that these large-pore materials have catalytic activity for the isomerization of xylene mixtures.

4.3.3. Oligomerization of Small Alkenes with Silicoaluminophosphate Molecular Sieves. Medium-pore silicoaluminophosphates have high activity and high selectivity for the oligomerization of propene to give iso hexenes, producing only minor amounts of C₉ isomers [38]. The results in Table IX demonstrate strong effects of catalyst pore size and acid strength in this reaction. The large-pore SAPO-5 presumably produces large oligomerizes which plug the pores and rapidly deactivate this catalyst. Conversely, the small-pore SAPO-34 is active for the conversion of propene; however, it is incapable of forming significant quantities of gasoline-range oligomerize due to its small pore size. Among the molecular sieves tested, all medium-pore materials, SAPO-11, SAPO-31, and the LZ-105-type zeolite used as a reference, are effective for the oligomerization of propene. However, here too, different degrees of molecular sieving effects are indicated by the liquid product boiling at temperature above 215°C. Clearly, the LZ-105 zeolite produces heavier products than the SAPO-11 molecular sieves, suggesting a slightly larger pore size for this zeolite catalyst. These results are consistent with the toluene methylation study described above, whereby the zeolite catalyst exhibited no p-xylene selectivity, in contrast to the results obtained with the medium-pore SAPO's.

Table VIII. Toluene methylation catalyzed by SAPO molecular sieves^a [38].

Molecular sieve type	SAPO-5	SAPO-11	SAPO-31	SAPO-40	SAPO-41	LZ-105	LZ-105
Pore size / Å	8	6	7	7	6	6	6
Temperature / °C	425	425	425	425	425	425	315
Pressure / psig	100	100	100	100	100	100	100
WHSV / g ⁻¹	5.6	5.6	5.6	5.6	5.6	5.6	21.0
Initial catalyst performance ^b							
Toluene conversion / %	46.5	56.2	29.2	5.7	15.6	55.8	19.0
Methylation selectivity ^d / %	41.3	99.7	97.7	99.7	98.1	21.9	99.7
Disproportionation selectivity ^c / %	58.7	0.3	2.3	0.3	1.9	78.1	0.3
Para isomer in xylene / %	22.6	48.6	34.7	30.6	31.4	23.8	25.7

^a Feed composition : 67 vol% toluene + 33 vol% methanol.^b Initial performance was obtained by linear regression of data collected during typical 5-h runs, extrapolated to time = 0.^c Disproportionating selectivity is given by 2 x (mols benzene yield)/(mols toluene converted) x100 and assumes 2 toluene → benzene + xylene.^d Methylation selectivity = 100 - disproportionation selectivity.

Table IX. Vapor-phase oligomerization of propene [38].

Molecular sieve	SAPO-5	SAPO-11	SAPO-31	SAPO-34	LZ-105
Pore Size / Å	8	6	7	4.3	6
Reaction temperature/°F	700	700	700	700	703
Pressure / psig	25	25	50	25	25
Time on feed / h	4.3	4.2	5.5	2.33	3.5
Propene WHSV / g ⁻¹	0.98	0.94	1.04	0.53	0.90
Propene conversion / %	0	86.3	76.2	41.6	81.6
C ₅ + selectivity / % ^a	-	77.0	82.7	19.5	37.2
Liquid product refractive index	-	1.43	1.43	-	1.52
215°C+ fraction of liquid product / %	-	8	10	-	20

^a C₅+ selectivity = (C₅+ yield, wt%)/(propene conversion, wt%) x 100.

The influence of acid strength on oligomerization selectivity is also apparent from the data in Table IX, and they confirm earlier reports of the mild acid character of the SAPO molecular sieves. While the SAPO-11, SAPO-31, and the reference zeolite catalyst are all medium-pore molecular sieves, the SAPO materials produce more alkene-rich products than are obtained with the zeolite. Correspondingly, the products obtained with the zeolite catalyst are rich both in aromatics and light alkanes. In contrast, the SAPO-11 and SAPO-31 catalysts have significantly lower hydrogen transfer activity than the zeolite reference, resulting in much higher selectivity to liquid alkene products.

5. REFERENCES

1. E.M. Flanigen, B.M. Lok, R.L. Patton, and S.T. Wilson, Proc. 7th Internat. Zeolite Conf., Tokyo, Japan, August 17-22 (1986), to be published.
2. G.C. Bond, M.R. Gelsthorpe, K.S.W. Sing, and C.R. Theocharis, J. Chem. Soc., Chem. Commun., 1056 (1985).
3. N.J. Tapp, N.B. Milestone, and L.J. Wright, J. Chem. Soc., Chem. Commun., 1801 (1985).
4. D.R. Pyke, P. Whitney, and H. Houghton, Appl. Catal. **18**, 173 (1985).
5. M. Tielen, M. Geelen, and P.A. Jacob, Proc. Zeolite Symp., p. 8, Siofok, Hungary, (1985).
6. D.M. Bibby and M.P. Dale, Nature (London) **317**, 157 (1985).

7. H.K. Beyer and I. Belenykaga, in Catalysis by Zeolites, p. 203, Elsevier (1980).
8. G.W. Skeels and D.W. Breck, Proc. 6th Internat. Zeolite Conf., p. 87, Reno, Nevada, July 10-15 (1984).
9. J.A. Rabo, R.J. Pellet, J.S. Magee, B.R. Mitchell, J.W. Moore, and W.S. Letzsch, Proc. 1986 NPRA Annual Meeting, Los Angeles, California, March 23-25 (1986).
- 9a. J.A. Rabo, Proc. 6th Internat. Zeolite Conf., p. 41 (1984).
10. M.W. Anderson, J. Klinowski, and L. Xinsheng, J. Chem. Soc., Chem. Commun., 1596 (1984).
11. C.D. Chang, C.T.W. Chu, J.N. Miale, R.F. Bridger, and R.B. Calvert, J. Am. Chem. Soc. 106, 8143 (1984).
12. C.D. Chang, S.D. Hellring, J.N. Miale, and K.D. Schmitt, J. Chem. Soc., Faraday Trans. 1 81, 2215 (1985).
13. R.M. Dessau and G.T. Kerr, Zeolites 4, 315 (1984).
14. J.M. Bennett, C.S. Blackwell, and D.E. Cox, J. Phys. Chem. 87, 3785 (1983) and 87, 5050 (1983).
J.V. Smith and C.S. Blackwell, Nature (London) 303, 223 (1983).
C.S. Blackwell, J.J. Pluth, and J.V. Smith, J. Phys. Chem. 89, 4420 (1985).
C.S. Blackwell and R.L. Patton, J. Phys. Chem. 88, 6135 (1984).
15. C.A. Fyfe, G.C. Gobbi, G.J. Kennedy, J.D. Graham, R.S. Ozubko, W.J. Murphy, A. Bothner-By, J. Dadok, and A.S. Chesnick, Zeolites 5, 179 (1985).
16. C.A. Fyfe, J.M. Thomas, J. Klinowski, and G.C. Gobbi, Angew. Chem., Int. Ed. Engl. 22, 259 (1983).
17. J. Klinowski, Progress in NMR Spectroscopy 16, 237 (1984).
18. J. Klinowski, C.A. Fyfe, and G.C. Gobbi, J. Chem. Soc., Faraday Trans. 1 81, 3003 (1985).
19. J.M. Thomas, Proc. 8th Internat. Congr. Catal. 1, 31 (1984).
J.M. Thomas, Proc. 6th Internat. Zeolite Conf., p. 793 (1984).
- 19a. O. Terasaki, J.M. Thomas, and G.R. Millward, submitted for publication.
20. H. Pfeifer, D. Freude, and M. Hunger, Zeolites 5, 274 (1985).
21. J.P. Fraissard, T. Ito, and L.C. de Menorval, Proc. 8th Internat. Congr. Catal. 3, 25 (1984).
22. M.A. Springuel-Huet, T. Ito, and J.P. Fraissard, in Structure and Reactivity of Modified Zeolites, p. 13 (1984).
23. T. Ito, L.C. de Menorval, E. Guerrier, and J.P. Fraissard, Chem. Phys. Lett., 271 (1984).
24. Ch. Baerlocher, The X-ray Rietveld System, Institut für Kristallographie Petrographie, ETH, Zurich, (1982).
25. Ch. Baerlocher and A. Hepp, Proc. Symp. on Accuracy in Powder Diffraction, p. 165, NBS, Gaithersburg, MD, June 11-15, (1980).
26. L.B. McCusker, C. Baerlocher, and R. Nawaz, Z. Kristallogr. 171, 281 (1985).
27. A. Alberti and G. Vezzalini, Proc. 6th Internat. Zeolite Conf., p. 834 (1984).
28. M.D. Baker, G.A. Ozin, and J. Godber, Catal. Rev.-Sci. Eng. 27, 591 (1985).

- 28a. G. Ozin, M.D. Baker, and J. Godber, J. Am. Chem. Soc. 107, 3033 (1985).
29. I.A. Brodskii, S.P. Zhdanov, and A.E. Stanevic, Opt. Spectrosc., 58 (1971).
30. G.N. Long, R.L. Chiang, R.J. Pellet, and J.A. Rabo, Proc. of the Katalistiks' 7th Annual Fluid Cat Cracking Symp., Venice, Italy, May 12 and 13 (1986).
31. J.S. Magee, W.E. Cormier, and G.M. Woltermann, Oil and Gas Journal Report, pp. 63-64 (1985).
32. J. Van Dijk and D.J. Rawlence, 'FCC Technology', presented at Internat. Symp. on Zeolites for Industry, Manchester, England, April 3-5 (1984).
33. A.W. Chester, W.E. Cormier, and W.A. Stover, U.S. Patent 4,309,279 (1982).
34. J.R. Bernard, Proc. 5th Internat. Conf. Zeolites, p. 686, Heyden, London (1980).
35. T.R. Hughes, W.C. Buss, P.W. Tamm, and R.L. Jacobson, Proc. 7th Internat. Zeolite Conf., Tokyo, Japan, August 17-22 (1986), to be published.
36. Y. Barron, D. Cornet, G. Maire, and F.G. Gault, J. Catal. 2, 152 (1963).
G. Maire, G. Plouidy, J.C. Prudhomme, and F.G. Gault, J. Catal. 4, 556 (1965).
Y. Barron, G. Maire, J.M. Muller, and F.G. Gault, J. Catal. 5, 428 (1966).
37. S.W. Kaiser, The Arabian Journal for Science and Engineering, 361 (1985).
38. R.J. Pellet, G.N. Long, and J.A. Rabo, Proc. 7th Internat. Zeolite Conf., Tokyo, Japan, August 17-22 (1986), to be published.

RECENT ADVANCES IN PILLARED CLAYS AND GROUP IV METAL PHOSPHATES

Abraham Clearfield
Department of Chemistry
Texas A&M University
College Station, Texas 77843
USA

ABSTRACT. The smectite family of clays swell in water and are thus able to exchange large cations such as $[Al_{13}O_4(OH)_{24}\cdot 12 H_2O]^{7+}$ and $[Zr(OH)_2\cdot 4 H_2O]^{8+}$. These ions act as pillars to prop open the clay layers thus creating porous structures. Pores larger than those possible in zeolites have been measured in the propped clays. Thus, their potential for the cracking of the heavy gas-oil fraction of petroleum has been examined.

The layered compound α -zirconium phosphate has been pillared by cross-linking the layers with aryl diphosphonic acids. The pillars can be spaced to produce different sized pores and the structures are stable in reducing atmospheres to 400°C. Their potential use as catalysts is discussed.

1. INTRODUCTION

Clays and layered silicate minerals have a long history of use as petroleum cracking catalysts [1]. These were largely replaced in the mid-sixties by zeolites [2]. The greater acidity, reactivity, and selectivity of zeolite catalysts allowed for closer control of cracking reactions and higher yields of desired products [3]. To date, more than 100 different zeolites have been synthesized [4], but of these only about a dozen are utilized on an industrial scale [5]. Zeolites A, X, Y, mordenite, erionite, and ZSM-5 represent more than 95% of the total worldwide usage. However, the limited pore size range of zeolites and the relatively high cost of those used in the petroleum industry have given impetus to the search for other types of porous compounds. The former limitation is a serious impediment to the possible use of zeolite catalysts for the conversion of synthetic and heavy crude oils to give commercially desirable products. In particular, molecular sieves with pore sizes of 8-40 Å are required for such purposes.

In the preceding two decades a new class of two-dimensional molecular sieves has been synthesized from certain types of aluminosilicate clay minerals. The general procedure is to incorporate a large inorganic cation between the layers to prop them open [6]. The props,

or pillars, are thermally cross-linked to the layers. It has long been known that various organic molecules such as amines and alkylammonium ions readily intercalate between clay layers [7], and that porous structures can be formed from such complexes [8]. In general these organically pillared structures suffer from the thermal instability of the organic component, although relatively stable complexes have been formed with cage-like amines [9-11]. However, since our emphasis is on catalytic reactions, for which robust structures are required, only inorganically pillared clays are described in this section (however, see section 8).

2. DESCRIPTION OF SMECTITES

The principal class of swelling clays is termed smectites. The smectites characteristically have alumina octahedra sandwiched between layers of silicate tetrahedra as shown in Fig. 1.

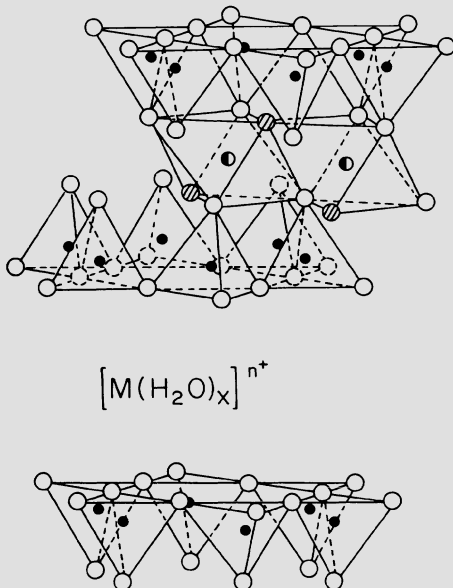


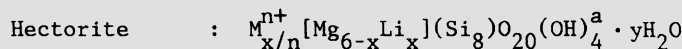
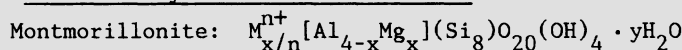
Figure 1. Schematic drawing of smectite clay: ● : octahedrally coordinated ion; ● : tetrahedrally coordinated ion; ○ : oxygen; Ⓜ : OH group.

The smectites are distinguished by the type and location of cations in the layered framework. In a unit cell formed from twenty oxygens and four hydroxyl groups there are eight tetrahedral sites and six octahedral sites. Idealized formulas are given in Table I. When all the

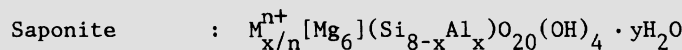
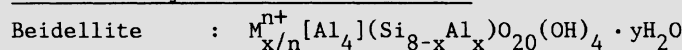
octahedral sites are filled with Mg^{2+} , a magnesium talc of ideal formula $[Mg_6](Si_8)(OH)_{40}O_{20}$ is the result. Pyrophyllite is like talc except that 2/3 of the octahedral sites are filled by Al^{3+} . In smectites, substitutions of Mg^{2+} for Al^{3+} and Li^+ for Mg^{2+} can take place in the octahedral sites, or M^{3+} ions can substitute for Si^{4+} in the tetrahedral sites. The deficiency of positive charge is balanced by the presence of hydrated cations between the layers [11]. Typically, the positive charge deficiency in smectites ranges from 0.4 to 1.2 e per Si_8O_{20} unit [12]. If the charge deficiency arises from octahedral substitution, then this excess negative charge is distributed over all the oxygens in the framework. These clays tend to be turbostratic, that is, the layers are randomly rotated about an axis perpendicular to the layers. However should the smectite have been formed by substitution at tetrahedral sites, then the extra charge is more localized and the resultant clay tends to exhibit greater three dimensional order [13].

Table I. Idealized structural formulae for principal smectite clays.

1. Octahedrally substituted smectites



2. Tetrahedrally substituted smectites



^a Some F^- may substitute for $(OH)^-$

The remarkable properties of the smectite clays are due to their relatively low layer charge. The interlayer cations are loosely held and therefore swelling via solvent sorption, ion exchange and intercalation of a variety of species is possible.

3. ION EXCHANGE BEHAVIOR OF SMECTITE CLAYS

I prefer to use the term "intercalation" for the incorporation of neutral species between the layers and the term "ion exchange" when there is a one for one exchange of species based on charge. The ion exchange capacity (IEC) of smectite clays ranges from about 0.5 to 1.5 meq/g. These capacities are low in comparison with those of sulfonated styrene-divinylbenzene resins (IEC ~ 5 meq/g) or α -zirconium phosphate (6.2 meq/g) [14]. Given the fact that the interlamellar surface is about $750\text{ m}^2/\text{g}$, univalent ions would be about 8.3 \AA apart in the interlayer space at an IEC of 1 meq/g.

An important property of the smectites is their ability to swell by intercalation of water or alcohols. The extent of the swelling

depends upon the layer charge, the interlayer cation and the nature of the swelling agent [15]. When the hydration forces of the interlayer cation are strong, and the layer charge low, the clay is most susceptible to swelling in water. Under the right conditions the layers can be separated by hundreds of Angstroms. The sequence of swelling and delamination is shown in Fig. 2. If such a dispersion is concentrated, gelation usually occurs. The gel is believed to have a "house-of-cards" structure (Fig. 3A) resulting from layer edge to face interactions [16]. This swelling behavior allows large complex ions, which can be used for catalytic purposes, to be exchanged into the interlamellar spaces (Fig. 4).

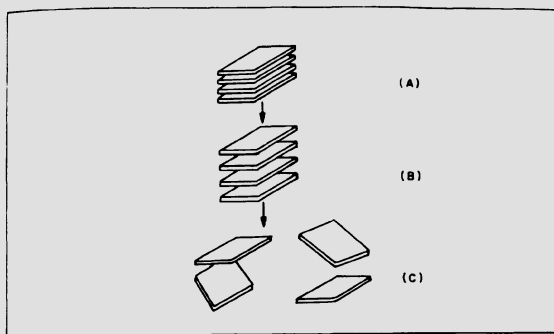


Figure 2. Scheme for the reversible dissociation of a montmorillonite crystal; (A): layers of a crystal, stacked parallel to each other; (B): increase in basal spacing (layer distance), following uptake of water (reduction of electrolyte concentration); (C): disintegration of a crystal into individual, kinetically independent layers at low electrolyte concentration ($C < 1 \times 10^{-3}$ M of a 1:1 electrolyte).

Reproduced from A. Weiss, *Angew. Chem., Int. Ed. Engl.* 20, 850 (1981), with permission.

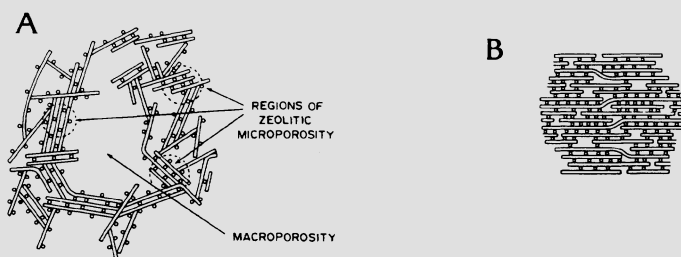


Figure 3. Models for the layer association in (A) delaminate (house of cards) structure with interlayer ions (open circles) and (B) pillared clays containing polyoxycations of aluminium (open circles).

Reproduced from Ref. 45, with permission.

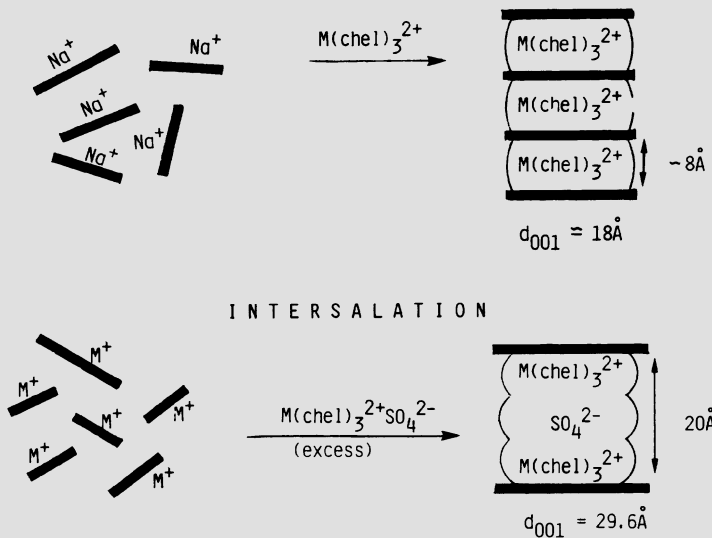


Figure 4. Two types of interlayer complexes are illustrated as forming with a swollen clay. In the first process, a complex ion may replace the original ions in the interlayer by ion exchange. (Some authors refer to this process as intercalation, not distinguishing between ion exchange and incorporation of neutral species in the interlayers). When excess complex ion is used, anions may also enter the interlayer. This process is referred to as intersalation.

According to Pinnavaia, in order for an interlamellar complex to be catalytically useful the interlayer molecules must be mobile under conditions of intermediate degrees of swelling, where the clay retains the properties of a genuine solid and not a gel [17]. Magnetic resonance (ESR, NMR) [18,19] and neutron scattering studies [20] have provided evidence for the interlayer motions and positioning of the interlamellar complex. For example, at low levels of swelling the $\text{Cu}(\text{H}_2\text{O})_6^{2+}$ complex ion is oriented with the C_4 symmetry axis perpendicular to the silicate sheets [21], as shown in Fig. 5A. Although oriented, the complex is still free to rotate about the C_4 axis. Swelling allows greater degrees of motion until, at about a 12 Å distance between the layers, the ions are free to tumble (Fig. 5B).

4. CATALYSIS BY COMPLEXES IN THE INTERLAYER

Pinnavaia *et al.* [22] pointed out that the rapid tumbling of ions and movement of free solvent in the clay interlayers indicated the possibility of carrying out catalyzed reactions in the intra-crystal space. Because the interlayers hosting the metal complex catalyst are of

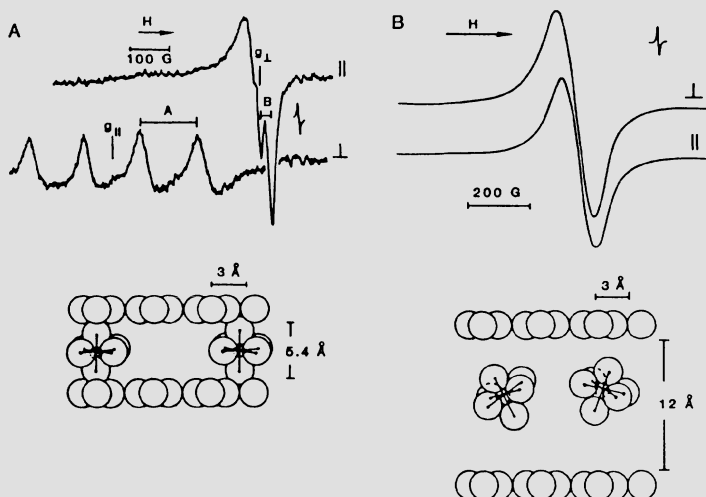
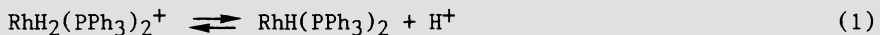


Figure 5. ESR spectra of $\text{Cu}(\text{H}_2\text{O})_6^{2+}$ ions in hectorite. (A): spectrum for complex ion with its C_4 axis perpendicular to the unswelled layers. (B): time-averaged spectra observed for the rapidly tumbling complex ion in swollen interlayer. Interlayer solvent (H_2O) molecules are not shown.

Reproduced from T. Pinnavaia, Science 220, 365 (1983), with permission.

uniform thickness and polarity, the possibility exists for selective sorption of reactant, and size and shape selectivity. In addition, preferred orientations of the interlayer complex may bring about differences between the behavior of the same catalyst in homogeneous solution and in the clay host.

The main thrust of this discussion deals with pillared clays, and we cite only two reactions to illustrate the catalytic behavior of metal complexes in unpillared clays. The hydrogenation of 1-hexene was carried out in methanol solution with a small amount of a solid consisting of rhodium triphenylphosphine complex, $\text{Rh}(\text{PPh}_3)_2^+$, exchanged into Na^+ hectorite. The complex could be introduced between the clay layers by direct ion exchange or by first exchanging Rh_2^{4+} into the clay and subsequently adding triphenylphosphine [23]. Essentially quantitative reduction of 1-hexene to give hexane was observed. In contrast, when the reaction was carried out in homogeneous solution, 2-hexene was formed in addition to hexane. In this system the reaction mechanism involves the formation of metal dihydride which is in equilibrium with monohydride [eq. (1)] [24].



The monohydride and accompanying proton formation favor isomerization. The dihydride species is favored in the clay because of the higher level of Brønsted acidity arising from hydrolysis of the hydrated interlamellar Na^+ ions [25]. It is well known that hydrated cations in the interlayers are more acidic than in solution due to the enhanced polarizing influence of the cation on its hydration shell in the restricted interlayers [26,27].

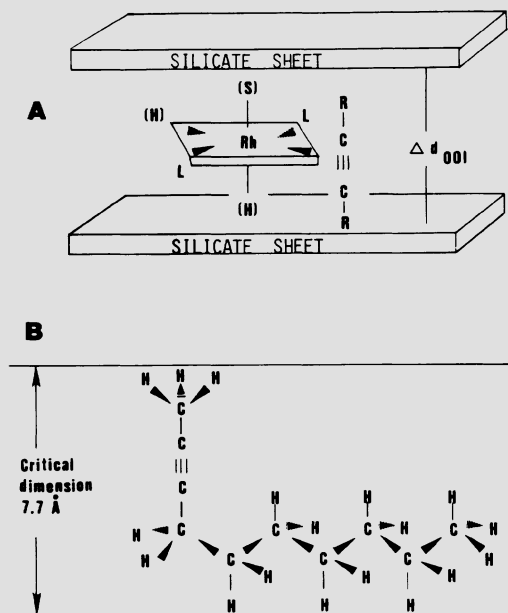


Figure 6. (A): proposed orientation for the reactive RhH_2L_2^+ -alkyne intermediate in the clay interlayer. (B): the 2-decyne critical dimension or minimum interlayer distance required to achieve a reactive configuration.

Reproduced from Ref. 22, with permission.

The importance of spatial factors was illustrated by the hydrogenation of alkynes by the same $\text{Rh}(\text{PPh}_3)_2^+$ -hectorite catalyst [22]. As the size of the R-group on either side of the triple bond increased (from 1-hexyne to diphenylacetylene) the relative rates of the reaction decreased dramatically. This effect was attributed to the relative positioning of catalyst and alkyne in the interlayer space as shown in Fig. 6A. The rates for 1-hexyne and 2-hexyne were roughly identical and Fig. 6B shows how the latter alkyne might position itself in the interlamellar space. The critical dimension in the (001) direction is then 7.7 Å which is equivalent to the spacing in the rhodium-hectorite catalyst. However 3-hexyne would not fit into this spacing and its rate

of hydrogenation is drastically less. Further swelling of the layers would be required to increase the reaction rate.

Rh(COD)(PPh₃)₂⁺-hectorite (COD = 1,5-cyclooctadiene) was examined as a hydroformylation catalyst [28]. Under hydroformylation conditions the rhodium complex forms neutral Rh(CO)_x(PPh₃)₂ ($x = 1,2$) and desorbs from the clay. Therefore a rhodium complex containing the positively charged phosphine-phosphonium ligand, Ph₂PCH₂CH₂⁺P(Ph₂)CH₂Ph, was prepared. This complex retained its charge during the hydroformylation and remained between the interlayers.

5. PILLARED INTERLAYERED CLAYS (PILCS)

As was mentioned in the introduction, the driving force for the preparation of PILCS is the desire to synthesize temperature-stable porous materials with large pores. For this purpose, inorganic polymeric species were chosen since they would form oxide particles on heating, which would act as props for the clay layers, as shown in Fig. 7.

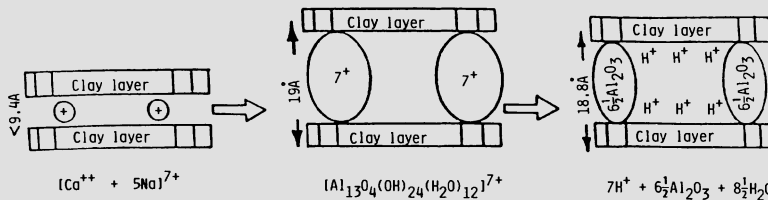


Figure 7. Schematic of the proposed formation of a pillared clay.
Reproduced from Ref. 39, with permission.

The initial work was done with either aluminum or zirconium polymers [29,30]. In the case of the aluminum pillaring, two types of solutions were used: an aluminum chloride solution to which was added up to 2.33 mol of NaOH per mol of Al [6], and a commercially available (Reheis Chemical Co., Chlorhydrol®) solution in which Al(OH)₃ or Al metal is dissolved in aluminum trichloride solutions, until the OH/Al ratio is equal to or slightly less than 2.5. Such solutions have been reported to contain polynuclear species with 6 to 400 aluminum atoms per structural unit [31,32]. However, the exact form of these species is unknown [33], but some of the proposed species are illustrated in Fig. 8 [34,35]. It has now been shown (see below) that in both types of solutions a major polymeric species is the Keggin ion, [Al₁₃O₄(OH)₂₄·12 H₂O]⁷⁺, having the structure shown in Fig. 9 [36]. However, NMR data have revealed some interesting differences between the two types of solution [37]. An aluminum chloride solution initially exhibits a single resonance characteristic of the Al(H₂O)₆³⁺ ion [38].

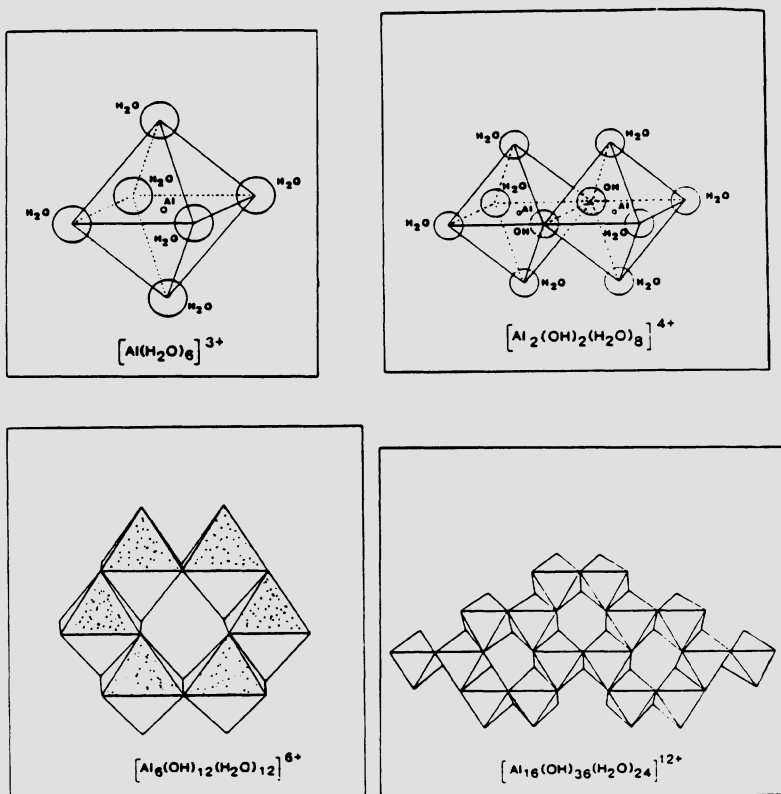


Figure 8. Proposed structures for complex aqueous aluminum species.
Reproduced from Ref. 35, with permission.

As base is added to this solution, a resonance at 62.8 ppm increases at the expense of a resonance indicative of the trivalent aluminum species. The new resonance is attributed to the Al_{13} Keggin ion, and when the OH/Al ratio is 2.42, it is the only species observed by NMR. In contrast, the Chlorhydrat[®] solution ($\text{OH}/\text{Al} = 2.50$) which was diluted from 6.2 M to 0.23 M exhibited the NMR spectra shown in Fig. 10 as it aged. The broad resonance at 10.8 ppm and the others at 70 and 0 ppm are attributed to species of higher nuclearity, but their identification has not been possible.

In all of the early pillararing studies irrespective of the type of solution used, the interlayer spacing of the smectite increased from approximately 9.3 Å to 18-19 Å [6,39,40]. This result is consistent with the incorporation of the Al_{13} Keggin ion, which has the shape of a prolate spheroid with a long axis of about 9.5 Å. The pillararing is illustrated (somewhat naively) in Fig. 7.

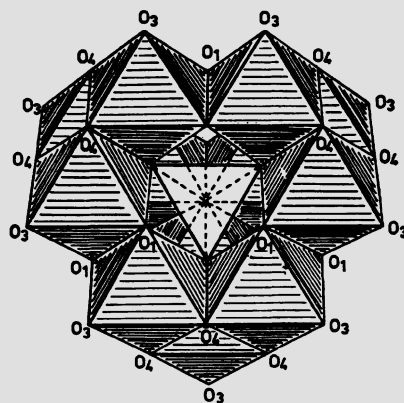


Figure 9. Schematic representation of the $[Al_{13}O_4(OH)_{24}(H_2O)_{12}]^{7+}$ ion.
Reproduced from Ref. 36, with permission.

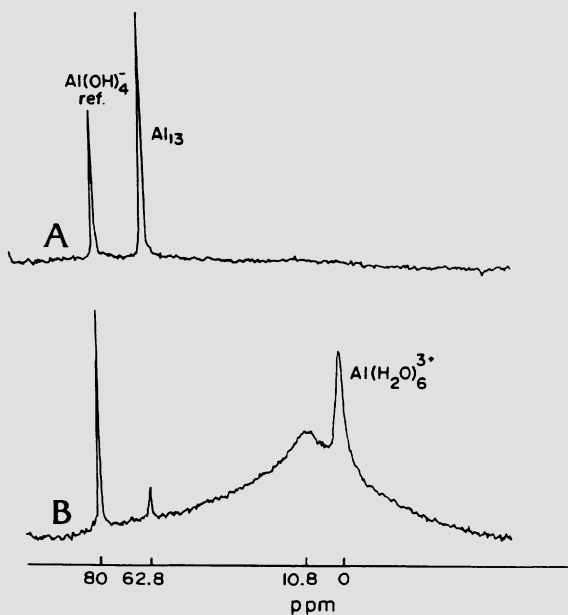


Figure 10. ^{27}Al spectra (46.9 MHz) of polyoxyaluminum pillaring reagents. (A): base-hydrolyzed $AlCl_3$, $OH/Al = 2.42$. (B): aluminum chlorohydrate, $OH/Al = 2.50$. The line near 80 ppm is the resonance of an external $NaAlO_2$ reference solution. Reproduced from Ref. 45, with permission.

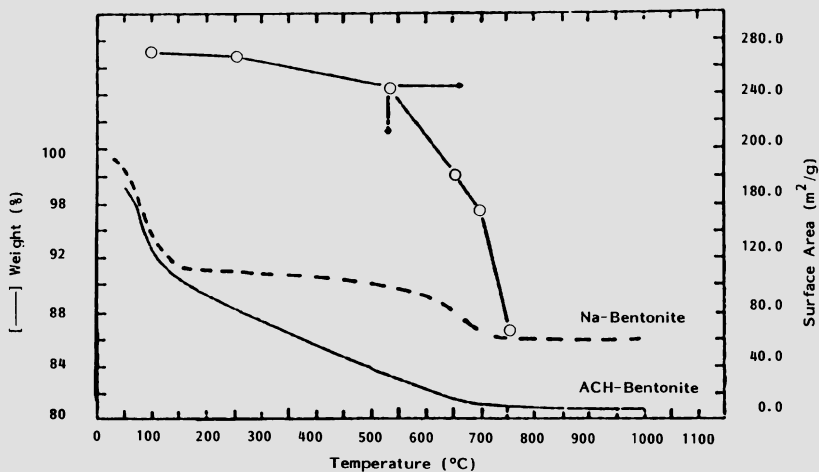


Figure 11. Thermogravimetric analysis of ACH-bentonite showing the correlation between weight and surface area losses.

Reproduced from Ref. 5, with permission.

On heating, the Keggin ion loses protons to the layers to balance the negative layer charge as the pillar is transformed to an oxide particle [40,41]. Surface areas of 200-300 m²/g have been observed [37]. Simultaneous thermal gravimetric analysis and surface area measurements show (Fig. 11) that about 50% of the water is lost at temperatures below 175°C; this is considered to be surface water. As the temperature is increased to 500°C, there is very little loss of surface area; the volume of the water lost roughly equals the pore volume. At higher temperatures, there is rapid loss of surface area accompanied by about a 1-Å loss in interlayer spacing, and at 700°C there is a total collapse of the structure [5].

Vaughan *et al.* [39,40] reported pore size distributions for two clays pillared by aluminum oxyocations. Their results are shown in Table II. In both examples, the majority of pores were less than 14 Å in diameter. However, there were significant numbers of pores between 14 and 20 Å and between 40 and 60 Å. The larger pores indicate some similarity to the amorphous catalyst. However, at low sorption pressures negligible amounts of large molecules are sorbed (Table III) [39,41]. Sorption data obtained by Occelli *et al.* [35,42] are shown in Table IV. Although the amount of straight chain hydrocarbons sorbed decreases with increasing chain length, the total volume occupied by the sorbed molecules is roughly constant and amounts to 60-70% of the total pore volume.

Table II. Pore size and surface area distributions for pillared clays and zeolites.

Pore Size Range, Å	Pillared Clay	Pillared Clay	NaY	Amorphous Catalyst	% N ₂ Surface Area
> 100	1.1	0.6	2.4	1.1	
100-80	0.5	0.2	0	3.0	
80-60	1.0	0.4	0	19.3	
60-40	16.5	19.0	0	47.5	
40-30	4.3	7.5	0	23.1	
30-20	0.7	0.0	0	6.0	
20-14	14.1	18.3	0	0	
< 14	61.9	64.0	97.6	0	
Average pore diameter, Å	23.6	21.9	18.2	51.4	
Total surface area, m ² /g	477	373	860	575	

Reproduced from Ref. 39, with permission.

Table III. Molecular sieve properties of pillared clays.

Probe molecule	Size, Å	Sorption Pressure, atm	Amount Sorbed, wt%
n-Butane	4.6	0.79	8.0
Cyclohexane	6.1	0.079	8.4
Carbon tetrachloride	6.9	0.139	11.5
1,3,5-Trimethylbenzene	7.6	0.012	5.3
1,2,3,5-Tetramethylbenzene	8.0	0.009	0
Perfluorotributylamine	10.4	0.041	0

Reproduced from Ref. 39, with permission.

One would imagine that the pore size of a particular pillared clay might depend upon the initial layer charge of the unpillared clay. Further, it is known that the charge distribution in smectite clays is highly irregular [43,44], which increases the expectation of non-uniform pillaring. However, it has been demonstrated that the pillars fill each interlayer region to essentially the same extent regardless of the layer charge, and the exchanging polynuclear hydroxo species apparently adjusts its charge by hydrolysis [29,37,45].

Table IV. Comparison of the sorptive properties of H-ZSM-5 and ACH-bentonite.

Sorbate	Sorbate size, Å ^a			Sorbate uptake, mmole g ⁻¹	
	b	t	l	H-ZSM-5	ACH-Bentonite
n-C ₆ H ₁₄	4.9	4.0	10.30	0.981	0.835
n-C ₇ H ₁₆	4.9	4.0	11.51	0.774	0.558
n-C ₈ H ₂₀	4.9	4.0	12.30	0.669	0.492
n-C ₁₀ H ₂₂	4.9	4.0	15.24	0.650	0.401
Mesitylene	9.0	4.0	8.60	<0.10	0.542

^a b = breadth; t = thickness; l = length.

Reproduced from Ref. 35, with permission.

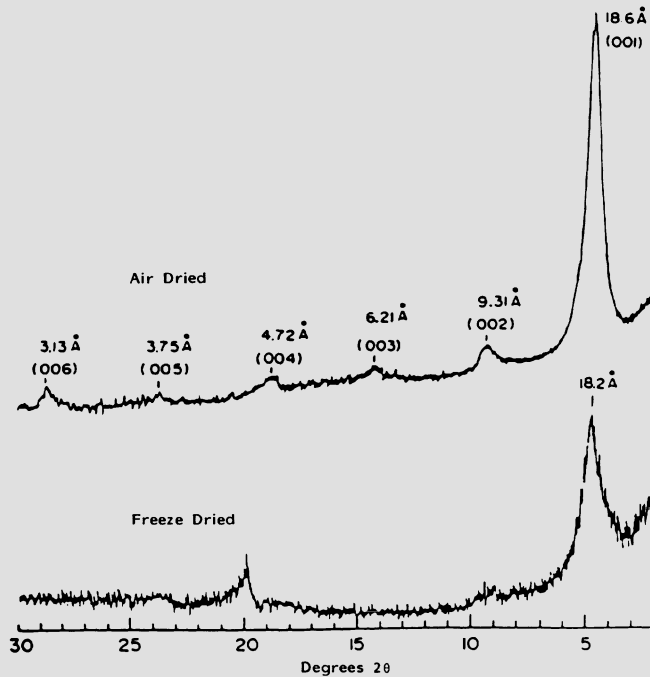


Figure 12. X-ray diffraction patterns of air-dried and freeze-dried forms of pillared montmorillonite (Sample II). Both samples were dispersed in water on glass slides and dried to constant water content at 110°C.

Reproduced from Ref. 37, with permission.

The pillar spacing appears to be decided by the radius of the ingoing cation. Selective adsorption studies demonstrate that the method used to dry the flocculated clay is far more important than the type of aluminum solution used for pillaring or the initial layer charge in determining the apparent pore size of the end product [37]. Air drying leads to a more crystalline product with relatively uniform pore sizes, whereas freeze-drying yields a more disordered product. This comparison is shown by the X-ray diffraction patterns of the clays prepared by the two different drying methods (Fig. 12). The air dried clay did not sorb 1,3,5-triethylbenzene (kinetic diameter 9.2 Å) but did sorb neopentane (kinetic diameter ~ 6.2 Å), whereas the freeze dried product sorbed appreciable amounts of molecules having a 10.4-Å kinetic diameter. Pinnavaia et al. attributed this result to the tendency of the air dried layers (formed by slow drying) to lie face to face, or flat, as shown in Fig. 13, whereas the rapidly freeze-dried product would tend to retain some delaminated structure, i.e., edge-to-face or edge-to-edge (Fig. 13). This pore structure holds at elevated temperatures also, as the adsorption measurements were made after heating the evacuated PILCS at 350°C for 3 hr. These considerations have important implications for the catalytic behavior of PILCS (vide infra).



Figure 13. A layer aggregation model for air-dried and freeze-dried pillared clays.

Reproduced from Ref. 45, with permission.

A quantitative interpretation of the solid state MAS-NMR spectra of both pillared and unpillared smectite clays has proved instructive [46]. The resonance for octahedrally coordinated ^{27}Al was clearly evident¹ in the spectrum of the pillared hectorite and the ratio oct/tet, obtained from the spectrum, indicated that the pillars were indeed the Al_{13} Keggin ions. When all the PILCS were heated, there was no evidence in the spectra that a reaction occurred between the pillar and layers for smectites with octahedral substitution i.e., montmorillonite and hectorite. However, for pillared beidellite, in which Al^{3+} substitutes in the tetrahedral sites, calcination at temperature

¹Only the Al_{tet} resonance is observed for the Al_{13} Keggin ion in solution (see Fig. 10). However, when the Al_{13} species is held rigidly in place as a pillar, the Al_{oct} resonance at approximately + 6 ppm is also observed.

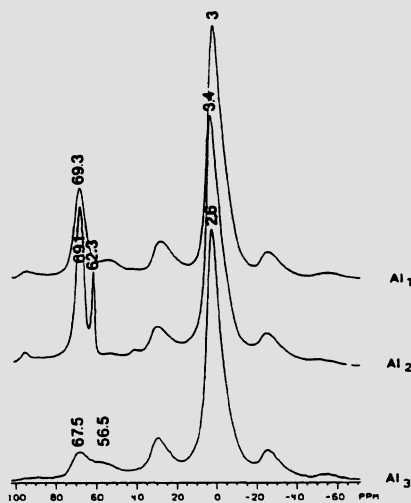
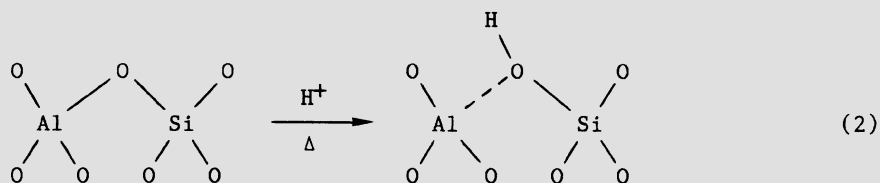


Figure 14. 11.7-T ^{27}Al MAS spectra, corresponding to a resonance frequency of 130.3 MHz, of beidellite (Al_1), pillared beidellite (Al_2), and calcined pillared beidellite (Al_3).

Reproduced from Ref. 46, with permission.

up to 350°C produced a drastic change in the sharpness and intensity of the ^{27}Al resonance for the tetrahedrally coordinated aluminums both in the clay layers, Al_s , and the pillar, Al_p . This spectral change, shown in Fig. 14, is interpreted in terms of a linkage between the layer and the pillar. Since the Al_{13} Keggin ion is acidic, it transfers protons to the layers upon calcination. The most likely point of attack is at an $\text{Al}-\text{O}-\text{Si}$ bridge, as shown in eq. (2), with formation of a silanol group.



Subsequent reaction with the pillar could lead to either $\text{Si}-\text{Al}_p^{\text{VI}}$ or $\text{Al}_s^{\text{IV}}-\text{Al}_p^{\text{VI}}$, where the Roman numerals denote the coordination of the Al and the subscripts s and p their location in the clay or pillar,

respectively. The spectral changes favor the latter type linkage and further indicate structural changes towards an all Al^{VI} pillar. The formation of silanol groups in beidellite makes it a much stronger acid than montmorillonite and accounts for its catalytic behavior in cracking [47] and hydroisomerization reactions [46].

Thomas et al. have also examined both pillared and unpillared clays by a variety of physical methods including NMR, FTIR and variable temperature powder X-ray diffractometry [48,49]. The clays studied were Gilwhite, a naturally occurring montmorillonite, and hectorite. In the unpillared clays it was shown that small cations such as Li⁺, or cations which generate protons at high temperatures (NH₄⁺, Al(H₂O)_x³⁺), show structural changes on heating to 500°C which are attributed to the diffusion of H⁺ or Li⁺ into the sheets. This effectively lowers the charge in the interlayer, resulting in reduced Brønsted acidity. At 700°C octahedrally coordinated aluminum is converted to 5-coordinate aluminum. Similarly, in the pillared clays the Brønsted acidity is also drastically reduced by diffusion of protons, generated from hydrolysis of the pillars, into the octahedral layer. At approximately 500°C, hydroxyl groups on the pillars condense with lattice hydroxyls on the clay sheets. The oxide pillars then become directly linked via oxygen to the aluminum and magnesium atoms in the octahedral layer.

6. PILLARING BY CATIONS OTHER THAN ALUMINUM

A variety of polynuclear cations other than the Al₁₃ Keggin ion have been used to pillar clays. Among them, we cite the zirconium tetramer [30,40,41,50,51], chromia polymers [52], bismuth [53], silicon [54], and niobium and tantalum halide clusters [55]. Of these, the most thoroughly studied have been zirconium polymers.

The cation species in the salt ZrOCl₂·8 H₂O is actually a tetramer, [Zr(OH)₂·4 H₂O]₄⁸⁺. The zirconium atoms form a square and are connected by double -ol (hydroxyl) bridges [56] as shown in Fig. 15. The same species has been shown to exist in solution in a more hydrolyzed form [57]. Boiling of zirconyl chloride solutions leads to the formation of colloidal, crystalline oxide particles [58]. The particles grow by -ol bridging between tetramers [59-61], forming a sheet-like structure [62]. Boiling for shorter periods yields a polydisperse system with average degrees of polymerization of 30-40 [63].

Burch et al. [50,51] prepared zirconium pillared montmorillonite. They obtained three different pillared products with gallery heights of 3-4 Å, 6.3-7.4 Å and 9.6-10.5 Å. By gallery height we mean the increase in interlayer spacing resulting from pillaring. Refluxing the Zr(IV) solution and dispersing the clay prior to pillaring produced PILCS with larger interplanar spacings, higher surface areas and greater stability. Surface areas were generally 200-300 m²/g. On the basis of the small increase in interlayer spacing it was proposed that the tetramers lie parallel to the clay layers. This result contrasts with the results of Yamanaka and Brindley [30], who obtained an interlayer increase of 10 Å with about 10% Zr uptake.

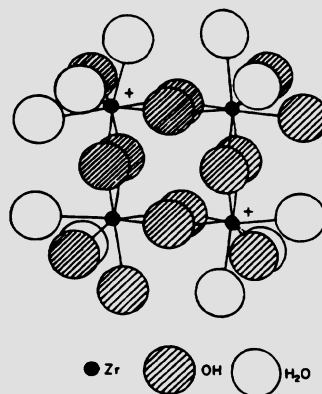


Figure 15. Schematic representation of the tetramer zirconyl ion in hydrolyzed form.

Based upon structures in Refs. 56 and 57.

From this Burch and Warburton [50] concluded that the tetramer species, the dimensions of which are $4.6 \text{ \AA} \times 10 \text{ \AA} \times 10 \text{ \AA}$, must stand perpendicular to the layers in the Yamanaka preparations. The free space in such pillared structures would arise only when the pillars are dehydrated (Fig. 16).

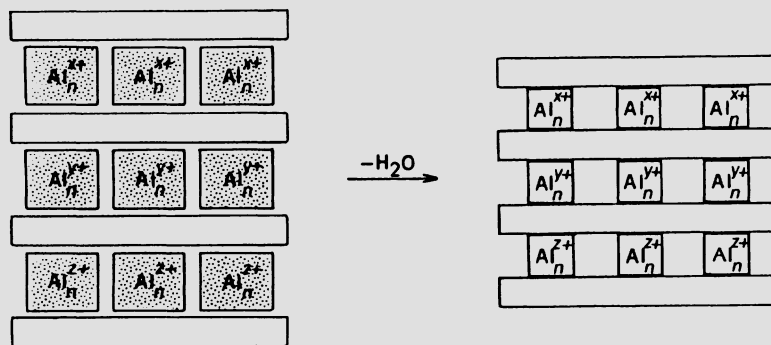


Figure 16. A model for the pillaring of smectite clays by hydrolyzed polyoxyaluminum cations, abbreviated Al_n^{X+} , Al_n^{Y+} , Al_n^{Z+} . The average charge per hydrolyzed cation is determined by the clay layer charge, but the nuclearity and population density of the hydrated pillars is independent of the clay layer charge.

Reproduced from Ref. 45, with permission.

In any event whether the pillars are parallel or perpendicular, the zirconium PILCS appear to have higher thermal and hydrothermal stability than the aluminum PILCS.

Chromium pillared clays represent an interesting case: it was possible to obtain products with 27 Å interlayer spacings [52]. These PILCS were prepared from hot basic chromium nitrate solution for which OH/Cr = 2. Surface areas were between 353 and 433 m²/g. Heating to 500°C reduced the interlayer spacing to 21 Å. Pore size data, however, are lacking.

A novel method of pillaring was utilized to prepare silica-clay intercalates [54]. The silicon acetylacetonato cation was exchanged with an oriented film of clay in acetone. Hydrolysis was then carried out in water. The pillared clays prepared in this fashion had expanded layer spacings of 12.6 Å and surface areas of 50 to 240 m²/g. These PILCS are stable to 500°C. Apparently the hydrolysis reaction forms silicic acid, which in turn forms SiO₂ pillars on heating. A related reaction involves exchanging [Nb₆Cl₁₂]²⁺ and [Ta₆Cl₁₂]²⁺ between clay layers. The clusters are probably incorporated as hydrates, and these hydrolyze to produce HCl and metal oxide on heating to 240°C. At temperatures near 400°C the interlayer distances decrease from approximately 19 Å to 10 Å.

7. CATALYSIS BY PILCS

Occelli and Tindwa [5] carried out an infrared study of an Al₁₃ pillared montmorillonite with adsorbed pyridine. Strong absorption bands at 1540 and 1490 cm⁻¹ confirmed the presence of Brønsted acid sites. However, equally strong or stronger bands at 1445 and 1600 cm⁻¹ showed the presence of a high proportion of Lewis acid sites. Heating to 400°C greatly diminished the ratio of Brønsted to Lewis acid sites. This result is interesting in the light of Thomas' finding that the Brønsted acid strength of pillared montmorillonite is reduced via migration of interlayer protons into the clay layer.

A number of acid catalyzed reactions have been examined in which the PILCS were compared to zeolites. Shabtai *et al.* [47] compared the rates of reaction for dealkylation of cumene and 1-isopropynaphthalene and for cracking of polycyclic naphthenes catalyzed by a pillared montmorillonite with rates of these reactions catalyzed by a Y-type zeolite. In each case the PILC, whether in the H⁺ or rare earth form, was found to have a higher activity. When the reactant molecule was larger than the zeolite windows, the rates of the PILC-catalyzed reaction were much greater than those of the zeolite-catalyzed reaction. Some of the data are summarized in Table V.

Pillared montmorillonite was also found to be highly active in cracking heavy gas oils to give gasoline [5,35,39,42,64]. However, it also exhibited high rates of coke formation. This result has been attributed to occlusion of hydrocarbons [65] which could be a serious deterrent to the use of PILCS for such reactions, since they are not as stable to regeneration by coke burn-off as are zeolites. A similar PILC also showed high initial activity for the conversion of methanol to

hydrocarbons, but the catalyst rapidly deactivated [35]. Regeneration at 425°C failed to restore the initial activity. This catalyst did not show shape selectivity in the alkylation of toluene. However, the deactivated catalyst could be restored to high activity by burning off the coke at 400°C.

Table V. Relative rates (V_{rel}) of dealkylation of 1-iso-Propylnaphthalene (2) with HY(I) and H-Al-CLM(II) catalysts.

Catalyst Temp., °C	H-Y(I) ^a $V_{rel\text{I}}$	H-Al-CLM(II) $V_{rel\text{II}}$	$V_{rel\text{II}}/V_{rel\text{I}}$
350	1.00	5.02	5.02
400	1.57	10.56	6.73
450	1.69	15.58	9.22
480	1.81	19.37	10.70

^a all rates relative to H-Y(I) at 350°C.

Shape selectivity in pillared montmorillonites has been considered by Kikuchi *et al.* [66,67]. Disproportionation of 1,2,4-trimethylbenzene yielded preferentially 1,2,4,5-tetramethylbenzene and α -xylene. A mechanism was proposed to account for the preferential formation of these products (which are not the most stable thermodynamically) based upon a restricted transition state selectivity [67]. Coke deposition, normally rapid, was prevented by supporting a small amount of Pd on the catalyst and using H_2 as a carrier gas.

Pillared montmorillonites were used to oligomerize propylene at 30-50 atm [68]. One of the catalysts was pillared with a mixed aluminum-zirconium polymer. The PILCS were much less active than H-zeolite omega or an aluminosilicate catalyst. However, the selectivity for gasoline was greater. The Al-Zr PILC exhibited a high selectivity for aromatics and less coke formation than the Al-PILC. The observed behavior was attributed to the large number of Lewis acid sites relative to Brønsted acid sites and to the microporosity of the PILCS.

An interesting comparison of catalytic activities of synthetic beidellite and montmorillonite and PILCS prepared from them was recently reported [69]. The reactions examined included secondary amine formation from cyclohexylamine, ester production from 1-hexene and acetic acid and ether synthesis from pentanol. In all cases, the reactivity of the PILCS was much lower than that of the unpillared clays, whereas the montmorillonite was generally more effective than the beidellite. These results are not surprising in that all of the reactions are Brønsted-acid-catalyzed and the observed decreased activity of the PILCS may derive from a greater loss of protons to the layers by the pillared clays. This is also in keeping with the findings of Occelli and Tindwa [5] that the PILCS are mainly Lewis acids after heat treatment.

Catalysis by PILCS is in its infancy and it is clear that much more characterization of the PILCS and controlled catalytic studies are required to place this field on a sound footing.

8. ORGANICALLY PILLARED GROUP(IV) PHOSPHATES

I would be remiss if I did not discuss in a small way ongoing work in my laboratory on organically pillared titanium and zirconium phosphates. The parent phosphates, having composition $M(HPO_4)_2 \cdot H_2O$ and possessing the α -phase structure, resemble smectites in that the metal atoms are sandwiched between phosphate groups [70]. The major difference results from the phosphate tetrahedra being inverted, as shown in Fig. 17.

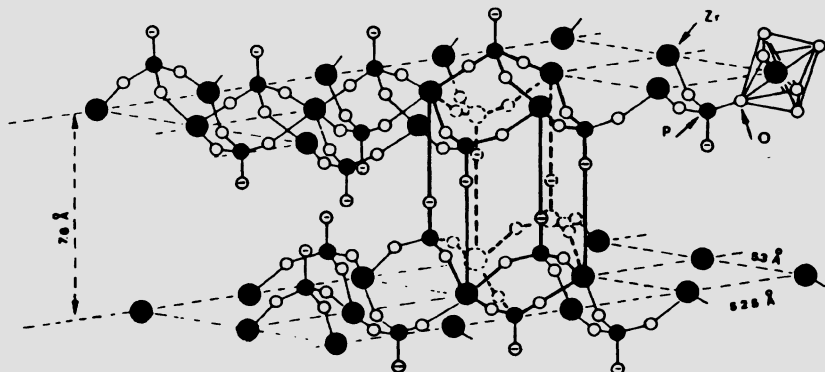


Figure 17. Idealized structure of α -zirconium phosphate showing one of the zeolitic cavities created by the arrangement of the layers.

From G. Alberti, in Study Week on Membranes (Ed. R. Passino), p.629, Pontificiae Academiae Scientiarum Scripta Varia, Rome (1976), with permission.

The octahedral coordination arises from the fact that each Zr or Ti is coordinated by six different phosphate groups which requires that each phosphate group bridge three metal atoms. All the charge then resides on the fourth oxygen, which points into the interlayer and is bonded to a hydrogen atom. By comparison with an Si_8 smectite unit, the formula is $(\text{Zr}_4)_{\text{oct}}(\text{P}_8)_{\text{tet}}\text{O}_{24}(\text{OH})_8$. Thus there is no substitution, either in the octahedra or the tetrahedra, and in this respect zirconium phosphate is more like a pyrophyllite than a smectite clay. The forces between layers are of the van der Waals type, and no swelling in water

takes place. Thus, pillaring by conventional methods used for clays is not possible.

Alberti *et al.* [71] were able to prepare organic derivatives with the α -structure by reacting a Zr(IV) solution with aryl or alkyl phosphonic acids. A schematic representation of the phenyl compound is shown in Fig. 18. Shortly thereafter, Dines *et al.* [72] prepared pillared derivatives by using diphosphonic acids in the preparation.

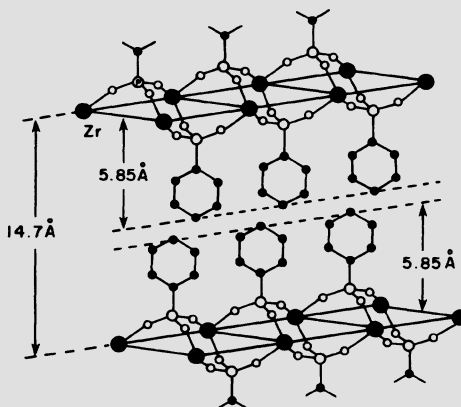


Figure 18. Idealized crystal structure of zirconium bis (benzenephosphonate). ●: Zr; ○: P; ○: O; •: C.

Reproduced from Ref. 71, with permission.

Since the distance between phosphate groups is 5.3 Å [70], there would be no room for inward diffusion of molecules if every position were thusly pillared. By mixing in either phosphoric or phosphorous acid, it is possible to space the pillars so as to create cavities (or rather diffusion paths) between layers [72,73]. This is illustrated schematically in Fig. 19. In this depiction, each pillar is equally spaced 10.6 Å apart. However, surface area and pore size measurements indicate that such may not be the case [74].

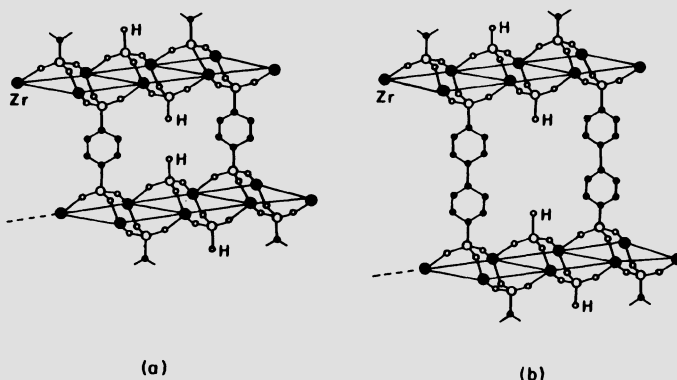
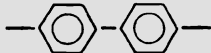
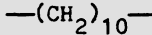


Figure 19. Schematic representation of monophenyl (a) and biphenyl (b) pillared zirconium phosphates.

The interlayer spacings obtained by pillaring with several different groups is given in Table VI. BET surface area measurements show that only the pillars which produce an interlayer distance of 12 Å or greater are sufficiently expanded to allow N_2 to penetrate into the interlamellar space. Surface areas of 100-400 m^2/g have been obtained by Dines [73] and also by us [74]. However, the surface area strongly depends upon the method of preparation. Rapid precipitation leads to small particle sizes of low crystallinity and a broad pore size distribution [74]. Slower precipitation from HF solution produces more crystalline products and better defined pores. However, it is easy under such conditions to obtain phase separation into $Zr(HPO_4)_2$ (or the corresponding phosphite) and an organically pillared product with much less spacing of the pillars. We are studying these synthetic procedures so as to learn how to direct the pillaring to achieve cavities of a desired size.

Only preliminary catalytic studies have been carried out with the organically pillared derivatives. Those with aryl pillars are stable to about 400°C in the absence of oxygen, whereas alkyl pillared products decompose at a temperature 50°C lower [72,73]. The conversion of methanol to hydrocarbons yielded mainly methane and coke together with smaller amounts of C₂-C₄ hydrocarbons [75]. However, with ethanol, a smooth conversion to ethylene in high yield was obtained [76].

Table VI. Interlayer distances of organically pillared α -zirconium phosphate.

Pillaring Unit R	Interlayer Spacing (\AA)
-	7.6
	9.6
	13.6
	18.5
	10.8
	17.2

Work with these organically pillared compounds is in its infancy. Given the wide choice of pillars and functional groups that can be utilized, a versatile family of catalysts may be expected to develop from these materials. For example, the protons of the HPO_4^{2-} groups (Fig. 19) may be exchanged for catalytically active metals. For divalent cations such as Pd^{2+} the distance between $\text{P}-\text{O}^-$ sites is large so that the cation is loosely held and mobile. Thus it is readily reduced to fine-grained reactive metal aggregates in the presence of H_2 under mild conditions. The Pd^{2+} ion can also be readily utilized in Wacker type chemistry [74]. Finally it should be mentioned that a variety of catalytically active complexes may be attached to the layers, such as, for example, those shown in Fig. 20 [77]. Because of the versatility with which derivatives of the layered group IV phosphates may be prepared, they have been referred to as "Molecularly Engineered Layers" or MELS [78].

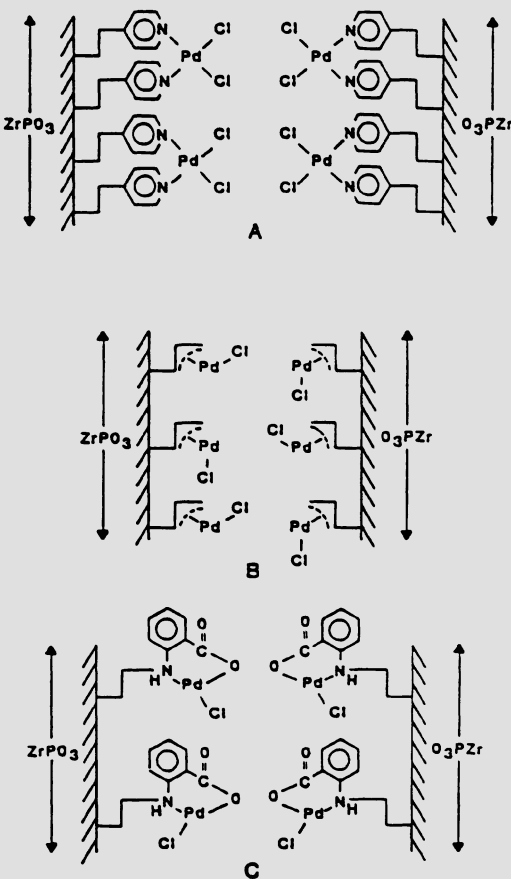


Figure 20. Palladium containing hydrogenation catalysts. (A): pyridyl; (B): allyl; (C): anthranilic acid.

Reproduced from Ref. 77, with permission.

9. CONCLUSIONS

The PILCS and MELS constitute new classes of porous materials with exceptional promise. Given the large number and diversity of potential pillaring species and the variety of layered materials which can be pillared it is evident that a wide range of products is possible. A great deal more work on the structure and properties of these materials

is required, and the anticipated knowledge should lead to the ability to create materials with pores of uniform, predictable sizes. These materials should join a growing array of catalysts which the chemist or engineer can tailor to the specific needs of a particular reaction.

10. ACKNOWLEDGMENT

The author wishes to express his thanks to Amoco Chemical Co. and Texaco, Inc., U.S.A., as well as to the Texas Advanced Technology Research Program for financial support.

11. REFERENCES

1. L.B. Ryland, M.W. Tamele, and J.N. Wilson, in Catalysis (Ed. P.H. Emmett), Reinhold Publ. Co, New York (1960).
2. E.M. Flanigen, Proc. 5th Int. Conf. on Zeolites (Ed. L.V. Rees), Heyden, London (1980).
3. J.H. Gary and G.E. Handwerk, Petroleum Refining: Technology and Economics (Eds. L.F. Albright, R.N. Maddox, and J.J. McKetta), Marcel Dekker, Inc., New York (1975).
4. D.W. Breck, Proc. Conf. on Properties and Application of Zeolites, Soc. Chem. Ind., London (1979).
5. M.L. Occelli and R.M. Tindwa, Clays and Clay Minerals 31, 22 (1983).
6. N. Lahav, V. Shani, and J. Shabtai, Clays and Clay Minerals 26 107 (1978).
7. B.K.G. Theng, The Chemistry of Clay-Organic Reactions, John Wiley & Sons, New York (1974).
8. R.M. Barrer, Zeolites and Clay Minerals as Sorbents and Molecular Sieves, Academic Press, New York (1978).
9. J. Shabtai, N. Frydmand, and R. Lazar, Proc. 6th Int. Congr. Catal. B5, 1 (1976).
10. M.M. Mortland and V. Berkheiser, Clays and Clay Minerals 24, 60 (1976).
11. S.W. Bailey, in Crystal Structures of Clay Minerals and Their X-ray Identification, (Eds G.W. Brindley and G. Brown), Mineral. Soc., London (1980).
12. G. Beson, A. Mifsud, C. Tchoubar, and J. Mering, Clays and Clay Minerals 22, 379 (1974).
13. H. Suquet, C. de la Calle, and H. Pezerat, Clays and Clay Minerals 23, 1 (1975).
14. A. Clearfield and J.A. Stynes, J. Inorg. Nucl. Chem. 26, 117 (1964).
15. M.M. Mortland, Trans. 9th Int. Congr. Soil Sci. 1, 691 (1968).
16. H. Van Olphen, An Introduction to Clay Colloid Chemistry, John Wiley & Sons, New York (1977). 2nd Ed.
17. T.J. Pinnavaia, Science 220, 365 (1983).

18. J.J. Fripiat, in Advanced Chemical Methods for Soil and Clay Minerals Research (Eds J.W. Stucki and W.L. Banwart), pp. 245-361, Reidel Publ. Co., Dordrecht, The Netherlands (1980).
19. T.J. Pinnavaia, in Advanced Techniques for Clay Mineral Analysis (Ed. J.J. Fripiat), pp. 139-161, Elsevier Publ. Co., New York (1981).
20. P.L. Hall, *ibid.*, pp. 51-75.
21. M.B. McBride, T.J. Pinnavaia, and M.M. Mortland, J. Phys. Chem. 79, 2430 (1975).
22. T.J. Pinnavaia, R. Raythatha, J.G.-S. Lee, L.J. Halloran, and J.F. Hoffman, J. Am. Chem. Soc. 101, 6891 (1979).
23. T.J. Pinnavaia and P.K. Welty, J. Am. Chem. Soc. 97, 3819 (1975).
24. R.R. Schrock and J.A. Osborn, J. Am. Chem. Soc. 98, 2134 (1976).
25. R. Raythatha and T.J. Pinnavaia, J. Catal. 80, 47 (1983).
26. M.M. Mortland, J.J. Fripiat, J. Chaussidon, and J. Uytterhoven, J. Phys. Chem. 67, 248 (1963).
27. J.J. Fripiat, A.C.S. Symp. Ser. 34, 261 (1976).
28. F. Farzaneh and T.J. Pinnavaia, Inorg. Chem. 22, 2216 (1983).
29. G.W. Brindley and R.E. Semple, Clays and Clay Minerals 26, 229 (1978).
30. S. Yamanaka and G.W. Brindley, Clays and Clay Minerals 26, 21 (1978).
31. J.D. Hem and C.E. Robertson, U.S. Geol. Surv. Water-Supply Pap. 1827-A, 55 pp. (1967).
32. R.W. Smith and J.D. Hem, U.S. Geol. Surv. Water-Supply Pap. 1827-D, 51 pp. (1972).
33. J.H. Patterson and S.Y. Tyree, Jr., J. Colloid Interface Sci. 43, 389 (1973).
34. P.H. Hsu and T.F. Bates, Soil Science 28, 763 (1964).
35. M.L. Occelli, R.A. Innes, F.S.S. Hure, and J.W. Hightower, J. Appl. Catal. 14, 69 (1985).
36. G. Johansson, Acta Chem. Scand. 14, 769 (1960).
37. T.J. Pinnavaia, M.-S. Tzou, S.D. Landau, and R.H. Raythatha, J. Mol. Catal. 27, 195 (1984).
38. See J.W. Akitt and A. Farthing, J. Magn. Reson. 32, 345 (1978); J. Chem. Soc., Dalton Trans., 1617 (1981); 1624 (1981) for further details on these assignments.
39. D.E.W. Vaughan and R.J. Lussier, 5th Int. Conf. on Zeolites, Naples, Italy, Heyden, London (1980).
40. D.E.W. Vaughan, R.J. Lussier, and J.S. Magee, Jr., U.S. Patent 4,271,043, June 2, (1981) (to W.R. Grace and Co.); U.S. Patent 4,176,090 (1977) (to W.R. Grace and Co.).
41. R.J. Lussier, J.S. Magee, Jr., and D.E.W. Vaughan, 7th Canadian Symp. Catal., Edmonton, Alberta, Oct. 19-22 (1980).
42. M.L. Occelli, V. Parulekar, and J. Hightower, Proc. 8th Int. Congr. Catal., Berlin (1984).
43. M.S. Stul and W.J. Mortier, Clays and Clay Minerals 22, 391 (1974).
44. P. Peogneur, A. Maes, and A. Cremers, *ibid.* 23, 71 (1975).
45. T.J. Pinnavaia, in Heterogeneous Catalysis (Ed. B. Shapiro), p. 18, Texas A&M University Press, College Station, Texas (1985).

46. D. Plee, F. Borg, L. Gatineau, and J.J. Fripiat, J. Am. Chem. Soc. 107, 2362 (1985).
47. J. Shabtai, R. Lazar, and A.G. Oblad, New Horizons Catal. 7, 828 (1981).
48. D.T.B. Tennakoon, J.M. Thomas, W. Jones, T.A. Carpenter, and S. Ramdas, J. Chem. Soc., Faraday Trans. 1 82, 545 (1986).
49. D.T.B. Tennakoon, W. Jones, and J.M. Thomas, ibid, submitted.
50. R. Burch and C.I. Warburton, J. Catal. 97, 503 (1986).
51. G.J.J. Bartley and R. Burch, J. Appl. Catal. 19, 175 (1985).
52. T.J. Pinnavaia, M.S. Tsou, and S.D. Landau, J. Am. Chem. Soc. 107, 4783 (1985).
53. S. Yamanaka, G. Yamashita, and M. Hattori, Clays and Clay Minerals 28, 281 (1980).
54. T. Endo, M.M. Mortland, and T.J. Pinnavaia, Clays and Clay Minerals 28, 105 (1980).
55. S.P. Christiano, J. Wang, and T.J. Pinnavaia, Inorg. Chem. 24, 1222 (1985).
56. A. Clearfield and P.A. Vaughan, Acta. Crystallogr. 9, 555 (1956).
57. G.M. Muha and P.A. Vaughan, J. Chem. Phys. 33, 194 (1960).
58. A. Clearfield, Inorg. Chem. 3, 146 (1964).
59. A. Clearfield, Rev. Pure Appl. Chem. 14, 91 (1964).
60. H. Rijnten, in Physical and Chemical Aspects of Adsorbents and Catalysts (Ed. B.G. Lensen), Academic Press, New York (1970).
61. A. Clearfield, G.H. Nancollas, and R.H. Blessing, in Ion Exchange and Solvent Extraction, (Eds. J.A. Marinsky and Y. Marcus), v.5, ch. 1, Marcel Dekker, Inc., New York (1973).
62. J.R. Fryer, J.L. Hutchinson, and R. Paterson, J. Colloid Interface Sci. 34, 238 (1970).
63. J.S. Johnson and K.A. Kraus, J. Am. Chem. Soc. 78, 3937 (1956).
64. M.L. Occelli, Ind. Eng. Chem. Prod. Res. Dev. 22, 553 (1983).
65. M.L. Occelli and J.E. Lester, Ind. Eng. Chem. Prod. Res. Dev. 24, 27 (1984).
66. E. Kikuchi, R. Hamana, M. Nakano, M. Takehara, and Y. Morita, J. Jpn. Pet. Inst. 26, 116 (1983).
67. E. Kikuchi, T. Matsuda, H. Fujiki, and Y. Morita, J. Appl. Catal. 11, 331 (1984).
68. M.L. Occelli, J.T. Hsu, and L.G. Galya, J. Mol. Catal. 33, 371 (1985).
69. P.A. Diddams, J.M. Thomas, W. Jones, J.A. Ballantine, and J.H. Purnell, J. Chem. Soc., Chem. Commun., 1340 (1984).
70. A. Clearfield and G.D. Smith, Inorg. Chem. 8, 775 (1969).
71. G. Alberti, U. Costantino, S. Allulli, and N. Tomassini, J. Inorg. Nucl. Chem. 40, 1113 (1978).
72. M.B. Dines and P.M. Di Giacomo, Inorg. Chem. 20, 92 (1981).
73. M.B. Dines, P.M. Di Giacomo, K.P. Callahan, P.C. Griffith, R.H. Lane, and R.E. Cooksey, in Chemically Modified Surfaces in Catalysis and Electrocatalysis (ACS Symp. Ser. 192) (Ed. J.S. Miller), ch. 1, A.C.S., Washington (1982).
74. A. Clearfield, G.-Z. Peng, and C.-Y. Yang, work in progress.
75. S. Cheng, G.-Z. Peng, and A. Clearfield, Ind. Eng. Chem. Prod. Res. Dev. 23, 219 (1984).

76. S. Cheng and A. Clearfield, J. Appl. Catal., in press.
77. R.H. Lane, K.P. Callahan, R. Cooksey, P.M. Di Giacomo, M.B. Dines, and P.C. Griffith, ACS Symp. on Immobilized Catalysts, A.C.S., Washington, D.C. (1982).
78. Catalytica Brochure, Catalytica Associates, Mountain View, CA 94043.

REACTIONS OF ORGANOMETALLICS WITH THE SURFACES OF ZEOLITES

Eric G. Derouane

Facultés Universitaires N.D. de la Paix
Center for Advanced Materials Research,
Laboratory of Catalysis
Rue de Bruxelles, 61
B-5000 Namur
Belgium

ABSTRACT. An account is given of the ways in which catalytically active organometallic species can be prepared or reacted within the intracrystalline volume of zeolites. Following a discussion of the chemical and physical factors influencing the interactions of metal complexes and zeolite frameworks, three types of intrazeolitic complexes are described: exchangeable cation-based complexes, occluded (neutral) organometallic species, and framework site-based coordination compounds.

Finally, some of the possible future trends are presented.

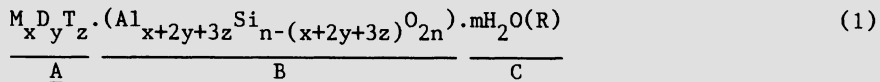
1. INTRODUCTION

The most stable family of crystal matrices is constituted by the zeolites, which, according to the generalized definition [1], encompass not only porous tectosilicates, but also other non-aluminosilicate molecular sieves. Preparing active organometallic catalytic species within the intracrystalline volumes of these structures is a challenge that is relevant to heterogeneous and homogeneous catalysis as well as enzyme modeling.

Several authors have reviewed established and promising applications in this field [2-4]. The present paper is not comprehensive, but is intended to offer some perspective, specifically, concerning methods of functionalizing the intracrystalline surfaces of zeolites, the chemical and physical nature of the interactions between the occluded species and the zeolite framework, and some principles describing the formation and behavior of organometallic compounds within the internal void volumes of zeolites.

2. INTRACRYSTALLINE ORGANOMETALLIC CHEMISTRY

Zeolite structures have the general chemical formula:



where A stands for exchangeable mono-(M), di-(D), or tri-(T) valent cations (which are H in the active acid catalyst); B represents the three-dimensional framework itself (including pores, channels, and cages); and C corresponds to sorbed (or occluded) water or other species (R) which can be removed, sometimes reversibly. Table I is a comparison of the pore structure and the typical Al content of some important pure zeolites. The channels and cavities of molecular dimensions determine the molecular shape selective properties of these catalysts [5,6], whereas the Si/Al ratio influences the (re)activity and stability.

Table I. Some common zeolites of industrial interest

Code	Name	Average channel size /nm	Cavity size /nm	Typical Si/Al ratio
LTA	Linde type	0.41(3D)	0.66;1.14	1.0-1.05
FAU(X)	Linde type X	0.74(3D)	0.66;1.18	1.2-1.30
FAU(Y)	Linde type Y	0.74(3D)	0.66;1.18	1.7-2.40
MAZ	Omega	0.74(1D)	-	2.6
LTL	Linde type	0.71(1D)	-	3.0
ERI	Erionite	0.36x0.52(3D)	0.63x1.30	3.0
OFF	Offretite	0.64(1D);0.36x0.52(2D)	0.60x0.74	3.5
MOR	Mordenite	0.67x0.70(1D)	-	5.0
MFI	ZSM-5	0.54x0.56-0.51x0.55(3D)	-	5.0-∞

1D, 2D, and 3D indicate uni-, bi-, and tri-dimensional channel networks respectively.

Three classes of interactions can be envisaged to lead to formation of organometallic compounds within zeolite frameworks; all three are illustrated schematically in Fig. 1. The structure include exchangeable cationic species, occluded complexes, and species incorporated in framework sites.

In all cases the zeolite structure will impose environmental conditions differing from those encountered on a "flat" surface. The zeolite will behave as a solid ionic solvent [7] and embed its guests within a high electrostatic field (10^{9-11} V.m⁻¹). Its anionic framework will be able to act as a macroanion or a polydentate ligand. Further, the finite size of the channels and intersections will limit the access to the internal void volume of the entities used in the preparation of

the organometallic and in catalysis; it will offer steric hindrance, causing virtual pressure effects; and it may also affect the catalytic activity of the organometallic. The occluded complexes will thus be held and affected by steric, electrostatic, and chemical forces. The exact nature, concentration, and properties of these species will depend on the nature, distribution, and accessibility of the anchoring sites (framework anions, exchangeable cations, or protons).

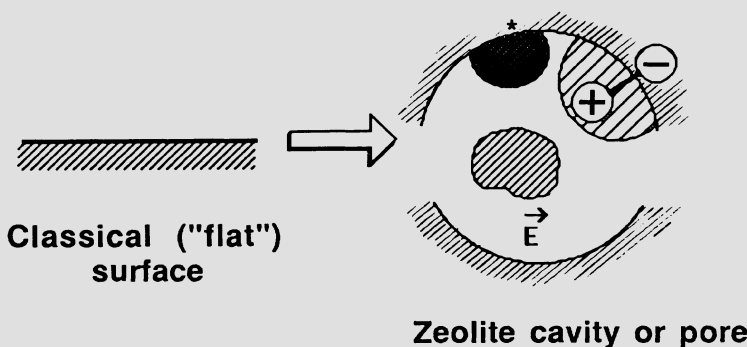


Figure 1. Schematic illustration of the different types of intracrystalline organometallic complexes: occluded species, exchangeable cation-based entities $[(+)-(-)]$, and framework (*) based species. E represents the internal electrostatic field.

Exchangeable cationic complexes are usually generated by in-situ complexation of transition metal ions. This process is obviously influenced by a variety of steric constraints. Occluded neutral species, either captured during synthesis or sorbed by the finished zeolite, may be subject to ligand substitution or react with structural (anionic or cationic) species. Complexes incorporated in framework sites have not been described so far; their formation will obviously necessitate in most cases the breakage of T-O-M bonds, T and M being metal lattice sites.

Examples of these intrazeolitic complexes are discussed below in more detail.

3. EXCHANGEABLE CATIONIC ORGANOMETALLIC COMPLEXES

It must be realized that fully coordinated complexes have little catalytic importance and that free, accessible coordination sites are necessary. Steric constraints arising from the particular and confined environment provided by the zeolite play an important role in determining the coordination. Further, the coordination number, as well as the position and oxidation state of an exchangeable cation can change within a zeolite cavity.

To illustrate these points, Fig. 2 shows the structures of adsorption complexes formed by contacting acetylene and NO with a Co(II)A zeolite [8]. In both cases, the Co(II) cation moves outside the plane of the six-membered ring window to achieve a more tetrahedral-like coordination with the sorbate. In the case of acetylene, a weak complex is formed which involves its polarizable π -orbitals. For NO sorption, however, electron transfer occurs, and the complex is best described as $\text{Co}(\text{III})\text{-NO}^-$. Although zeolite A is a small-pore material and has restricted applications to catalysis, model studies such as these are relevant to large-pore zeolites as well.

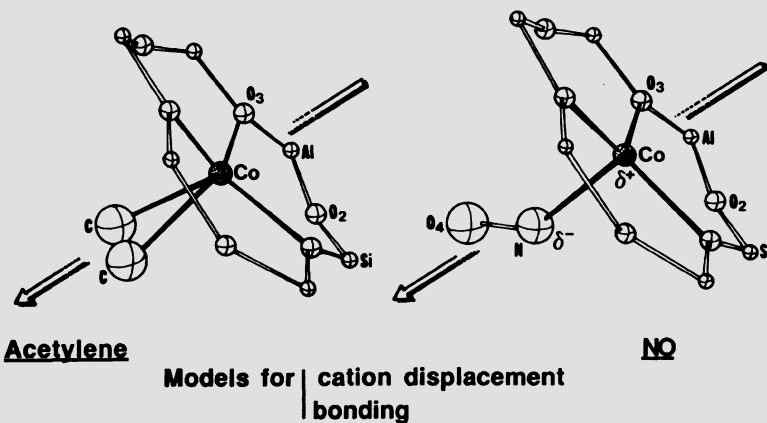


Figure 2. Acetylene and NO sorption complexes in Co(II) in zeolite A (adapted from [8]).

The reaction of Co(II) ions in zeolite Y with 2,2'-bipyridine (bpy) and 2,2',2"-terpyridine (terpy) has been used to prepare structures believed to be mixed ligand five-coordinate $[\text{Co}^{\text{II}}(\text{bpy})(\text{terpy})]^{2+}$ complexes [9,10]. As shown in Table II, higher temperatures favor the synthesis of mixed species, and the presence of other cations has a profound, albeit not fully rationalized, effect on complex formation. Cations can change diffusional properties affecting the transport of reactants entering a zeolite by modifying the effective (pore) window size. Since the cations may have various hydration states and occupy various positions, they may offer various steric constraints.

The cobalt complex mentioned above can be used to selectively and reversibly sorb oxygen from air, according to the scheme:

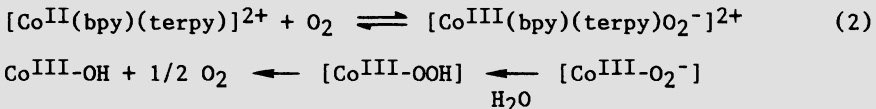


Table II. Effect of other cations in zeolite Y on the complex formation of Co(II) with bipyridine and terpyridine ligands ($7 \cdot 10^{-5}$ mol Co/g of zeolite Y; Co:bpy:terpy = 1:1:1) (adapted from [10]).

Zeolite	Reaction		Complex formed	Co-based yield (%)
	Temperature /K	Time /h		
CaY	623	18.5	[Co ^{II} (bpy)(terpy)] ²⁺	1.5
NH ₄ Y	523	85	[Co ^{II} (terpy) ₂] ²⁺	26.4
NH ₄ Y	583	23	[Co ^{II} (terpy) ₂] ²⁺	22.0
KY	523	47	[Co ^{II} (terpy) ₂] ²⁺ [Co ^{II} (bpy) ₂] ²⁺	49.9
NaY	523	24	[Co ^{II} (bpy)(terpy)] ²⁺ [Co ^{II} (terpy) ₂] ²⁺	7.2 8.5
NaY	613	14	[Co ^{II} (bpy)(terpy)] ²⁺ [Co ^{II} (terpy) ₂] ²⁺	20.2 17.8
LiY	653	14	[Co ^{II} (bpy)(terpy)] ²⁺ [Co ^{II} (terpy) ₂] ²⁺	27.1 9.1
LiY	703	2	[Co ^{II} (bpy)(terpy)] ²⁺ [Co ^{II} (terpy) ₂] ²⁺	45.3 4.1

in which both the oxidation and coordination states of the Co are changed [10]. O₂/N₂ separation factors of 5-20 can be achieved with the LiY zeolite as base material. The presence of water has a detrimental effect: it converts the superoxide anions into hydroperoxy species which, in turn, irreversibly oxidize Co(II) into Co(III).

Spectroscopic measurements characterizing encaged complexes support the view that chemical (and physical) interactions with the zeolite framework produce high virtual pressure effects. Such findings are in line with the so-called "concentration effect" [11], recent NMR results [12], and the "nest effect" proposal [13]. For example, when dimethylglyoxime is sorbed in Ni(II)Y or Co(II)Y zeolites, tetrahedrally coordinated species are initially formed $[(Ni,Co)(dmgh)]^{2+}$ (Fig. 3) [14]. They are converted at higher dimethylglyoxime concentrations into square-planar $[(Ni,Co)(dmgh)_2]^{2+}$ complexes, which experience a virtual pressure of about 0.74 kbar, as evidenced by the bathochromic shift of the 524-nm band characterizing an electron transition perpendicular to the plane of the molecule [15].

Even larger virtual pressure effects (up to about 30 kbar) are observed when bulkier molecules, such as metal phthalocyanines, are synthesized *in-situ* within zeolite Y cages [3,16]. Fig. 4 represents an encaged Co-phthalocyanine complex within a faujasite framework supercage, experiencing distortions which are reflected in the electronic vibration transitions of the macrocycle.

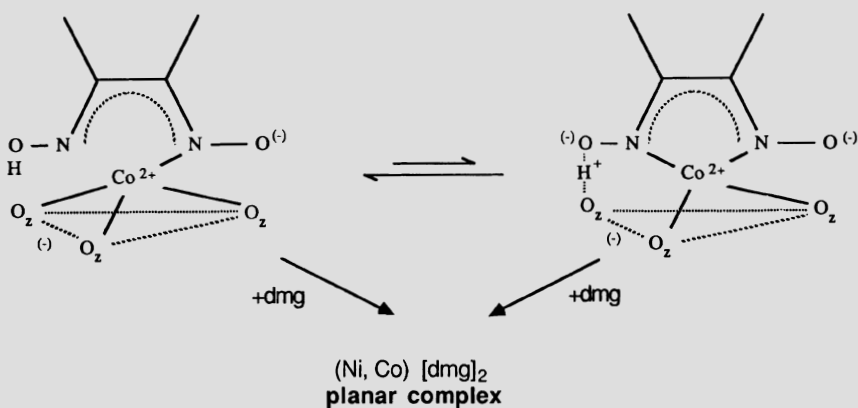


Figure 3. Tetrahedral intermediates formed upon vapor adsorption of dimethylglyoxime in Co(II)Y zeolite (adapted from [14]).

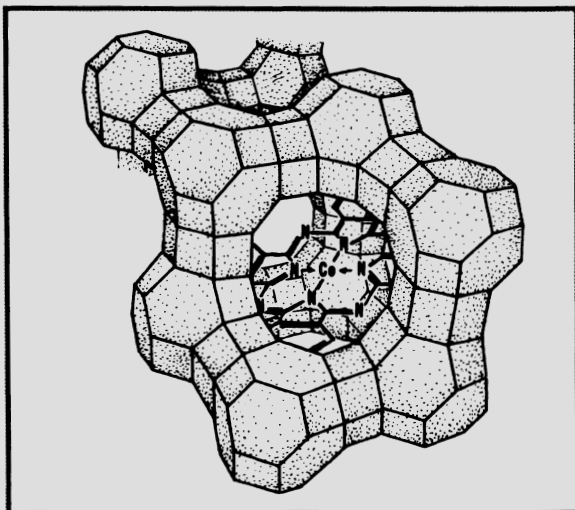


Figure 4. Representation of a Co-phthalocyanine molecule trapped in a faujasite zeolite supercage (adapted from [4]).

4. OCCLUDED (NEUTRAL) ORGANOMETALLIC SPECIES

Occluded, possibly neutral, complexes can be prepared by capture in the zeolite cages during synthesis, by post-synthesis sorption from either the gas or liquid phase, or by *in-situ* preparation [17]. Such species are submitted to the high electrostatic fields of the zeolite cages ($10^{9-11} \text{ V.m}^{-1}$) and may interact with nearby acidic sites; both factors are likely to alter their electronic structure (oxidation state). Metal carbonyl complexes are probably the most common organometallics which can be used to illustrate this situation [18].

Table III shows ^{13}C NMR data characterizing $\text{Ni}(\text{CO})_4$ and $\text{Fe}(\text{CO})_5$ sorbed on HY and NaY zeolites [19,20]. The interactions of the metal carbonyls with the Na form of the zeolite are weak and unspecific, as shown by the lack of change in the chemical shifts. For zeolite HY, however, different behavior is observed for the Ni and for the Fe species, and the difference can be ascribed to the different accessibilities of the carbonyl metal centers. In contrast to the carbonyl of Fe, $\text{Ni}(\text{CO})_4$ can adopt a square planar configuration, which exposes the Ni atom to the acidic sites. Exposure to such electron-deficient centers decreases the amount of M-C=O backbonding, destabilizes the π^* level on CO, and results in a shift on the ^{13}C resonance toward higher fields.

Table III. Interaction of Ni and Fe carbonyl complexes with HY and NaY zeolites. A ^{13}C NMR study: δ (ppm) are referred to TMS, values in () are linewidths (Hz), both at (294 K).

Metal carbonyl	$\delta_{\text{ppm}}(\Delta H(\text{Hz})) - (294 \text{ K})$			
	CDCl ₃ solution	Zeolite		
		H-Y	Na-Y	
$\text{Ni}(\text{CO})_4$	192 (5)	184.7 (50)	193.8 (30)	
$\text{Fe}(\text{CO})_5$	211.1 (20)	211.5 (50)	-----	
CO _{gas} (Ref.)	-----	~ 181	-----	

The same argument can be used to explain differences between the thermal and the photochemical decompositions of $\text{Fe}(\text{CO})_5$, as illustrated in Fig. 5 [20]. The important variation in the chemical shift of CO occurring upon photodecomposition indicates an increasing positive charge transfer between the zeolite and the carbonyl complex as CO molecules are progressively removed; i.e., there is a rather strong interaction of the acid sites of the zeolite with the metal carbonyl. In contrast, the opposite situation is found upon mild thermal

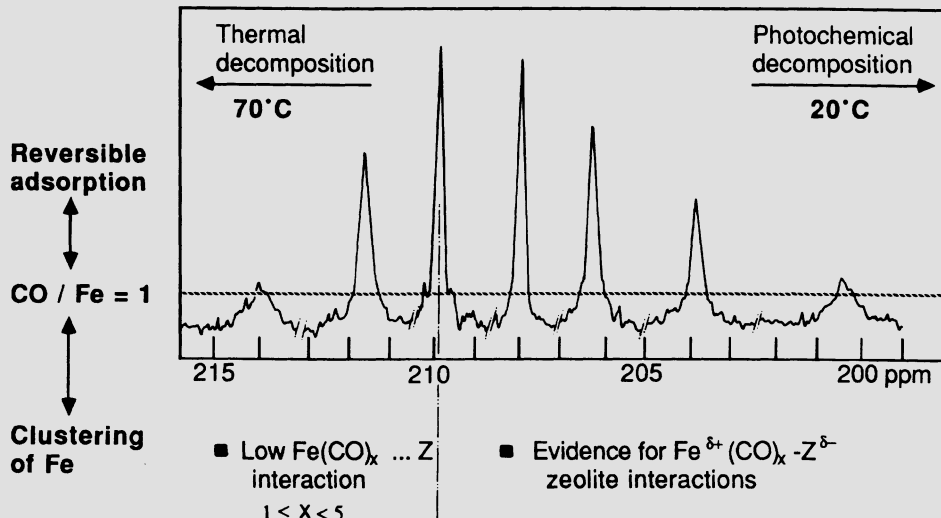
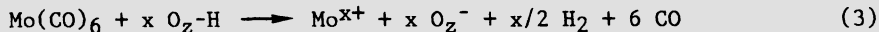


Figure 5. ^{13}C NMR spectra observed during the thermal and photochemical decompositions of $\text{Fe}(\text{CO})_5$ in zeolite HY (adapted from [20]).

treatment; the interaction with the zeolite surface is now small, and backbonding to the remaining CO ligands increases as the average number of CO ligands per molecule decreases (increasing electronic charge density on Fe).

At higher temperature, exposure of a metal carbonyl to zeolitic acid sites can lead to its complete decomposition and oxidation. For example, the following redox reaction has been proposed to account for the decomposition of $\text{Mo}(\text{CO})_6$ [21]:



It may thus lead to oxidized Mo species which are not homogeneously distributed. Note, however, that the resulting catalysts were still active, in this case, for propylene epoxidation.

As a further illustration of the intracrystalline transformations which such compounds may undergo is provided by recent and exhaustive (infrared and NMR) investigations of the chemistry of Rh(I) carbonyl species in various zeolite matrices [22]. Dimerization of $\text{Rh}^{\text{I}}(\text{CO})_2$ in

NaY, upon water sorption, was demonstrated by infrared spectroscopy to occur according to the equilibria shown in Fig. 6. This scheme also implies that water favors the migration of Rh(I) dicarbonyl species in the zeolite matrix, which thus behaves as a "solid solvent".

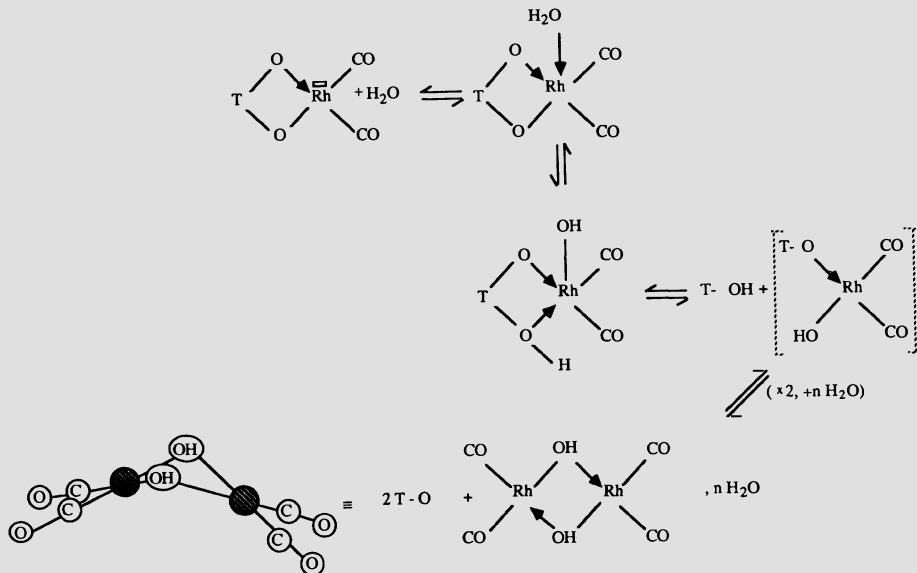
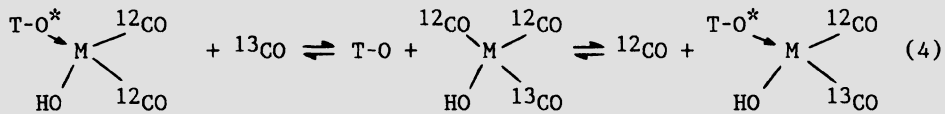


Figure 6. Effect of water on the conversion of $\text{Rh}^{\text{I}}(\text{CO})_x$ species in zeolite NaY [22].

Isotopic ^{13}CO -exchange was used in the same work [22] to investigate the effect of the zeolite matrix on the lability (rate of exchange) of the CO ligands according to the following reaction scheme, M = Rh(I):



The only framework oxygen anions which can stabilize (by coordination) the dicarbonyl species and retard the formation of the tricarbonyl intermediates are those which have an enhanced and localized negative charge. The occurrence of such anions is governed by the density of TO_4^- (tetrahedral) entities related to the presence of structural Al species. Thus, an increasing rate of CO exchange is expected for zeolites characterized by higher Si/Al ratios, which will displace the equilibria toward the formation of the tricarbonyl structure. This expectation has been confirmed for the series $\text{NaX} < \text{NaY} < \text{Na-mordenite}$

< Na-ZSM-11; the result illustrates further the capacity of zeolite frameworks to act as macroanionic ligands.

5. FRAMEWORK SITE COORDINATION CHEMISTRY

Free coordination sites can also be generated, in principle, by manipulation of the zeolite framework, as indicated in Fig. 7. If T is a framework site (in particular, a metal which may have tetrahedral as well as other coordinations), the equilibria will be displaced toward the formation of free ligand positions on site T as the electronegativity of the counterion M (if T is trivalent) and/or the electronegativity of T itself increase(s). Such sites should thus become available for reaction with other ligands (L), which would lead to their stabilization.

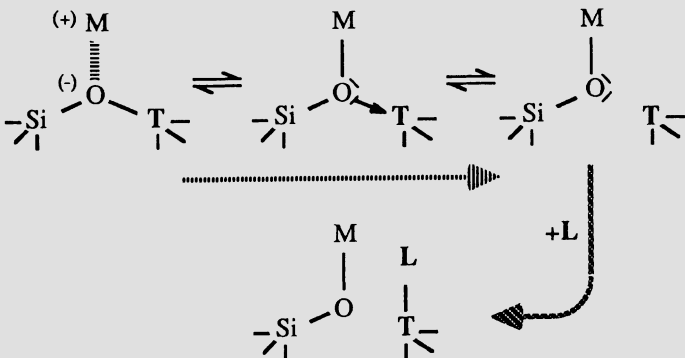


Figure 7. Framework site chemistry: formation of coordinatively unsaturated sites.

These sites should be suitable for reactions such as ligand substitution or addition, oxidative addition, and reductive elimination. However, no convincing examples of such chemistry are available for these materials and this should be a field for innovative developments.

Directions which could be explored in this area are the following:

- (1) Isomorphous substitutions in high-silica zeolites, for which the essential principles have recently been reviewed [23].
- (2) Investigations of the potential of new molecular sieve structures, e.g., metallophosphates, titanoaluminophosphates (TAPOs) [24], ferroaluminophosphates (FAPOs) [25], etc., as the corresponding aluminophosphate structures sometimes show the presence of sites with a coordination virtually higher than tetrahedral [26].

- (3) Studies of mixed framework sieves [27], consisting of corner-sharing Mo_6 octahedra and $\text{M}'\text{O}_4$ tetrahedra and involving transition metal ions, e.g., Mo, Ti, etc., which offer new types of open frameworks and possibilities for "coordination chemistry engineering".

6. PERSPECTIVES AND TRENDS

Obviously, the catalytic future of zeolite-occluded clusters and organometallics is two-fold. They can be used as coordination-type catalysts or act as zeolite-entrapped metal precursors. In both cases, the zeolite will provide its solid solvent property, its bifunctional capability (in a broad sense, either its acidic or macroanionic properties), and its unique shape-selective properties.

Future developments will probably include some of the possibilities discussed above (framework site coordination chemistry) and the application of zeolite frameworks with larger pores, such as those of zeolite Omega, Beta, and ZSM-20, which should be able to host relatively large organometallic compounds.

There is little doubt that increasing advantage will be taken of the ability of the zeolite framework to function as a polydentate ligand, enabling, in addition, the achievement of distinct steric and electronic configurations because of its unique matrix and electrostatic field effects.

7. REFERENCES

1. F. Liebau, Zeolites 3, 191 (1983).
2. T.J. Pinnavaia and R.A. Schoonheydt, Eds., Metal Complex Catalysts in Intracrystalline Environment, J. Mol. Catal. 27 (1984) (special volume), and references therein.
3. B.V. Romanovsky, Acta Phys. Chem. 31, 215 (1985), and references therein.
4. N. Jaeger, P. Plath, and G. Schulz-Ekloff, Acta Phys. Chem. 31, 189 (1985).
5. P.B. Weisz, Pure Appl. Chem. 52, 2091 (1980).
6. E.G. Derouane, in Catalysis on the Energy Scene (Eds. S. Kaliaguine and A. Mahay), Elsevier, Amsterdam; Stud. Surf. Sci. Catal. 19, 1 (1984).
7. D. Barthomeuf, J. Phys. Chem. 83, 249 (1979).
8. K. Seff, Acc. Chem. Res. 9, 121 (1976).
9. K. Mizuno, S. Imamura, and J.H. Lunsford, Inorg. Chem. 23, 3510 (1984).
10. S. Imamura and J.H. Lunsford, Langmuir 1, 326 (1985).
11. J.A. Rabo, R.D. Bezman, and M.L. Poutsma, Acta Phys. Chem. 24, 39 (1978).
12. J. Fraissard, in Catalysis by Zeolites (Eds. B. Imelik et al.), Elsevier, Amsterdam; Stud. Surf. Sci. Catal. 5, 343 (1980).
13. E.G. Derouane, J. Catal. 100, 541 (1986).

14. H. Diegruber and P.J. Plath, in Metal Microstructures in Zeolites (Eds. P. Jacobs et al.), Elsevier, Amsterdam; Stud. Surf. Sci. Catal. 12, 23 (1982).
15. L. Edwards and M. Gouterman, J. Mol. Spectrosc. 33, 292 (1970).
16. H. Diegruber, Ph.D. Thesis, Universität Bremen (1984).
17. J. Zwart and R. Snel, J. Mol. Catal. 30, 305 (1985).
18. D.C. Bailey and S.H. Langer, Chem. Rev. 81, 109 (1981).
19. E.G. Derouane, J.B. Nagy, and J.C. Vedrine, J. Catal. 46, 434 (1977).
20. J.B. Nagy, M. van Eeno, and E.G. Derouane, J. Catal. 58, 230 (1979).
21. M.B. Ward, K. Mizuno, and J. Lunsford, J. Mol. Catal. 27, 1 (1984).
22. F. Lefebvre, Ph.D. Thesis, Lyon (1985).
23. M. Tielen, M. Geelen, and P.A. Jacobs, Acta Phys. Chem. 31, 1 (1985).
24. B.M. Lok, M.B. Kristoffersen, and E.M. Flanigen, Eur. Patent Appl. 121,232 (1984).
25. C.A. Messina, B.M. Lok, and E.M. Flanigen, Eur. Patent Appl. 131,946 (1985).
26. J.B. Parise, J. Chem. Soc., Chem. Commun., 686 (1985).
27. A. Leclaire, M.M. Borel, A. Grandin, and B. Raveau, Mater. Chem. Phys. 12, 537 (1985).

INDEX

- acetoxylation**
 - aromatics 30, 111, 112
 - benzene 112
 - butadiene 108
 - butenes 108, 109
- acetylene, sorption in Co(II)-zeolites 302
- acid catalysis, in hydrocarbon conversion 24
- acrolein, by oxidation of propene 98
- acrylic acid, by oxidation of propene 109-111
- acrylonitrile
 - by ammoxidation of propene 98, 188, 189
 - hydrogenation 130
- actinide organocomplexes, reactivity with alumina 62-64
- adsorption
 - of carbon monoxide 41, 43, 132, 134, 137, 140, 148, 164
 - of hydrogen 148, 151
 - of pyridine
 - on alumina 44
 - on pillared clays 288
 - of water, on oxide surfaces 41
 - of xenon 39, 40, 258, 259
 - sites, on magnesia 38, 50
- Al₁₃ Keggin ion 278-281, 284, 285
- alcohols
 - by oxidation of alkenes 102-104
 - condensation, with niobotungstic acid 178
 - dehydration, by molybdochosphate esters 180
 - oxidation, by molybdochosphate esters 180
 - reactions, with molybdenum trioxide 174, 177
- aldehydes
 - by allylic oxidation of alkenes 107
 - by oxidation of alcohols 174, 180
 - oxidation 174
 - reaction with imido complexes 192
- alkanes
 - activation 30, 60
 - dehydrocyclization 263
 - formation, in methanol conversion 292
 - hydrogenolysis 83-85, 89
 - hydroxylation 119
 - isomerization 84
 - oxidation 100, 119-122
- alkenes
 - allylic oxidation 98, 107-110
 - by dehydration of alcohols 180
 - epoxidation 31, 98, 101-106
 - from methanol 265

glycolation 101
hydroformylation 65, 78
hydrogenation 65, 66, 78, 84, 86, 89
hydrosilylation 65
isomerization 84, 89
metathesis 15, 27, 51, 61, 174, 197, 198, 215
oligomerization 266, 289
oxidation 31, 65, 98, 101-111, 174, 198
oxidative carbonylation 31, 110, 111
oxygenation 104
polymerization 59-62
vinylic oxidation 98

alkoxides
 bridging groups 175
 surface-bound 177, 178, 181
 tridentate chelating ligands 175

alkoxy groups 174, 177-179, 189, 191

alkyl-metal complexes, on supports 59, 130

alkylation, of aromatics 266

alkynes
 hydrogenation 78, 277
 oxidation 198

allyl
 complexes, oxide supported 59-62
 radicals 189, 193, 194

allylic
 acetoxylation, of butenes 109
 O to N rearrangement 189, 194
 oxidation, of alkenes 98, 107-110

allylic acetates, by oxidation of alkenes 107, 108

allylic alcohols
 ammonoxidation 194
 epoxidation 101, 103
 formation, in oxidation of alkenes 102, 103

alumina
 aprotic surface sites on 43, 49
 CO adsorption on 43
 hydroxyl groups of 42, 49
 pyridine adsorption on 44
 reactivity of, with organometallics 52-64
 structure of (γ) and (η) 41, 42
 surface defect sites on 44
 surface models of 42, 44
 surface site relaxation 44
 X-sites on 44

aluminophosphate-based molecular sieves 19, 21, 241, 242, 246-250

aluminum polymer, in pillared clays 278

amido complexes 194

amination, of aromatics 30

amines 272, 289
 amine to imido ligand exchange 190, 192

amine-bis(imido) complex 190, 191
benzylidene-*t*-butyl amine 193
t-butyl amine 190
geranyl amine 194
neryl amine 194
ammonoxidation 187-196
 allylic alcohols 194
 propene 187-196
 toluene 194
anchoring sites, in zeolites 301
 π -aromatic ligands 197-219
 acentric coordination, in Re complexes 205, 207-214
aromatics
 acetoxylation 30, 112
 alkylation 266
 amination 30
 hydrogenolysis 84
 hydroxylation 112
 oxidation 99, 100, 111-118
 oxidative carbonylation 113, 114
 selective hydrogenation 30
aromatization, of hydrocarbons 263, 264

beams of metal clusters 91, 144
benzene
 acetoxylation 30, 112
 amination 30
 dehydrogenation 151
 hydrogenation 30, 137, 138
 hydroxylation 112
 oxidation 99
benzophenone, hydrosilation 78
benzopinacolato complexes 191
benzyl radicals 116, 193, 194
benzylidene-*t*-butyl amine 193
bimetallic crystallites (see also 'bimetallic supported catalysts' and
 'bimetallic supported particles') 58, 160, 161
bimetallic films 160
bimetallic molecular clusters 8, 57, 58, 80, 84, 147, 160-162
 metal frame 160-162
 precursors of bimetallic supported catalysts 80, 84
 reactivity with oxide supports 57, 58
bimetallic supported catalysts
 Co-Cu 135
 Co-Pd 138, 139
 Co-Rh 57
 Fe-Co 58, 147
 Fe-Cu 135
 Fe-Os 58, 147
 Fe-Pd 138

Fe-Ru 58, 147
Mn-Pd 139
Pb-Ni 130
Pt-Mo 148
Pt-Sn 130
Rh-Cu 135
Rh-Os 58
Rh-Pd 137, 138
Rh-Sn 130
Ru-Cu 135
Ru-Os 57, 84
Ru-Pd 132-136
bimetallic supported particles
 by reaction of organometallics with metal surfaces 127-140, 148
 from bimetallic molecular clusters 8, 58, 80, 147
biomimetic systems, for alkane oxidation 122
bipyridine, reaction with Co(II) ions, in zeolites 302, 303
bismuth molybdate-based catalysts 98, 174, 188
Brønsted acid sites, in clays 277, 286, 288, 289
butane, oxidation 100
butenes
 acetoxylation 108, 109
 allylic oxidation 108-110

carbide
 carbonyl clusters 84-87, 149, 163-168
 exposed 166
 interstitial 163, 166
 proton-induced conversion of 168
 reactivity of 166, 167
 surface bound 166
carbidization 164
carbon monoxide
 adsorption 132, 134, 137, 140, 148, 164
 hydrogenation 68, 83-87, 135, 136, 152
 probe molecule for surface of oxides 40, 41, 43
 reduction 79, 168
carbonyl
 complexes
 in zeolites 305-308
 reactivity with oxide surfaces 51-59
 groups 174
 molecular metal clusters 6, 13, 15, 17, 47-68, 78-89, 128-134,
 147-152, 157-168
carbonylation, oxidative 110-114
carboxyl groups 174
carboxylic acids, by oxidation of aldehydes 174
cationic organometallic complexes
 in clay interlayers 275-277
 in zeolites 301-304

chromium

 allyl complexes, oxide supported 60, 61
 bis(cyclopentadienyl) complex, on silica 61
 bis(fluorenyl) complex, on silica 61
 bis(indenyl) complex, on silica 61
 carbide 163, 164

carbonyls

 on supported Cu 131
 on supported Pd 131
 oxide supported 52, 53
 imido complexes 187, 189, 190, 193, 194
 organometallic oxides 198, 199

clays (see also 'PILCS' and 'smectite clays') 271-290

clusters (see 'metal clusters' and 'molecular metal clusters')

cluster beams (see also 'naked metal clusters') 91, 144

cluster-surface, analogy 158

cobalt

 carbide carbonyl clusters 165, 167
 complexes

 as oxidation catalysts 100, 104, 116, 119, 120
 in zeolite 302-304
 -Fe bimetallic clusters 58, 147
 on supported Cu 131, 135
 on supported Pd 131, 135, 138, 139
 -Pd bimetallic catalysts 139, 152
 -Rh bimetallic catalysts 57

copper

 -based catalyst, on silica 130, 131, 135
 -catalyzed oxidation of phenols 99, 100, 114, 115
 CO hydrogenation on 135
 complexes

 for oxidation of alkenes 106, 110, 111
 in clay interlayers 276

cracking process 262, 263, 271, 288

crystal facets, on oxide surfaces 37

crystal growth, in zeolite synthesis 232-237

crystallites (see also 'metal particles') 84

 bimetallic 58, 160, 161
 growth of 158

crystallization rates, in zeolite synthesis 234, 239

cumene, dealkylation 288

cyclohexane

 dehydrogenation 151
 oxidation 100

cyclohexene, oxidation 103

cyclopentadienyl ligands 61, 197-219

 acentric coordination, in Re complexes 205, 207-214

dealkylation

 cumene 288

- 1-isopropynaphthalene 288, 289
- dehydrocyclization, of alkanes 263
- dimethylglyoxime, sorption in Co(II)- and Ni(II)-zeolites 303, 304
- diols, as chelating ligands 190, 191
- dodecasil-1H 225, 227, 228
- π -donor ligands 197-219
- dynamics
 - of ligands 13
 - of metal framework 13
- EELS (electron energy loss spectroscopy) 38
- electronic effects
 - in bimetallic catalysts 130, 137
 - in organometallic oxides of Re 208-214
- elementary steps 6, 7, 25
- enzymatic oxidation, of aromatics 118
- epitaxial effect 150
- epoxidation
 - of alkenes 31, 98, 101-106
 - of allylic alcohols 101, 103
- epoxy alcohol, by oxidation of alkenes 102-104
- erionite zeolites 222, 247, 271, 300
- ethane, hydrogenolysis 84, 85, 134-139
- ethylene
 - epoxidation 98
 - formation, in methanol conversion 292
 - hydrogenation 78, 84, 87
 - oxidation 98, 106
 - polymerization 62
- ethylene glycol
 - by oxidation of ethylene 106
 - by reduction of carbon monoxide 79
- EXAFS (extended X-ray absorption fine structure) 54-57, 66, 81, 82, 132, 133, 148, 149
- extraction, of surface complexes 7
- faujasite zeolites 222, 225, 229, 234-238
- FEG-STEM (field emission gun - scanning transmission electron microscopy) 147
- Fischer-Tropsch synthesis (see also 'carbon monoxide hydrogenation' and 'synthesis gas') 27, 33, 68, 83-85, 135, 168
- fluorosilicate treatments, of zeolites 251, 252
- formaldehyde
 - adduct, in polyoxomolybdates 175
 - by oxidative cleavage of methyl aromatics 116, 117
 - formation, in decomposition of polyoxomolybdates 176
 - from methanol 174
- framework
 - clusters 163

zeolites 221-223, 247, 261, 300, 301, 308, 309
functionalized silica, reactivity, with Rh complexes 64

Gibbs-Duhem relation 226

glycol, by ethylene oxidation 106

glycolates 190-192

glycolation, of alkenes 101

guest-host interaction, in porous materials 20, 225-228

halides ligands, in Re complexes 201, 208

heterometallic carbonyl clusters (see also 'bimetallic molecular clusters') 78

heteronuclear molecular clusters (see 'bimetallic molecular clusters')

heteropolyanions 173-186

1-hexene

hydrogenation 276

isomerization 276

hydride ligands 7, 12, 57, 84-88, 147, 160, 161, 214, 276

hydrocarbons

aromatization 263, 264

conversion, by acid catalysis 24

from methanol 265, 292

from synthesis gas 83, 84

oxidation 97-126, 174

hydrocarbyl metal complexes, reactivity with oxide surfaces 59

hydrodenitrogenation 25

hydrodesulfurization 25

hydroformylation 78, 88, 152, 153, 278

hydrogenation

acrylonitrile 130

alkynes 78, 277

aromatics 30

benzene 30, 137, 138

carbon monoxide 68, 83-87, 135, 138

catalysts 128, 135-138, 276, 277, 294

ethylene 78, 84, 86, 87

1-hexene 276

propene 62

hydrogenolysis 83-85, 89, 134, 135, 138, 139, 152

hydrosilation, of benzophenone 78

hydroxyl groups

in zeolites 252, 257, 258

on oxide surfaces 40, 41, 180

stretching frequencies of 41, 43

hydroxylation

aromatics 112

light alkanes 119

imido complexes
 of group VI metals 187-196
 of Re 206
imido/oxo interconversion 189, 190
intercalated porous compounds 20, 22, 288
intercalation 273, 275
interlayers
 in clays 274, 275, 279, 281, 284, 286, 293
 in group IV metal phosphates 292, 293
intersalation 275
intracrystalline surfaces, functionalization 299-310
ion exchange
 in clays 273-275
 in molecular sieves 251-254
 in zeolites 301-304
ion vacancies, on oxide surfaces 38
IP (ionization potential) 151
iridium
 carbonyl clusters
 formation of, in zeolites 148
 precursors of metal particles 147
 metal clusters 144, 147, 148
iron
 carbides 164
 carbide carbonyl clusters 166
 carbonyl, in zeolites 305, 306
 carbonyls, reactivity with oxides 53, 54
 cluster-derived catalysts 83-85
 -Co bimetallic clusters 58, 147
 complex, for hydrocarbon oxidation 105, 121
 on supported Cu 131, 135
 on supported Pd 131, 138
 -Os bimetallic clusters 58, 147
 -Pd bimetallic catalysts 139
 -Pd carbonyl clusters 160
 -Ru bimetallic clusters 58, 147
isobutane, autoxidation 100
isobutene, oxidation 110
isomerization
 alkanes 84
 catalysts 84, 277
 1-hexene 276
 xylene 266
1-isopropylnaphthalene, dealkylation 288, 289

Keggin ion (see 'Al₁₃ Keggin ion')
ketones
 by oxidation of alcohols 180
 by oxidation of alkenes 104, 107

lead, -Ni bimetallic catalyst 130
LEED (low energy electron diffraction) 37
Lewis acid sites, in pillared clays 288, 289
ligand tethered organometallic complexes 64
linalool 194
Linde type zeolites 223, 246, 300
Löwenstein
 limit 224, 239
 rule 254, 255

magnesia
 adsorption sites on 38, 50
 electronic properties 38
 optical spectra 38, 39, 50
 reactivity, with organometallics 53, 54
 structure 36
 surface bonding characteristics 37
 surface defects 37, 38
 surface relaxation in 37

magnetic behavior, of molecular metal carbonyl clusters 165

manganese
 complex, for alkene epoxidation 105, 106
 on supported Cu 131
 on supported Pd 131, 138
 -Pd bimetallic catalysts 140

MAS NMR (magic angle spinning nuclear magnetic resonance) 63, 191, 254-258, 284

MELS (molecularly engineered layers) (see also 'organically pillared group IV phosphates') 293

metal
 catalysis 24
 crystallites 84, 161
 dynamics 13
 films 129
 lattices-large molecular clusters, analogy 158, 161
 particles (see also 'crystallites', 'metal clusters', and 'naked metal clusters') 7, 8, 58, 143-152
 characterization techniques 81, 132, 144-148
 colloidal 76, 79
 growth sequence 158
 molecular models of 12-18, 143, 157-165
 size effects 82, 83
 supported 7, 8, 58, 80, 129, 133, 151, 158
 unsupported 90, 91, 128
 surface reconstruction 160
 surfaces
 molecular models of 12-18
 reaction of organometallics with 5-11, 130-140

metal-carbene complexes 27, 121

metal carbide (see also 'carbide') 163-165
metal-carbon bond distances, in cyclopentadienyl rhenium complexes 201-203, 210, 212, 213
metal clusters (see also 'metal particles', 'molecular metal clusters' and 'naked metal clusters') 75-95, 143-153, 157-172
generation in the gas phase 90, 91
homogeneous catalysis by 78, 79
heterogeneous catalysis by 79-89
supported
 catalytic behavior 82-89
 characterization 80-82
 preparation 79, 80
metal-nitrogen bond, exchange for a metal-oxo bond 192
metal-oxygen bonds, in polyoxoanions, reactivity 176, 177, 181, 182
metal vapour chemistry 90
metallacycle
 intermediates, in alkene oxidation 103, 104, 106
 osmate esters 106
 Re complexes 208
metalloporphyrin complexes, catalysts for alkene epoxidation 105, 106
metathesis
 alkenes 15, 27, 51, 174, 197, 198, 215
 propene 59, 61, 84, 174
methacrolein, conversion into methacrylic acid 174
methacrylic acid, from methacrolein 174
methane
 in conversion of methanol 265, 292
 oxidation 30, 100, 119-121, 174
 oxidative coupling 30, 120-121
methanol
 alkylation of toluene by 266
 by oxidation of methane 30
 conversion 265, 288, 292
 from CO-H₂ 135
 oxidation 174
methyl aromatics, oxidation 116, 117
mixed metal clusters (see 'bimetallic molecular clusters')
molecular metal clusters
 bimetallic 57, 58, 80, 84, 147, 160-162
 bonding theories 162
 carbide carbonyl 84-87, 149, 163-168
 carbonyl 6, 13, 15, 17, 47-68, 78-89, 128-134, 147-152, 157-168
 catalysis by 78, 79
 definition 157
 degradation 157-168
 five-fold symmetry, in large 161
 formation
 from metal cations 148
 from metal halide salts 148, 149
 from naked metal clusters 86, 90, 148
 interaction with oxide surfaces 6, 47-68, 79

interaction with surfaces of supported metals 130-140
interstitial carbide atoms in 163, 164
magnetic behavior 165
metal frame 163
models of metal particles 12-16, 143, 157, 165
models of surface complexes 13-17, 32, 33
precursors of metal particles 58, 75, 80, 146, 147
precursors of supported catalysts 32, 34, 75, 79-89
reactivity 166, 167
structure 158-161
-surface, analogy 166, 168

molecular models
of intermediates in surface catalysis
 organic derivatives of polyoxoanions 173-186
 organoimido complexes 187-196
 organometallic oxides 197-219
of metal particles and metal surfaces 12-18, 157-168
of oxide surfaces 12-18, 36
 of surface complexes 12-18, 32, 33

molecular sieves (see also 'porous supports' and 'zeolites') 221-244,
245-270, 299-310

aluminophosphate-based 246-250
 containing transition metal atoms 249
 structure 246-249
 synthesis 246-250

aluminum enrichment 252-254

catalytic properties 262-268

characterization 254-262
 electron microscopy 259
 far-infrared spectroscopy 261
 MAS NMR spectroscopy 254-259
 X-ray crystallography 260, 261

hydrothermal stability 248, 251

pore size 247, 248

silicon enrichment 250-252

thermal stability 248, 251

molybdates
 bismuth molybdate 98, 174, 188
 cesium phosphovanadomolybdate 174
 ferric molybdate 174
 polyoxomolybdates 173-175

molybdenum
 alkyl, oxide supported 59
 allyl, reactivity with oxides 61, 62
 -based catalyst, for epoxidation of propene 98
 carbonyl
 in zeolites 306
 on supported Pt 148
 reactivity with oxides 51-53
 imido complexes 187-196
 -Pt bimetallic catalysts 148, 152

molybdenum oxides
MoO₃ 174, 180, 182
organometallic oxides 198, 199
polyoxoalkoxides 175
reactions catalyzed by 174
reactions with alcohols 177
molybdophosphate esters 180-184
decomposition, thermal and photochemical 183
structure 183
synthesis 182, 183
montmorillonite 274, 286, 288, 289
mordenite zeolites 97, 146, 222, 240, 258, 261, 300, 307

naked metal clusters (see also 'metal clusters' and 'metal particles')
143-155
beams of 91, 144
encaged in zeolites 144-146
epitaxial interaction with support 150
from molecular clusters 146, 147
nuclearity 144-149
precursors of molecular clusters 86, 90, 148
reactivity 150-152
structural flexibility 149, 150
supported 144, 145, 151, 152
unsupported 144, 150, 151

nickel
carbides 164
carbide carbonyl clusters 165, 166
carbonyl, in zeolites 305, 306
complexes, in zeolites 303
-Pb bimetallic catalyst 130
-Pt carbonyl cluster 159-161
-Sn carbonyl cluster 161, 162

niob tungstic acid
condensation with alcohol 178
esterification 178
preparation 178
self-condensation 178

niob tungstic anhydrid 178, 179

niob tungstic anion
decomposition 176
reactivity 177
structure 177

niob tungstic esters 178, 179

nitro complexes, for epoxidation of alkenes 104, 105

nitrogen activation 34

nitrogen monoxide, sorption in Co(II)-zeolites 302

NMR (nuclear magnetic resonance) (see also 'MAS NMR') 63, 191, 254-258, 278-280, 284, 285, 305, 306

NMR magnetization transfer studies 191, 192

nucleation, in zeolite synthesis 229-231, 236, 237

offretite zeolites 229, 300

olefins (see 'alkenes')

oligomerization

 alkenes 266

 propene 289

organically pillared group IV phosphates 290-294

organoactinide complexes, reactivity with alumina 62, 63

osmium

 carbide carbonyls 84, 85, 87

 carbonyls

 from metal particles 86

 magnetic behavior 165

 precursors of supported catalysts 81, 84-87

 reactivity with oxides 53, 55, 56, 86, 147

 cluster-derived catalysts 82-88

 -Fe bimetallic catalyst 58, 147

 oxyhalides, in alkene oxidation 106

 -Rh bimetallic catalyst 58

 -Ru bimetallic catalyst 57, 84

 tethered complexes 66, 67

Ostwald's rule, in zeolite synthesis 237, 238

oxidation

 alcohols 174, 180

 aldehydes 174

 alkanes 100, 101, 119-122

 alkenes 31, 65, 98, 101-111, 174, 198

 alkynes 198

 aromatics 99, 111-118

 benzene 99

 butane 100

 butenes 108-110

 catalysts, homogeneous and heterogeneous 97-126

 cyclohexane 100

 cyclohexene 103

 ethylene 98, 106

 hydrocarbons 97-126, 174

 methane 30, 100, 119, 120, 174

 methanol 174

 methyl aromatics 116, 117

 phenol 99, 100, 114, 115

 propene 106, 191

 toluene 117

oxidative carbonylation

 alkenes 110, 111

 aromatics 113, 114

oxidative coupling, of methane 30, 120, 121

oxidative trapping, of radicals 187-196

oxides, of transition metals
molecular models for 173-186
organometallic, with π -aromatic ligands 197-219
 oxoalkyl complexes 208
 oxohalide complexes 198, 199, 201-207
 Re complexes 197-219

oxide surfaces
 aprotic sites on 41, 43
 characterization techniques 7, 13, 14, 40, 44
 CO adsorption on 41, 43
 crystal facets on 37
 defect sites on 37, 38
 dehydrated 180
 electronic properties 38
 functionalization of 48, 50, 64-67
 hydroxyl groups on 41-43, 180
 ion vacancies on 38
 models of 12-18, 36, 42, 44
 O-H stretching frequencies on 41-43
 probes for 7, 40, 44
 reactivity of, with organometallics 5-11, 51-64
 relaxation of surface sites 42, 44
 single crystals 36
 terraces on 37
 water adsorption on 41

oxo ligand
 in homogeneous models of ammonoxidation catalysts 189, 190, 192
 in hydrocarbon oxidation catalysts 102, 106, 112
 in organometallic oxides of transition metals 197-219
 in polyoxoanions 173-186
 trans influence, in cyclopentadienyl Re complexes 211, 213

oxo-imido interconversion 189

oxometalloporphyrin, for alkene oxidation 105, 106

oxygenation, of alkenes 104

palladium
 -based catalysts 98-114, 130-140
 carbonyl cluster 159
 -Co bimetallic catalysts 138, 152
 complexes, for hydrocarbon oxidation 104-113
 -Fe carbonyl cluster 160
 ion, in pillared group IV phosphates 293, 294
 -Rh bimetallic catalysts 137, 138
 -Ru bimetallic catalysts 133, 134, 136, 137
 trifluoroacetate oxidation catalyst 107, 111

PAX (photoemission of adsorbed xenon) 40

perfluoropinacolato complexes 190

phenol, oxidation 99, 100, 114, 115

phenyl acetate
 by benzene acetoxylation 112

by toluene oxidation 117

phosphorus

- cesium phosphovanadomolybdate 174
- molybdophosphate esters 180-183
- P-O bond, reactivity 182
- pillared group IV metal phosphates 290-294
- vanadyl pyrophosphate 100

PILCS (pillared interlayered clays) 20, 278-290

- Al_{13} Keggin ion, in 278-281, 284, 285
- aluminum polymer, in 278
- Al-Zr PILCS 288
- Brønsted acid sites 286, 288, 289
- catalytic behavior 284, 288, 289
- deactivation 289
- interlayers 279, 281, 284, 286
- Lewis acid sites 288, 289
- molecular sieve properties 281-283
- pore size 271, 281, 282, 284
- sorption of organic molecules 281-283
- surface area 281, 282, 286, 288, 291, 292
- thermal stability 278, 288, 292
- zirconium polymer, in 286

pillared clays (see also 'PILCS') 20, 271-290

pinacolato complexes 190, 191

platinum

- based catalysts 128, 130
- carbonyl clusters 84, 159, 161
- cluster-derived catalyst 84
- metal clusters 144, 145, 150, 151
- Mo clusters, in zeolites 148, 152
- Ni carbonyl cluster 159, 161
- Rh carbonyl cluster 159, 161
- Sn bimetallic catalyst 130

poisoning effect 137

polymerization

- alkenes 60, 61
- ethylene 62

polymolybdates (see also 'molybdates') 173-175

polyoxoanions 173-186

pore size 247, 248, 271, 281, 282, 284, 291, 300, 302

porosils 224, 225

porous supports 19-23

- molecular sieves 221-244, 245-270
- organically pillared group IV phosphates 290-294
- pillared clays 271-290
- zeolites 221-244, 245-270, 299-310

propene

- ammoxidation 187-196
- epoxidation 98
- hydrogenation 62
- metathesis 59, 61, 84, 174

- oligomerization 266, 268, 289
- oxidation 98, 99, 106, 191
- propylene glycol 106
- propylene oxide 100
- pyridine, adsorption 44, 288
- quinones, by oxidation of phenols 114, 115
- RDA (radial distribution of atoms) 132, 133, 148
- RED (radial electron distribution) 144, 148, 149
 - characterization of Rh clusters by 148, 149
 - nuclearity of Pt clusters by 144
- reforming catalysts 130
- rhenium
 - carbonyls, oxide supported 84, 130
 - cyclopentadienyl compounds 197-219
 - acentric coordination, of π -aromatic ligand, in 205, 207-214
 - carbonyl complexes 200, 210, 213
 - electronic properties 208-214
 - hydrido complexes 214
 - imido complexes 206
 - metal-carbon bond distances in 201-203, 210, 212, 213
 - oxo complexes 197-219
 - oxoalkyl complexes 208
 - oxohalides complexes 201-207
 - reactivity 197-208
 - structural properties 208-214
 - synthesis 197-208
 - trioxo(η^5 -pentamethylcyclopentadienyl)rhenium(VII) 197-219
- rhodium
 - allyl complex, reactivity with silica 59, 60
 - carbide carbonyl clusters 165
 - carbonyls
 - as homogeneous catalysts 79
 - in zeolites 148, 306, 307
 - large molecular metal clusters 159
 - on supported Cu 131, 135
 - on supported Pd 131
 - reactivity with oxides 56, 147, 148
 - Co bimetallic catalysts 57
 - complexes, in clays 276-278
 - Cu bimetallic catalysts 135
 - Os bimetallic catalysts 58
 - Pd bimetallic catalysts 134, 137, 138
 - Pt carbonyl cluster 159, 161
 - Sb carbonyl cluster 161, 162
 - Sn bimetallic catalysts 130
 - tethered clusters on silica 65, 66

ruthenium
carbide carbonyls 84, 149
carbonyls
 on supported Cu 131, 135
 on supported Pd 131-133, 136
 precursors of supported catalysts 78, 81, 84
 reactivity with oxides 54, 57
cluster-derived catalysts 81, 83, 84
complex, for alkene epoxidation 106
-Cu bimetallic catalysts 135
-Fe bimetallic cluster 58, 147
-Os bimetallic catalysts 57, 84
-Pd bimetallic catalysts 133-137
tethered clusters, on silica 65, 67

rutile
CO adsorption on 40
Xe adsorption on 39, 40

SAPO's (silicoaluminophosphates) 248, 265-267
shape selectivity, in pillared clays 276, 289
silica
 -clay intercalates 288
 functionalization of 50, 51
 morphology 49
 phosphinated 66
 reactivity of, with organometallics 51-62
 surface hydroxyl groups on 49
 tethered complexes on 64-67
silver catalyst, for epoxidation of ethylene 98
silyl ester, of niobotungstic acid 178
site isolation effect 65
size selectivity, in pillared clays 276
smectite clays 272-278, 284
 catalysis by complexes in the interlayer 275-278
 description 272, 273
 ion exchange behavior 273
 octahedral sites 272, 273
 swelling 274, 275, 278
 tetrahedral sites 272, 273
sodalite 224, 225, 230, 250
sorption
 of acetylene in Co(II)-zeolites 302
 of dimethylglyoxime in Co(II)- and Ni(II)-zeolites 303, 304
 of nitrogen monoxide in Co(II)-zeolites 302
 of organic molecules
 in pillared clays 281-283
 in zeolites 226-228, 283
STEM (scanning transmission electron microscopy) (see also 'TEM') 147
surface area
 of oxides 36

- of pillared compounds 281, 282, 286, 288, 291, 292
- swelling, of clays 274, 275, 278
- synergetic effect 152
- synthesis gas (see also 'carbon monoxide hydrogenation' and 'Fischer-Tropsch synthesis')
 - conversion 59
 - to anhydride 34
 - to glycol 34
 - to hydrocarbons 84
 - to methanol 84, 135
 - to oxygenates 34
 - to polymethylene 68
 - from methane 100
- tailor-made catalysts 5, 9, 10
- tectosilicates 299
- TEM (transmission electron microscopy) 144, 147, 148, 259
- templates 228, 229, 246
- terpyridine, reaction with Co(II) ions, in zeolites 302, 303
- terraces, on oxide surfaces 37
- tethering, of organometallic compounds 64-67
- tin
 - Ni carbonyl cluster 161, 162
 - Pt bimetallic catalysts 130
 - Rh bimetallic catalysts 130
- titania
 - CO adsorption on 40
 - photoemission of adsorbed xenon on 40
 - surface sites 50
 - surface structure 40
- titanium phosphates 290
- titanium-tetrabenzyl 59
- toluene
 - alkylation by methanol 266
 - ammonoxidation 194
 - oxidation 111-117
- TPD (temperature programmed desorption) 148
- trans influence, of an oxo ligand, in Re complexes 211, 213
- trioxo(η^5 -pentamethylcyclopentadienyl)rhenium(VII) 197-219
- tungsten
 - hexacarbonyl, on silica 52
 - imido complexes 190-192, 194
 - organometallic oxide complexes 198, 199
- unsupported metal clusters 144
- vanadium
 - cesium phosphovanadomolybdate 174

complexes, for hydrocarbon oxidation 102, 103, 112
organometallic oxide complexes 198, 199
oxide, for hydrocarbon oxidation 100, 110, 111
peroxo complex, for hydroxylation 112
pyrophosphate 100
vinylic acetates, by oxidation of alkenes 107, 108
vinylic oxidation, of alkenes 98

Wacker chemistry 107, 110, 111, 293

xenon adsorption
on rutile 40
on zeolites 258, 259
xylene, isomerization 266

zeolites (see also 'molecular sieves' and 'porous supports') 221-244,
245-270, 299-310
aluminum enrichment 252-254
anchoring sites 301
catalytic properties 262-268
cationic organometallic complexes in 301-304
characterization 254-262
clusters encaged in 144-146
Co(II) complexes in 302-304
crystal growth 232-236
crystallization rates 234, 239
fluorosilicate treatments 251, 252
framework site coordination chemistry 308, 309
framework topology 221-223, 247, 261, 300, 301
guest-host interaction 20, 225-228
hydrothermal stability 251, 252
intracrystalline organometallic chemistry 300, 301
intracrystalline surfaces, functionalization 299-310
isomorphous replacement 241, 242, 249, 308
Löwenstein limit 224, 239
Löwenstein rule 254, 255
natural 222
nucleation 229-231, 236, 237
organometallic species occluded in 305-308
Ostwald's rule 237, 238
pH effect, in synthesis 239, 240
porosils 224, 225
reaction of organometallics with 8, 299-310
reaction variables, in synthesis 238-241
Si/Al ratios 224, 225, 250-252, 300
silicon enrichment 250-252
sorption of organic molecules 226-228, 283, 302-304
successive transformations 237, 238

synthesis 19-21, 221-244
synthetic 223
templates 228, 229, 246
thermal stability 251
transition metal ions in 261, 263, 301-304
Ziegler-Natta catalysts 59
zirconium phosphates 273, 290, 293
zirconium polymers, in pillared clays 286
ZSM-5 zeolites 223, 225, 227-229, 254, 263, 271, 283, 300